Effect of lipids on the infectivity of influenza A viruses

By

Lamyaa Mohammed Al-Dalawi

B.V.Sc. & M.V.Sc.

Thesis submitted to the University of Nottingham for the degree of Doctor of Philosophy

School of Veterinary Medicine and Science

The University of Nottingham

January 2019

Abstract

Influenza is an enveloped, single stranded negative sense RNA virus that subverts host cell factors like lipids for its own replication. Airway epithelium contributes towards the host defence against pulmonary pathogens by a number of mechanisms including the production of cytokines, chemokines and surfactant phospholipids and proteins. Phosphatidylcholine (PC) and phosphatidylglycerol (PG) make up the major of the composition of pulmonary surfactant. Therefore, this project aimed to explore the potential antiviral activity of exogenous phospholipids against influenza A viruses *in vitro*. The specific aims were to investigate the potential of these lipids to reduce the infectivity of influenza A virus and to measure the potential toxicity of specific exogenous phospholipids, using human adenocarcinomic alveolar basal epithelial (A549) and Madin Darby canine kidney (MDCK) cell lines and chicken red blood cells.

Two types of phospholipids were used at concentrations of 5, 50 and 500 μM to treat avian influenza virus H2N3, equine influenza virus H3N8 or pandemic influenza virus H1N1. The first type are phospholipids composed of two aliphatic chain including 1,2-dipalmitoyl-sn-glycero-3- phospho-L-serine (DPPS), 1,2-dipalmitoyl-sn-glycero-3-phospho-(1'-rac-glycerol) (DPPG), 1,2-dipalmitoyl-sn-glycero-3-phosphocholine (DPPC). The second type are lyso-derived lipids including 1-palmitoyl-2-hydroxy-sn-glycero-3-phospho-L-serine (LPS), 1-palmitoyl-2-hydroxy-sn- glycero-3 -phospho-(1'-rac-

glycerol) (LPG), 1-palmitoyl-2-hydroxy-sn-glycero-3-phosphocholine (LPC).

Lipids make up the bilayer membranes of both virus particles and host cells. The potential toxicity of these lipids was assessed using chicken RBCs; incubation with DPPC deformed the RBC as they became round and nuclear loss occurred after 5-30 mins of incubation with 500μM DPPC However, no changes were observed when excess lipids were removed by ultrafiltration prior to incubation using two sequential filtration steps with an Amicon Ultra-15 Filter (50KDa MWCO; molecular weight cut-off). This result was further confirmed through ultrafiltration of phospholipids DPPG, LPG, DPPC, LPC, DPPS, or LPS prior to incubating them with cells as no significant changes were measured in both cell size and granularity of suspension MDCK cells or on the cell viability of adherent MDCK or A549 cells. Therefore, the use of ultrafiltration to remove excess lipids using the Amicon filtration system prior to incubating them with cells was used for further experiments to avoid any direct toxicity of the lipids on the cells.

Modifying the lipid envelope of influenza A virus by cholesterol depletion using methyl-β-cyclodextrin (MβCD) reduced H2N3 infectivity of MDCK cells in a dose-dependent manner suggesting that it disrupts the natural packing of influenza viral envelope lipids. Regarding the importance of phospholipid head charge and size, pre-treated H2N3 with charged and small lipid heads, such as DPPG

reduced virus infectivity more than when DPPS or DPPC were used. However, treating H2N3 virus with various lyso-lipids including LPS, LPC, or LPG produced a significant inhibition to < 15 % of virus infection in MDCK cells, suggesting that the lipid head and the number of aliphatic chains are an essential factors in the modulation of virus infectivity by phospholipids. Similarly, pre-treatment of H1N1 and H3N8 with phosphatidylglycerol (DPPG or LPG) significantly reduced the virus infectivity in a dose-dependent manner, although, the use of DPPG on the filamentous H3N8 virus showed less reduction than that of H2N3 and H1N1. In a similar manner, pre-treatment of LPAI H2N3 with LPG and DPPG reduced virus infectivity in both A549 and MDCK cells, but it was more noticeable in A549 than MDCK cells suggesting some differences in the receptor/binding characteristics between these cell lines.

Transmission electron microscopy (TEM) revealed changes in influenza virus H2N3 and H3N8 morphology upon treatment of H2N3 or H3N8 with exogenous lipid treatment, H2N3 displayed extensive fusions between virions and liposomes and formed giant particles with an uneven surface distribution of viral glycoprotein. The lyso-lipids had a greater impact on morphology of both virus strains, suggesting that the exogenous lipids may have been inserted into only one leaflet of the virion, leading to disruption of the viral envelope and therefore reduction in influenza virus infectivity.

The physicochemical structure of the lipid head has an impact on influenza virus adhesion and fusion to liposomes. The results showed that the two aliphatic chains, negatively charged lipid head domain DPPG and DPPS blocked virus haemagglutinin unit (HAU) 16 and 32 at ≥ 500 μM or 250 μM, respectively. However, flow cytometry results showed that only LPG, LPC, LPS, DPPC and DPPG pre-treatment significantly blocked the binding of H2N3 to MDCK cells, in a dose-dependent manner, while DPPS pre-treatment did not reduce virus binding. These flow cytometry results were confirmed by immunofluorescence staining of virus protein using MDCK and A459 cells infected with H2N3 or H3N8, pre-treated with 50 and 500 μM of LPG and DPPG at 4°C. This suggested that pre-incubating the virus with phospholipids seemed to have an impact on the ability of the virus to bind either by inhibiting virus binding to cellular receptors or by causing disruption of the viral envelope.

Expression of cytokine mRNA for IL-8 and TNF-α were significantly reduced in MDCK or A549 cells infected with H2N3 or MDCK cells infected with H1N1 and H3N8 following pre-treatment of virus with DPPG or LPG. However, no significant reduction of TNF-α was observed under the same conditions following pretreatment of H3N8 virus. Impact of pre-treatment of virus with either 500μM of DPPG or LPG in reducing H2N3 infectivity correlated with reduction of IFN-β mRNA expression at 6 and 4 hrs pi when compared to un-treated virus. This suggested that the virus may have been altered upon lipid pre-treatment leading to reduced cytokine expression levels due to a

reduced binding and entry of virus to cells. A significant reduction in virus M gene RNA expression was also observed following pre-treatment of H2N3 with phospholipid in both MDCK (DPPG: 42%, LPG 37%) and A549 cells (DPPG: 13%, LPG 58%).

In conclusion, the type of polar head and the number of aliphatic chains are the two variables to consider when modulating virus infectivity with lipids. Altering the lipid composition or structure/shape of the virus using exogenous lipids can be envisaged as a potential treatment for influenza.

Declaration

I declare the work in this thesis followed the University of Nottingham rules and regulations. It has not been submitted for another degree or qualification at the University of Nottingham or any other university or institute.

Name: LAMYAA Al–DALAWI

Signed:
Date:

Conferences, Posters and Oral Presentations

1. Al-Dalawi LM, Rauch C, Dunham SP (2015). Understanding the role of membrane biophysical properties of influenza viruses in virus infectivity (Poster Presentation). Emerging Viruses 2015 on 27—29th July 2015 (School of Veterinary Medicine & Science University of Nottingham, UK).
2. Al-Dalawi LM, Rauch C, Dunham SP (2015). Understanding the role of membrane biophysical properties of influenza viruses in virus infectivity (Poster Presentation). AVTRW 2015 Annual Meeting on September 2nd-3rd, Royal Veterinary College London.
3. Animal infection and immunity themed meeting December 2015. Understanding the role of the biophysical properties of influenza virus membranes in virus infectivity, Nottingham University (oral and Poster Presentation).
4. Al-Dalawi LM, Rauch C, Dunham SP (2016). Membrane biophysical properties of influenza viruses in virus infectivity (Poster Presentation). Society for General Microbiology (SGM) Spring Conference, Liverpool Central 21-24 March.
5. Al-Dalawi LM, Dunham SP, Rauch C (2016). Understanding the role of membrane biophysical properties of influenza viruses in virus infectivity (Poster Presentation). Influenza 2016: St Hilda’s College, Oxford, UK. 13-15 September.
6. Research Day; Oral Presentation, in Veterinary Medicine and Science; 2nd and 3rd of July 2015.

7. Research Day (second year); Oral Presentation, in Veterinary Medicine and Science; 4th of July 2016.
8. Research Day (third year); Oral Presentation, in the School of Biosciences and School of Veterinary Medicine & Science16th and 17th of May 2017.
9. Al-Dalawi LM, Rauch C, Dunham SP (2017). Determining the molecular and biophysical importance of phospholipids on the avian influenza virus infectivity (Oral Presentation). Society for General Microbiology (SGM) Spring Conference 2017, Edinburgh 3-6 April.
10. Al-Dalawi LM, Rauch C, Dunham SP (2017). Determining the molecular and biophysical importance of phospholipids on the avian influenza virus infectivity (Poster Presentation). Emerging Viruses of Zoonotic and Veterinary Importance, Churchill College Cambridge 26-27th of July.
11. Al-Dalawi LM, Rauch C, Dunham SP. The molecular and biophysical importance of phospholipids on the influenza A viruses' infectivity (Poster Presentation). Conference 2018, Austria, Vienna 2-4th July.
12. Al-Dalawi LM, Rauch C, Dunham SP. Investigate the potential of phospholipid to reduce avian influenza virus infectivity (Poster Presentation). AVTRW Annual Conference 2018, UK, University of Nottingham 17 -18 September.

Acknowledgements

I would like firstly to express my deepest gratefulness to my supervisors, Dr Cyril Rauch and Dr Steve Dunham for their guidance, advice and input throughout the years during my study. Their patience and full support during my work on my thesis provided me with a much needed helping hand during my PhD.

I am very thankful for the Janet-Dunham group and the virology group for their consistent support and helpful suggestions as well as selflessly sharing their scientific knowledge in the virology field. I would also like to say a special thank you for all staff members at the University of Nottingham, especially Denise Christie from the School of Biomedical Science/ Electron Microscopy and Dr David Onion and Nicola Croxall from the School of Life science/ Flow cytometry for their fantastic support throughout my work, which gave me a reassuring feeling that I was not on my own.

To my friends and colleagues in veterinary medicine and science, I would like to thank you from the depths of my heart for your continuous moral support and valuable friendship along the years.

To the strongest woman I have come across, my mother, thank you for your support and prayers during this journey of mine and your spirit will always be in my life, encouraging me to be stronger and walk the extra mile in order never stop improving and learning. I would also like to thank my brothers and sisters for their continuous support and motivation throughout this journey. I am heavily appreciative for my husband Mohammed, my daughter Ruya and my son Mustafa for their support through this PhD.

Finally, I am deeply grateful to the Iraqi government's Ministry of Higher Education and Scientific Research for this great experience to have Overseas Scholarship that allowed me to broaden my horizons considerably.

Table of Contents

List of Figures

List of Tables

List of Abbreviations

AI	Avian Influenza
AMPK	Adenosine 5’ monophosphate-activated protein kinase
APHA	Animal and Plant Health Agency
AHT	Animal Health Trust
A549	Adenocarcinomic human alveolar basal epithelial cells
BSA	Bovine serum albumin
$^{\circ}$C	Degree Celsius
CD4	Cluster of differentiation 4
cDNA	Complementary Deoxyribonucleic Acid
CL	Cardiolipin
Cm	Centimetre
CPE	Cytopathic effect
Cryo-EM	Cryoelectron microscope
D	Diameter
DAPI	4’, 6–Diamidino–2–phenylindole
DCs	Dendritic cells
DMEM	Dulbecco’s modified Eagle’s medium
DMEM-10	Dulbecco’s modified Eagle’s medium containing 10% FCS and penicillin-streptomycin
DMSO	Dimethyl sulphoxide
DPPC	Dipalmitoylphosphatidylcholine
DPPG	Dipalmitoylphosphatidylglycerol
DNase	Deoxyribonuclease

DPPS	Dipalmitoyl-sn-glycero-3-phospho-L-serine
EM	Electron Microscope
ER	Endoplasmic reticulum
FCS	Fetal calf serum
Ffu	Focus forming Unit
FITC	Fluorescein isothiocyanate
FSc	Forward scatter
GM	Ganglioside monosialic acid
GPLs	Glycerophospholipids
GTP	Guanosine-5-triphosphate
HA	Haemagglutinin
HAU	Haemagglutinin unit
HPAI	Highly pathogenic avian influenza
hr	Hour(s)
HRP	Horseradish peroxidase
IAV	Influenza A virus
IFN	Interferon
Ig	Immunoglobulin
IL	Interleukine
L	Length
LBP	LPS-binding protein
LPAI	Low Pathogenic Avian Influenza
LPC	Lysophosphatidylcholine
LPG	Lysophosphatidylglycerol

LPS	Lipopolysaccharide
Lyso-PA	Lysophosphatidic acid
M	Matrix
MβCD	Methyl-β-Cyclodextrin
MDCK	Madin Darby Canine Kidney cells
min	Minute(s)
ml	Millilitre
mm	Millimetre
MOI	Multiplicity of infection
mRNA	Messenger Ribonucleic acid
µg	Microgram
µL	Microlitre
µM	Micro molar
NA	Neuraminidase
NAD	Nicotinamide adenine dinucleotide
NGC	Negative Gaussian curvature
IM	Infection media
NEP	Nuclear export protein
NES	Nuclear Export Signal
ng	Nanogram
NI	Neuraminidase inhibitors
NK	Natural Killer cells
NLR	NOD-like receptor
NLS	Nuclear localisation signal

nm	Nanometer
NP	Nucleoprotein
NOD	Nucleotide-binding oligomerisation domains
NS	Non structural
PA	Polymerase acidic
PAMPs	Pathogen-associated marker patterns
PB1	Polymerase basic 1
PB2	Polymerase basic 2
PBS	Phosphate buffered saline
PC	Phosphatidylcholine
PE	Phosphatidylethanolamine
PFA	Paraformaldehyde
PG	Phosphatidylglycerol
PI	Phosphatidylinositol
pi	Post infection
PRRs	Pattern–recognition receptor
RLRs	Pattern–recognition like receptors
POPG	Palmitoyl-2-oleoyl-sn-glycero-3-phosphoglycerol
PS	Phosphatidylserine
RBC	Red blood cells
RNA	Ribonucleic acid
RNase	Ribonuclease
RNP	Ribonucleoprotein
RT–PCR	Reverse transcriptase polymerase chain reaction

RT	Room temperature
RSV	Respiratory syncytial virus
s	Second(s)
SAα2,3–Gal	Sialic acid linked to galactose by α2,3 linkage
SAα2,6–Gal	Sialic acid linked to galactose by α2,6 linkage
SD	Standard error
SM	Sphingomyelin
SSc	Side scatter
TBS	Tris buffered saline
TEM	Transmission electron microscope
TLR	Toll like receptors
TNF	Tumour necrosis factor
TPCK	Tosyl phenylalanyl chloromethyl ketone
U	Unit(s)
VLPs	Virus–like particles
vRNA	Viral ribonucleic acid
UV	Ultra–violet
WHO	World Health Organization
xg	Gravitational force

Chapter 1: Introduction

1.1 Influenza virus

Influenza (”flu”) is a viral disease that affects birds and mammals and is associated with severe public health consequences (Noda and Kawaoka, 2010).

The term ‘influenza’ was initially used in Italy to connect occurrences of flu symptoms with an astrological influence later termed influenza delfreddo, referring to the influence of cold. For the first time, the 1745 European outbreak was described as influenza in English (Kapoor and Dhama, 2014). Influenza A virus infects a wide variety of host species, including humans, other mammals and birds (Koçer et al., 2013). The World Health Organization reports 3–5 million cases of serious influenza infections and 250 000–500 000 deaths resulting from the virus annually (Fernandez-Sesma et al., 2006). Influenza in humans can vary from slight, to moderate, to severe pulmonary infections, associated with manifestations such as fever, headache, cough and pulmonary failure, with mild to severe upper respiratory infection (Davis et al., 2015). Influenza affects animals and birds causing fever and variable signs including coughing, diarrhoea and decreased egg production in laying birds; thus, it is associated, with negative health and economic burdens (Medina and García-Sastre, 2011).

The disease has zoonotic implications due to the potential for genetic reassortment between influenza virus subtypes, posing a pandemic threat because of the emergence of new viral strains. The most

significant influenza virus pandemic recorded in history is the "Spanish flu" pandemic of 1918–1919, which is believed to have been responsible for approximately 50 million human deaths worldwide (Taubenberger and Morens, 2006). Other important documented outbreaks include Asian flu (1957) and Hong Kong flu (1968) (Claas et al., 1998). The most recent influenza pandemic was originated in Mexico (2009) and was caused by swine-origin H1N1 (Neumann et al., 2009).

1.2 Avian influenza

Avian influenza (AI) infection was recorded for the first time in poultry in Italy in 1878 (Ligon, 2005). AI virus outbreaks have been widely reported in poultry farms (especially turkey and chicken) and can infect any domestic or captive fowl population worldwide, often resulting from contact with feral birds (Alexander, 2000). Waterfowl are the main reservoir for most AI virus strains (Koopmans et al., 2004). Long-distance poultry and bird migration have been shown to have an essential role in spreading highly pathogenic strains that have been associated with severe flu outbreaks in Europe, the Middle East and Africa (Medina and García-Sastre, 2011, Neumann and Kawaoka, 2015).

1.3 Influenza viruses

Influenza viruses belong to the *Orthomyxoviridae* family, which is characterised by negative-sense, single-stranded, enveloped, segmented RNA viruses (Arranz et al., 2012, Baker et al., 2014). The family consists of seven genera: influenza viruses A, B; C and D;

Thogotovirus; *Isavirus* and *Quaranjavirus.* Isaviruses mainly infect salmon, and Thogoto viruses predominantly infect invertebrates. Influenza virus subtype A has been shown to affect a variety of hosts, such as aquatic birds, humans, pigs and horses; subtype B has been mostly associated with humans and seals, and subtype C has been associated with pigs and humans (Noda and Kawaoka, 2010). Recently a new genus of Orthomyxoviridae family was identified, designated as influenza D, closely related to Influenza C virus, which was first isolated in pigs with serological assessment suggesting that cattle are the natural host reservoir (Ferguson et al., 2015).

Research on the genomic structure of these influenza viruses has revealed that subtypes A and B contain eight RNA segments, differing from influenza C, which includes only seven segments. Furthermore, the A, B and C subtypes can be classified according to differences in their viral nucleoprotein and matrix proteins (Fontana and Steven, 2015). The classification of influenza A viruses is based on genus, species, location, serial number, year of isolation and the subtype according to the surface glycoproteins haemagglutinin (HA) and neuraminidase (NA), for example, A/goose/Guangdong/1/96 (H5N1) (Knipe and Howley, 2013).

1.4 Structural and molecular biology of influenza A virus

Influenza A viruses possess a pleomorphic structure that varies from spherical to elongated with a diameter between 100 and 300 nm (Harris et al., 2006). Influenza viruses derive their lipid envelopes on budding from the host cell plasma membrane. Within the envelope are

embedded glycoprotein molecules, including HA, which are trimeric rod-shaped molecules, and NA spikes, which are tetrameric mushroom-shaped molecules with box-shaped heads, organised in a four to one HA/NA ratio (Knipe and Howley, 2013). Other envelope glycoproteins include matrix protein 2 (M2), which projects from the surface and has a homotetramer structure (Roberts et al., 2013). The matrix protein 1 (M1) is located inside the virion under the viral lipid envelope (Harris et al., 2006, Li et al., 2014). Within the viral core are eight viral RNA segments, and the non-structural proteins; non-structural protein1 (NS1) and nuclear export protein NEP/NS2. The genome is coated by nucleoprotein (NP) and polymerase proteins forming a ribonucleoprotein complex (RNP), an essential unit during the influenza virus life cycle (Arranz et al., 2012) (Figure 1.1). A cell-derived lipid envelope is acquired by the virus as it emerges from the virus host cell membrane. Three glycoproteins are embedded in the envelope forming "spikes", namely HA, NA and M2. There are 18 HA (1–18) and 11 NA (1–11) subtypes used to classify the IAV viruses further. Under the lipid bilayer, M1 acts as a bridge between the viral surface and viral core (Crisci et al., 2013, Pflug et al., 2014).

The influenza virus core, known as the ribonucleoprotein complex (RNPs), includes viral RNA (Noda and Kawaoka, 2010), nucleoprotein (Opasawatchai and Matangkasombut, 2015) with a small amount of nuclear export protein (Koçer et al., 2013) and a complex of three dependent RNA polymerases, namely polymerase basic 1 (PB1)(Dudek et al., 2011), polymerase basic 2 (PB2), and polymerase acidic (PA).

Electron microscopy (EM) has shown that budding virions appear with eight RNPs arranged with one in the centre surrounded by the other seven RNPs (Noda, 2012, Pflug et al., 2014).

The polymerase protein complex consists of PB1, PB2 and PA (Li et al., 2014). Accessory proteins, such as PB1-F2 and N40, are encoded on an alternate reading frame near the 5' end of PB1 gene. The gene transcribes an 87 amino acid PB1-F2 polypeptide that has been shown to have pro-apoptotic properties (Tscherne and García-Sastre, 2011). However, PB1-F2 is not present in influenza B or C (Knipe and Howley, 2013). Influenza A virus RNA segments are categorised according to length: long segments comprise the three polymerase subunits (PB1, PB2 and PA), intermediate length segments are HA and NA and short segments are M, NS, and NP (Noda and Kawaoka, 2010).

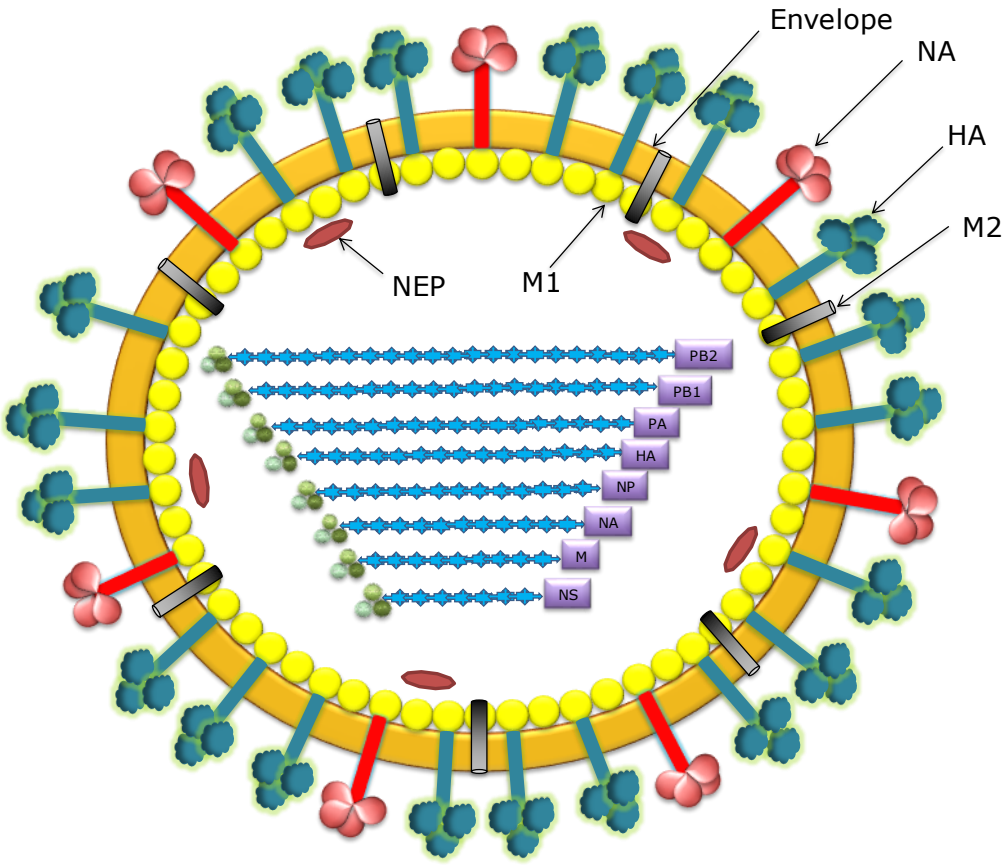

Figure 1:1 Schematic diagram of influenza virus A.
The glycoprotein molecules, including haemagglutinin (HA), neuraminidase (NA) and M2 proteins are implanted in the viral lipid envelope. Underlying the lipid layer, there is the matrix (M1) protein. The viral core has eight RNA segments coated by nucleoproteins and connected to polymerase proteins PB1, PB2, and PA, forming ribonucleoprotein (RNP) adapted from Medina and García-Sastre (2011).

The organisation of RNPs depends on the morphology and size of the virion; for example, filamentous virions have a regular arrangement of eight RNPs that bind to the interior virion at the distal end. In contrast, in purified spherical virions, RNPs are compressed, showing a more disordered arrangement (Noda and Kawaoka, 2010).

The RNA molecules vary in lengths from 2341 to 890 nucleotides. Influenza A virus RNA segments have two complementary ends, 3' and 5', and are known as the core promoter (Noda and Kawaoka, 2010). At the 5' end, RNA from influenza A virus contains 13

conserved nucleotides, and there are 12 conserved nucleotides at the 3’ end. Following these conserved regions, there are untranslated regions and then non-coding regions, which contain promotor regions identified by polymerase proteins for the initiation of the replication and translation processes, these components also form the viral packaging signal system (Noda and Kawaoka, 2010). Influenza virus RNA is surrounded by NP and RNPs that are folded back and coiled on themselves, forming a twisted rod-shaped structure. Then, heterotrimeric RNA polymerases come into contact with the viral complimentary 5’ and 3’ ends (Figure 1.2) (Noda and Kawaoka, 2010, Eisfeld et al., 2014).

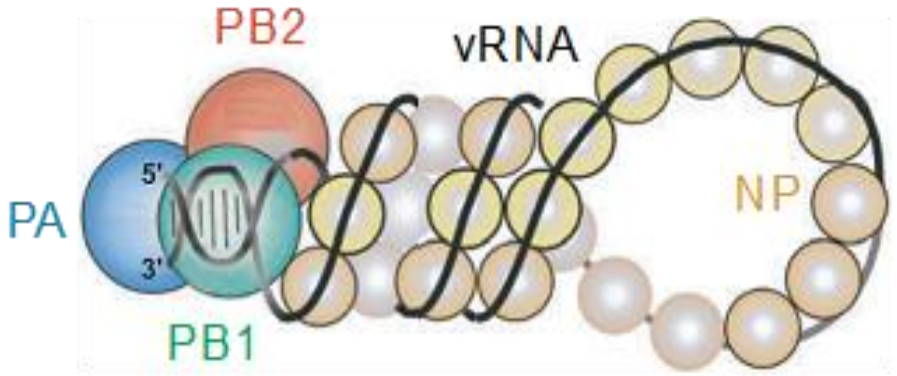

Figure 1:2 Structure of influenza virus ribonucleoprotein (RNP).

Influenza virus RNA, represented by black line coated with NP monomers, described as a sphere. RNPs are folded back and coiled on themselves forming a twisted–rod shape structure. Heterotrimeric RNA polymerases come into contact with the viral complimentary 5’ and 3’ ends. Figure adapted from Ruigrok et al. (2010).

The viral genome encodes for ten main viral proteins that have been shown to have diverse roles in the virus life cycle (Table 1.1). Haemagglutinin consists of two subunits: HA1 binds to the receptor pocket while the HA2 subunit fusion protein enables the release of RNPs (Knipe and Howley, 2013). NA is connected with the lipid

membrane via a stalk and is vital in the release of progeny viruses via the destruction of the sialic acid/ neuraminic receptor on the cell surface (Noda and Kawaoka, 2010).

Table 1:1 Influenza virus genome segments, major proteins and their function modified from Akila et al. (2012).

Segment number	Protein	Name of protein (ID)	Length in amino acids	Function
1	Polymerase basic 2	PB2	759	IAV replication
2	Polymerase basic 1	PB1	757	IAV replication
3	Polymerase acid	PA	716	IAV replication
4	Haemagglutinin	HA	566	Attachment and fusion
5	Nucleoprotein	NP	498	IAV replication
6	Neuraminidase	NA	454	Release
7	Matrix proteins	M1 M2	252 97	Viral morphology, assembly, budding, and uncoating processes
8	Non-Structural proteins	NS1 NEP	230 121	Immunity via antagonism of the host interferon response

The M1 protein has a role in determining viral morphology and formation of filamentous virions in addition to involvement in viral assembly and budding functions (Noda and Kawaoka, 2010, Rossman et al., 2010). M2 protein has been shown to function as an ion channel that regulates acidic pH in the endosomal membrane which is responsible for the initiation of the viral uncoating process in the endosome, releasing RNP. Polymerase protein PB1 acts as a core particle by binding to both PB2 and PA (Noda and Kawaoka, 2010). A

polymerase complex is necessary for forming messenger RNA (mRNA) and complementary RNA (cRNA) leading to the transcription and translation processes. PB2 identifies the cap on the host mRNA structure and allows for the creation of primers for transcription, PB1 is a catalytic subunit and PA is involved in viral RNA replication (Pflug et al., 2014). NS2 (also called nuclear export protein or NEP) plays a role in the exportation of RNPs from the nucleus to the cytoplasm during viral replication. It also regulates virus transcription and replication processes (Numata et al., 2010) and studies have demonstrated the essential role of NS1 protein in inhibiting the host immune response by inhibiting interferon (IFN) production (Hale et al., 2009), inhibiting the production of IFN-β (Munir et al., 2013) and preventing the activation of transcription factors such as nuclear factor kappa B (NF-κB) (Munir et al., 2011).

1.5 Influenza A virus replication

The influenza A virus life cycle involves several stages: attachment and entry into the host cell; fusion and uncoating; transcription and replication of viral genome and budding and release from the host cell plasma membrane. Each stage of the viral life cycle is explained briefly below (Figure 1.3).

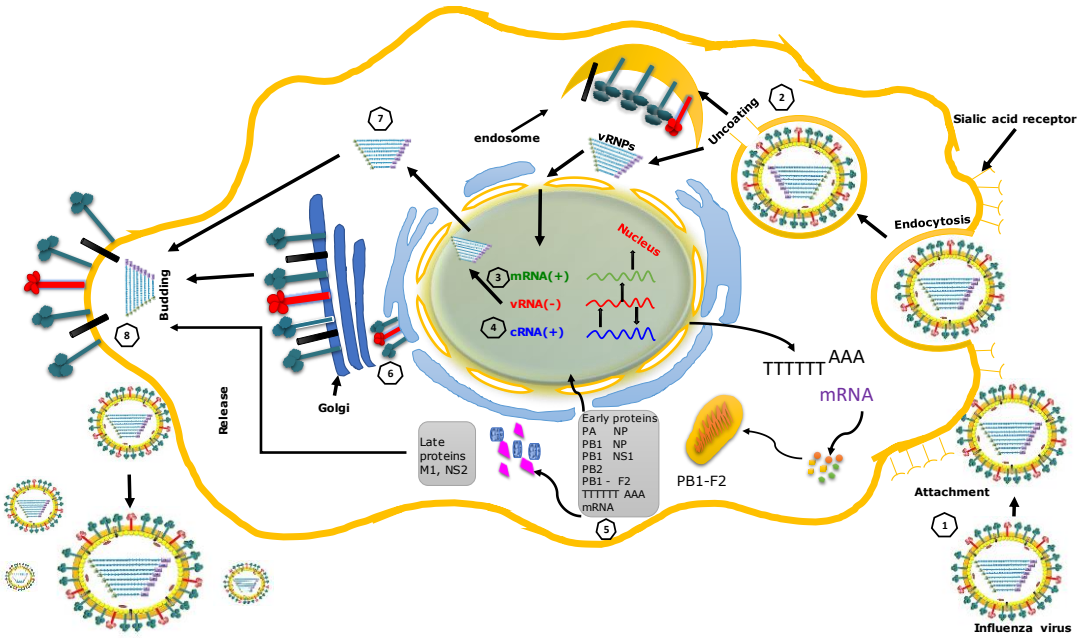

Figure 1:3 Stages of the influenza virus life cycle.
1. Attachment and entry of virus.
2. Virus uncoating and RNPs release.
3. Transcription and translation.
4. Replication of viral RNA.
5. Production of proteins.
6. Creation of envelope proteins and their movement to the cell membrane.
7. Viral RNP packaging.
8. Budding and release of new virions adapted from Medina and García-Sastre (2011).

1.5.1 **Virus attachment and entry**

IAV enters the host cell through endocytosis by interacting with the glycosaminoglycan or glycosphingolipid of the host cell membrane (Mazzon and Mercer, 2014). The structural components of influenza virus glycoproteins affect virus binding to the host cell as IAV attachment depends on the affinity of the HA receptor to binding sites on the surface of the host cell (Mair et al., 2014). The viral life cycle is initiated by surface influenza virus glycoprotein HA attaching and binding to host cell sialic acid receptor (Lesse, 2016). Viruses bind to N-acetylneuraminic acid moieties, which are linked to galactose via alpha 2-6 linkage (SA α2-6 Gal) in human tracheal epithelium, while

IAV in the intestinal tract of avian species (Knipe and Howley, 2013) and equine influenza virus in the equine upper respiratory tract (Daly et al., 2011) binds with sialic acid linked to galactose via an alpha 2-3 linkage (SA α 2-3 Gal). Both SA α2-6 Gal and SA α 2-3 Gal are presented in the respiratory tract of pigs (Nelli et al., 2010). There are two alternative endocytosis pathways utilised by IAV for cell entry: clathrin-dependent and non-clathrin dependent. The HA precursor, HA0, is activated due to cleavage by proteases, into HA1 and HA2. The HA1 portion as viral binding receptor has the antigenic sites, and HA2 acts as a fusion protein and allows entry the virus into the cell cytosol forming endosomes at the host plasma membrane (Tscherne and García-Sastre, 2011). Influenza virus virulence is determined by the cleavage sequence of HA0 (Zambon, 1999).

1.5.2 **Fusion and un-coating process**

After virus attachment and entry, the low pH in the endosome activates the fusion of the outer leaflet of the viral membrane with the inner leaflet of the endosome membrane because of the conformational change in the HA protein (Mazzon and Mercer, 2014). The "fusion peptide" of HA2 domain interacts with the endosomal membrane, leading to close apposition of the endosome and viral membranes. The hemifusion stalk then opens, forming a fusion pore (Mazzon and Mercer, 2014). Un-coating depends firstly on the presence of weak bases, such as ammonium chloride, chloroquine or ionophores (Knipe and Howley, 2013). After the initial uncoating, activity within the M2 ion channel allows protons to enter the virus

particle. This insertion of hydrogen ions interrupts protein-protein interaction and releases RNP from M1 protein, which enters the host cell cytoplasm (Roberts et al., 2013).

1.5.3 **Transcription and replication**

The RNP complex is a fundamental structure required for viral genome transcription and replication (York and Fodor, 2013). Viral replication starts after the transportation of RNPs to the nucleus, mediated by the nuclear localisation signal (NLS) on viral proteins (Roberts et al., 2013). Viral RNA (vRNA) acts as a template for both mRNA and cRNA. Genome replication occurs in two steps. Firstly, a full length, positive-sense copy of the vRNA is made; this is called cRNA synthesis. Secondly, the positive cRNA acts as a template for the synthesis of negative sense vRNA, which participates in forming new viral RNP (Knipe and Howley, 2013).

Transcription begins with the binding of the 5’ end of the vRNA to the PB1 subunit. This binding allows PB2 to recognise and bind to the cap structure of host pre-mRNA. Upon binding, the endonuclease activity of PB1 is activated. This results in the cleavage of the bound pre-mRNA by PA, this cleavage occurs ten to thirteen nucleotides from the 5’ cap (Elton et al., 2006). Transcription occurs via the addition of guanine residues to the primer by PB1 until a string of uridine residues is added as a signal for polyadenylation, which is induced by an uninterrupted string of five to seven uridine residues (Knipe and Howley, 2013). Positive sense mRNA is exported to the host cell

cytoplasm, where it initiates the translation process by ribosomes (York and Fodor, 2013).

1.5.4 **Protein synthesis**

HA, NA and M2 RNA is translated in membrane bound ribosomes in the ER, where they undergo post-translational modification, folding in the Golgi apparatus, followed by transport to the cell surface through an exocytic pathway (Noda and Kawaoka, 2010). PB2, PB1, PA, NS, NP and M1 are synthesised in the cytoplasm. These proteins then re-enter the nucleus to interact with new viral RNA particles and form new RNPs, which diffuse passively into the cytoplasm; this is mediated by nuclear export protein (Noda and Kawaoka, 2010).

1.5.5 **Assembly and packaging**

The newly formed RNP complex relocates to the apical plasma membrane via the activity of two proteins, M1 and NEP/NS2 (Noda and Kawaoka, 2010). Cross-nuclear membrane transport is an energy driven mechanism that relies on an active nuclear export mechanism via recognising nucleoprotein an NLS-containing cargo protein (Ozawa et al., 2007). At the plasma membrane, the new RNPs interact with viral glycoproteins HA, NA and M2, to package virus particles (Noda and Kawaoka, 2010). HA interacts with the lipid layer which is rich in cholesterol, glycerophospholipids (GPLs) and sphingolipids. From these lipids, the virion obtains the lipids that surround the virus particles, forming the envelope. The packaging of

the influenza A virus genome has been postulated to be either random with different eight segments randomly incorporated or specific with packaging of one copy from each viral segment. Viral RNPs are likely packaged by a selective process which ensures that each virion contains one of each viral segment, creating an infectious virion (Fujii et al., 2003).

1.5.6 **Budding and release**

The newly packaged RNPs connect with the cytoplasmic tails of glycoproteins, forming a budding site which is then cleaved from the sialic acid receptor of the host cell membrane via the sialidase activity of NA (Harris et al., 2006).

Budding and assembly start with the concentration of both viral glycoproteins, HA and NA, in the lipid domains of host cell plasma membrane; M1 binds to HA and NA and recruits the RNA complex, while viral surface glycoprotein M2 is concentrated in the apical plasma membrane, allowing for more change in the membrane and causing positive membrane curvature. At this point, new virions are released (Rossman et al., 2010).

1.6 Pathogenicity of influenza A virus

The infectivity of the influenza virus depends on successful HA cleavage by host proteolytic enzymes, which is crucial for the spread of replication (Garten and Klenk, 1999). AI may be classified according to the viral pathogenicity as either low pathogenic avian

influenza (LPAI) or highly pathogenic avian influenza (HPAI) (Adams and Sandrock, 2010). HPAI, is confined to H5 and H7 subtypes and characterised by the presence of a multibasic cleavage site, containing arginine and lysine residues in the cleavage site of HA of these subtypes (e.g. PQRESRRKK/GLF). This allows the viral HA to be cleaved by ubiquitous host proteases and thus infect a wide range of host tissues, causing severe systemic disease (Tscherne and García-Sastre, 2011). In contrast, LPAI has only one or two basic amino acids in the cleavage site of HA (e.g. PEKQTR/GLF) (Offlu, 2018) and is cleaved by host trypsin like proteases present in the respiratory or gastrointestinal tract. Thus LPAI causes mild to moderate respiratory or gastrointestinal clinical signs (Medina and García-Sastre, 2011, Pflug et al., 2014). Low pathogenic influenza virus can mutate to the highly pathogenic through accumulating basic amino acid in the viral HA gene (Adams and Sandrock, 2010).

1.7 Genetic variation of influenza virus

Influenza A virus infection has considerable health and economic impacts due to the ability of this virus to avoid the immune system and undergo genetic change, potentially leading to either antigenic drift or antigenic shift, allowing re-infection of the same population. Such changes can enable the virus to escape antiviral immune response and reduce the efficacy of vaccine

1.7.1 **Antigenic drift**

Antigenic drift occurs due to the natural occurrence of errors during viral replication because of the lack of proofreading activity of the viral RNA polymerase. This results in frequent genetic mutation which may lead to viral avoidance of the immune response due to alterations in the antibody-binding sites in either one or both of HA and NA. Antigenic drift decreases vaccine effectiveness, causing the recurrence of seasonal influenza epidemics in human populations (Carrat and Flahault, 2007). For example, the European 2003–2004 influenza season was dominated by the spread of a new drift variant, A/Fujian/411/2002-like virus, a variant of the vaccine strain of influenza H3N2 that is associated with recorded clinical cases (Paget et al., 2005). Also, viral HA mutation increases the opportunity for the cross-species transmission of AI virus to human hosts (Koopmans et al., 2004, Smrt et al., 2014). Thus, the production of an effective influenza vaccine is a major challenge due to the need to monitor antigenic drift and continually change vaccine stocks to reflect the most recent circulating virus strain.

1.7.2 **Antigenic shift**

The reassortment of genomic segments can occur if two different influenza virus strains infect a single host cell, leading to the creation of a viral strain with altered genetic material, which differs from the initial strains. This rapid change in virus phenotype can lead to widespread disease (pandemics and panzootics) due to the lack of

host immunity (Figure 1.4) (Nelson and Vincent, 2015, Carrat and Flahault, 2007). The antigenic shift of IAV mostly is particularly relevant if a virus acquires a novel HA resulting in evasion of existing host antibody response to the surface glycoprotein (Neumann and Kawaoka, 2015).

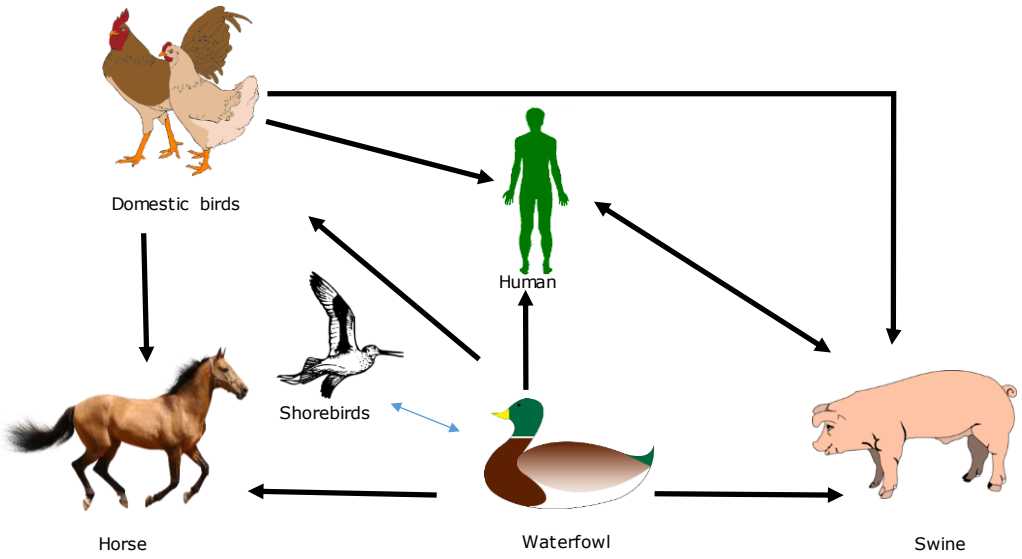

Figure 1:4 The animal and human influenza life cycle.
Influenza A viruses circulate in aquatic birds (shorebirds and waterfowl) as a reservoir host, transmitting the virus to both humans and animals. The AI virus transmits to domestic birds and swine. Domestic birds and swine may transmit the virus to humans. Swine act as intermediate hosts and because they are susceptible to both avian and human influenza viruses may be important hosts for viral recombination (genetic shift) (Shi et al., 2014).

Research into the evolution of influenza pandemics in 1957 and 1968 has shown them to be the result of the reassortment of avian and human influenza viruses, leading to high infectivity in humans (Belshe, 2005). Live poultry markets and farms are a potential source of influenza pandemics and a threat to public health due to the opportunity for close contact between infected birds and humans (Li et al., 2014). Pigs possess host cell receptors for both human and avian viruses (sialic α2-6 gal-and sialic α2-3 gal, respectively) so can

be infected by both avian and human influenza and act as an intermediate host for new stains with novel segment combinations (Neumann and Kawaoka, 2015).

1.7.3 **Innate immunity**

Innate immunity against viral infection involves multiple mechanisms with cellular components such as natural killer cells (NK), macrophages, dendritic cells (DCs) and epithelial cells (lining the respiratory tract). Antigen-presenting cells recognise microbial particles via their surface markers designated pathogen-associated marker patterns (PAMPs), which are identified by cellular pattern recognition receptors (PRRs) (Kreijtz et al., 2011). Interaction of melanoma differentiation associated gene 5 (MDA5) of NK cells with macrophages and DCs leads to release of type-1 IFNs, which have antiviral activity, leading to the activation of hundreds of IFN-stimulated genes in neighbouring cells and transcript factors like NF-$_k$B and activators of transcription (STATs), which activate cytokine expression to initiate an 'antiviral state' (Fernandez-Sesma et al., 2006, Iwasaki and Pillai, 2014). Pattern-recognition receptors (PRRs) include Toll-like receptors (TLR3, 7 and 8 are mainly involved in recognition of influenza viruses), retinoic acid-inducible gene I (RIG 1) and nucleotide-binding oligomerisation domains (NOD-like receptors); these receptors detect viral RNA, which results in endosome formation. This starts intracellular cascade steps leading to the secretion of antiviral substances, such as IFNs, pro-inflammatory cytokines and eicosanoids (fatty acids with 20 carbon

molecules). In turn, this leads to local and general inflammation, resulting in elevated host temperature, anorexia and chemokine enhanced recruitment of further immune cells including neutrophils, monocytes and NK cells which recognise cells infected by the influenza virus (Iwasaki and Pillai, 2014).

1.7.4 **Adaptive immunity**

Adaptive immunity is the second line of defence against influenza infection, and it is comprised of two defined responses: humoral and cellular immunity.

1.7.4.1 **Cellular immunity**

Cellular immunity is initiated in response to virus infection of host cells. MHC class II proteins on the surface of antigen-presenting cells present viral peptides, forming an MHC II–antigenic peptide complex on their cell surface. This complex is recognised by CD4 (Cluster of differentiation 4) + T-lymphocytes called helper T cells, which produce cytokines and may enhance both the humoral and cellular immune responses. The DCs of the airway epithelium barrier and basal membrane mediate their antiviral activity by migrating to the lymph nodes and activating T cells in germinal centres (García-Sastre, 2011, Iwasaki and Pillai, 2014). In virus-infected cells, viral peptides bind with the extracellular domain of MHC I and then transfer these peptides to the cell surface, exposing them to CD8+ lymphocytes; stimulation of these cells leads to the destruction of virus-infected cells (Yewdell et al., 1985).

1.7.4.2 **Humoral immunity**

Serum antibodies (immunoglobulin (IgM and IgG)) are stimulated following viral infection and can provide long-term protection; mucosal IgA antibodies initiate local and general immunity (Schmitz et al., 2005, Lee et al., 2008). The production of a specific antibody is mediated by B lymphocytes against specific viral antigens, such as the influenza virus HA glycoprotein (Kreijtz et al., 2011). Antibodies can bind to HA and inhibit viral attachment and entry. Furthermore, specific antibodies bind to NA, blocking NA's role in the cleavage of sialic acid and thus preventing virus release and spread (Ekiert et al., 2009).

1.8 Vaccination

Influenza vaccine efficacy depends on the content of the presently circulating strain and can provide adequate protection when this is optimised. The World Health Organization (WHO) organised a global influenza network in 1952 to observe antigenic changes and confirm that the annual vaccine is the same as the predominant circulating strain(s) (Carrat and Flahault, 2007). Most influenza vaccines are prepared using embryonated hens' eggs as a trivalent or quadrivalent preparation which consists of HA and NA glycoproteins. These are derived from representative circulating strains (Iwasaki and Pillai, 2014). Such traditional vaccines are then inactivated, for example by treatment with formaldehyde, and the vaccine antigen purified. Live Live-attenuated vaccines, such as Flu Mist (Med Immune), are

created through adapting live viral strains which replicate at low temperatures, or by inactivating NS1 via the truncation of the gene or the modification of the M1 protein (Kreijtz et al., 2011).

Traditional inactivated vaccines aim to induce broadly protective influenza virus-specific antibodies, such as those recognising the globular head of HA (Kreijtz et al., 2011). A whole killed virus can elicit the induction of memory cytotoxic T lymphocytes, whereas the subunit vaccine can not (Fernandez-Sesma et al., 2006). The idea of DNA vaccination against influenza virus using influenza viral NP antigen may also deliver cross-strain protection due to the highly conserved of NP gene among most Influenza A virus subtypes (Dunham, 2002). It is possible to increase vaccine efficacy by adding an adjuvant such as MF59 or by using a virosomal vaccine. Virosomes are virus–like particles that have no genetic material (Carrat and Flahault, 2007). Recombinant virus-like particles (VLPs) have been shown to induce protective immunity against H5N1 viral infection; purified H5 VLP immunisation is able to reduce a more robust immune responce than inactivated vaccination with all viral components (Song et al., 2011, Lei et al., 2015).

1.9 Antiviral compounds

Antiviral medication can be used either prophylactically or as a treatment to decrease the duration and severity of disease in humans. The two main types of treatment are M2 channel blockers and

neuraminidase inhibitors (NI) (Oxford and Lambkin, 2006). The first M2 inhibitors are the anti-influenza drugs amantadine and rimantadine. At high concentrations, the use of these drugs inhibits HA cleavage by increasing the pH of the endosomal membrane and preventing viral fusion. At low concentrations, they block M2 ion channel activity and prevent uncoating and release of virus from endosomes (Gasparini et al., 2015). Amantadine and rimantadine resistance has led to a limit on the use of these drugs (Gubareva et al., 2000).

Viral neuraminidase activity allows progeny virions to detach from the cell membrane during the viral life cycle. Neuraminidase inhibitors zanamivir (Relenza) and oseltamivir (Tamiflu) are neuraminic acid derivatives that mimic sialic acid and block viral NA binding (Gasparini et al., 2015). NI medication has been used as a prophylaxis and treatment because it provides a broad antiviral spectrum with less development of resistance (Gubareva et al., 2000). Another neuraminidase inhibitor which exhibits a prolonged anti-influenza virus activity compared to zanamivir and oseltamivir, is known as R-125489 (4S, 5R, 6R)-5-Acetamido-4-guanidino-6-((1R, 2R)-2,3-dihydroxy-1-methoxypropyl)-5,6-dihydro-4H-pyran-2-carboxylic acid) (Yamashita et al., 2009). A more potent and drug has been reported which targets the polymerization activity of influenza A virus RNA dependent RNA polymerase such as favipiravir (T-705), which acts as a nucleoside inhibitor of IV RdRP (Loregian et al., 2014).

Other non-specific antiviral medications such as Ribavirin (Virazole), decrease the concentration of guanosine-5-triphosphate (GTP) and inhibit viral protein production, as well as blocking viral RNA replication. The use of this drug is limited by the requirement for relatively large doses (Gasparini et al., 2015). A new antiviral strategy targets the cellular protein GTPase Rac1, which is necessary for viral replication, via the application of Rac 1 inhibitors such as NSC23766; this has been shown to reduce viral replication for a wide range of influenza virus strains, even highly pathogenic strains (Dierkes et al., 2014).

1.10 Role of lipids in the influenza virus life cycle

Host cell lipids are cellular elements that play essential roles in the entry and release of viruses through the modification and re-organisation of the membrane lipid bilayer (Mazzon and Mercer, 2014). The influenza virus has a lipid envelope that is acquired from the host plasma membrane. The virus envelope plays an essential role during several steps of the virus life cycle, from entry and fusion to replication and virion release (Martín-Acebes et al., 2013).

1.10.1 **Lipid structure**

Amphipathic lipids are heterogeneous molecules that are mainly composed of a hydrophobic domain (aliphatic or carbonated chain(s)) and a hydrophilic domain (Légaré and Lagüe, 2014) that can be polarised and/or charged. Because the carbonated chains have no

affinity with water, they tend to aggregate together, forming bilayer vesicle/membrane (Figure 1.5). Indirectly, these unique properties play essential roles in cell membrane budding, fusion and trafficking (Chan et al., 2010).

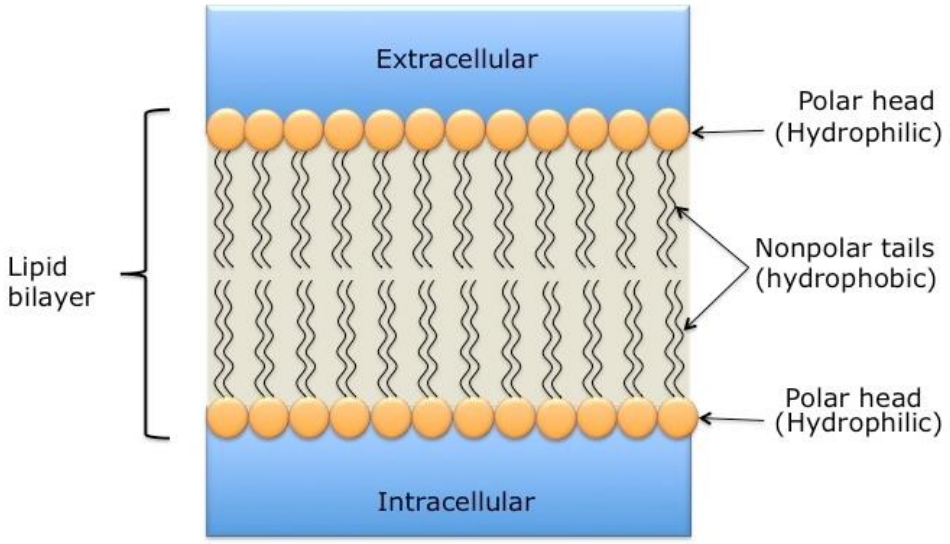

Figure 1:5 Basic structure of the lipid bilayer.
A lipid molecule has two portions, a hydrophilic portion (Légaré and Lagüe, 2014), which interacts with water, and a hydrophobic portion called (lipid tail), which has no affinity with water. Figure modified from Luckey (2014).

The lipids present in plasma membranes are phospholipids (constituting more than half of total lipids), cholesterol and glycosphingolipids (i.e. glycolipids and sphingomyelin) (Knipe and Howley, 2013). The main phospholipids are glycerophospholipids including phosphatidylcholine (PC), phosphatidylethanolamine (PE), phosphatidylserine (PS), phosphatidylinositol (PI) and phosphatidic acid. PC forms approximately 50% of the cell membrane and has a cylindrical molecular geometry with two aliphatic chains and its polar head group facing the aqueous phase, while PE has a conical shape with a smaller head group (Willson et al., 2009).

The sphingolipids present in the mammalian cell membrane are sphingomyelin (SM) and glycosphingolipids (GSLs) (Merrill Jr, 2011, Seo et al., 2010, Fujii et al., 2003). GSLs can act as influenza virus receptors via their carbohydrate structure, which can be an uncharged sugar, such as glucose, or an ionised functional molecule, such as sialic acid (Chan et al., 2010).

Furthermore, the bilayer membrane is not randomly composed. For example, phosphatidylcholine and sphingomyelin are enriched on the outer membrane layer whereas PS and PE are mostly located in the inner layer. This asymmetry can be disrupted by cellular processes. For example, during apoptosis, PS becomes externalised, acting as a positive signal for phagocytosis (Vance, 2008). The main organelle for lipid synthesis is the endoplasmic reticulum and the Golgi apparatus is an essential organelle for lipid export to the cell membrane (Willson et al., 2009).

1.10.2 **Lipid biophysics**

Lipid molecules are composed of two parts: a hydrophilic "head" and a hydrophobic "tail". As a result of these two opposing properties, they tend to form aggregates in aqueous environments to optimise the exposure of the head to water and minimise the contact between the tail and the water. Because their chemical compositions can differ, their physical shapes can vary as well. Usually, a single lipid shape can fall into one of three categories: cylindrical, conical and wedge-shaped. The shape of cylindrical lipids is driven by near identical cross

sectional areas between the tails and heads once inserted in a membrane. One well-known biological phospholipid in this family that is also a major component of biological membranes is PC (Figure 1.6, A). The conical shape comes as a result of the fact that lipids have a head cross-sectional area larger or smaller than that of the tails (once inserted in a bilayer membrane). For example, lyso-lipids that only contain one aliphatic tail fall into this category very often (e.g., Lyso-PC,) (Figure 1.6, B). Finally, wedge-shaped lipids are those with smaller heads as compared to tail. These include phosphatidylglycerol (PG) (Figure 1.6C). It is essential, however, to keep in mind that these shapes may vary as a function of the ionic environment, for example, if the head of the lipid is charged, like PS (Figure 1.6D).

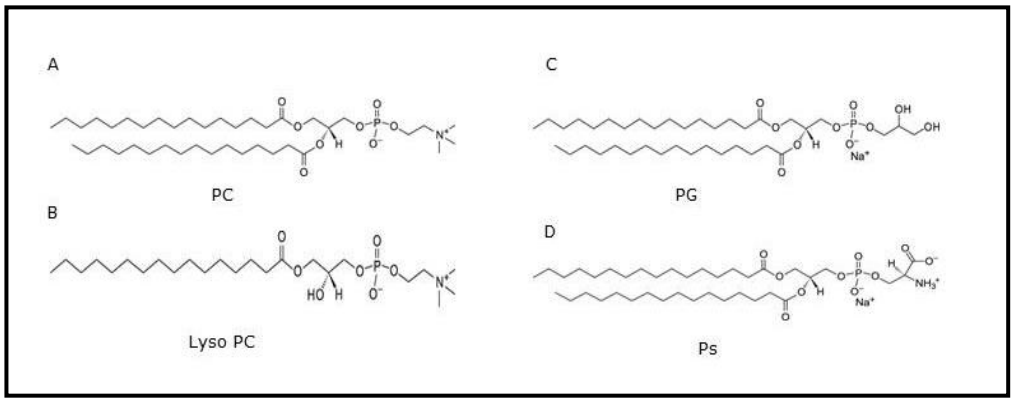

Figure 1:6 Structures of the major glycerophospholipids.
The major glycophospholipid components of a biological membrane are A) Phosphatidylcholine (PC), with a polar head and two aliphatic chain; B) Lyso PC with a polar head longer than one aliphatic chain; C) Phosphatidylglycerol, with a negatively charged and two aliphatic chains and D) Phosphatidylserine (PS), with a charged head with two aliphatic chains adapted from (Luckey, 2014).

The size of the head is not necessarily strictly related to the steric hindrance between PS molecules but the electrostatic repulsion between the heads. However, the electrostatic repulsion can change

depending on the ionic strength of the environment (Figure 1.7). Thus, the size of heads may vary, and a cylindrical lipid can become wedge-shaped or conical.

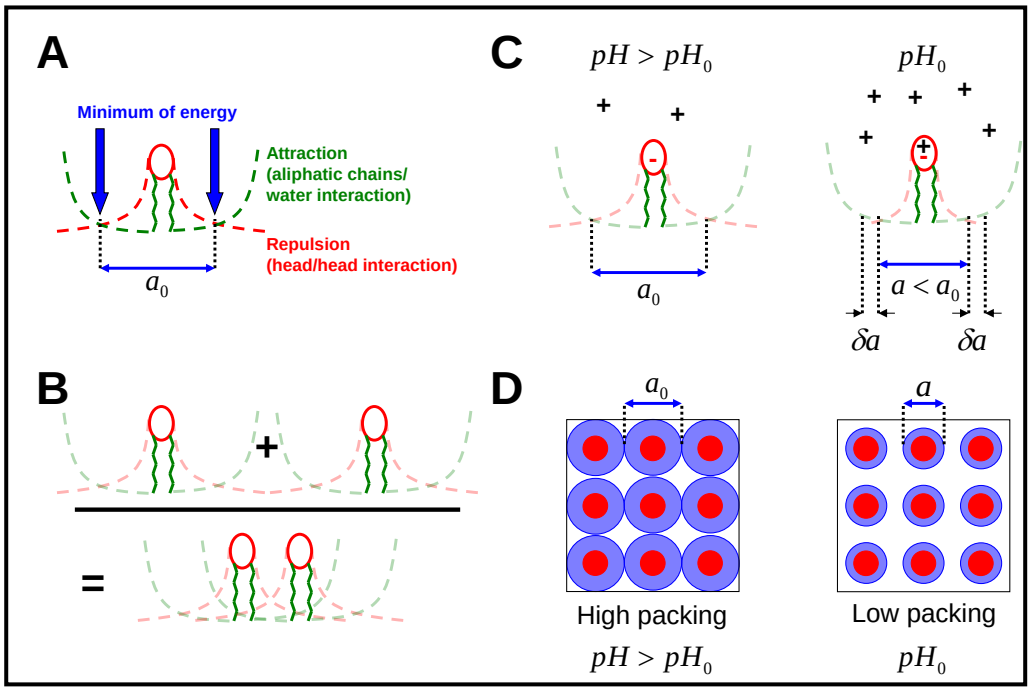

Figure 1:7 Effect of pH on lipid packing.

(A) Assuming a leaflet is composed of charged lipids, the optimal area per lipid is determined by the competition between attractive energy that reflects lipids attraction linked to their hydrophobic tails and repulsion energy which we will assume to be linked to a net charge carried by all the lipids. The competition between these two defines a minimum of energy. Note that in the figures, a_0 corresponds to the optimal distance between adjacent lipid heads. (B) Thus the minimum of energy provides the optimal distance between lipids including their optimal area in the monolayer. Note that the packing of lipids is not always defined by hard core contact/steric repulsion and that, accordingly, there is room to change this packing. (C) With regard to negatively-charged lipids, an increase in the concentration of hydrogen ions allows more hydrogen ions to interact with lipids' head. Thus by masking their negative charges, the long-range repulsion between lipids is disturbed. The effect will be an alteration of the positioning of the energy minimum, which will move closer to the lipids. (D) Top view of a portion of a membrane. The lipid's head core head is coloured in red and the optimal area per lipid has driven by repulsive/attractive interactions is drawn in blue. Changes in pH are expected to redefine the optimal area per lipid and thus their packing. In the figure, a decrease in the pH is represented. In conclusion, a low cytosolic pH is expected to decrease the surface area per lipid. Figure modified from Rauch (2009b).

To conclude, the incorporation of lipids in bilayer membranes can affect the biophysical properties of the membrane, and the cell makes full use of those properties to function normally (Rauch and Farge, 2000, Rauch, 2009a, Rauch, 2009b).

1.10.3 Role of lipids in influenza virus structure

The influenza virus uses cellular lipids and a lipid signal mechanism for entry into host cells. Then, it uses specific lipids for successful assembly and budding (Mazzon and Mercer, 2014). Cholesterol, glycosphingolipids, glycophosphatidylinositol-anchored proteins and transmembrane proteins gather and form lipid raft domains utilised by influenza virus (Chan et al., 2010). In addition, opened wedge-shaped dioleoyl phosphatidyl ethanolamine lipids (Figure 1.8) allow the membrane to take a specific conformation, allowing the formation of a neck through the generation of a negative Gaussian curvature (NGC), which enhances membrane fusion. In contrast, the closed wedge-shaped LPC reduces the fusion by destabilising the membrane NGC (Smrt et al., 2014). Lipid rafts at the apical plasma membranes of polarised epithelial cells are the primary site of influenza virus assembly and budding. Lipids can play an essential role in the enveloped virus lifecycle, as this depends on the lipid composition of target membrane and can affect the interaction rate between viral glycoproteins and host cell lipid membrane which can influence the rate of virus binding and fusion (Martín-Acebes et al., 2013).

The lipid envelope of the influenza virus is derived from the host cell membrane but differs qualitatively from the host. It has been found that the apical plasma membrane of infected MDCK is enriched with sphingolipids (SPs) and cholesterol. However, GPLs are reduced in influenza envelope membrane compared with the apical membrane of MDCK cells. The viral membrane shows further enrichment in SPs and cholesterol. Viral GPLs consist mostly of PS and PE but have reduced proportion of PC, PG and PI (Gerl et al., 2012). Infected host cell membrane pre-treated with 25μg of unsaturated fatty acids decreases IAV virus infectivity by "dissolving" the viral membrane as shown in EM images (Kohn et al., 1980). Physically and metabolically, lipid remodelling acts as a scaffold for viruses to transition successfully through the lifecycle and avoid vRNA recognition via host immunity. In contrast, viral infection can be blocked through reduced biological cell membrane fluidity due to greater expression of interferon-induced transmembrane proteins, which inhibit virus fusion (Rowse et al., 2015). In viral infection, adenosine monophosphate-activated protein kinase can block lipid synthesis, thereby inhibiting viral processes (Chukkapalli et al., 2012).

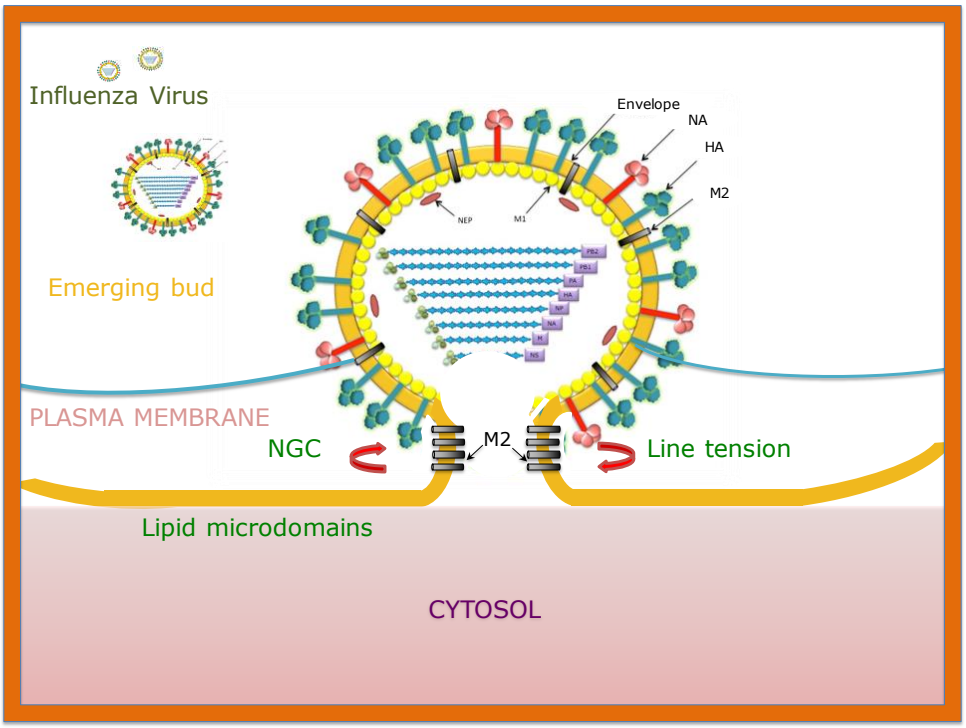

Figure 1:8 Negative Gaussian curvatures.
Influenza viruses use lipid raft domains in the apical plasma membrane of polarised epithelial cells as sites for budding. The viral glycoprotein is embedded in lipid microdomains and incorporated into the virion, and M2 proteins concentrate at the neck of the budding virus altering local membrane curvature. Figure modified from Heaton and Randall (2011).

The importance of membrane topology in viral infection has been underlined. M2 can induce high levels of membrane curvatures of different sizes (Schmidt et al., 2013). The host cell lipid raft domains are important in virus life cycle as lipid composition analysis in Influenza A viruses (H1N1, H3N2, and H5N1) and noninfected allantoic fluid (NAF) (Bonnafous et al., 2014) showed that sphingomyelin increased significantly in these viruses compared to NAF, which could explain the importance of these lipids to infect host cells.

1.10.4 The role of pulmonary surfactant in respiratory infections

Pulmonary surfactant organises the biophysical and immunological responses of the respiratory system (Numata et al., 2013) and acts as a natural body-defence mechanism against a number of different microorganisms, like viruses, as these phospholipids have been confirmed as natural barriers against viral infection (Perino et al., 2011).

Lipids compose 90% of the pulmonary surfactant molecular weight; 80% of these lipids are phospholipids, like PC and PG, and 10% are neutral lipids (Figure 1.9). The most common phospholipid is dipalmitoylphosphatidylcholine (DPPC) phosphatidylcholine, which comprises 70% of surfactant lipids and is mainly saturated (Glasser and Mallampalli, 2012, Han and Mallampalli, 2015).

Phosphatidylglycerol is also an abundant surfactant phospholipid comprising about 7–18% of the total phospholipid mass that modulates the inflammatory response of alveolar macrophages (Kuronuma et al., 2009). From the phosphatidylglycerol lipids, 1,2-dipalmitoyl phosphatidylglycerol (DPPG) has a vital role in the lung via tubular myelin formation (Quintero and Wright, 2000). Cholesterol, PS, PE and sphingomyelin are all present but in small percentages in lung surfactant (Han and Mallampalli, 2015). It has been found that unsaturated phospholipid POPG, that is found in the lung, exhibited inhibition of viral infection with reduced cytokine expression (Numata et al., 2013).

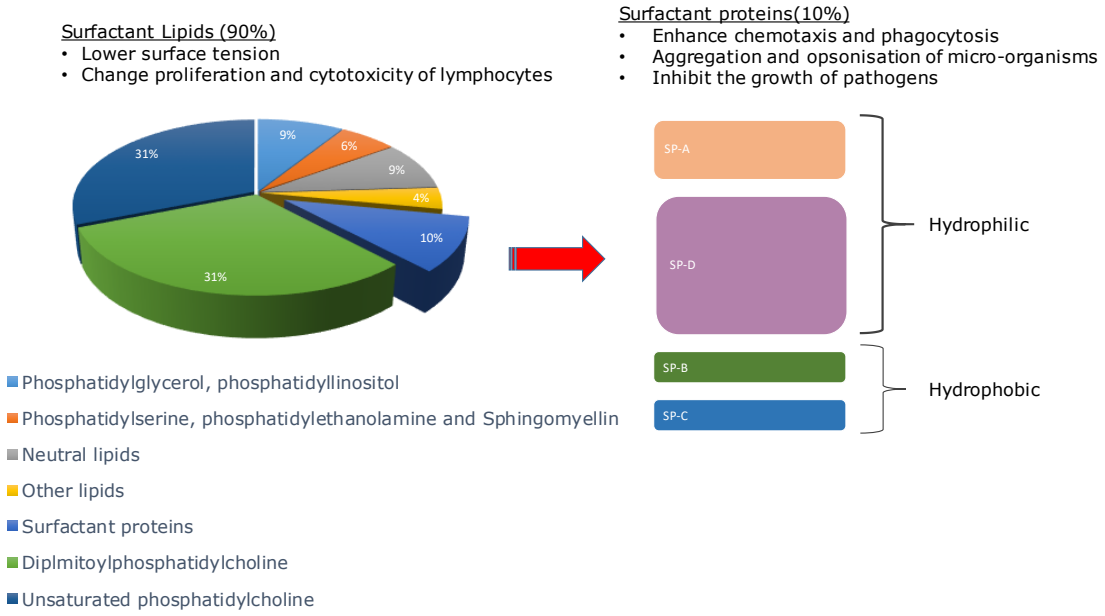

Figure 1:9 Pulmonary surfactant composition and function.
Lipids comprise 90% of the surfactant while the remaining 10% of the surfactant is composed of proteins. This figure adapted from Han and Mallampalli (2015).

Surfactant proteins (SP) constitute 10% of the surfactant composition and are believed to play an essential role in regulating surfactant tension properties in addition to possessing antimicrobial activity. In particular, SP-A and SP-D appear to have roles as pulmonary anti-inflammatory components by binding with Toll-like receptor 4 and modulating lipopolysaccharide (LPS) induced pro-inflammatory cytokines that clear pathogens from the body (Han and Mallampalli, 2015, Kuronuma et al., 2009). The basic functions of pulmonary surfactant are to reduce the surface tension at the air-liquid interface of the alveolus. This specific property was first highlighted by Neergaard (1929), (as reviewed by (Willson et al., 2009). This property prevents the collapse of the alveolus at the end of exhalation by enabling low and stable surface tension (1–2 mN/m)

during the respiratory cycle (Schürch et al., 2001). Pulmonary surfactant phospholipids, especially DPPC, have a critical role in maintaining surface tension (<1 mN/m) at low lung volume to prevent alveolus atelectasis (Perez-Gil and Weaver, 2010).

Pulmonary surfactant plays a critical role in phagocytosis, modulating cytokine production. Pulmonary phospholipids like 1-palmitoyl-2-oleoyl-sn-glycero-3-phosphoglycerol (POPG) alter the immune response by interfering with TLR interaction with the protein molecules CD-14 and MD-2 (Kuronuma et al., 2009). The pulmonary surfactant protein collectins increase the number of bronchoalveolar macrophages and enhance TNF-α expression in host defence against fungal infection such as *Blastomyces dermatitidis* (Lekkala et al., 2006) and bacterial infection such as *Pseudomonas aeruginosa* (LeVine et al., 1998). Surfactant inhibits human immunodeficiency virus type-1 (HIV-1) life-cycle by the binding of SP-D with viral glycoprotein-120, blocking viral entry and inhibiting CD4 and glycoprotein-120 interaction (Pandit et al., 2014).

Surfactant lysophospholipids also have important physiological and biological properties against atherosclerosis and pulmonary inflammation. Lyso-lipids like lysophosphatidylcholine (lyso-PC) and lysophosphatidic acids (lyso-PAs) have been noted for their anti-inflammatory action in the pulmonary system, as lyso PC regulates adhesion of molecules, gene growth factors, cyclooxygenase-2 and attracts monocyte and T-lymphocytes (Ryborg et al., 1994).

Interestingly, lysophospholipids play a role in the immune response as studies have also revealed the impact of lyso-PA and lyso-PC in the treatment of sepsis and organ failure (Murch et al., 2006, Yan et al., 2004). Exogenous surfactant is also the treatment of choice for neonates with NRDS (neonatal respiratory distress syndrome) caused by a deficiency of alveolar type-II epithelial cells (Raghavendran et al., 2011).

1.10.4.1 **Role of lipids in influenza virus infection**

Virus infection induces morphological changes in the cellular membrane which, in turn, acts as a platform enhancing viral replication through recruitment of several cellular and viral factors (Mazzon and Mercer, 2014). Enveloped viruses utilise the host cell machinery involved in lipid metabolisms (Table 1.2), such as sterol biosynthesis, fatty acid metabolism and phosphoinositide synthesis pathways, to replicate (Mazzon and Mercer, 2014).

Membrane lipids can act as scaffolding molecules to anchor viral proteins or viral replication complex also participating in spontaneous membrane curvature (Chukkapalli et al., 2012). Alterations in lipid molecules, for example, the head group or acyl chain composition, can protect the virus from, or expose the virus to, the host's innate immune response (Martín-Acebes et al., 2013). For example, adenosine 5' monophosphate-activated protein kinase (AMPK) is an enzyme involved in lipid metabolism. During viral infections AMPK

prevents lipid synthesis thus releasing ATP as a result of apoptosis, initiating the innate immune response (Chukkapalli et al., 2012).

Lipid metabolism is a potential target for the treatment of infection with enveloped viruses and the direct inhibition of fatty acid biosynthesis can block virus budding (Munger et al., 2008).

Table 1:2 The main types and roles of each lipid molecule in the influenza virus life cycle, modified from Chan et al. (2010).

Stage	Lipid class	Mode of action	Reference
Fusion	Phosphatidylserines	Annexins are hijacked as co-receptors by PS expressed in the virus envelope	(Huang et al., 1996)
	Sterol	Virus surface glycoproteins and receptors are clustered in a lipid raft	(Takeda et al., 2003)
	Sphingolipids	Glycan-glycan interactions between host and virus stabilise virus attachment	(Huang, 1976, Leskawa et al., 1986, Kasson and Pande, 2008)
Assembly/ budding	Sterol	Surface exposed polybasic domains of similar matrix proteins also use phosphoinositide or other anionic phospholipids for "lipid-raft" induction of membrane curvature	(Ruigrok et al., 2000, Thaa et al., 2009)
	Sphingolipids	Cholesterol depletion enhances virus budding "lipid-raft" dependent viruses do not co-localize on the plasma membrane	(Barman and Nayak, 2007, Khurana et al., 2007, Leung et al., 2008).
	Fatty acids	Several viral proteins have myristoyl and palmitoyl covalent modifications for "lipid–raft" targeting	Reviewed in (Hruby and Franke, 1993, Maurer-Stroh and Eisenhaber, 2004)
Extracellular	Sterols/sterol esters	Cholesterol depletion of virus envelope leads to virus inactivation due to the loss of protein core and genome integrity	(Barman and Nayak, 2007)
	Lipid molecular geometry	Inverted cone-shaped lipids, such as lyso PC, inhibit virus envelope fusion with the target membrane while cone shaped lipids, such as PE may facilitate membrane dynamics	(Günther-Ausborn et al., 1995, Chernomordik et al., 1998).

As a summary, it is often routine to think pharmacologically, i.e. in terms of drug-target or lipid-virus chemical interaction. However, given the complexity of enveloped membrane viruses, it is unclear to what extent the addition of lipids perturbs the membrane biophysics of viruses especially as blebs appear upon lipids treatment (Numata et al., 2012). The efficacy of lipids against viral infections therefore needs to be optimised. The basic geometry or topology of lipids is a key determinant as it indicates the type of micelles that can be formed in solution once the critical micellar concentration (cmc) has been reached. In this context, lyso-lipids, i.e. single chain phospholipids, have a tendency to form single unilayer structures whereas two aliphatic chains lipids form bilayer liposomes (Israelachvili, 2011). Although bilayer liposomes can fuse together (Nomura et al., 2004) and with viruses (Perino et al., 2011), by being a single layer of lipids, unilayer structure made of lyso-lipids are expected to be smaller (Israelachvili, 2011) and should not have access to the inner leaflet of the virus upon fusion. This should result in a different response regarding infectivity that, in turn and conceptually, can be a starting point to investigate the hypothesis suggesting that the membrane biophysics of viruses may be a key factor in the antiviral activity of lipids, for example in pulmonary surfactant.

1.11 Aims and objectives of the study

The major aims of this study were to investigate the impact of lipids on influenza A viruses to determine:

1. The effect of exogenous phospholipids on host cell metabolic activity.
2. The effect of exogenous lipids on the infectivity of LPAI H2N3, H1N1 and H3N8 by incubating the viruses with lipids of interest prior to incubating them with cells for 6hrs post infection using immunocytochemical staining for viral nucleoprotein.
3. The impact of phospholipids on H2N3 and H3N8 morphologies.
4. Influenza A virus H2N3 and H3N8 binding to the host cell membrane before and after incubation with exogenous phospholipids for 0-30 mins post infection using immunofluorescence to detect viral HA.
5. The impact of exogenous phospholipids on cytokine and viral gene expression in host cells infected with H2N3, H1N1 and H3N8.

Chapter 2: General Materials and Methods

2.1 Virus production and titration

2.1.1 **Viruses**

Three influenza A viruses were used in this study: AI H2N3 (A/mallard duck/England/7277/06) and pandemic influenza A (H1N1) virus (A/California/7/2009), were kindly provided by Dr Ian Brown (Animal and Plant Health Agency (APHA), UK), equine influenza H3N8 (A/equine/Newmarket/5/03), as kindly provided by Dr Debra Elton (Animal Health Trust (AHT), UK). Viruses were propagated in the allantoic fluid of embryonated hen's eggs.

In order to confirm that the effect of phospholipid treatment was not exclusive to H2N3, the effect of phospholipid treatments on H1N1 and H3N8 were also investigated.

These three strains have different morphologies; H1N1 is uniformly round, H2N3 is spherical, whilst H3N8 is filamentous, so we would hypothesise that due to, their different shape and surface areas they might interact differently with exogenous lipids and therefore show different degrees of inhibition.

2.1.2 **Influenza virus growth**

Influenza virus was propagated in Dekalb white fertile hen's eggs from Sussex chicken breed that were obtained from Henry Stewart & Co. Ltd, UK. A virus stock was diluted to 1:2000 in Dulbecco's phosphate buffer saline (Invitrogen) with 2% tryptose phosphate broth (Sigma-Aldrich) and 1% of penicillin/streptomycin at 10,000

units/µg per mL (Invitrogen). The fertilised eggs were incubated in an egg incubator (Brinsea, UK) at 37°C for ten days, and then, candling (Brinsea, UK) was used to observe the embryo in a dark room and outline the air sacs using a pencil to define the site for injection. The eggs were washed with 70% ethanol, and a hole was made in the shell at the site of injection using a needle and to avoid damage to the shell membrane and reduce the pressure during inoculation, a second hole was made above the air sac of the egg. The virus (0.1 mL) was injected into the allantoic cavity, the hole was sealed with molten paraffin wax, and the eggs incubated for 24 hrs at 37°C. Eggs containing dead embryos were detected via candling and were discarded. The remaining embryos were incubated for a further 48 hrs and then chilled at 4°C overnight to kill the embryo. The shell over the egg air sac was opened with sterile scissors in a Class 2 safety cabinet, and the allantoic fluid was collected using a disposable pipette (Figure 2.1). The harvested virus was aliquoted into cryovials and kept at -80°C for long-term storage.

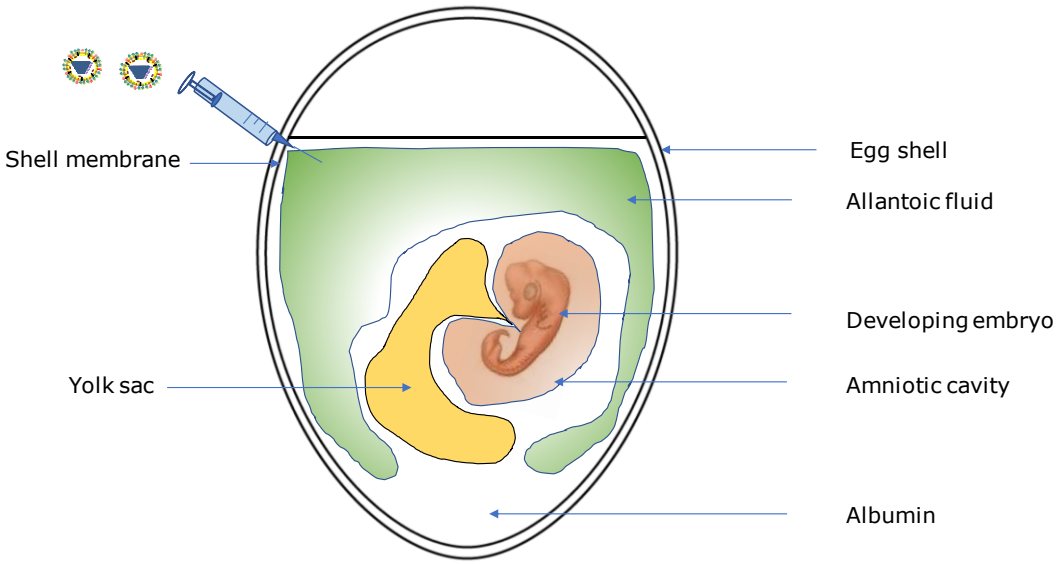

Figure 2:1 Inoculation of influenza virus H2N3 in a healthy chicken embryo age ten day
Influenza virus (0.1ml) was inoculated with a 1ml insulin syringe with 25 gauge needle at depth around 22mm into the allantoic cavity of a healthy ten day old embryonated hen's egg.

2.2 Cell culture

2.2.1 Continuous cell lines

MDCK and A549 cells were were seeded into a cell culture flask (Nunc) with Dulbecco's modified Eagle's medium (DMEM, Glutamax), along with 10% fetal calf serum (FCS; Invitrogen) and a broad-spectrum antibiotic, 1% penicillin-streptomycin (100u and 100µg /mL, respectively) (Invitrogen); the complete media was designated DMEM-10. Then, the cells were seeded into flasks at a cell density of 5000–6000 cells/cm² and grown to confluence (90–100%), and the culture media was discarded. The monolayer cells were washed twice with PBS. Then, these cells were trypsinised using 0.05% trypsin (Invitrogen). The flask was returned to the incubator at 37°C for another 5 min until the cells became detached from the flask surface.

Trypsin was neutralised using DMEM-10. The cell suspension was then centrifuged at 1200xg for 5 min. Finally, the supernatant was discarded, and the pellet was re-suspended in fresh DMEM-10 and inoculated into new flasks at 37°C. Typically, MDCK cells were split 1:4 to 1:5 flasks every 2–3 days.

2.2.2 **Cryo-preservation of cells**

Media for cryo-preservation was prepared using DMEM with 50% FCS and 10% dimethyl sulphoxide (DMSO, Sigma). The sub-confluent monolayer (90% cells) was passaged, as described above. After centrifugation, the pellet with media was transferred into cryovials (Nunc), placed in an isopropanol-filled "Mr. Frosty" freezing container (Nalgene) and stored at -80°C overnight. The next day, cryovials were frozen at -196°C in liquid nitrogen until required. When required, the cells were thawed rapidly via immersion in a water bath at 37°C. When thawed, the cryovials were placed at 37°C, with the addition of 10 mL DMEM-10 and centrifuged at 1200 xg for 5 min. The supernatant was discarded, and the pellet was re-suspended and used to seed a new culture flask.

2.2.3 **Cell counting**

A Neubauer haemocytometer chamber was used to count the resuspended cells prepared in a counting solution (10 µL of cell suspension and 10 µL of 0.4% trypan blue. A cover slide was placed on the mounting area of the chamber, and 10 microlitres of the counting solution was pipetted on both sides of the counting chamber.

The number of viable cells (that do not incorporate trypan blue) was counted. Precisely, the number of non-blue cells were determined in five squares (two on the right, two on the left, and one in the central area) using an x10 magnification objective. To determine the concentrations of cells per millilitre, the average number of cells per square was multiplied by the dilution factor and 10^4. The cells were then diluted appropriately and seeded in culture flasks at an appropriate density (typically 5000–6000 cell/cm²).

2.3 Measurement of virus infection

2.3.1 Virus infection of MDCK

MDCK cells were plated in a T75 flask (Nunc) and allowed to grow to 90% confluence before these cells were split via trypsinisation and seeded at a density of 5,000 cells per cm² into 96-well plates with DMEM-10 and incubated at 37°C. After 24 hrs, cells reached 95% confluence. The media was discarded, and the cells were washed three times with PBS prior to being infected with 50 µL of media containing virus diluted from 10^{-1} to 10^{-10} using serum free medium Ultraculture (Lonza, UK) supplemented with 1% penicillin/streptomycin, 1% L-glutamine and 2 µg/mL tosyl phenylalanyl chloromethyl ketone (TPCK) trypsin (Sigma); designated infection media (IM). Mock-infected and uninfected cells containing media only were seeded in wells, in triplicate. Cells were incubated at 37°C for 2 hrs then rinsed three times with PBS, followed by the addition of 100 µL IM per well for each dilution of the virus and

incubated at 37°C with 5% CO2 for 4 hrs. After 6 hrs post-infection, the cells were washed three times with PBS and fixed using cold (4°C) 1:1 acetone-methanol for 10 mins at room temperature (RT). The plates were kept at 4°C prior to immunocytochemical staining, overlaid with Tris-buffered saline (TBS).

2.3.2 **Immunocytochemical staining**

Infected MDCK and A549 cells were immunostained using the Envision system-HRP (DAB; DAKO, Ely, UK) to detect influenza H2N3, H1N1, or H3N8 viral nucleoprotein via immunocytochemical staining (Figure 2.2). Fixed cells were rinsed three times with 1 x of Tris-buffered saline (TBS) and blocked by using peroxidase blocking reagent at room temperature for 10 min. Cells were then washed three times with 1 x Tris-buffered saline (TBS) and incubated at room temperature with 1:1000 mouse monoclonal antibody raised against the influenza nucleoprotein (AA5H, Abcam, UK) for 1 hr. The cells were then washed three times using 1x TBS before incubating with Envision reagent of enzyme horseradish peroxidase phosphate (HRP) conjugated dextran polymer backbone labelled anti-mouse IgG secondary antibody for 40 min. Finally, the cells were washed three times using 1x TBS and incubated at room temperature for 10 min with a substrate-chromogen solution (1 drop of DAB mixed with 1 mL of substrate buffer). After three final washes with 1xTBS, the cells were examined using a light microscope. The multiplicity of infection (MOI) of 1.0 was determined according to the amount of virus that produced 95–100% positive cell labelling for NP.

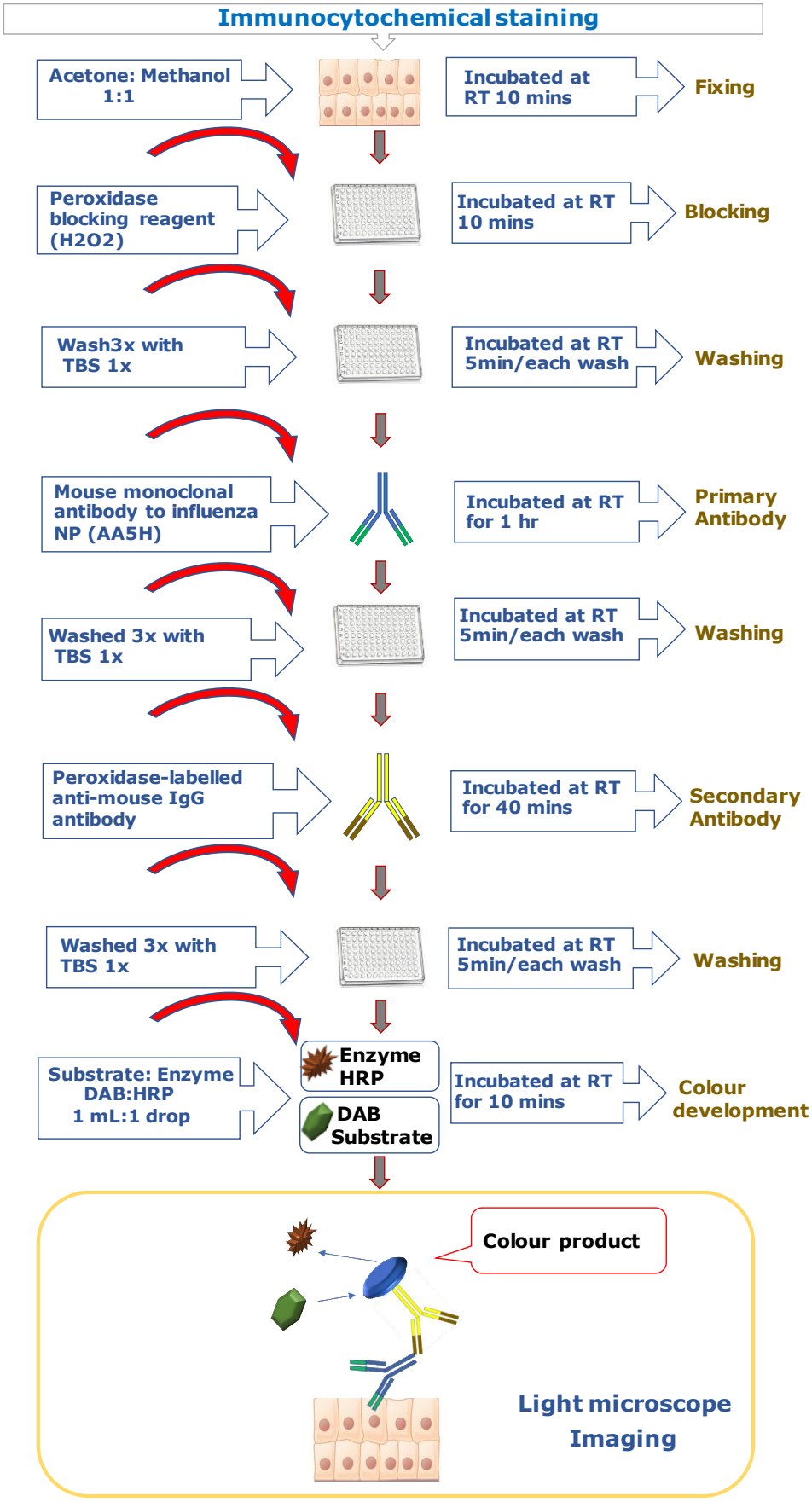

Figure 2:2 Immunocytochemical staining of Influenza nucleoprotein.

2.3.3 Quantification of virus titre by focus forming assay (ffu)

Confluent MDCK cells were used to determine virus titre in cell culture supernatants. Culture supernatants derived from IAV infected cells were added to a 96 well plate in triplicate, incubated at 37°C for 2 hrs and then washed three times with PBS. The wells were incubated with a fresh IM for a further 4 hrs. Then, the cells were fixed, and immunocytochemical staining performed for viral NP, as detailed above (Kawaoka and Neumann, 2012). Images were captured from five random fields from each well under 10 X magnification and infected cells were counted, to calculate an average number of infected cells per field, using Image J software (image 1.47v, National Institute of Health, USA).

2.4 Effect of lipid treatment on influenza A viruses infection

To examine the effect of phospholipids on H2N3, H1N1 and H3N8 infection, viruses were treated with various types of phospholipids (Avanti Polar Lipids, Inc.), including DPPS, LPS, DPPG, LPG, DPPC and LPC (Table 2.1). Lipids were prepared at three different concentrations (5, 50, and 500 μM), and an N2 generator (Peak Scientific Instruments Ltd, UK) was used to evaporate the lipid's solvent (chloroform) for 5–10 min, then infection medium was added and the lipid solution sonicated using an ultrasonic bath at 60 KHz for 10–15 min.

Table 2:1 Types of phospholipids used in our study and their abbreviations and chemical structures (Luckey, 2014)

Lipid name	Abbreviation	Chemical structure
Phospholipid with two aliphatic chain		
1,2-dipalmitoyl-sn-glycero-3-phospho-L-serine	DPPS	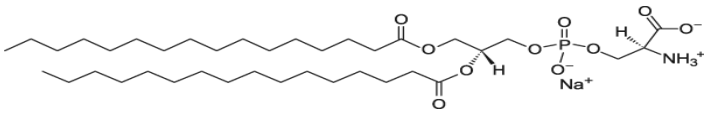 Polar, large negatively charged lipid head domain and two aliphatic chains (C16)
1,2-dipalmitoyl-sn-glycero-3-phospho-(1'-rac-glycerol)	DPPG	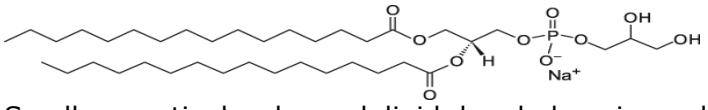 Small, negatively charged lipid head domain and two aliphatic chains (C16)
1,2-dipalmitoyl-*sn*-glycero-3-phosphocholine	DPPC	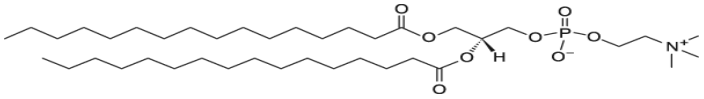 Large, neutral lipid head domain and two aliphatic chains (C16)
Lysolipids mean single aliphatic change		
1-palmitoyl-2-hydroxy-sn-glycero-3-phospho-L-serine	LPS	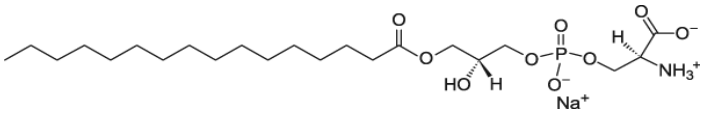 Polar, large, negatively charged lipid head domain and one aliphatic chain (C16)
1-palmitoyl-2-hydroxy-sn-glycero-3-phospho-(1'-rac-glycerol)	LPG	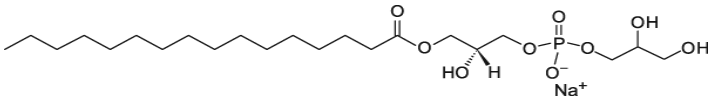 Small, negatively charged lipid head domain and one aliphatic chain (C16)
1-palmitoyl-2-hydroxy-sn-glycero-3-phosphocholine	LPC	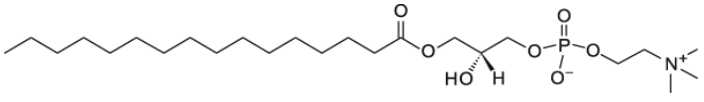 Polar, large neutral lipid head domain and one aliphatic chain (C16)

The lipid solution was mixed with influenza A viruses for 5, 30 mins or 2hrs at 37°C and the solution centrifuged at 5000xg for 10 min twice using an Amicon Ultra-15 filter (50K MWCO) (Fisher Scientific, UK Ltd) to separate unbound lipids from the viruses. The virus preparations were then resuspended in IM and incubated with confluent MDCK or A549 cells for different incubation times at an MOI of 1.0 at 37°C. Cells infected with influenza A virus (with or without lipid treatment) and mock (i.e. uninfected) cells were fixed as previously described, followed by immunocytochemical staining against viral nucleoprotein (Figure 2.3), as described in 2.3.2. The infectivity was measured using the focus forming assay (ffu/mL), as described in 2.3.3.

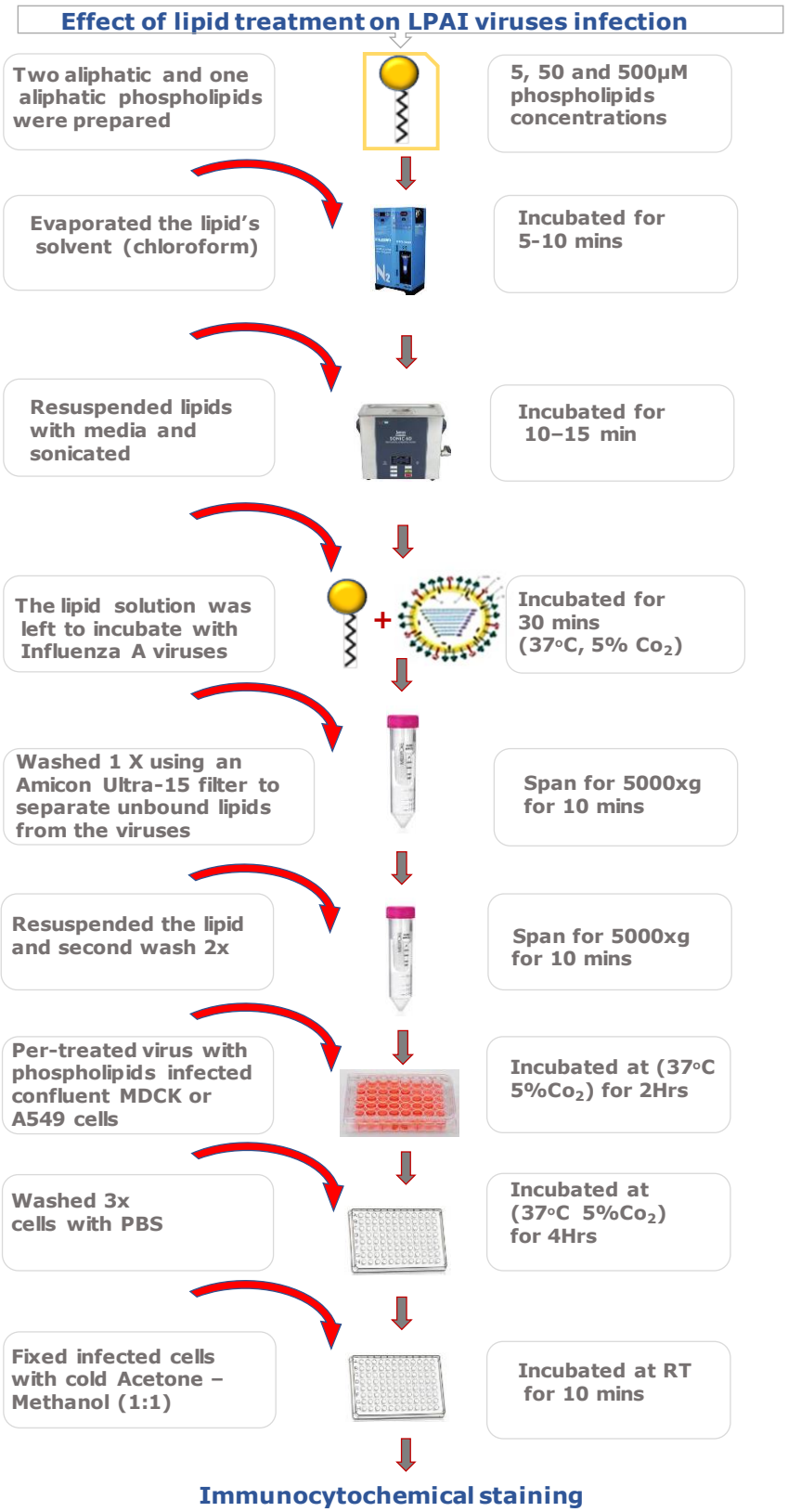

Figure 2:3 Pre-treatment of influenza virus with exogenous phospholipids.
Virus was treated with phospholipids followed by two wash steps performed using Amicon ultra-15 filtration.

Chapter 3: Determination of the effects of the lipids on cell metabolic activity, size, shape and complexity

3.1 Introduction

Monitoring cell size, viability, and shape in medical and/or biological research settings are used in many cell culture laboratories to investigate apoptosis or to determine the impact of treatment(s) on the host cell *in vivo or in vitro* (Jiang et al., 2016).

3.1.1 Biological functions of phospholipids

The initial observation that the cell membrane is composed of two layers of lipids was first recorded almost a century ago (Gorter and Grendel, 1925). The permeability and electrical properties of cells were discussed in terms of lipid properties by Danielli and Davson (1935). We know now that lipids also represent a source of energy and a fundamental matrix for raft domain formation, enzyme and chemical reactions (Van Meer et al., 2008, Edidin, 2003). The importance of phospholipid is shown by the administration of phospholipids as 'replacement therapy' in aged people and patients with fatigue symptoms due to mitochondria dysfunction-Patients showed improvements following therapy in cellular function resulting from mitochondria dysfunction (impaired oxidative glycerophospholipid accumulated through the ageing progress) (Nicolson and Ash, 2014).

3.1.2 **Detection of cell toxicity by flow cytometry assay**

Cell viability in suspension, measured by flow cytometry, provides a method to assess single cell size and granularity as a function of light scattering occurring in both forward scatter (FSc) and side scatter (SSc) directions (Figure 3.1) (Adan et al., 2017). Thus, flow cytometry is a suitable method to study the impact of lipid treatment on individual cells. In apoptosis, a drop in cell size and an increase in complexity was has been observed using SSc/FSc (Jiang et al., 2016). When mouse renal proximal tubular cells were treated with Lyso-PA, cell viability was raised by 59%, which indicated an inhibitory effect of this lipid on apoptosis induced by incubating cells with growth factor–free medium (Levine et al., 1997).

It has been shown that the monounsaturated fatty acids are less harmful to cell metabolic activity through their effect on membrane integrity compared to polyunsaturated fatty acids. Incubation of these fatty acids directly with cells results in a decrease in cell volume and an increase in granularity, as well as changes in mitochondrial membrane and phosphatidylserine externalisation (Cury-Boaventura et al., 2004).

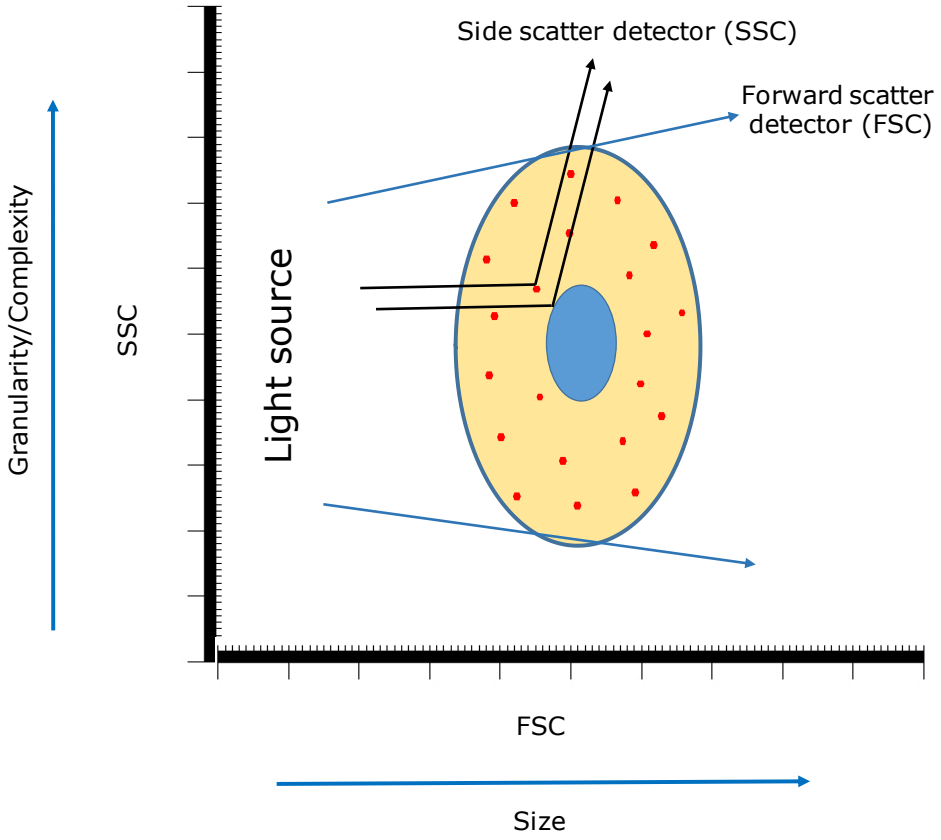

Figure 3:1 Flow cytometry measures biological cell size and granularity/complexity using forward (FSc) and side (SSc) light scatterings.

3.1.3 Properties of red blood cells

Red blood cells (RBC) are the most abundant blood cells circulating in the blood vessels that transfer the oxygen to body tissues. RBCs are synthesised in the bone marrow and circulate in the body for 100–120 days (Raut Deepika et al., 2013). RBCs can be used to study the toxicity of medicines in relation to their morphology (Campbell and Ellis, 2013).

In humans, RBCs are characterised by a biconcave shape (Raut Deepika et al., 2013, Viallat and Abkarian, 2014). The red cell membrane is composed of protein 52%, and lipid 40% carbohydrate

8% and phospholipids are asymmetrically distributed in the membrane and packed in a bilayer, the outer layer composed of 30% of PC and 25% of SM; negatively charged phospholipids, PE and PS are concentrated in the inner layer at 28%, and 14% respectively (Mohandas and Evans, 1994). Human RBCs can deform when flowing through smaller blood vessels or due to exogenous chemical and medicines. These deformities are characterised by a change in cell shape and size, which can vary up to 10 times (from a diameter of ~10μm in large vessels to ~0.5 μm in capillaries of the red pulp of the spleen). Furthermore, RBC deformities are affected by changes in their membrane properties, cell viscosity, surface area and cell size (Raut Deepika et al., 2013, Viallat and Abkarian, 2014).

RBCs are made of a bilayer membrane including transmembrane proteins and a cortical cytoskeleton composed of spectrin proteins forming a bi-dimensional network made of hexagonal mesh. This network is attached to the lipid bilayer through transmembrane protein (Mohandas and Gallagher, 2008). The lipid membrane composition and membrane proteins can slip against each other (Discher and Carl, 2001). Morphological disorders of RBC are seen in a number of diseases like sickle cell anaemia, due to changes in spectrin network binding with the bilayer phospholipids (Mohandas and Gallagher, 2008, Ghosh et al., 2014).

Avian blood is used for different haematological laboratory tests in avian farms and industry; this was initiated in 1960 by (Lucas and

Jamroz, 1961). Chicken RBCs differ from those in mammals, as they have a larger size and are characterised by their elliptical shape and central nucleus (Campbell and Ellis, 2013).

3.1.4 **Use of RBCs in biological assays**

Chicken blood has been used to investigate treatment responses and diagnose diseases rapidly by measuring the cellular and nuclear size, shapes and colours (Campbell and Ellis, 2013). Use of RBC from an appropriate species, RBC should be considered when measuring influenza haemagglutination for a particular influenza virus strain (World Health Organization, 2002). Rapid detection of influenza infection is possible using chicken blood due to the high affinity between the virus surface haemagglutinin and the sialic acid receptor of chicken RBCs. However, AI virus may not haemagglutinate chicken RBC unless grown in embryonated hens' eggs. In that case, turkey RBCs are considered to be more sensitive to AI virus (Killian, 2014). For example, turkey RBCs showed a higher titre in haemagglutination inhibition assay compared to guinea pigs RBCs against influenza virus H1N1 suggested that the RBCs of turkey contain a higher proportion of SAα2,6Gal than guinea pig RBCs. The nucleated RBCs of turkey also settle more quickly in haemagglutination inhibition assay and form buttons instead of halos making the assay endpoint easier to determine (cf. guinea pigs RBC) (Ovsyannikova et al., 2014).

Both cholesterol and lysophosphatidylcholine (LPC) lipids have an impact on the shape of RBCs leading to echinocytosis (i.e. RBCs with

many thorny membrane projections) (Lange and Slayton, 1982). It has been shown that lysopalmitoyl phosphatidylcholine modulates human RBC shape causing either echinocytosis if this lipid is concentrated in the outer leaflet or stomatocytosis if the lipid is concentrated in the inner leaflet (Mohandas et al., 1978). LPC phospholipid can move from the outer to the inner layer after being acylated to phosphatidylcholine (Shohet and Nathan, 1970). It was also shown that cells with high cholesterol content absorbed more LPC than when cholesterol is depleted (Lange and Slayton, 1982).

3.1.5 **Cell metabolic activity**

Measurement of cellular metabolic activity can be used to estimate the viability of cells in a multi-well plate using assays involving different colourimetric reagents, such as tetrazolium reagents and resazurin reduction. Viable cell number, cell proliferation and the cytotoxic effect of chemicals can be determined using such assays (Riss et al., 2004). MTT assay and Alamar blue techniques are used to measure the number of viable cells based on their metabolic properties given that dead cells do not display the ability to metabolise their chemicals in solution (Stockert et al., 2012).

The MTT dye 3-(4, 5-dimethylthiazol-2-yl)-2, 5-diphenyltetrazolium is a yellowish solution that is widely used to detect cell metabolic activity through the reduction of tetrazolium to form purple formazan by mitochondrial succinate dehydrogenases. The metabolite formazan can be identified by a plate reader (Figure 3.2). The purple colour of

formazan is an obvious indication of active metabolism in cells (Stockert et al., 2012, Riss et al., 2004). Formazan signals viable cell metabolism and reading this signal is also dependent on MTT concentration, time of incubation, and the number of viable cells (Riss et al., 2004).

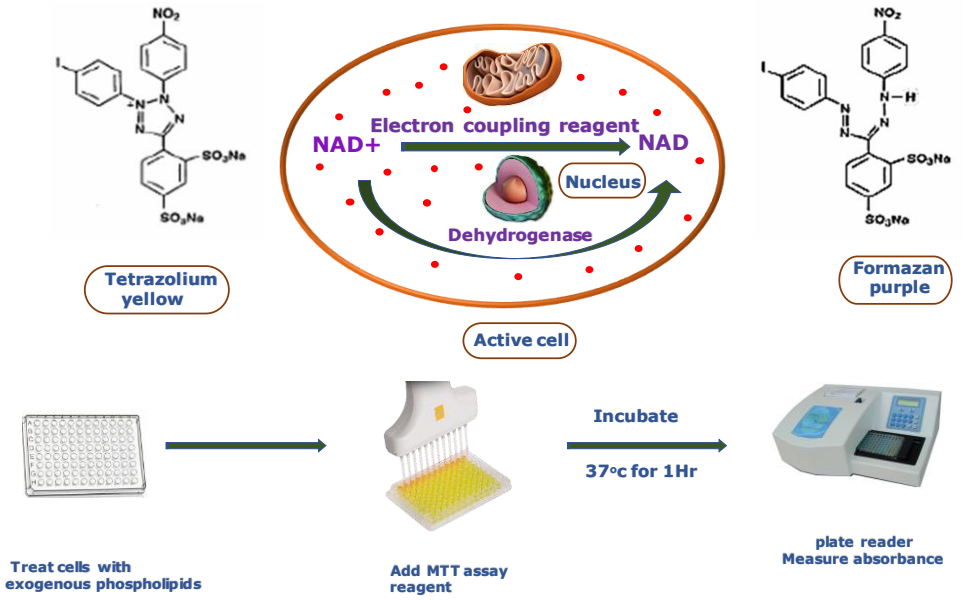

Figure 3:2 MTT assay cell metabolic activity.
Reduction of tetrazolium to formazan in living cells by mitochondrial activity and absorbance 490nm. NAD: Nicotinamide adenine dinucleotide.

Likewise, Alamar blue dye solution can be used to examine the metabolic activity of viable cells as blue resazurin (7-Hydroxy-3H-phenoxazine-3-one 10-oxide) reduces to pink resorufin, which can be detected at a 590 nm absorbance with a plate reader (Figure 3.3). Compared to tetrazolium, resazurin provides more sensitive results and is less toxic (Riss et al., 2004).

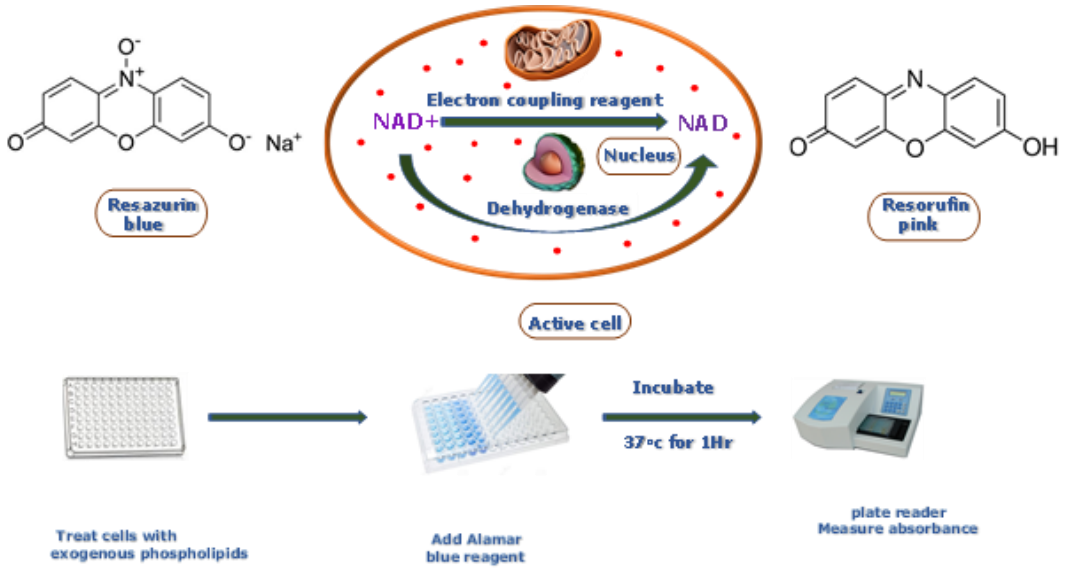

Figure 3:3 Alamar blue cell metabolic activity.
Mitochondrial activity in living cells is measured by the reduction of Resazurin to resorufin and absorbance at 592nm.

3.2 Aims

The main aims of this chapter are:

1. To determine the influence of exogenous phospholipids on RBC shape, size, surface area and agglutination.
2. To evaluate the impact of these phospholipids on cell size and granularity.
3. To determine the potential toxicity of each phospholipid using mammalian cell culture (MDCK or A549 cells) by measuring cell metabolic activity.

3.3 Material and Methods

To examine the effects of phospholipids on cell viability, size, and morphology, using DPPS, LPS, DPPG, LPG, DPPC, and LPC (Avanti Polar Lipids, Inc.), lipids were prepared at three concentrations (5, 50, and 500 µM). Cells were incubated with lipids directly or following two washes using an Amicon Ultra-15 Filter (50K MWCO) at 5000 xg for 10 min (as described in Section 2.4). The lipid solution was then incubated with the cells at different time points.

3.3.1 Lipid influence on the shape, size, and complexity of biological cells

The impact of lipids on living cells was investigated by incubating MDCK cells and chicken RBCs (TCS Biosciences Ltd, UK) with phospholipids.

3.3.1.1 Impact of phospholipids on chicken RBC morphology

To examine the effects of phospholipids on chicken RBC morphology, various types of phospholipids were used, including DPPS, LPS, DPPG, LPG, DPPC, and LPC (Avanti Polar Lipids, Inc.). Lipids were prepared as described in Section.4.2. Either the lipid solutions were used directly without Amicon filtration incubated with the chicken RBCs or the lipid was removed washing twice using an Amicon Ultra-15 Filter (50K MWCO; Molecular weight cut-off refers to the lowest molecular weight of solute (in daltons) at 5000 xg for 10 min. The phospholipids were then were incubated with chicken RBCs for different time points

of 5, 10, 20, and 30 min and imaged using an inverted microscope (Leica, UK).

3.3.1.2 Quantification of the influence of phospholipids on RBCs size

To quantify the influence of DPPC on RBC size, the short (L) and long (D) axes of RBCs were measured using Image J software and their ratio was plotted for each time point and lipid concentration.

3.3.1.3 Measurement of the impact of phospholipids on chicken RBC using haemagglutination

Fifty microlitres of PBS was added to each V-bottom well on a 96-well plate (wells 1 to 12). Fifty microlitres of lipid solution (500 μM)was then added to the first well and transferred to subsequent wells to produce a two-fold serial dilution (50 μL). Finally, 50 μL of RBCs working suspension at 0.5% of RBC was added to each well, mixed gently, and then left for 30 min at RT. The negative control used 50 μL of PBS with 0.5% of RBC but without lipids.

3.3.1.4 Determination of the impact of phospholipids on MDCK cells

MDCK cells were treated with phospholipids and processed for flow cytometry. To assess the impact of the lipid on MDCK cell size and granularity, two different techniques were used: one using Amicon filtration to remove excess lipids and the other without the filtration step.

3.3.1.4.1 Preparing individual MDCK cells for flow cytometry

MDCK cells were cultured in a T75 flask (Nunc) using DMEM-10. Once confluent (90–95%), the medium was discarded and the cells were washed twice with cold PBS at 4°C. Then, the flask was incubated in versene (Ethylenediamine-tetra-acetic acid, Gibco, UK) at 37°C for 10 min to detach the cells from the flask. DMEM-10 was used to neutralise versene and the cell suspension was centrifuged at 1200 xg for 6 min. Finally, the supernatant was discarded, and the pellet was resuspended at a concentration of 1 x 10^6 cells/ml in IM. Cell suspensions were then incubated with phospholipids. Ten thousand events were analysed for each sample. Two approaches were used to minimise the potential toxicity of phospholipids on biological cell including: 1) removal of lipids using Amicon ultrafiltration, 2) up to three washes with PBS after ultrafiltration.

3.3.1.4.2 Impact of lipids on the MDCK cells without Amicon filtration

Individual cell suspensions were incubated with phospholipids at three different concentrations (5, 50, and 500 µM) prepared without Amicon filtration for 10 min at 37°C. Either the treated cells were fixed directly using 1% paraformaldehyde (PFA; Fisher, UK) for 20 min at RT after treatment; or treated cells were washed three times with cold PBS

and then fixed with 1% PFA for 20 min at RT (Figure 3.4). The samples were kept at 4°C overnight and then examined with the FC500 Flow Cytometer (Beckman Coulter, UK) the following day.

3.3.1.4.3 Impact of lipids on the MDCK cells with Amicon filtration

Three different concentrations of each lipid (LPG, LPC, LPS, DPPG, DPPC and DPPS) were prepared as detailed in Section 2.4, followed by two washes using an Amicon Ultra-15 Filter and re-suspended in cold infection (4°C) media. Individual MDCK cell suspensions were treated with these lipid solutions for 10 min at 37°C. All samples were either directly fixed by 1% PFA or washed thrice with cold PBS and then fixed for 20 min using 1% PFA (Figure 3.4). This resulted in four treatment groups:

1. Without Amicon filtration, without washing steps.
2. Without Amicon filtration, with three washing steps.
3. Amicon filtration, without three washing steps.
4. Amicon filtration, with three washing steps.

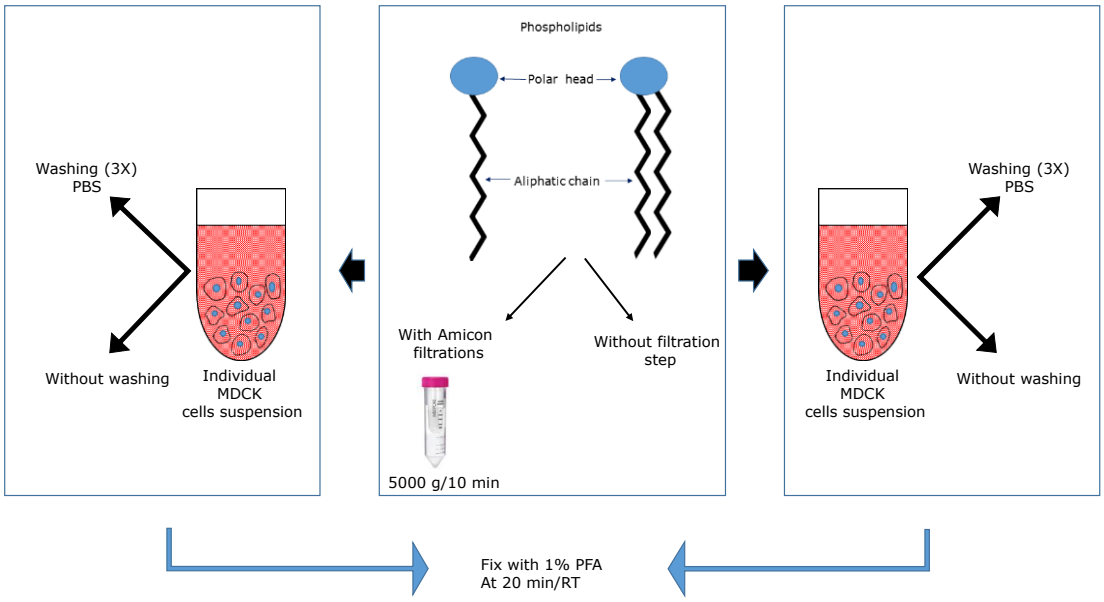

Figure 3:4 Phospholipid incubation with or without Amicon filtration steps.

3.3.2 Effect of phospholipids treatment on cell metabolic activity

MDCK or A549 cells were seeded in 96 well plates (Nunc) at 5x10³ cells /well with DMEM-10 at 37°C and 5% CO_2. After 24hrs the cells reached 95% confluence. The culture media was discarded, and the cells washed three times with PBS, then incubated with 100 µL of IM in quadruplicate wells with or without three different concentrations of phospholipids (5, 50, and 500 µM). Triton 1% was used as a positive control. Cells were then incubated at 37°C for 30, 60 min or 6 hrs. After each time point of incubation, cell metabolic activity was determined by using MTT reagent (CellTiter 96® Aqueous one solution for cell proliferation assay; Promega) following the manufacturer's instructions. Absorbance was read at 492 nm using a plate reader (Labtech International LTD., UK). In parallel assays, Alamar blue

reagent was added to each well, instead of MTT, for 4 hrs at 37°C, following manufacturer's instructions (Alamar blue, Cell viability Reagent, Invitrogen, UK) and the absorbance was read at 590nm.

3.4 Statistical analysis

To determine the presence of a statistical difference between phospholipid treated cells and untreated cells, with the three concentrations of phospholipids, at different times points of incubation, each experiment was performed three times and a one-way ANOVA performed followed by Dennett's multiple comparisons test using GraphPad Prism version 7.01 were used (graph pad software, Inc., USA).

3.5 Results

3.5.1 The effect of lipids on chicken RBC morphology and size

Chicken RBC were incubated with 500μM of the two-aliphatic chain phospholipid DPPC without Amicon infiltration for 5, 10, 20 and 30 min. After 10 min incubation, cells started to appear swollen with a clear deformity in some cells. After 20 and 30 min chicken RBCs became more rounded and showed more visible deformity without a clear nucleus. Following incubation of RBC with one aliphatic chain phospholipid LPC (500 μM) there was a clear absence of RBCs suggesting they are lysed through this specific treatment, after 10 min incubation (Figure 3.5).

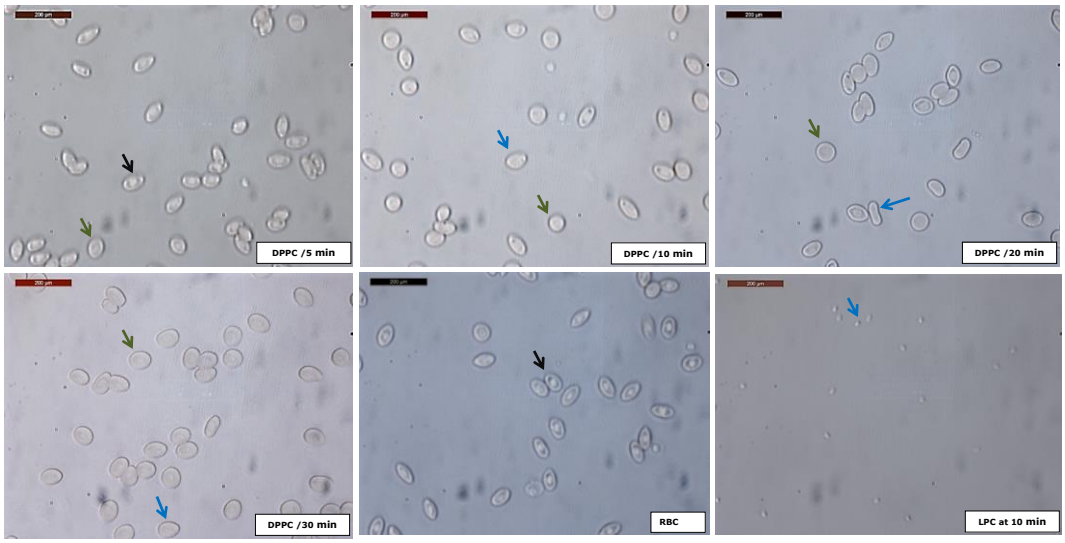

Figure 3:5 Impact of phospholipids on chicken RBC morphology. The direct impact of lipids without the two filtration steps showed a change in RBC shape. Black arrows point to normal RBCs shape; green arrows point to rounded RBCs, blue arrows point various deformations in cell shape.

Measurement of RBC dimensions was performed for RBC treated with DPPC (Figure 3.6) A ratio D/L~1 signifies a round cell, a ratio D/L

different from 1 signifies an elliptical cell. Untreated chicken RBC had a D/L ratio of approximately mean 1.7. Chicken RBC treated for 5min with DPPC without Amicon filtration showed significant alteration in cell shape with cells becoming more spherical, (approximately an average of 1.2 D/L ratio) at DPPC concentrations of 5 and 500μM compared to RBCs without treatment. No apparent change in the RBC shape was observed after 10 and 20 min incubation. However, incubation of RBCs for 30min with 500 μM of DPPC showed a significant ($p<0.05$) change in RBC shape compared to either untreated RBCs or RBCs treated with 50 μM of DPPC. RBCs treated with DPPC solutions prepared with Amicon filtration showed no significant changes in RBC shape comparing with untreated cells at any of the incubation times (Figure 3.6). These results confirmed that Amicon filtration was effective at removing excess 'toxic' effect of phospholipid.

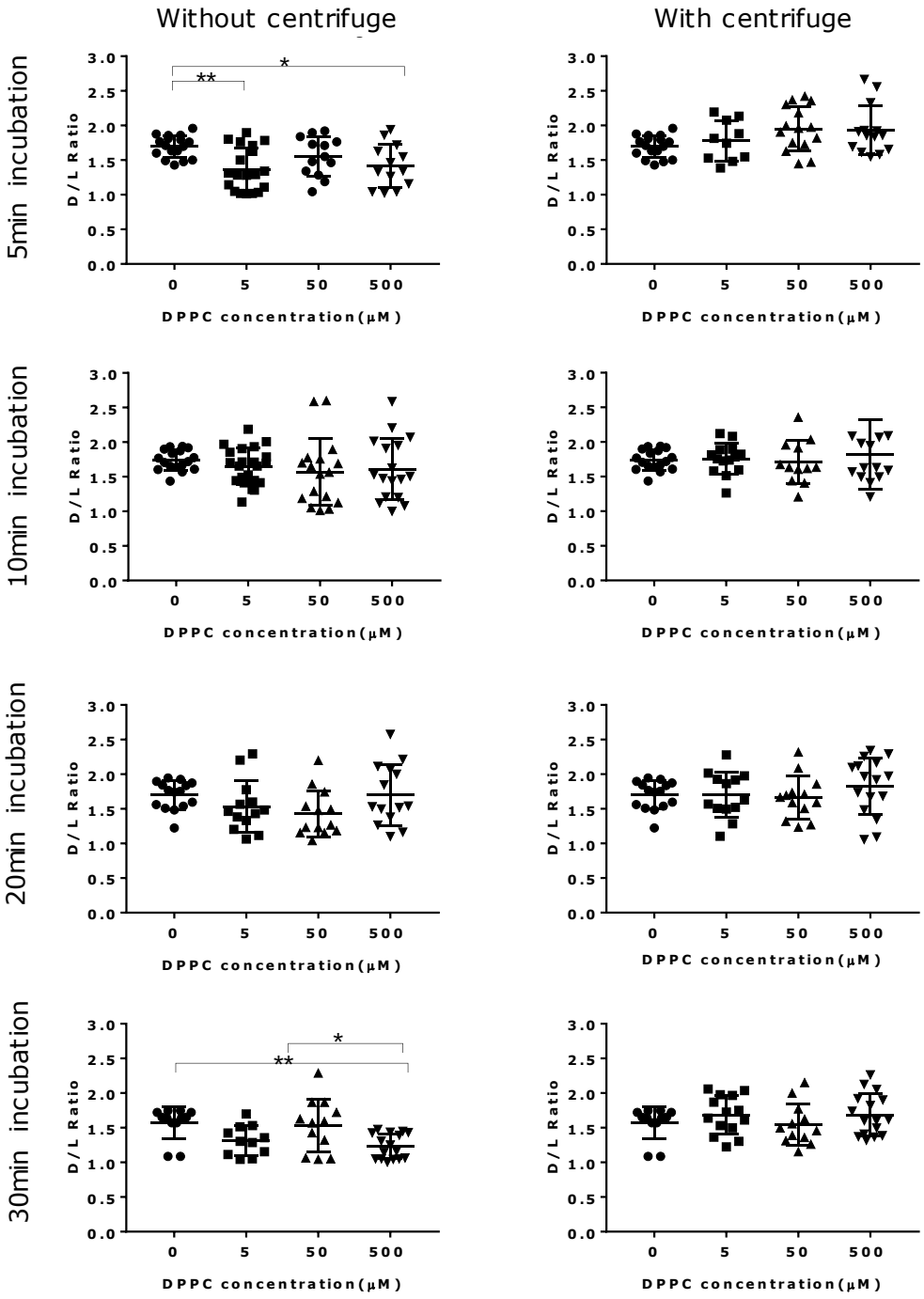

Figure 3:6 Measurements of the D/L ratio of chicken RBCs pre-treated with phospholipids.
DPPC was prepared with or without Amicon filtration. RBCs and lipids were incubated at different times. RBCs imaging was carried out using an inverted microscope, and then the D and L ratio of each cell were measured using Image J software. RBCs pre-incubated with 500μM DPPC without filtration step showed a significant impact on RBC shape (*p<0.05, **p<0.01; one-way ANOVA).

3.5.2 **The effect of lipids on chicken RBC agglutination**

A two-fold serial dilution of six different types of phospholipids (DPPG, DPPC, DPPS, LPG, LPC and LPS) was used to observe their effect on the agglutination of chicken RBC starting at a concentration of 500 µM. The results were compared with a negative control including chicken RBC without lipids. The double aliphatic chain phospholipids did not show any impact on RBC agglutination apart from the first working concentration of DPPG (500 µM). However, Lyso Lipids showed an impact on RBC agglutination as LPG and LPS showed agglutination at dilution (1:32) and LPC at (1:16) (Figure 3.7).

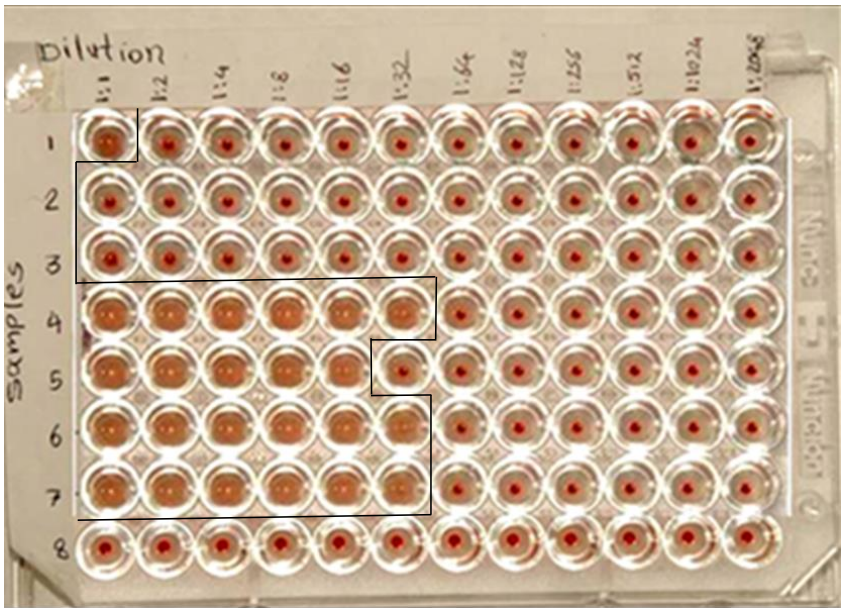

Figure 3:7 Impact of phospholipids on chicken RBCs agglutination. The HA image shows the endpoint dilutions for each treatment. Different phospholipids represent different endpoints. LPG and LPS agglutinate at a dilution of 1:32 and LPC at a dilution of 1:16. DPPG demonstrates partial agglutination at a dilution of 1:1 only.

3.5.3 **Effect of phospholipid treatment on MDCK size and complexity**

To identify the impact of phospholipids on cell complexity and size, forward and side scatter was measured by flow cytometry. MDCK cells

treated with different doses of exogenous phospholipid showed an increased in size and granularity as measured by selection of the R1 population below shown in figure 3.8.

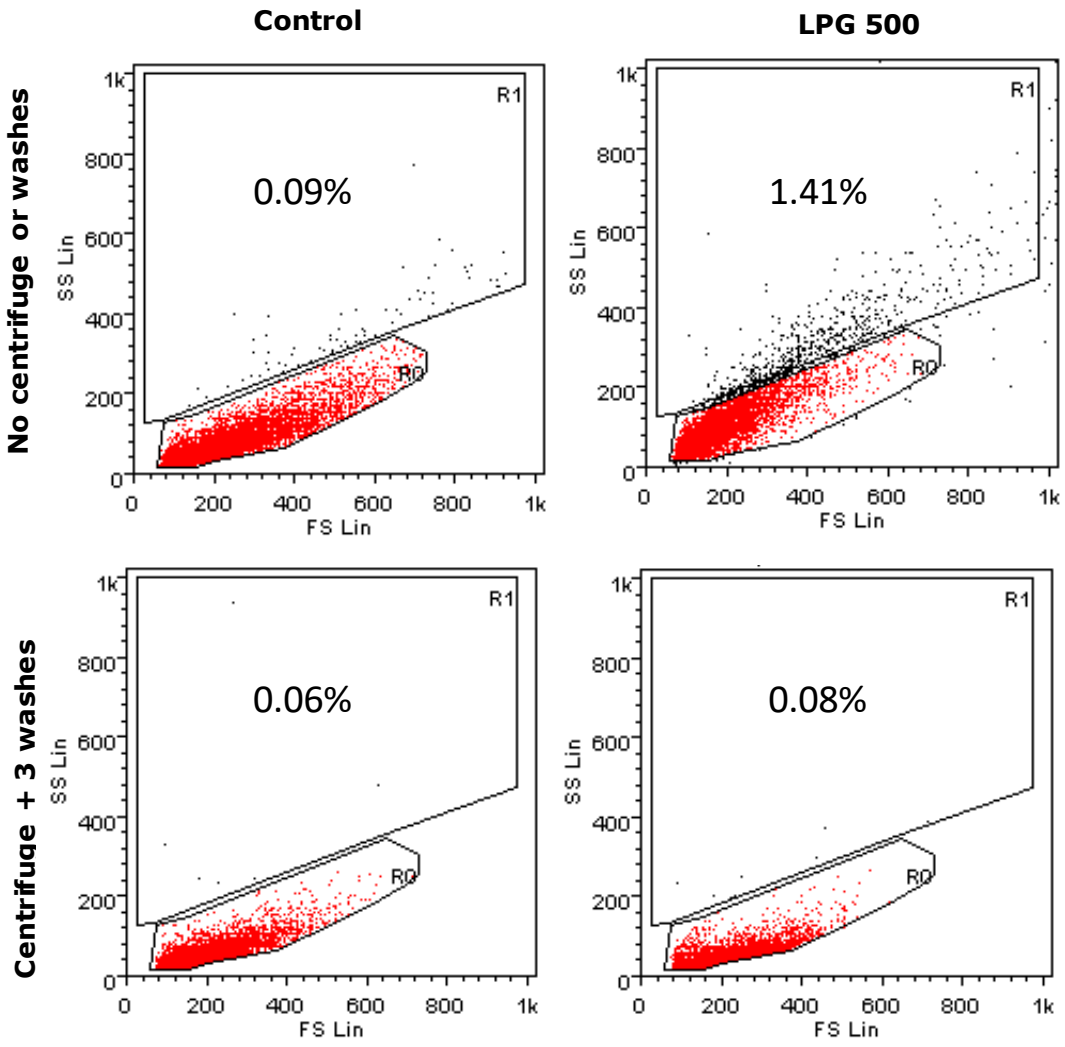

Figure 3:8 Impact of phospholipid after Amicon filtration with three washing steps on MDCK cell populations.
Pre-incubation of LPG at a concentration of 500 µM with individual MDCK cells for 10 min at 37°C then fixed using 1% PFA. R0) control gate healthy cells; R1) Cells showing an increase in cell size and granularity compared to R0.

Incubation of MDCK cells with DPPG, DPPC, DPPS, LPG, LPC or LPS prepared without Amicon filtration had a clear impact on cell size and complexity which is represented by the R1 gate population as compared with control MDCK cells without phospholipids. When MDCK

cells were pre-treated with 5μM phospholipids without Amicon filtration or washing steps, the R1 gate percentage was 2%, which was reduced to 1% with three washing steps. At 50 μM the majority of phospholipids without Amicon filtration increased the cell gate R1 percentage to 2.5%, while with DPPC, it increased to 3% and with DPPS to 4%. With further washing steps, the R1 percentage was reduced to 1% for the majority of phospholipids and to 1.5% and to 2% for DPPC and DPPS, respectively. At 500 μM a notable increase to 5% of cells in R1 was measured for most lipids without filtration, whilst the increase in R1 for DPPS was 20%. However, at this concentration, the washing steps were not able to reduce the R1-percentage for DPPS (Figure 3.9).

The addition of Amicon filtration without additional washing steps reduced the R1 gate percentage for most phospholipids incubated at 5 μM (Figure 3.9). At 50 μM the most noticeable R1 gate percentages were for DPPC and DPPS (0.8 % and 0.4%, respectively). The addition of further washing steps reduced the R1 population to levels of untreated cells. Cells treated with 500 μM phospholipid followed by filtration showed an increased percentage of the R1 gated population (when compared to control level) for most phospholipids to 1%, apart for DPPC (2%) and DPPS (9%). With the addition of three further PBS wash steps there was a further reduction, such that there was significant ($P>0.05$) difference when compared to the percentage of the R1 gated cell of untreated control cells (Figure 3.9). That confirms the effectiveness of Amicon filtration at removing the toxic effect of

phospholipids and that adding three PBS wash steps further decreases the toxicity of the phospholipids on MDCK cells.

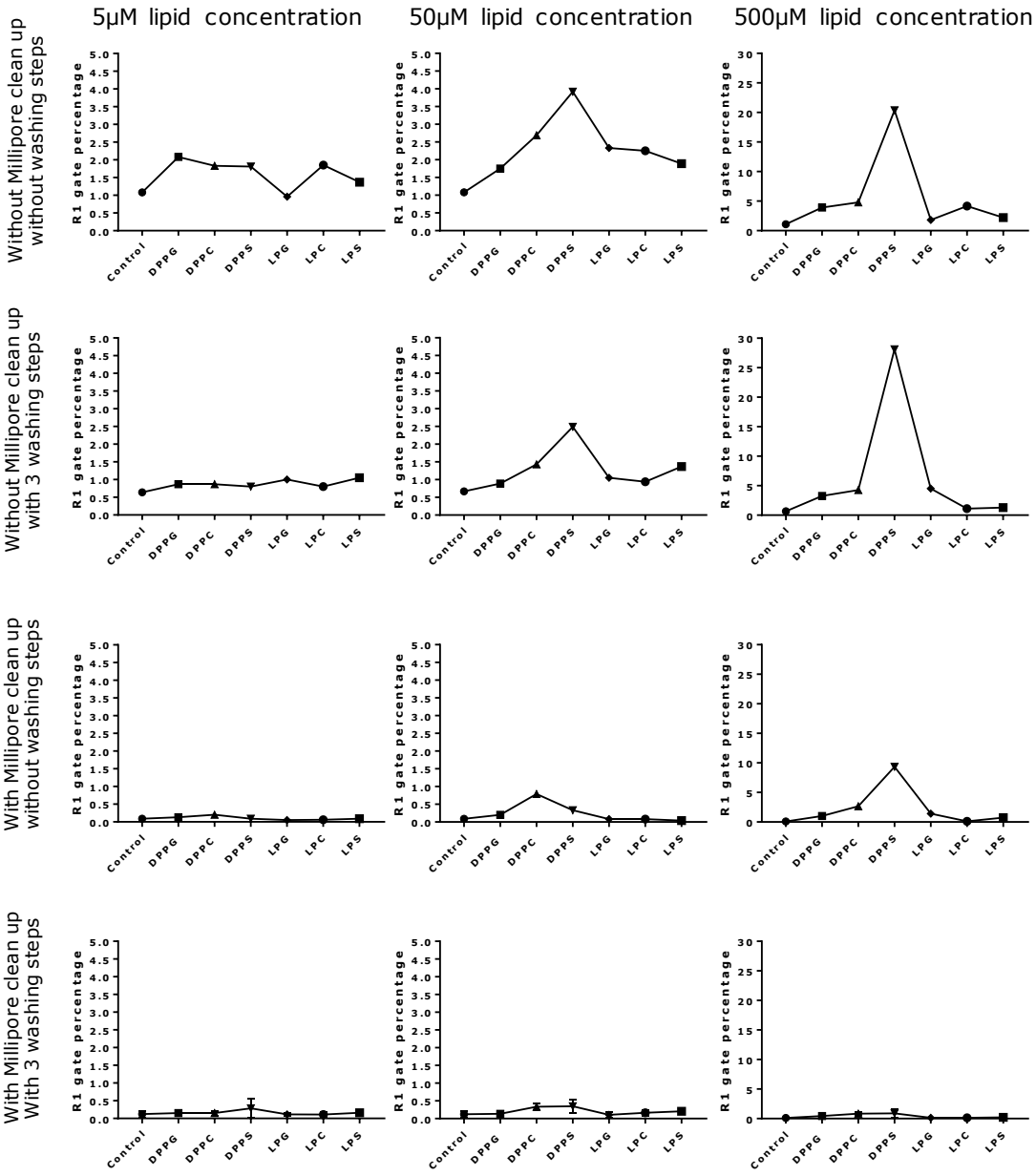

Figure 3:9 Analysis of MDCK cell population size and complexity after pre-treatment with lipids.
MDCK cells were incubated with phospholipids at three different concentrations (5, 50, and 500 µM) with or without Amicon filtration followed or not by three washing steps. 'R1 gate' represent all cells that underwent changes in cell size and complexity by measuring the forward and sideways scatters, respectively.

3.5.4 **Metabolic activity of MDCK cells following phospholipid treatment**

Cell metabolic activity was assessed by measuring the absorbance value of specific colourimetric reagents normalised to the number of adherent cells. MDCK cells were incubated with DPPG, LPG, DPPC, LPC, DPPS or LPS at 5, 50 or 500μM for 30, 60 min or 6 hr. The results showed that there was no significant reduction in metabolic activity when treated and untreated populations were compared using either the MTT assay (Figure 3.10) or the Alamar blue assay (Figure 3.11). However, DPPG and DPPS showed a significant increase ($P<0.05$) in cell metabolic activity compared to untreated cells in a dose dependent manner. Cells treated with 1% triton showed a notable significant reduction in the cell metabolic activity when compared to untreated cells ($P<0.0001$).

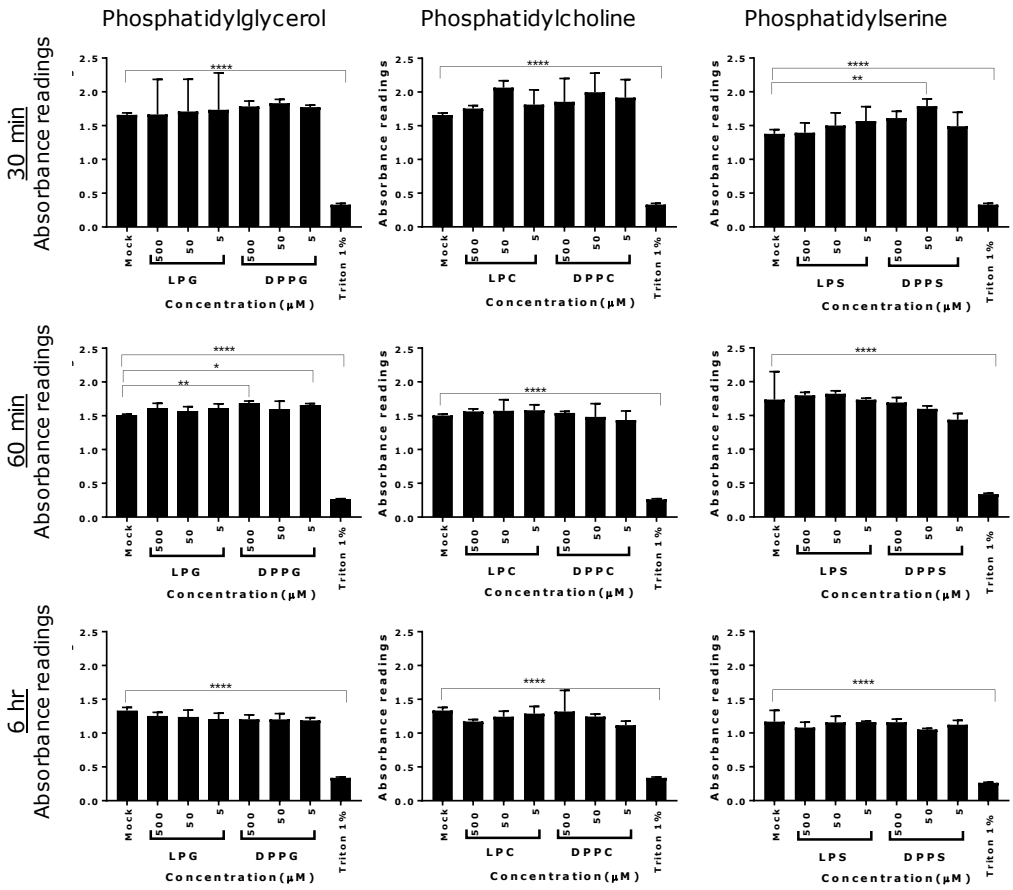

Figure 3:10 Cell metabolic activity of MDCK cells with and without incubation with phospholipids using MTT assay.

Metabolic activity of MDCK cells treated with phospholipids. The data represent the mean of quadruplicate wells; error bars indicate the SD. A significant increase (*P<0.05, **p<0.01) was observed with both DPPG at concentration 5 μM and 50 μM for 60 min incubation and DPPS at concentration 50 μM for 30 min incubation. Triton, as a positive control, showed a significant reduction in cell metabolic activity (**** p<0.0001).

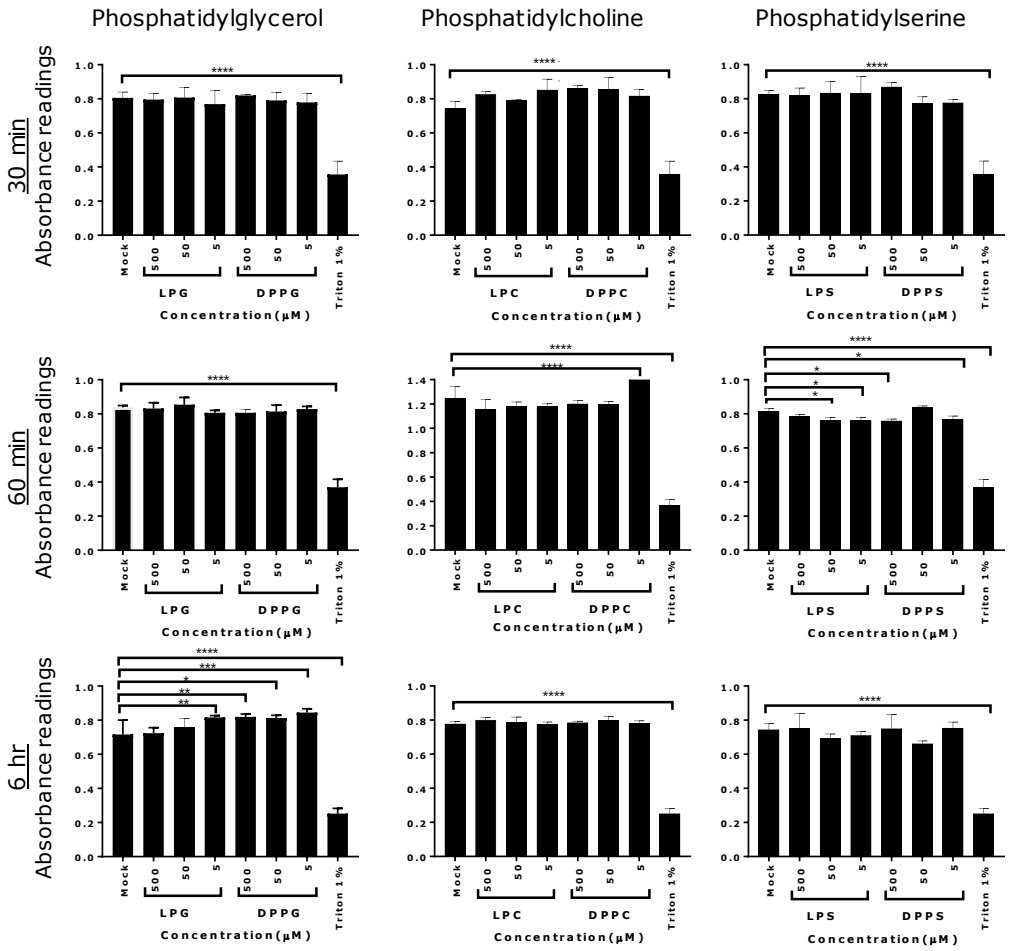

Figure 3:11 MDCK cell metabolic activity with or without phospholipids treatments by Alamar blue assay.
Cell metabolic activity was determined in mock-untreated or treated MDCK cells with different concentrations of phospholipids for 30 min, 60 min, and 6hrs. Alamar blue assay showed that there is no decrease in cell metabolic activity ($p>0.05$; one-way ANOVA). However, 50 μM DPPG at and 5 μM DPPS showed a significant increase in cell metabolic activity (**$p<0.01$), while Triton as positive control showed a significant decrease in cell metabolic activity (**** $p<0.0001$). The data indicate the mean of triplicate well; Error bars show the SD.

3.5.5 **Cell metabolic activity of A549 cells**

A459 cells treated with 1% triton showed, as expected, a significant reduction in metabolic activity ($p<0.0001$). In spite of treated A549 cells with DPPG, LPG, DPPC or LPC for 30, 60 min and 6 hr showed no significant ($p>0.05$) influence of the phospholipid treatment on the cell metabolic activity compared with untreated cells (Figure 3.12).

There was a tendency for 6hrs incubation with 500μM DPPC to decrease cell metabolic activity but this was not statistically significant.

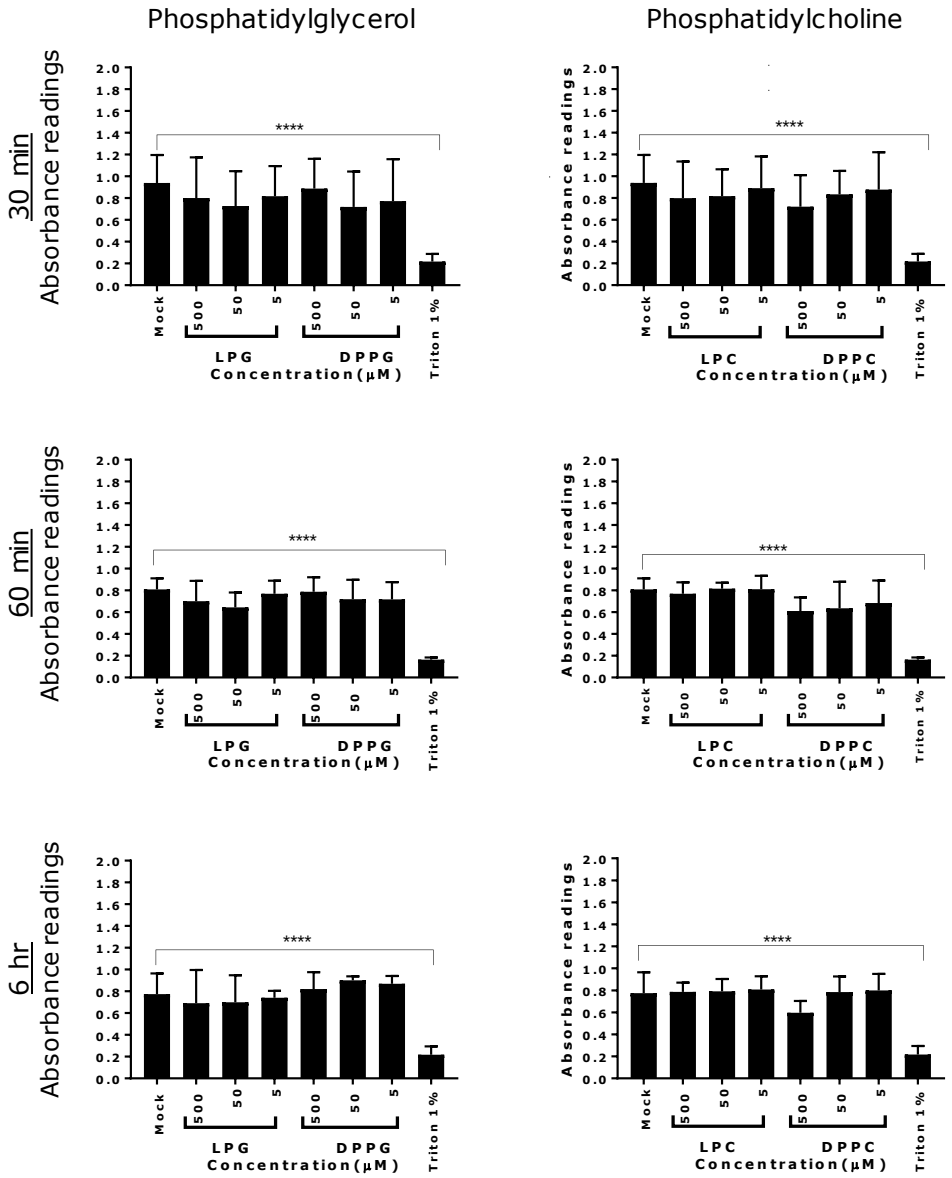

Figure 3:12 Metabolic activity of A549 cells incubated with different phospholipids at different incubation time.
Confluent human lung carcinoma A549 cells with or without treatment with three concentrations of different phospholipids, at different time points. The data represent the mean of quadruplicate wells; error bars show the SD. There was no significant reduction in cell metabolic activity ($p>0.05$; one-way ANOVA). Triton 1% showed a significant reduction in the cell metabolic activity (**** $p<0.0001$).

3.6 Discussion

Chicken RBC was used as a simple system to study the impact of phospholipids on cell shape. Phospholipids were chosen with a range of polar head types and number of aliphatic chains. Results demonstrate that after 5 min of DPPC incubation without Amicon filtration some RBCs were rounder than usual and started to swell while others showed deformity with loss of a clear nucleus after 10 to 20 min. Lysophospholipids had a greater impact probably because they are more soluble due to the presence of a unique aliphatic chain. In this case, RBCs were rounded and deformed at concentrations of 5 and 50 μM. However, we did not obtain a clear view or image of RBCs at 500 μM suggesting that the lipid may have led to cell rupture. In contrast, when the lipids were prepared in the same way but with Amicon filtration, they showed a much lower impact on chicken RBC and only lysophospholipids at high doses had a measurable effect on RBCs.

RBC deformity is mostly related to stress. Indeed, mammalian RBCs deform to take a spherical shape in pathological cases or upon an increase in blood plasma drug concentration (Raut Deepika et al., 2013, Viallat and Abkarian, 2014, Ghosh et al., 2014). Lange and Slayton (1982) mentioned that the endogenous distribution of membrane lipids is key to control of cell shape. This theory agrees with our results where adding a small amount of lysophospholipids,

more prone to solubilisation, show greater impact on RBC leading to changes in shape.

The effect of phospholipids on chicken RBCs was also tested using HA. Data showed that the two aliphatic chain phospholipids had no effect on RBC haemagglutination, even at high concentrations. Meanwhile, lysophospholipids at relatively higher concentrations showed clear lattice formation.

Given the impact that phospholipid had on RBC shape, we also compared the effect of phospholipids on MDCK cells using flow cytometry. The results showed that microfiltration (Amicon filtration) at 5000 xg for 10 mins before treating the MDCK cell suspension for 10 minutes followed by triple washing with PBS reduced phospholipid toxicity and had a much lower impact on the cells. FSc and SSc determined by flow cytometry have already been used to measure apoptosis in cells via their change in size and complexity (Jiang et al., 2016). More specifically FSc and SSc values have been used to determine the impact of polyunsaturated and monounsaturated fatty acids incubation with Jurkat cells (Cury-Boaventura et al., 2004); Gemini-lipid nanoparticles in murine PAM212 epidermal keratinocyte cells which enhanced delivery of skin therapy (Gharagozloo et al., 2015); Lyso-PA as cellular anti-apoptotic factor (Levine et al., 1997). In all these cases a change in cell size, i.e. becoming smaller, with increased complexity is related to reduced cell metabolic activity.

To understand the potential impact of exogenous phospholipids used in this study on relevant cell lines, viability was measured through assessing mitochondrial enzyme activity. Although no reduction in cell viability was detected in these assays following treatment of cells with phospholipids. The results confirmed that microcentrifugation (Amicon filtration) followed by three washing steps did not significantly reduce cells viability when compared to control. The MTT and alamar blue assays were therefore less sensitive than flow cytomtery or use of chicken RBC to detect the impact of phospholipid. However, it was interesting to observe that DPPG at concentrations 5 and 50 μM increased cell metabolic activity. While this has never been shown for DPPG, the ability of specific lipids or fatty acids to improve 'viability' by restoring mitochondrial damage or by changing the biophysical properties of the plasma membrane has been previously demonstrated (Levine et al., 1997, Nicolson and Ash, 2014, Levental et al., 2016).

This method of preparing phospholipids with two steps of Amicon filtration followed by three washing steps to treat influenza virus was used subsequently throughout the experiments.

Chapter 4: Effect of lipids on influenza A virus infection

4.1 Introduction

Influenza A virus is an enveloped, single-stranded RNA virus that enters the host cell endosome mostly using clathrin-dependent receptor-mediated (Sidorenko and Reichl, 2004). Then the acidic pH in late endosomes leads to conformational changes of the HA glycoprotein, which enable virus uncoating.

The genetic and structural components of viral surface glycoproteins affect influenza virus binding to sialic acid receptors on the host cells (Frensing et al., 2016). Influenza virus glycoprotein HA recognises N-acetylneuraminic acid ligands which may differ depending cell type (Critchley and Dimmock, 2004). MDCK and A549 cells are the most suitable cell lines to study influenza virus replication and cytopathic effect (CPE) (Lieber et al., 1976). The CPE of influenza virus infection become notable after 2–48 hours pi as most of the infected cells detach from the culture plate (Daidoji et al., 2008, Tan et al., 2016). The influenza viral genome segments are exported from the nucleus from around 4 hours post infection followed by the consistent release of new virions at 16 hrs which also leads to cell death (Frensing et al., 2016). Thus, early cell apoptosis following influenza viral infection may impair virus replication, whereas late apoptosis following infection increases the release of new virions (Herold et al., 2012).

.

4.2 Influence of host cell lipid during viral infection

The host cell membrane consists of two layers of lipid with embedded proteins. Cell membranes contain 63 types of lipids with 14 different head groups and 11 different tails (Bagatolli et al., 2010, Ingólfsson et al., 2014). The outer layer is mostly enriched in neutral lipids such as PC, SM, and ganglioside monosialic acid (GM), while anionic lipids like PE, PS, and other charged lipids such as PG and PA are mostly present in the inner layer. Cholesterol is distributed symmetrically in both layers (Van Meer et al., 2008). The level of acyl chain saturation and the number of chains per lipid varies between the membrane leaflets, e.g. lysophosphatidylcholine is mostly present in the inner layer (Ingólfsson et al., 2014). The lipid bilayer becomes significantly more ordered and packed in the cell membrane with a higher content of cholesterol. Lipids are also distributed heterogeneously as patches or rafts with a high local density of cholesterol (Ingólfsson et al., 2014).

Lipids contribute to the multiple steps of enveloped virus lifecycle and the reprogramming of host cell lipid synthesis is critical to form a suitable environment to promote virus replication, assembly and release (Chukkapalli et al., 2012, Mazzon and Mercer, 2014). Besides the qualitative difference in the type of lipids between the membrane of the virus and the host cell, the biophysical properties of the membrane such as the fluidity seems to play an important role. Glycolipids and cholesterol are involved in defining the membrane fluidity and the depletion of cholesterol from influenza virus by MβCD

reduces virus infectivity (Sun and Whittaker, 2003, Mazzon and Mercer, 2014). Moreover, cholesterol and negatively-charged phospholipids have been indicated as important for the entry of enveloped viruses. For example, phosphatidylserine is known to be a receptor for vesicular stomatitis virus through interaction with viral glycoprotein G (Carneiro et al., 2006). Pulmonary surfactant acts as a natural defence barrier against inhaled pathogens and 80% of the composition of pulmonary surfactant is made up by phospholipids (Han and Mallampalli, 2015). In order to understand the contribution of different phospholipids to this host defence against viruses, we therefore treated influenza virus with a range of exogenous phospholipids.

4.3 Hypothesis

Treatment of influenza A virus with phospholipids reduces virus infection of permissive cells.

4.4 Aims and Objective

1. To determine the effect of cholesterol depletion using MβCD treatment on influenza A virus infectivity.

2. To determine the impact of exogenous lipid treatment on the infectivity of IAV by pre-incubating avian influenza virus H2N3 with phospholipids. To achieve this, two cell lines, MDCK and A549 were

infected with or without lipids at three different concentrations: 5, 50, and 500 μM.

3. To determine the impact of these phospholipids on the infection of MDCK cells by other influenza A virus subtypes, such as equine influenza virus H3N8 and pandemic influenza virus H1N1.

4. To evaluate the impact of exogenous phospholipids treatment on H2N3 virus infection of MDCK cells 6hr to 72hr pi.

4.5 Material and Methods

4.5.1 Effect of lipid treatment on virus infection

4.5.1.1 Infection of MDCK cells with LPAI H2N3 pre-treated with cholesterol

Confluent MDCK cells were seeded in 12 well plates and infected with LPAI H2N3 at MOI of 1.0 pre-treated with 100μM cholesterol (Avanti, USA) at 37°C for 2 hrs. Cells were also infected with untreated virus. Infections were performed in triplicate. The cells were then washed three times with PBS. Supernatants were collected at 2 hrs, 4 hrs, 6 hrs, 12 hrs, 24 hrs, and 48 hrs post-infection. Supernatants were kept at -80°C before determination of the viral titers. The viral titer in supernatants was determined through the infection of confluent MDCK in 96–well plates. The experiment was repeated three times and immunocytochemical staining of the virus nucleoprotein was performed, as described above, and used to determine the titer of virus (see section 2.3.3).

The CPE of H2N3 virus pre-treated with or without 100μM of cholesterol on MDCK cells was determined by following the morphological changes of the infected cell post-infection of 12, 24 and 48 hrs, using an inverted microscope.

4.5.1.2 **Infection of MDCK cells with IAV H2N3 pre-treated with methyl-beta-Cyclodextrin**

To examine the role of cholesterol in influenza virus infectivity, H2N3 virus was incubated with MβCD (Acros Organics, UK) to deplete cholesterol from the influenza virus membrane (Figure 4.1) in IM (serum-free media). MβCD was incubated with the virus at concentrations: 2.5, 5, 10, 20 or 25mM at 37°C for 30 min prior to ultrafiltration twice using Amicon filtration (as described in Section 2.4) to remove axcess unbound MβCD. Then the virus was reconstituted in IM and incubated for 2 hrs with the cells at an MOI of 1.0 at 37°C. The cells were then washed three times with PBS and incubated in culture media for a further 4 hrs. The cells were then fixed using cold (4°C) 1:1 acetone-methanol for 10 mins and washed with TBS three times. The infected cells were then stained by immunocytochemical staining using the influenza mouse anti–NP antibody (see section 2.3.2).

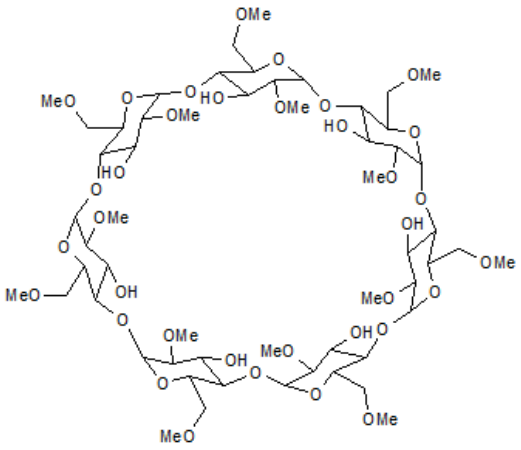

Figure 4:1 Chemical structure of Methyl-beta-Cyclodextrin.
Methyl-beta-Cyclodextrin is composed of seven glucopyranoside units, forming a cone shape.

4.5.1.3 **Phospholipid treatment**

Phospholipids (Avanti polar Lipids, Inc.), DPPS, LPS, DPPG, LPG, LPC and DPPC were prepared at 5, 50, and 500 µM concentrations

4.5.1.4 **Infection of MDCK cells with IAV H2N3 pre-treated with phospholipids for different incubation periods**

The chloroform solvent was evaporated from the lipid samples using a N2 generator. A negative control was prepared by evaporating chloroform in the same manner (e.g. chloroform without lipid). Phospholipids were incubated with LPAI H2N3 for 5 mins, 30 mins, or 2 hrs at 37^{o}C and followed by two washing steps to remove the lipids not bound to the virus using the Amicon ultrafiltration. The viruses were then resuspended in IM and incubated with confluent MDCK for 2 hrs at an MOI of 1.0 at 37^{o}C. Then, the cells were washed three times and incubated in the fresh IM for 4 hrs. The cells were then fixed using ice cold acetone-methanol, followed by immunocytochemical staining against viral nucleoprotein. Finally, the number of infected cells were counted (see section 2.3.3).

4.5.1.5 **Pre-treated LPAI H2N3 with phospholipids for 30 mins and infection of MDCK and A549 cells**

H2N3 virus with or without pre-incubation with DPPG, LPG, DPPC, and LPC at three different concentrations 5, 50, and 500µM for 30 mins at 37^{o}C were used to infect MDCK and A549 cells. An Amicon Ultra-15

filter was used to remove lipids in excess. The resuspended H2N3 virus infected confluent MDCK and A549 cells for 6 hrs pi. Finally, cells were fixed and stained by immunocytochemical staining (see section 2.3.2) and focus forming units of infected cells were measured (see section 2.3.3).

4.5.1.6 Infection of MDCK cells with Influenza Virus A H1N1 and H3N8 pre-treated with phospholipids

Influenza A virus H1N1 and H3N8 at MOI of 1 were pre-treated DPPG, LPG, DPPC and LPC for 30 mins at 37°C. After two washing steps with Amicon filtration, the virus with or without treatment were infected MDCK cells for 6 hrs (see section 4.5.4.4).

4.5.1.7 LPAI H2N3 at an MOI of 0.1 pre-treated with phospholipids followed by MDCK infection

LPAI H2N3 at an MOI of 0.1 was pre-treated with DPPG or LPG at 50 or 500μM for 30 mins at 37°C. Virus was washed twice with Amicon ultrafiltration and incubated with confluent MDCK at 37°C for 2 hrs. Cells were then washed with PBS and re-incubated for 4, 22, 46, or 70 hrs in media. Infected cells were fixed, immunostained for influenza NP and the number of infected cells were counted to measure the ffu/mL value (section 2.3.3).

4.5.2 **Statistical analysis**

Statistical analysis was performed using GraphPad Prism Student (Version 6.07). A T-test was used to analyse the data for H2N3 infection with or without cholesterol treatment, a one-way ANOVA with Turkey's multiple comparisons test was used to analyse data from infection of cells with virus pre-treated with lipid in comparism to untreated virus. Differences were considered significant at p values < 0.05.

4.6 Results

4.6.1 **Determination of multiplicity of infection (MOI) of virus stocks**

Using serial dilutions of virus on confluent MDCK monolayer cells followed by immunocytochemical staining for viral nucleoprotein allowed determination of the MOI of the influenza virus stocks. The lowest dilution causing >95% infection (cells immunostained with influenza NP) was determined to be equivalent to an MOI of 1.0. Uninfected cells showed no evidence of staining (Figure 4.2). This MOI determination was then used for all subsequent experiments.

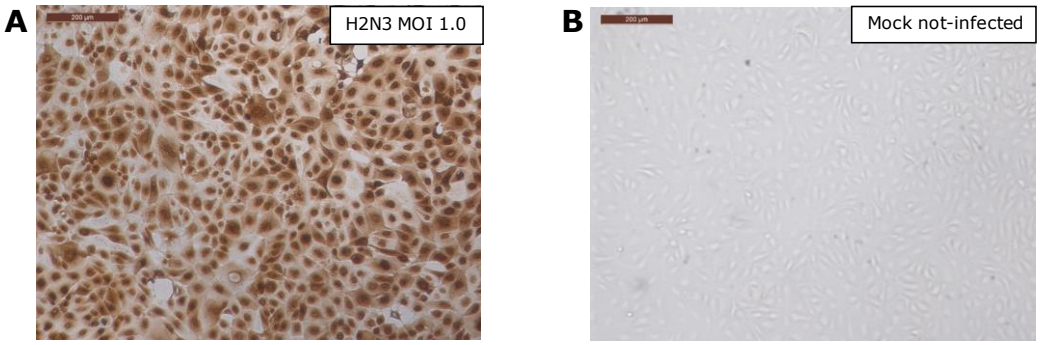

Figure 4:2 Determination of multiplicity of infection (MOI).
MDCK cells infected with H2N3 and immunostained against influenza virus nucleoprotein. A) Positive control with 95-100% infected cells with the lowest dilution defined as an MOI of 1. B) Mock or negative control shows no staining of uninfected cells.

4.6.2 **Effect of pre-treatment of H2N3 with cholesterol on the efficiency of MDCK infection**

The influenza virus infection observed in MDCK cells after H2N3 infection showed a significant CPE that was characterised by rounded cells after 24 hr pi, which became separated from the culture surface,

showing shrinking and necrosis, with large gaps in the cell culture at 48hrs pi. The CPE of the virus was similar in cells that were pre-treated with cholesterol as compared to untreated cells, suggesting no exacerbation of CPE following cholesterol treatment of cells (Figure 4.3).

Figure 4:3 Cytopathic effect of H2N3 with or without cholesterol. The MDCK cells infected with H2N3 with or without cholesterol at various time points (12, 24, 48 hrs) were examined under a light microscope, which revealed morphological changes in both cases. A) The MDCK cells infected with H2N3 without cholesterol. B) The MDCK cells infected with H2N3 co-incubated with cholesterol.

Furthermore, confluent MDCK cells were infected with the influenza virus H2N3 pre-treated with 100 μM cholesterol. The virus titre in cell culture supernatants was measured via focus-forming assay 2–48 hrs pi. The addition of cholesterol had no significant effect on virus replication ($p>0.05$; students t test) at all infection time points of the experiment (Figure 4.4).

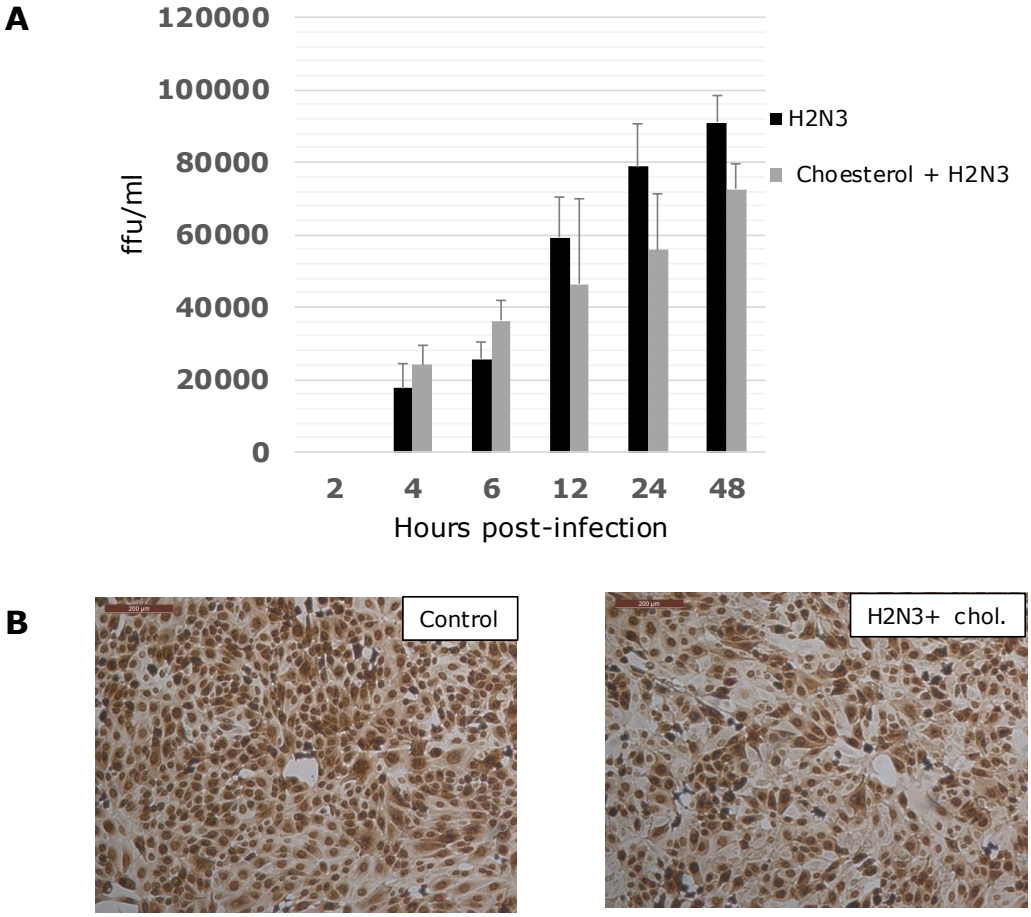

Figure 4:4 H2N3 infectivity when pre-treated with cholesterol. Supernatants were collected 2, 4, 6, 12, 24 and 48 hrs pi. A) Virus titration showed there were no significant differences ($p>0.05$) between MDCK cells infected by LPAI H2N3 pre-treatment with or without cholesterol. The titres were determined via focus-forming assay. B) Immunocytochemical staining with positive control H2N3 without cholesterol and virus pre-treated with cholesterol at 100 µM. Bars show the mean of triplicate infection; error bars indicate the SD.

4.6.3 Effect of pre-treatment of H2N3 with methyl-beta-Cyclodextrin on the efficiency of MDCK infection

LPAI H2N3 was pre-treated with MβCD to deplete cholesterol from the virus. The proportion of infected cells decreased following the treatment with MβCD in a dose-dependent manner ($p<0.05$) (Figure 4.5), with 5 mM MβCD producing >40% reduction in the number of infected cells and further significant reduction to <10% with 25 mM

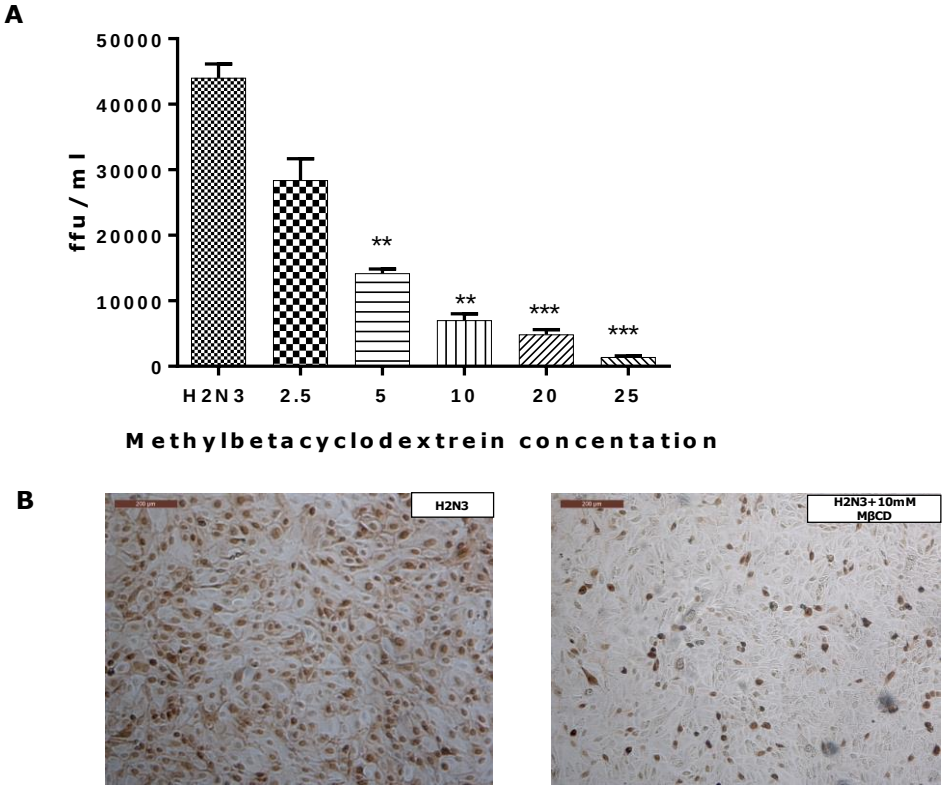

Figure 4:5 Cholesterol depletion via methyl-beta-Cyclodextrin. Pre-treatment of H2N3 with MβCD at different concentrations for 30 min at 37°C prior to infection of MDCK cells for 6 hrs. A) Virus titration showed there was a significant reduction in virus infectivity (**p<0.01, ***p<0. 001; one-way ANOVA), which was dose-dependent. B). Immunocytochemical staining of cells infected with virus pre-treated with 10 mM MβCD and a positive H2N3 control without treatment. Bars show the mean of triplicate infections, with error bars indicating the SD.

4.6.4 **Effect of lipid pre-treatment of H2N3 on MDCK infection**

4.6.4.1 **MDCK infected with LPAI H2N3 pre-treated with 1, 2-dipalmitoyl-sn-glycero-3-phospho-L-serine (DPPS)**

Pre-treatment of LPAI H2N3 with DPPS had no significant effect on the level of infection of MDCK (p>0.05; one-way ANOVA) at concentrations ranging from 5 to 500 μM. The cells infected with either untreated virus or virus treated with DPPS at different

incubation time points showed approximately 100% infection, as demonstrated via the focus-forming assay results. The percentage of infected cells with H2N3 pre-treated at 5, 30 mins and 2 hrs showed no changes between the different time points for each concentration used, i.e. 5, 50 and 500 μM (Figure 4.6). The control sample (chloroform without lipid) incubated with H2N3 virus confirmed that chloroform evaporation using N2 generator did not impact on influenza virus infectivity compared to an untreated virus.

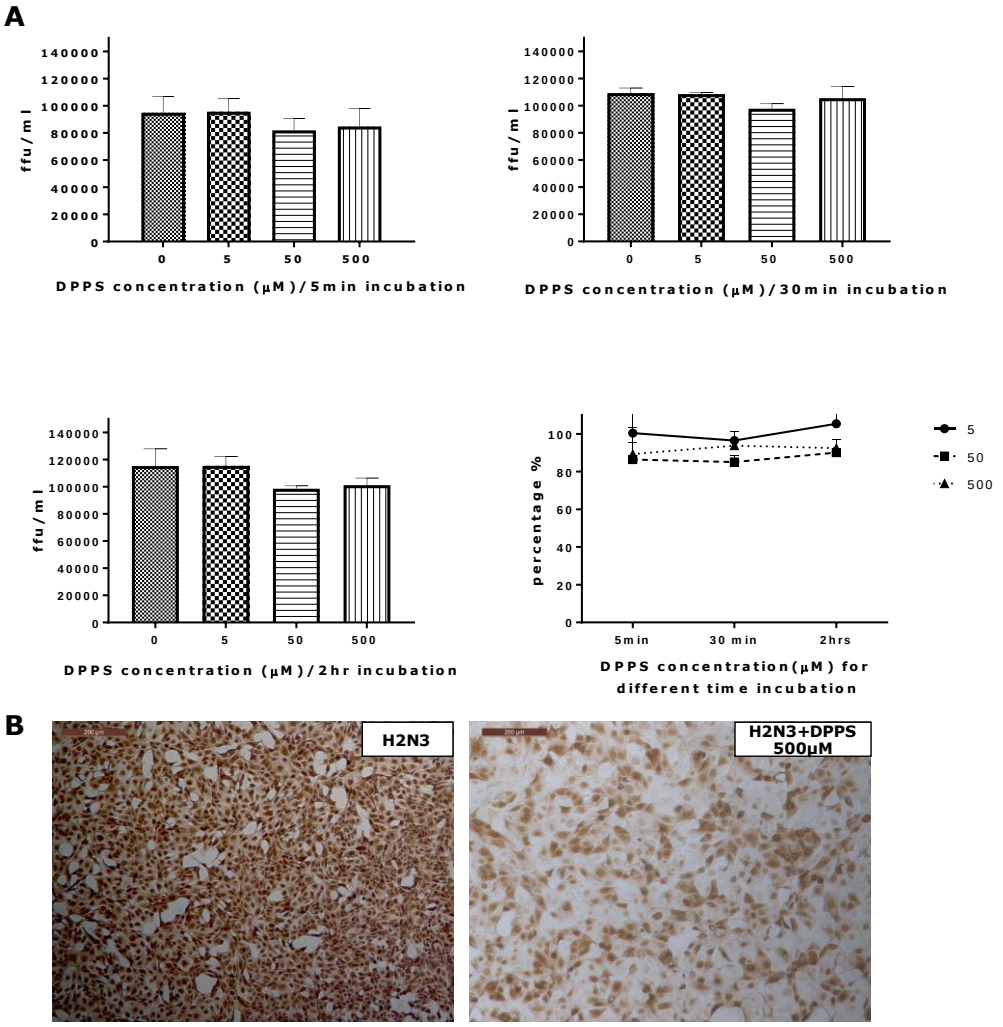

Figure 4:6 MDCK cells infected with H2N3 pre-treated with DPPS. MDCK cells were infected with H2N3 at an MOI of 1.0. The virus was pre-treated with DPPS at different concentrations and cells infected over different incubation times. Six hours pi, the cells were fixed, followed by immunostaining for virus NP. A) Virus titration showed that there was no significant reduction in virus infectivity ($p>0.05$; one-way ANOVA) and no significant decrease between the different incubation times for each concentration ($p>0.05$; one-way ANOVA) the error bars correspond to the SD. B) Immunocytochemical staining with H2N3 without treatment used as positive control and virus pre-treated with 500 µM DPPS.

4.6.4.2 **MDCK infected with LPAI H2N3 pre-treated with 1-palmitoyl-2-hydroxy-sn-glycero-3-phospho-L-serine**

The effect of pre-treatment of H2N3 at an MOI 1.0 with 5, 50 or 500 µM of Lyso PS for 5, 30 mins or 2hr was measured by infecting MDCK cells for 6hrs followed by immunocytochemical staining of cells for virus NP (Figure 4.7). Results reveal that virus infectivity was

significantly reduced in a dose dependent manner ($P<0.05$, one-way Anova) compared with the virus without lipid pre-treatment. Pre-incubating H2N3 virus for 5 mins with 5μM of Lyso PS prior to infecting MDCK cells showed a significant ($P<0.05$) reduction in virus infectivity (from 100% to 76%) which was further enhanced at 50 μM (from 100% to 58 %, $P<0.01$) and 500 μM (from 100% to 17%, $P<0.0001$).

Pre-incubating H2N3 virus for 30 mins with 5μM of Lyso PS showed no significant decrease in virus infectivity, whilst treating H2N3 virus with 50 μM of lyso PS showed a significant reduction ($P<0.0001$) of virus infectivity to 68%. A greater reduction in virus infectivity to 0.3% was seen with 500 μM Lyso PS treatment. Pre-incubating H2N3 virus for 2hr with 5 μM Lyso PS showed no significant reduction in virus infectivity, whilst doing so with 50 μM of Lyso PS reduced the infectivity significantly ($P<0.001$) to 39.7% and the infectivity was further reduced to 7.3% following incubation with 500 μM of Lyso PS.

Analysis of the effect on time of incubation on virus infectivity showed some differences although there were not consistent for each concentration of lipid (Figure 4.7). At 500 μM lipid, incubation was maximal at either 30 mins or 2hrs. At 50 μM, 2hrs incubation led to greater inhibition than 5mins or 30 mins. With 5 μM lipid, incubation for 30 mins reduced infectivity less than with 5 mins or 2hrs incubation.

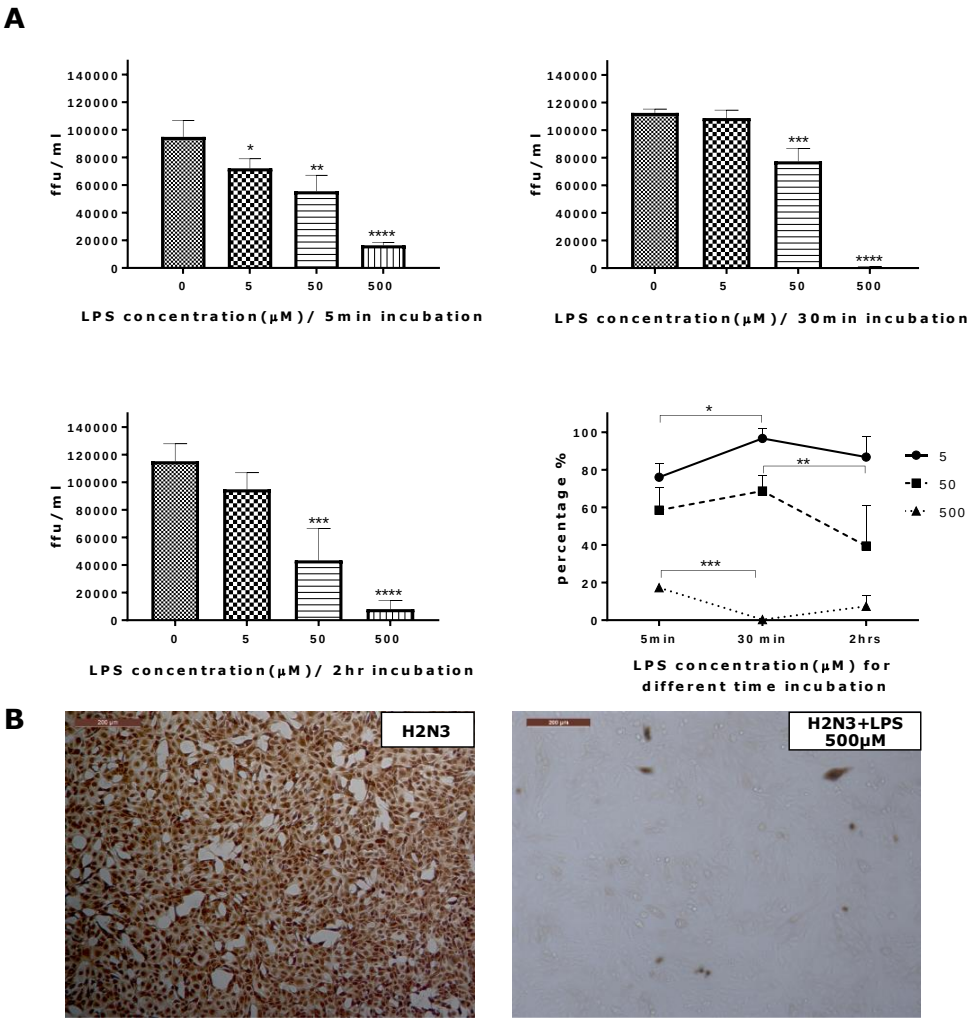

Figure 4:7 MDCK cells infected with H2N3 pre-treated with Lyso PS. H2N3 pre-treated with Lyso PS at different concentrations for 5, 30 and 2 hrs at 37°C were used to infect MDCK cells at an MOI of 1.0. The cells were fixed 6 hrs pi and then immunostained for viral NP. Results show a significant reduction in virus infectivity (*p<0.05, **p<0.01, ***p<0.001; one-way ANOVA). A) Means of triplicate infected wells, with error bars were showing the SD. B) Immunocytochemical staining observed following infection of MDCK cells with H2N3 at an MOI of 1.0 for 6hr without or with treatment with 500µM Lyso PS.

4.6.4.3 **MDCK infected with LPAI H2N3 pre-treated with 1, 2-dipalmitoyl-sn-glycero-3-phospho-(1'-rac-glycerol) (DPPG)**

MDCK cells were infected with H2N3 influenza virus, which was pre-treated with DPPG. Virus treatment with DPPG significantly reduced the number of infected cells forming foci in a dose-dependent manner ($p<0.05$; one-way ANOVA). Pre-incubating H2N3 virus for 5 mins with

5 μM of DPPG showed a significant reduction in the percentage of virus infectivity to 50% and a further significant reduction ($p<0.001$) to 40%, with 50μM of DPPG, and to 30% following DPPG treatment at 500μM concentration. Pre-treatment H2N3 virus for 30mins with 5 μM of DPPG showed a significant reduction of virus infectivity to 53.5% and further a significant reduction of virus infectivity to 40.2% and 32.1% treatment with 50 or 500 μM respectively. Two-hour incubation of H2N3 virus with 5 μM showed a significant reduction to 41% when compared to virus without pre-treatment. Similarly, 50 and 500 μM of DPPG further reduced virus infectivity to 37 and 29% respectively.

No significant difference ($p>0.05$; one-way ANOVA) was observed in the percentage of viral infectivity between different incubation time of H2N3 with DPPG (Figure 4.8).

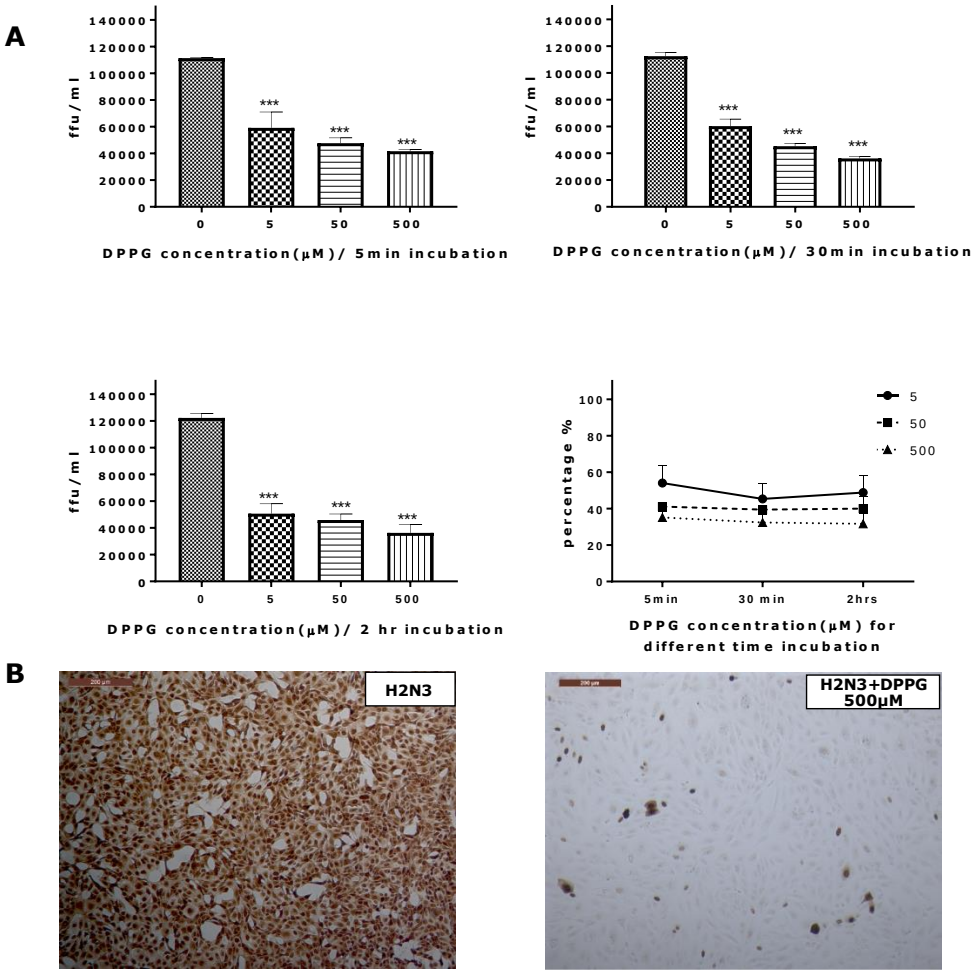

Figure 4:8 MDCK cells infected with H2N3 pre-treated with DPPG.

LPAI H2N3 pre-treated with DPPG at 5, 50 and 500 µM for three different incubation times was used to infect MDCK at an MOI of 1.0. The cells were fixed and immunostained for virus NP. A) Mean focus forming units (ffu) with error bars showing the SD (*p<0.05, **p<0.01, ***p<0.001, one-way ANOVA). B) Immunocytochemical staining with H2N3 without treatment used as positive control and virus pre-treated with 500 µM DPPG.

4.6.4.4 **MDCK infected with LPAI H2N3 pre-treated with 1-palmitoyl-2-hydroxy-Sn-glycero-3-phospho-(1'-rac-glycerol) (LPG)**

Confluent MDCK cells were infected with H2N3 pre-treated with LPG containing only one aliphatic chain, showing the high effectiveness of this lipid in reducing H2N3 infectivity with a near-complete blocking of virus infection at 500 µM. H2N3 pre-treatment for 5 min with 5 or

50 μM of LPG showed a significant reduction ($p<0.05$) in the percentage of virus infectivity to approximately 70 % and a further significant ($p<0.0001$) reduction to around 12% with 500 μM of LPG.

At 30 mins incubation a significant further reduction ($P<0.0001$) in a percentage of virus infectivity was measured to approximately 50% and a further decrease to <10% with 500μM. Pre-treatment of H2N3 virus for 2hrs with 5 μM of LPG showed a significant ($p<0.05$) reduction in virus infectivity to 83% and a further significant reduction ($p<0.01$) of virus infectivity with 50μM to around 65% and to <10% with 500μM ($p<0.0001$). Virus infectivity with LPG overtime demonstrated that the 30 mins time point was significantly lower when compared to 5 min and 2hrs incubation, for 5 and 50 μM of LPG. However, with 500 μM there were no significant differences over the treatment times ($p>0.05$; one-way ANOVA) (Figure 4.9).

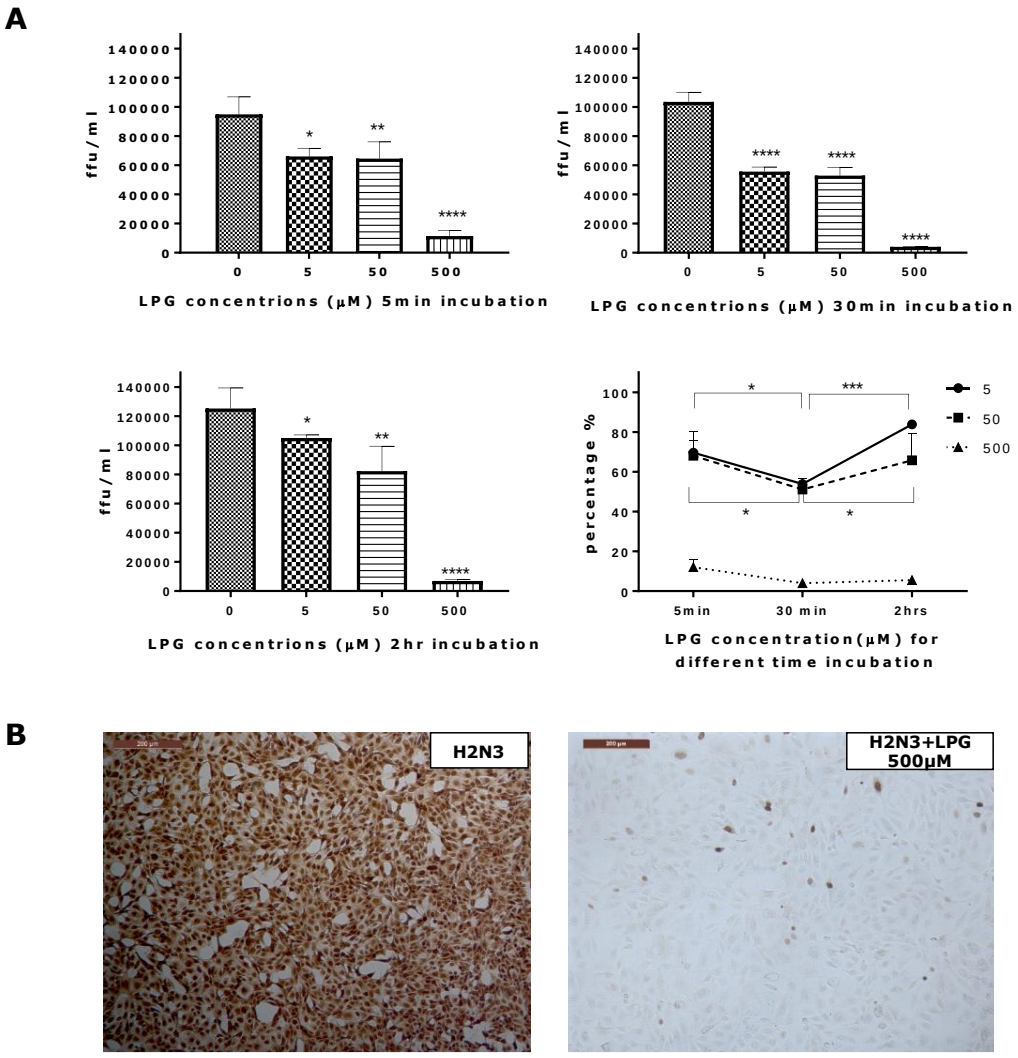

Figure 4:9 MDCK cells infected with H2N3 pre-treated with Lyso PG. LPAI H2N3 at an MOI of 1.0 pre-treated with Lyso PG at 5, 50 and 500 µM concentrations for 5, 30 and 2 hrs at 37°C. A) Virus titration showed a significant reduction in virus infectivity (*p<0.05; **p<0.01; one-way ANOVA) that was dose dependent. B) Example of immunocytochemical with H2N3 without treatment used as positive control and virus pre-treated with 500 µM LPG.

4.6.4.5 **MDCK infected with LPAI H2N3 pre-treated with 1, 2-dipalmitoyl-*sn*- glycero-3-phosphocholine (DPPC)**

Treatment of H2N3 influenza virus with the lipid made of two aliphatic chains, DPPC, for 5, 30min and 2hr showed no significant decrease in virus infectivity ($p>0.05$; one-way ANOVA) when DPPC was used at either 5 or 50 µM. However, a significant ($p<0.01$) reduction in the percentage of virus infectivity to approximately 70% was measured at

both 30mins and 2hrs incubation time for 500 μM of DPPC. Virus infectivity with DPPC overtime demonstrated no significant difference between incubation times for each concentration of lipid (Figure 4.10).

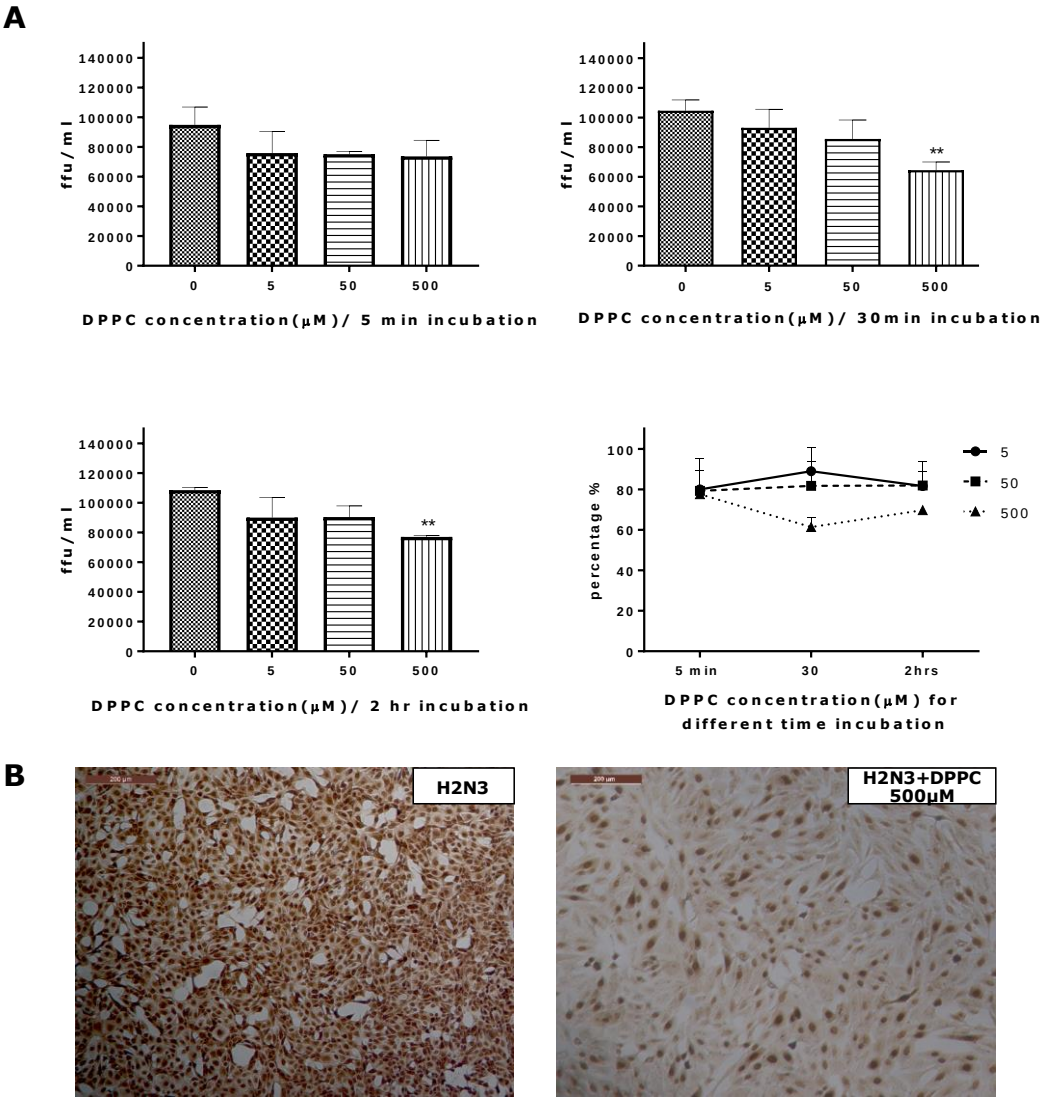

Figure 4:10 MDCK cells infected with H2N3 pre-treated with DPPC. LPAI H2N3 treated with DPPC for different time points, prior to infection of MDCK at an MOI of 1.0. A) Virus titration showing the mean of infected cells with the error bars representing the SD; ffu: focus forming units (**p<0.01; one-way ANOVA). B) Example of immunocytochemical staining with H2N3 without treatment used as positive control and virus pre-treated with 500 μM DPPC.

4.6.4.6 **MDCK infected with LPAI H2N3 pre-treated with 1-palmitoyl-2-hydroxy-sn-glycero-3-phosphocholine (Lyso PC)**

H2N3 influenza, when pre-treated with Lyso PC made of one aliphatic chain, exhibited reduced infectivity ($p<0.05$; one-way ANOVA). Pre-incubating H2N3 virus for 5 mins with 5 μM of Lyso PC showed no significant reduction in virus infectivity, whilst treating H2N3 virus with 50 μM of Lyso PC showed a significant reduction ($p<0.01$) of virus infectivity to 47% and to <10% with 500 μM of Lyso PC ($p<0.0001$). The percentage of virus infectivity was further reduced to approximately 60% with 5 or 50 μM at 30 min and the infection was completely blocked at 500 μM. Pre-incubating H2N3 virus for 2hr with 5 μM showed significant ($p<0.05$) reduction of virus infectivity to 75% and a further reduction ($p<0.01$) of virus infectivity to 57% with 50 μM and to < 10 % with 500 μM ($p<0.0001$). There was no significant influence of incubation times on virus infectivity (Figure 4.11).

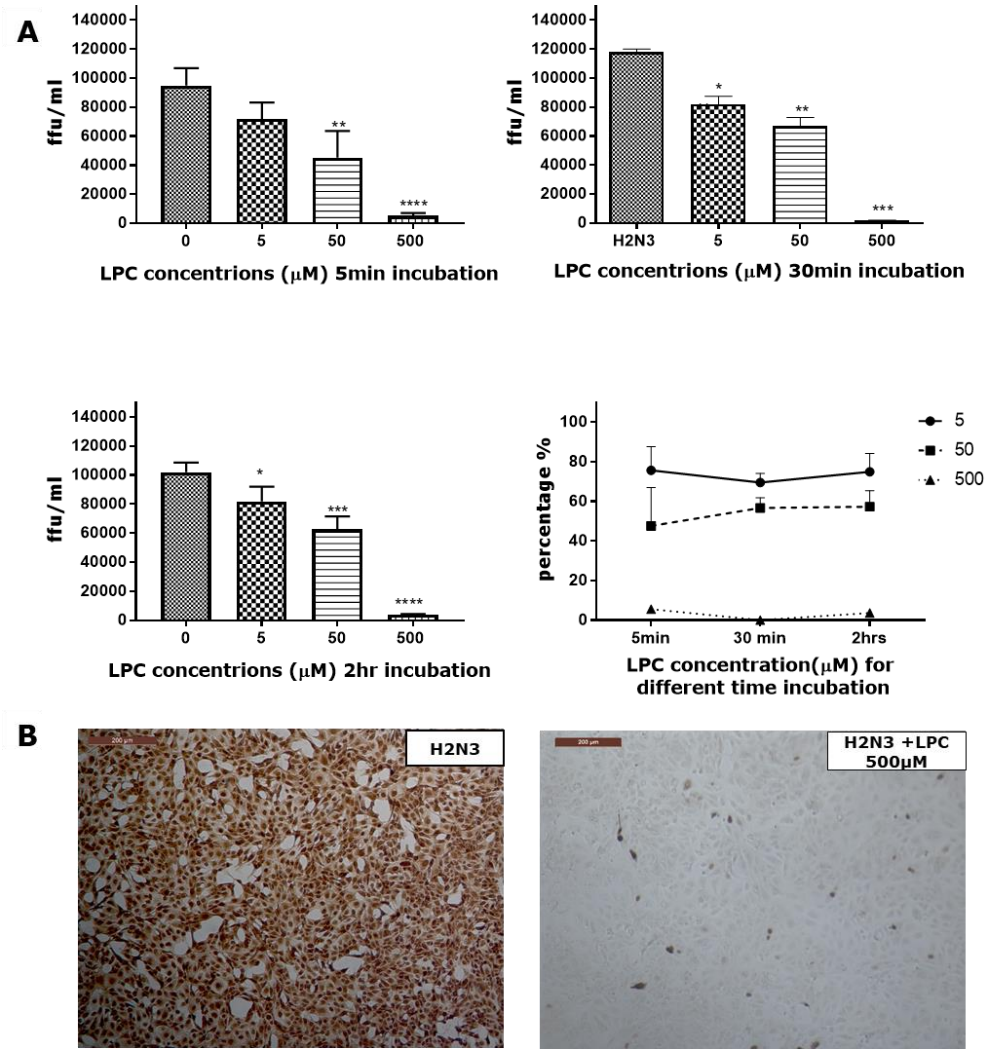

Figure 4:11 MDCK cells infected with H2N3 pre-treated with Lyso PC. The MDCK cells infected with H2N3 at an MOI of 1.0 when the virus was pre-treated with Lyso PC at various concentrations for three different time points. A) Immunostaining of cells showed a significant decrease in the number of infected cells at concentrations above 5 μM (*p<0.05, ***p<0.001, ****p<0.0001; one-way ANOVA). B) Example of immunocytochemical staining with H2N3 without treatment used as positive control and virus pre-treated with 500 μM LPC.

4.6.5 **Effect of phospholipids on H1N1 or H3N8 infectivity**

In order to confirm that the effect of phospholipid treatment was not exclusive to H2N3, the effect of phospholipid treatments on H1N1 and H3N8 were also investigated. Influenza A viruses, AI virus H2N3, pandemic influenza virus H1N1, and equine influenza virus H3N8 were pre-treated with DPPG and LPG for 30 mins, prior to infecting MDCK

cells. Virus pre-treatment with DPPG significantly reduced the number of infected cells in a dose-dependent manner ($p<0.05$; one-way ANOVA) for all the viruses used. More specifically pre-treating IAV with 500 μM of DPPG showed a significant reduction in the percentage of virus infectivity when compared to the untreated virus (H2N3: 32.1%; H1N1: 4.6%; H3N8: 51.2%).

However, the use of LPG at a similar concentration of 500 μM had a much greater impact on infectivity overall (H2N3: 3.5%; H1N1: 1.3%; H3N8: 7.4%). This differential impact between lipid types on viruses seemed to be dose dependent as at a concentration of 5 μM there was no substantial difference between DPPG or LPG on infectivity (DPPG/H2N3: 53.5% & LPG/H2N3: 49.5%; DPPG/H1N1: 71.6% & LPG/H1N1: 76.8%; DPPG/H3N8: 74.4% & LPG/H3N8: 70.6%).

Finally at the intermediate concentration of 50 μM of either DPPG or LPG the results demonstrated that H2N3 was less sensitive to the nature of the lipid used (DPPG/H2N3: 40.2%; LPG/H2N3: 46.9%) when compared to H1N1 (DPPG/H1N1: 46.5%; LPG/H1N1: 5.8%) or H3N8 (DPPG/H3N8: 54.4%; LPG/H3N8: 14.7%) (Figure 4.12).

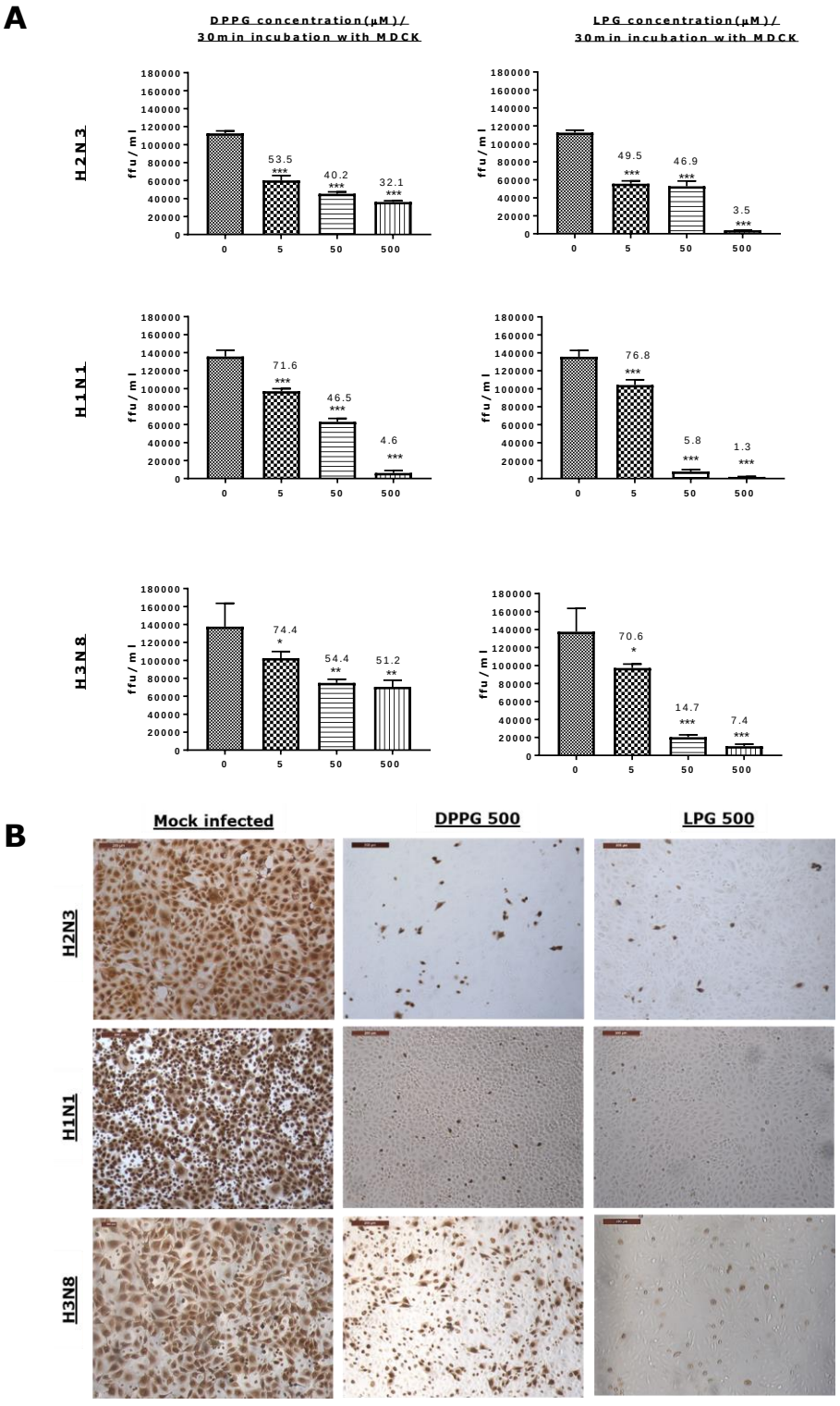

Figure 4:12 MDCK cells infected by influenza A viruses pre-treated with exogenous phosphatidylglycerol.
Influenza viruses H2N3, H1N1 and H3N8 at an MOI of 1.0 were pre-treated with Lyso PG and DPPG at 5, 50 and 500 µM for 30 min at 37°C. A) Focus forming units per ml showed a significant reduction in virus H2N3, H1N1 and H3N8 infectivity (*$p<0.05$; **$p<0.01$, ***$p<0.001$; one-way ANOVA) that was dose dependent with a higher reduction in the percentage of virus infectivity of treated virus compared with the untreated virus. Error bars presenting the SD; ffu/ml. B) Example of immunocytochemical staining.

The table below summarises the results discussed in the section 4.6.5

Table 4:1 Reduction in the percentage of virus infectivity compared to untreated virus (100%)

Phospholipid	Concentration	H2N3 % of virus infectivity	H1N1 % of virus infectivity	H3N8 % of virus infectivity
DPPG	5	53.5	71.6	74.4
	50	40.2	46.5	54.4
	500	32.1	4.6	51.2
LPG	5	49.5	76.8	70.6
	50	46.9	5.8	14.7
	500	3.5	1.3	7.3

4.6.6 **Impact of lipids on H2N3 infectivity of different host cell lines**

To assess whether the results were specific to the cell culture used A549 and MDCK cells were infected with LPAI H2N3 at an MOI 1.0 pre-treated with DPPG and LPG at concentrations (5, 50 and 500 μM) for 30 mins at 37^{o}C. The results revealed that there was a statistically significant reduction in H2N3 virus infectivity following pre-incubation with DPPG or LPG using either A549 or MDCK cells. However, DPPG at concentration 500 μM was more potent at reducing virus infectivity in A549 cells (DPPG/H2N3: 15.5%) when compared to MDCK cells (DPPG/H2N3: 32.1%). However, this difference was reduced at low (5 μM) or intermediate (50 μM) concentrations of DPPG. Likewise,

virus pre-incubated with 50 μM and 500 μM showed to be more effective in reducing virus infectivity in A549 (50 μM of LPG: 5.5%) and (500 μM of LPG: 0.4%) when compared with MDCK cells (50 μM of LPG: 46.9%) and (500 μM of LPG: 3.5%). However, with 5 μM of LPG, no difference was seen between cell types (Figure 4.13).

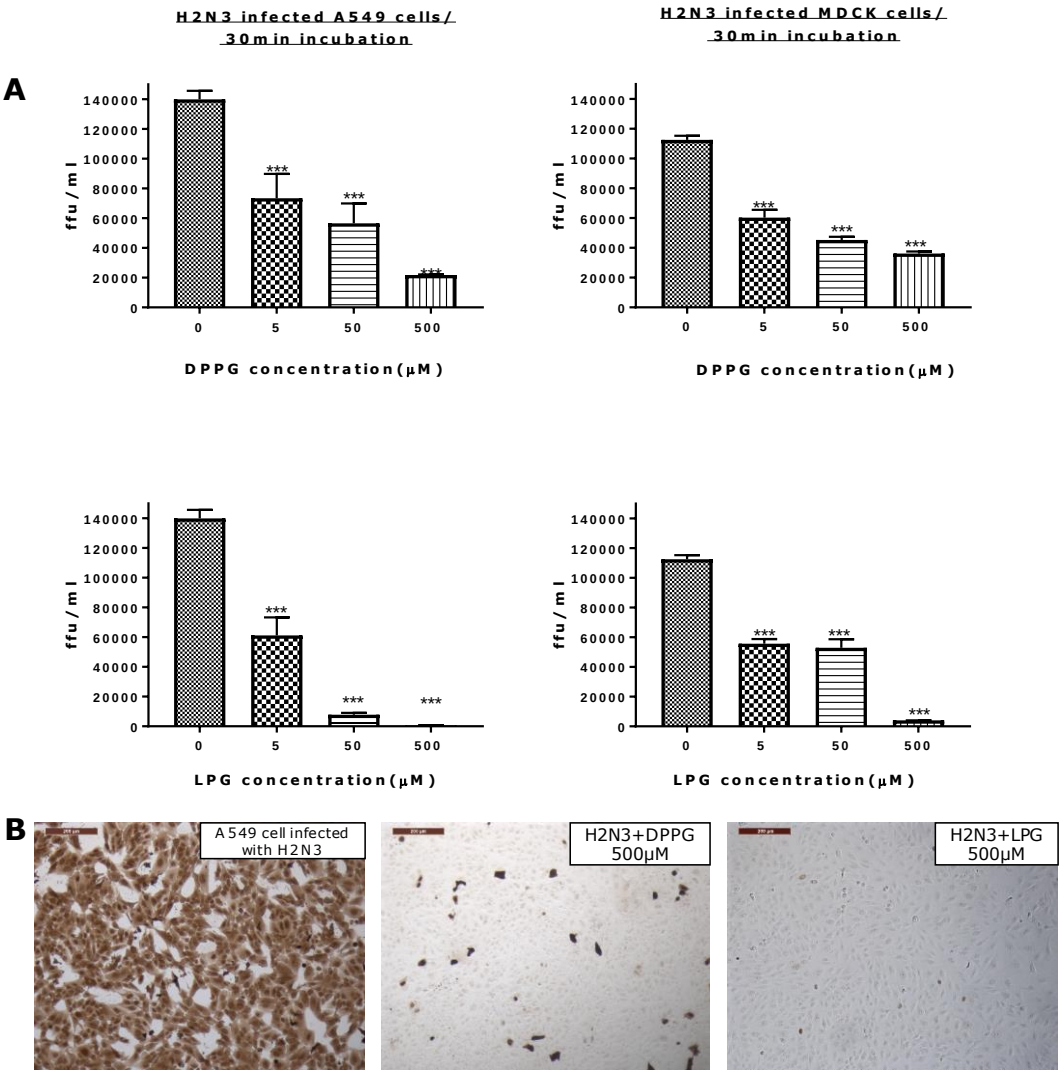

Figure 4:13 A549 and MDCK cells were infected with H2N3 pre-treated DPPG or LPG.

H2N3 virus infectivity at an MOI of 1.0 pre-incubated with phosphatidylglycerol (LPG and DPPG) at 5, 50 and 500 μM in A459 and MDCK cells. The cells were fixed after 6 hrs pi and immunostained for virus NP. A) There was a significant decrease showed in virus infectivity (***$p<0.001$; one-way ANOVA) the error bars indicate the SDs. B) Example of immunocytochemical staining for A549 cells infected with H2N3 pre-treated with 500 μM of DPPG or LPG or with no lipid treatment.

The table below summarises the results discussed in the section 4.6.6

Table 4:2 Reduction in the percentage of virus infectivity

Phospholipid	Concentration	H2N3/MDCK % of virus infectivity	H2N3/A549 % of virus infectivity
DPPG	5	53.5	53.0
	50	40.2	40.0
	500	32.1	15.5
LPG	5	49.5	50.0
	50	46.9	5.5
	500	3.5	0.4

4.6.7 **MDCK infected with LPAI H2N3 at MOI 0.1 pre-treated with DPPG and LPG**

All the previous experiments were carried out following 2 hrs direct incubation with the virus at an MOI of 1 followed by three washes and a 4 hrs incubation time. In order to address the kinetics of infection following a 2 hrs incubation with H2N3, a dynamic study was also carried out to determine whether inhibition of virus growth extended beyond 6 hrs using, an MOI of 0.1. Viral foci were quantified following immunostaining at 6, 24, 48 and 72 hrs pi following infection with H2N3 pre-treated with 50 or 500 μM DPPG or LPG (for 30 mins at 37^{o}C). Despite the low titration of H2N3 (at a MOI of 0.1), the infectivity increased throughout the incubation time for the control. As expected, a lower level infection was measured in the presence of DPPG (500 μM) and LPG (500 μM and 50 μM). The number of focus forming units increased over time in each case (Figure 4.14).

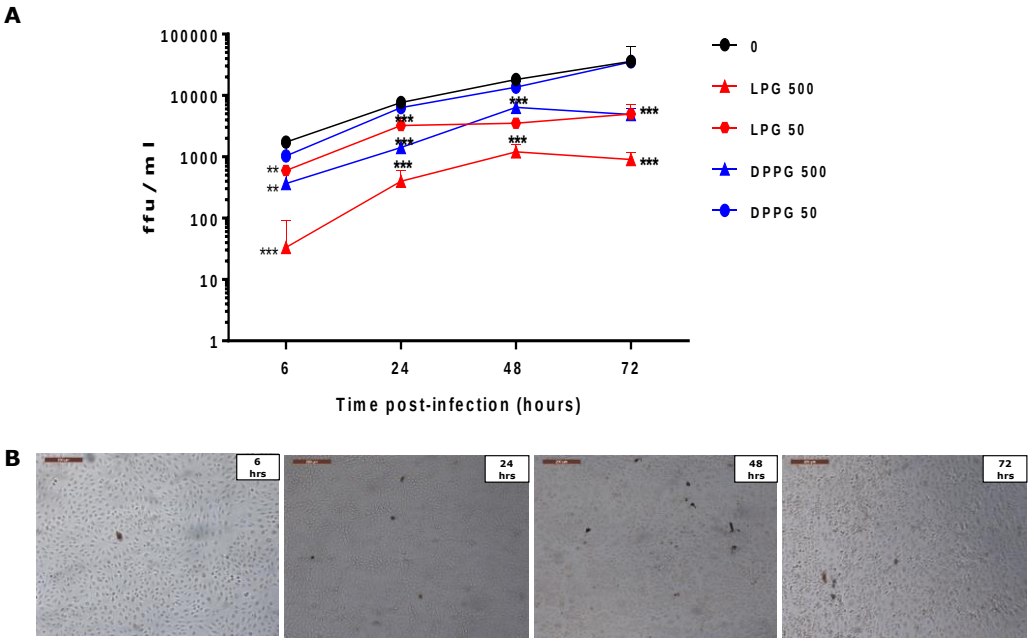

Figure 4:14 LPA H2N3 at MOI of 0.1 with or without pre-treatment with DPPG and LPG infect MDCK cells at different time points.
Confluent MDCK cells were incubated with H2N3 at the MOI of 0.1 with and without pre-treatment with 50 and 500 μM concentrations of DPPG and LPG for 30 min at 37°C. A) Virus titration showed a significant decrease in virus infectivity in a time dependent manner after infection with lipid pre-treated H2N3 compared with notreated virus (**p<0.01, ***p<0.001; one-way ANOVA). The error bars represent the SD. B) Example of immunocytochemical staining.

4.7 Discussion

Our results showed that the addition of cholesterol to MDCK did not affect virus infectivity. In contrast, pre-incubation of LPAI H2N3 with MβCD, with the aim of depleting cholesterol from the virus envelope, showed reduced virus infectivity. Depletion of the cholesterol of influenza viruses disrupts the natural packing of their molecules (López et al., 2011). Cholesterol is essential for the formation of ordered, tightly-packed raft microdomains, and the removal of more than 50% of virus-cholesterol by using MβCD can destabilise the virus structure and permeabilize the virus membrane (Hawkes et al., 2015). Indirect immunofluorescent microscopy of IAV entry following

cholesterol depletion using 50mM of MβCD, showed reduced virus fusion and infectivity after 5hrs post infection (Sun and Whittaker, 2003). Other studies have reported that the influenza haemagglutinin trimers are packed closer together after cholesterol is removed, with the HA trimer-trimer spacing decreasing from 92.6 angstroms to 84.9 angstroms which expands after the re-addition of cholesterol (Dunning et al., 2015).

The addition of exogenous phospholipids of various types had a variable effect on the infectivity of H2N3 on the MDCK cells. LPG, LPC, and LPS were particularly effective at decreasing virus infectivity, in a dose-dependent manner. The change in virus infectivity is dependent on the charge in the phospholipid head and the number of aliphatic chains. Regarding the importance of phospholipid head charge and size, our results have revealed that charged and small lipid heads, such as DPPG, reduced virus infectivity more than when DPPS or DPPC, are used. Furthermore, the addition of lysolipids containing one aliphatic chain had a significant impact on reducing H2N3 influenza virus infectivity in cell cultures, especially at the higher dose of lipids used in this study (500 μM). Another study found that treating MDCK cells using low (200 μg/ml, equivalent to 267μM) or high (1 mg/mL, equivalent to 1335μM) concentrations of POPG (negatively charged hydrophilic domain) inhibited influenza viral infection, reducing virus infectivity by 80% and matrix protein expression by 75%, while palmitoyl oleoyl-phosphatidylcholine (POPC, neutral hydrophilic domain) did not alter the infectivity,

presumably because the two lipids differ in their hydrophilic domains (Numata et al., 2012). Other research has revealed the critical role of pulmonary surfactant phospholipids as a natural barrier, with the presence of PG blocking vaccinia viral infections of Vero cells (Perino et al., 2011).

Phosphatidylserine (PS) has been shown to increase the infectivity of retroviruses. Increasing cell surface levels of PS in human fibrosarcoma cells to 320 μM PS led to an increase in virus infectivity (Coil and Miller, 2005). LPC, on the other hand, with a large head group and one aliphatic chain forming a positive curvature in the outer domain of lipid bilayer, is thought to inhibit the negative curvature needed for the inward budding of viruses to occur (Ciechonska and Duncan, 2014).

Phosphatidylglycerol showed a significant influence in reducing the infectivity of influenza A viruses H2N3, H1N1, and H3N8. Phospholipid DPPG significantly reduced the virus infectivity in a dose-dependent manner, however, the use of DPPG on the filamentous virus showed less reduction than that of H2N3 and H1N1. 500μM of lyso PG showed a greater decrease in influenza A virus infectivity by nearly completely blocking H1N1, H2N3, and H3N8 virus infectivity at 500 μM.

Phospholipids of influenza A viruses are derived from the host cell but different in term of composition. The most dominant lipid composition of the host cell membrane is PC while in purified influenza virus PE

and PS become the most abundant phospholipids. However, the lowest lipid concentration measured in the IAV lipid envelope were PG and LPG (Ivanova et al., 2015), which could explain why those lipids have a greater impact in reducing the viral infectivity. Our study observed that two different cell lines A549 and MDCK cells showed reduced infection with LPAI H2N3 after treatment with LPG and DPPG at 500 μM but it was more marked in A549 than MDCK cells suggesting some differences in the receptor/binding characteristics between these cell lines.

Chapter 5: Impact of lipid on virus morphology and size determined by transmission electron microscopy

5.1 Introduction

5.1.1 IAV morphology

Influenza viruses are enveloped viruses and are composed of two layers. The internal layer comprises the viral genome and RNP complex. This layer is surrounded by the external layer, containing the viral glycoproteins HA and NA and the channel protein M2 in the virus envelope. Both layers, external and internal, incorporate the M1 protein (Treanor, 2014, Zhirnov and Manykin, 2015). Electron microscopy has allowed the characterisation of the morphology of influenza virus, which typically exhibits one of two structures: (i) 100–300 nm diameter spherical virions (Ozawa et al.) and (ii) filamentous virions reaching a length up to 20 μm (Treanor, 2014, Zhirnov and Manykin, 2015). Cryo-electron tomography has shown that influenza A virus H3N2 demonstrates a variable morphology, from spherical to elongated, with spikes of viral glycoproteins in the outer surface of virions. Underneath these spikes, there are two layers with similar density: the lipid envelope and M2 protein. The core of virion particle contains viral RNPs arranged in seven to eight loops. In the filamentous virion, RNPs look more ordered forming parallel bundles having similar endings to matrix proteins. However, RNP in a spherical virion appears less ordered and more dispersed in the virion core. The outer spikes of both HA and NA appear in cryo-electron tomography as having different surface densities with NA being longer with a shorter bulging head (Harris et al., 2006). RNP structure variations in influenza virus might be a result of pliable nucleoprotein interaction;

electron tomography images show RNP segments of filamentous influenza virus with variant length and curvature (Gallagher et al., 2017).

EM can be used to study virus entry, trafficking, assembly and virus budding (Harris et al., 2006). Negative staining using transmission electron microscopy (TEM) can be used to assess virus morphology accurately, for example, avian influenza virus H5N1 which consists of spherical particles of diameter ranging between 80–120 nm with viral glycoprotein spikes on the particle surface (Sarachai et al., 2014). Environmental factors such as acidic medium and lipid membrane (Zhirnov and Manykin, 2015) as well as host cell factors play a critical role in determining influenza virus morphology.

5.1.2 **Sample preparation for negative staining**

Negative staining was first used in 1959 by Sydney Brenner and Robert W. Horn, who established the negative staining process for viruses (Harris, 2015). Virus specimens detected by EM are mostly derived from body fluids, which can be processed within a few minutes through the negative staining technique. Low-speed centrifuging at 2000 x g/5 mins is used to spin large particles, while supernatant is placed on the grid for 10–15 mins. The concentrated virus is mixed with water in an ultracentrifuge to obtain a clear image (Goldsmith and Miller, 2009). However, it is necessary for influenza virus grown in eggs to be centrifuged at 20000 x g in order to remove cell debris

and virus aggregates in samples (Fera et al., 2012). It was reported that influenza virus morphology changed with ultracentrifugation of the sample to increase the concentration of virions for the negative staining. Prior fixation of the virions with glutaraldehyde or osmium tetroxide reduced the impact of the ultracentrifuge on the change in virus morphology (Sugita et al., 2011). One the other hand, concentrating the sample by centrifugation increased the ability of EM to detect small amount of virus (Schramlová et al., 2010). EM images with negative stain will appear as light images with darkness surrounding the virus (Harris, 2015). Determining the type of negative stain that should be used depends on different parameters. For instance, 0.01–2% uranyl acetate works as a fixative and a precipitate in the presence of phosphate salt, while ammonium molybdate forms granules that help clarify some details. Moreover, staining with 1–2% phosphotungstic acid (PTA) can break down some viruses if the imaging is not done within a few hours; at the same time, it does not precipitate in presence phosphate salts, and the spikes of enveloped viruses are outlined without causing positive staining, as with uranyl acetate (Goldsmith and Miller, 2009). Immunological procedures that use gold-labelled antibody can provide results that are more visible to confirm detection of specific viruses or virus structure (Fera et al., 2012).

5.2 Hypothesis

We hypothesise that treatment of influenza viruses H2N3 and H3N8 with exogenous lipids may affect virus morphology.

5.3 Aim and objectives

This study sought to examine cell culture supernatant using TEM with negative staining, in order to identify LPAI virus H2N3 and H3N8 morphology before and after treatment with exogenous lipids.

5.4 Material and Method

5.4.1 Viruses

Low pathogenic avian influenza (LPAI) virus H2N3 and equine influenza virus H3N8 (see section 2.1.1) were used for experiments described in this chapter.

5.4.2 Virus infection of MDCK

MDCK cells were seeded in a T75 flask (Nunc) in Dulbecco's modified eagle's medium (DMEM), containing 10% fetal calf serum (FCS) and 1% penicillin/streptomycin. The cells were incubated at 37°C and allowed to grow to 95% confluence. The cells were washed three times with phosphate-buffered saline (PBS, Invitrogen) and infected with either H2N3 or H3N8 at a multiplicity of infection (MOI) 1 in 10 mL of IM. Infected cells were incubated at 37°C for 2 hr, rinsed three times with PBS, and reincubated in 10 mL of IM at 37°C with 5% CO_2 for 70 hr. At 72 hr pi, the supernatant of the infected cells was harvested, aliquoted into cryovials (Nunc) and stored at –80°C prior to processing for EM.

5.4.3 Processing the supernatant for transmission electron microscopy

The virus-containing supernatant was clarified by centrifugation at 12000 x g for 2 mins. In order to examine the effect of phospholipids

on the morphology of LPAI-H2N3 and H3N8, the viruses were treated with a selection of phospholipids (Avanti Polar Lipids, Inc.), including LPG, LPC, DPPG and DPPC.

Lipids were prepared at two concentrations (50 and 500 μM), followed by sonication using an ultrasonic bath (as described in section 2.4). The lipid solution was then incubated with influenza A viruses H2N3 or H3N8 for 30 min at 37°C. Virus stability for TEM was increased by using holey carbon support film with 3.05-mm copper grids including 300 hexagonal mesh (EM Resolution, UK). For the examination, 10 μL of the supernatant of infected cells was deposited onto the grid and left for 10 mins; then, filter paper was used to remove any excess of the viral suspension. An ultraviolet (UV) stimulator (254 nm/20 min; Flowgen, UK) was employed to deactivate the sample and enhance virus adhesion to the grids (Goldsmith and Miller, 2009). The film was stained with 10 μL negative stain containing 2% PTA at pH 7.4 (Sigma, UK) for 30 s; excess stain was removed using filter paper. The grids were then left at room temperature (RT) for 30 mins to dry before the Tecnai G212 Bio Twin Digital TEM System was used to image the samples from different areas of the grids (Figure 5.1).

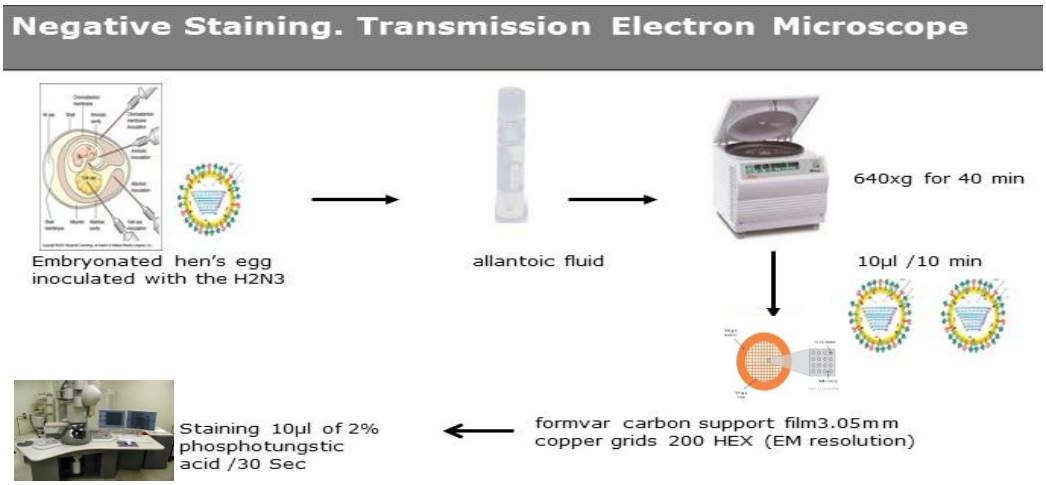

Figure 5:1 Negative staining of the influenza A virus with or without pre-treatment with phospholipid.

The size and dimensions of influenza virus H2N3 pre-treated with or without two concentrations of phospholipids (50 and 500 µM) were measured using Image J (Image J 1.47v, National Institute of Health, USA). The aspect ratio of viruses, namely the ratio between the apparent short axis (noted: diameter (D)) and long axis (noted: length (L)), (Figure 5.2) was assessed for 18-20 virus particles for each untreated and treated virus.

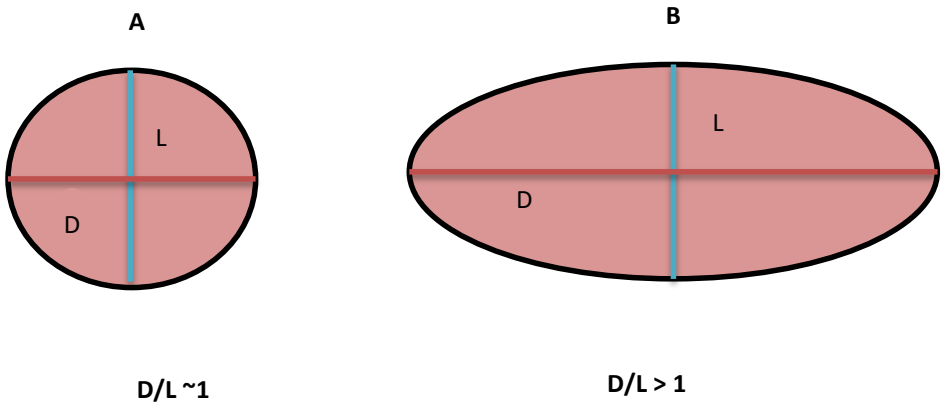

Figure 5:2 Diameter and length axis measurements
The measurement including both diameter (D) and length (L), was carried out using Image software. (A) Particles with an asymmetrical size of approximately 1, and (B) Particles in which one particle axis is longer than the other such that the D/L ratio is more than 1.

5.5 Results

Influenza A viruses H2N3 and H3N8 were imaged with EM in the absence of phospholipid to determine normal virus morphology before imaging following phospholipid treatment.

5.5.1 The morphology of avian H2N3 and equine influenza virus H3N8

H2N3 virus harvested from MDCK supernatant appeared spherical to slightly elliptical with a diameter ranging from 100 to 120 nm, with clear visible surface spikes (Figure 5.3).

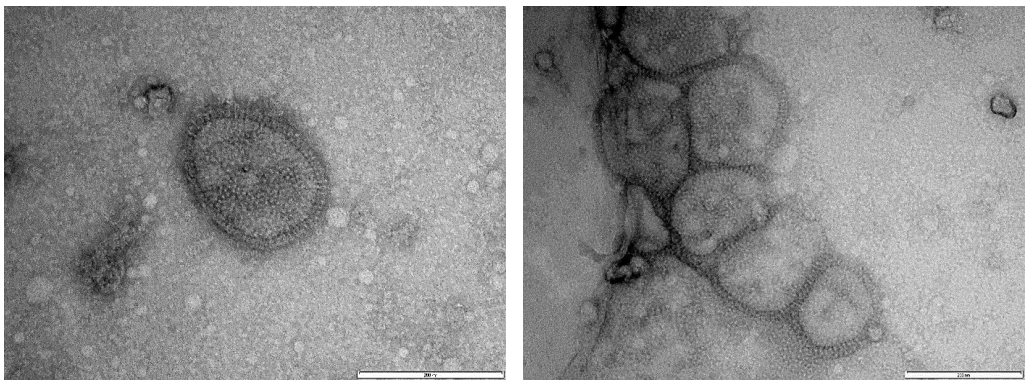

Figure 5:3 Negative staining (TEM) of LPAI H2N3 virus.
Electron microscopy images reveal spherical particles with clearly visible surface spikes (scale bar 200 nm).

In contrast, and as expected, H3N8 virion particles mostly showed the filamentous morphology of various length and diameter, with noticeable viral glycoprotein spikes around the outer surface of the virion (Figure 5.4).

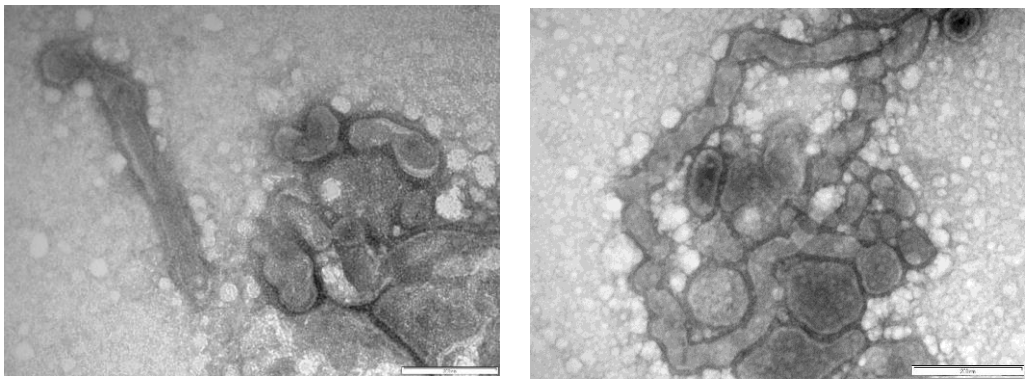

Figure 5:4 Negative staining (TEM) of the LPAI H3N8 virus. Filamentous particles with clearly visible surface were observed by EM within the supernatant of infected MDCK cells at 72 hr postinfection (scale bar 200 nm).

5.5.2 **The morphology of H2N3 and H3N8 pre-treated with exogenous phospholipids**

The morphology of LPAI H2N3 and H3N8 viruses was assessed by EM after treatment with phospholipid at either 50 or 500 μM.

5.5.2.1 **H2N3 and H3N8 pre-treated with phospholipids at a concentration of 500 μM**

Images taken using EM of avian influenza H2N3 virions pre-treated with phospholipids showed changes in the virus morphology. H2N3 virus pre-treated with LPG demonstrated either virus enlargement with what looks resembled disrupted virion membrane (Figure 5.5 A) or single virions surrounded by liposomes (Figure 5.5 B). Pre-treatment with LPC showed viruses with enlarged size (Figure 5.5 C) with an uneven surface distribution of what looks like glycoprotein spikes (Figure 5.5 D). Similarly, H2N3 virus pre-incubated with DPPG showed a number of fused and enlarged virions (Figure 5.5 E) with

an uneven distribution of glycoprotein spikes in some parts of virion where it bound with liposomes (Figure 5.5 F). H2N3 virions pre-treated with DPPC demonstrated virions interacting with liposomes (Figure 5.5 G), with a change in the virus morphology and some perturbation of the surface distribution of HA (Figure 5.5 H).

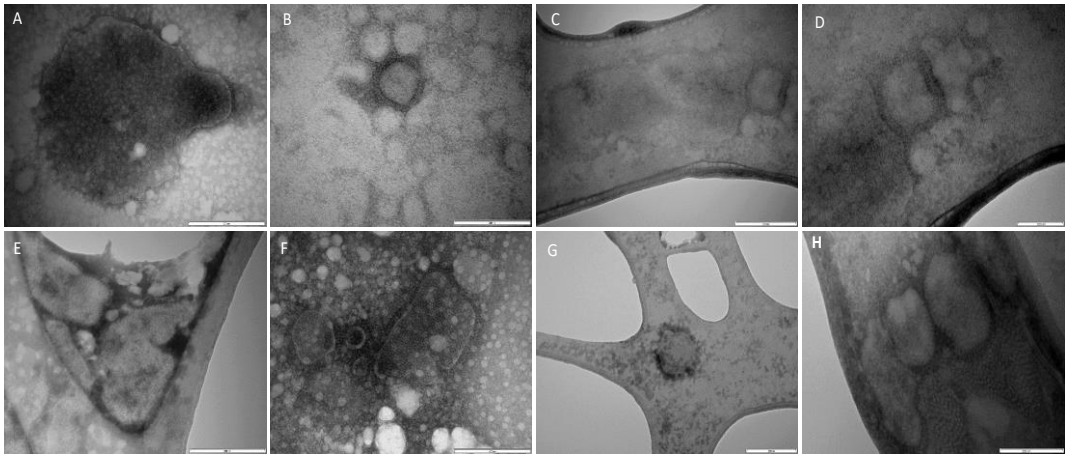

Figure 5:5 TEM images of H2N3 virus pre-treated with 500 μM of phospholipids.
Images A and B show H2N3 virus pre-treated with LPG indicating the enlarged size and surrounded by liposomes. Images C and D show the changes in virus morphology after pre-treatment with LPC. Images E and F show H2N3 that is pre-incubated with DPPG with a number of fused and enlarged virions. Images G and H show H2N3 virions pre-treated with DPPC, demonstrating virions interacting with liposomes, with a change in virus morphology (scale bar 200 nm). These images are representative of three independent experiments.

The negative staining of equine influenza virus H3N8 pre-treated with 500 μM LPG or LPC was difficult to image; possibly due to a disintegration of virions associated with marked damage to the viral membrane. In images A-D (Figure 5.6) some virions showed interaction with liposomes and membrane spikes are also unclear following lipid pre-incubation. In addition, virus that was pre-treated with DPPG showed observable change in virus morphology (Figure 5.6

E) and extensive fusion with liposomes (Figure 5.6 F). H3N8 treated with DPPC showed filamentous virus surrounded by liposomes (Figure 5.6 G). DPPC appeared to have less impact on virus morphology (Figure 5.6 H) when compared to LPG, LPC or DPPG phospholipid.

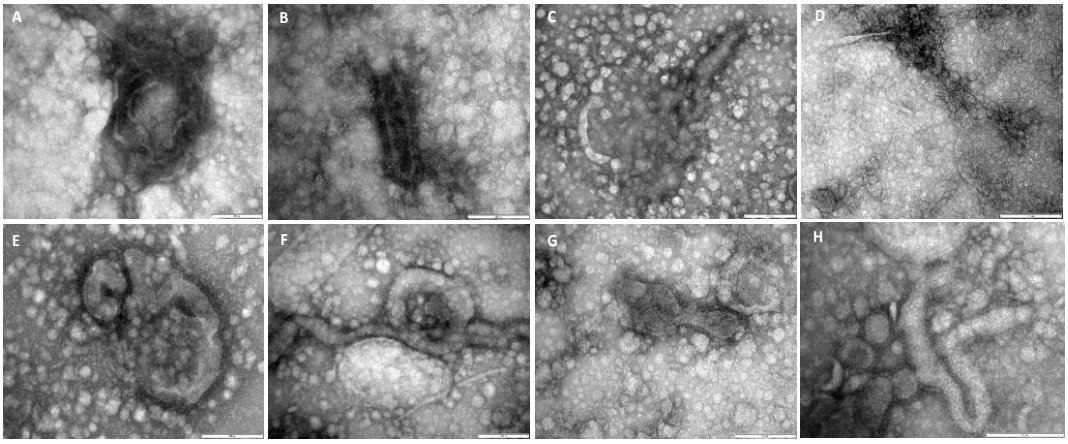

Figure 5:6 TEM images of the H3N8 virus pre-treated with 500 µM of phospholipids.
Images A and B show equine influenza H3N8 virus pre-incubated with LPG. The virions seemed to burst and are surrounded by a number of liposomes. Images C and D indicate filamentous H3N8 pre-treated with LPC, with changes in virus morphology including membrane rupture in some parts of the virus. Images E and F show an alteration in virus shape and bound liposome with virus pretreated with DPPG. Pre-incubated H3N8 virions with DPPC in images G and H represent filamentous virus particles rounded by liposomes, an observable change in virus morphology (scale bar 200 nm). These images are representative of three independent experiments.

5.5.2.2 **H2N3 and H3N8 pre-treated with phospholipids at a concentration of 50 µM.**

Influenza A viruses H2N3 and H3N8 were negatively stained and processed for TEM after pre-treatment with a 50 µM of phospholipid for 30 min at 37°C. The results of pre-treatment H2N3 virus with LPG showed a large aggregation of virus, surrounded by liposomes (Figure 5.7 A-B). Additionally, some virions pre-treated with LPC showed a change in virus morphology surrounded by liposomes (Figure 5.7 C-D). Some virions showed neck-like structures. H2N3 virus treated

with DPPG (Figure 5.7 E-F) or DPPC (Figure 5.7 G-H) showed some virions fused with liposomes with unclear visible influenza glycoprotein spikes while others showed no change in virus morphology.

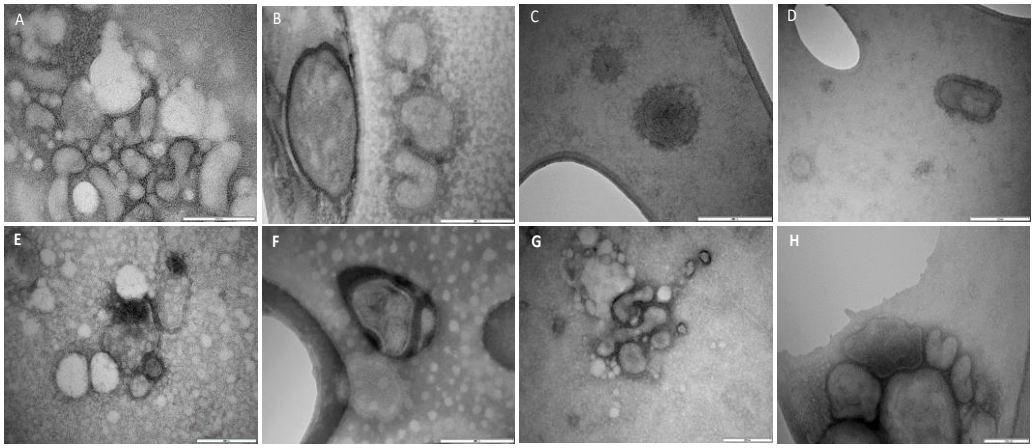

Figure 5:7 Negative staining of influenza virus H2N3 pre-incubated with 50 μM of phospholipids.
In TEM, images A and B, LPAI H2N3 was pre-treated with LPG; a large aggregation of virions and some virions forming a neck-like structures are visible. In images C and D, H2N3 is treated with LPC showing smaller virions surrounded by lipids. In images, E and F, the virions treated with DPPG showed virions fused with liposomes and a change in virus shape. Images G and H present virions treated with DPPC; some virions are fused with liposomes and showed an irregular shape (scale bar 200 nm). These images are representative of three independent experiments.

Similarly, TEM images of H3N8 virus pre-incubated with 50 μM show the effect of phospholipids on virus morphology and viral glycoprotein distribution. Images of H3N8 virus treated with LPG, LPC, and DPPG showed swelling and bulging in some parts of virus particles, fragmentation, and alteration in the virus particle morphology. Altogether, treated virions were mostly fused with liposomes with unclear spikes. DPPC did not show much change in virus morphology (Figure 5.8).

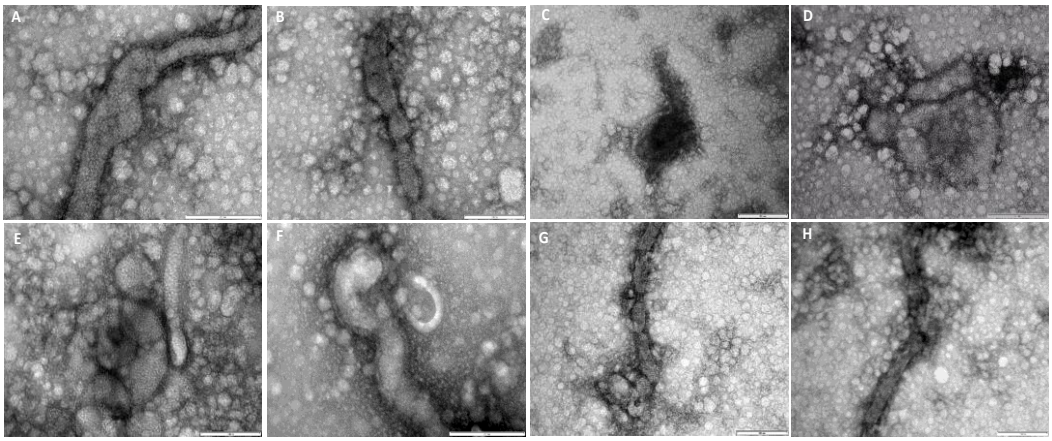

Figure 5:8 Negative staining of H3N8 equine influenza virus pre-incubated with 50 μM of phospholipids
Low pathogenic equine influenza virus was incubated with 50 μM phospholipid. In images A and B, H3N8 virions were incubated with LPG; liposomes surrounded and fused with virions caused a change in virus morphology. In images C and D, H3N8 was incubated with LPC, showing complex virion morphologies with an irregular distribution of influenza glycoproteins. Images E and F show virions treated with DPPG, with virions and liposomes interacting and associated changes in virus morphology. Images G and H show equine influenza virions treated with DPPC; while virions are surrounded by liposomes, no apparent change in virus morphology was noticed (scale bar 200 nm). These images are representative of three independent experiments.

5.5.2.3 **Measurement of the aspect ratio and surface area for LPAI H2N3 particles**

Measurement of the aspect ratio of viruses (the D/L ratio) with or without treatment showed that H2N3 virus treated with phospholipids had a significant change in their aspect ratio that was dose-dependent with increasing concentration of lipid increasing the D/L ratio further ($p < 0.05$; one-way ANOVA).

H2N3 virus treated for 30 mins with 50 or 500μM of LPG or LPC had a significant change in virus aspect ratio ($p<0.05$ or $p<0.01$,

respectively). Increase in the D/L ratios of virions treated with DPPG (50 μM: P<0.001, 500μM: P<0.01) and DPPC (50 μM: P<0.01, 500μM: P<0.05) were also measured although the latter ratios were lower compared to the use of lyso-lipids (Figure 5.9). Treatment with LPG, DPPG, LPC or DPPC at either 50 or 500 μM led to greater variation in the virion surface area compared to untreated virus with viruses showing both increases and decrease in virus surface area (Figure 5.10).

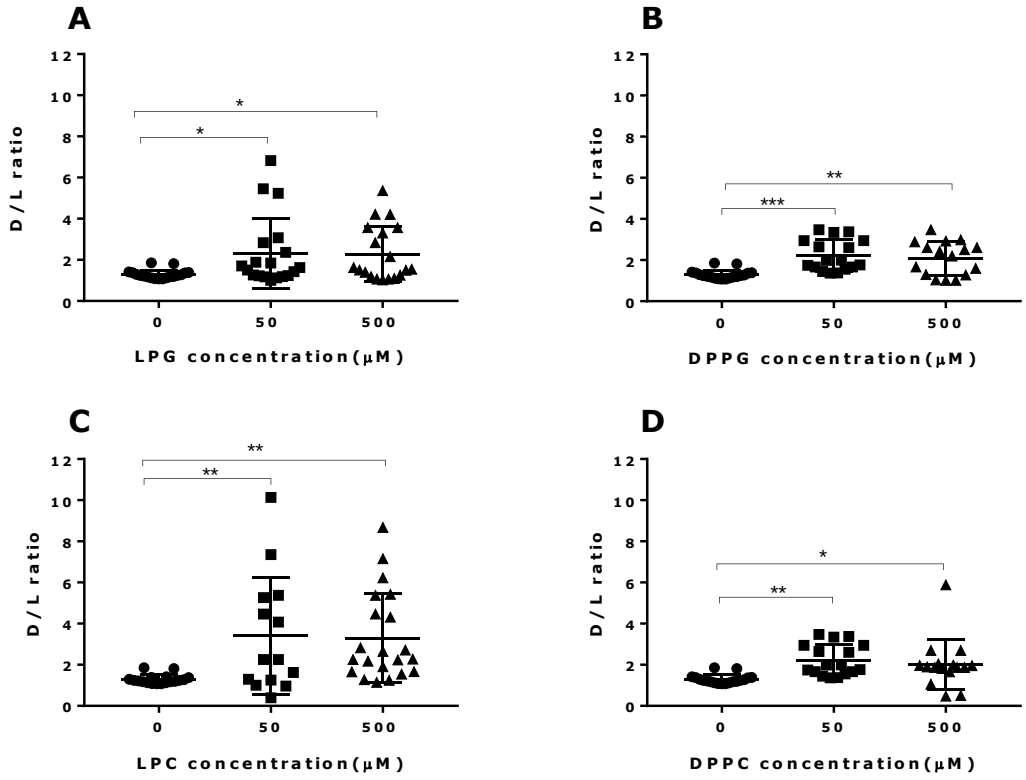

Figure 5:9 Size and dimensions of the influenza H2N3 with or without pre-incubation with phospholipids.
Influenza H2N3 virus pre-treated with A (LPG), B (DPPG), C (LPC), D (DPPC). The mean D/L measurements showed a significant effect of DPPG (**p < 0.01, ***p < 0.001; one way ANOVA), DPPC (*p < 0.05, **p < 0.01) and LPG and LPC (*p < 0.05; one-way ANOVA) pre-treatment on the shape of H2N3 virus particles.

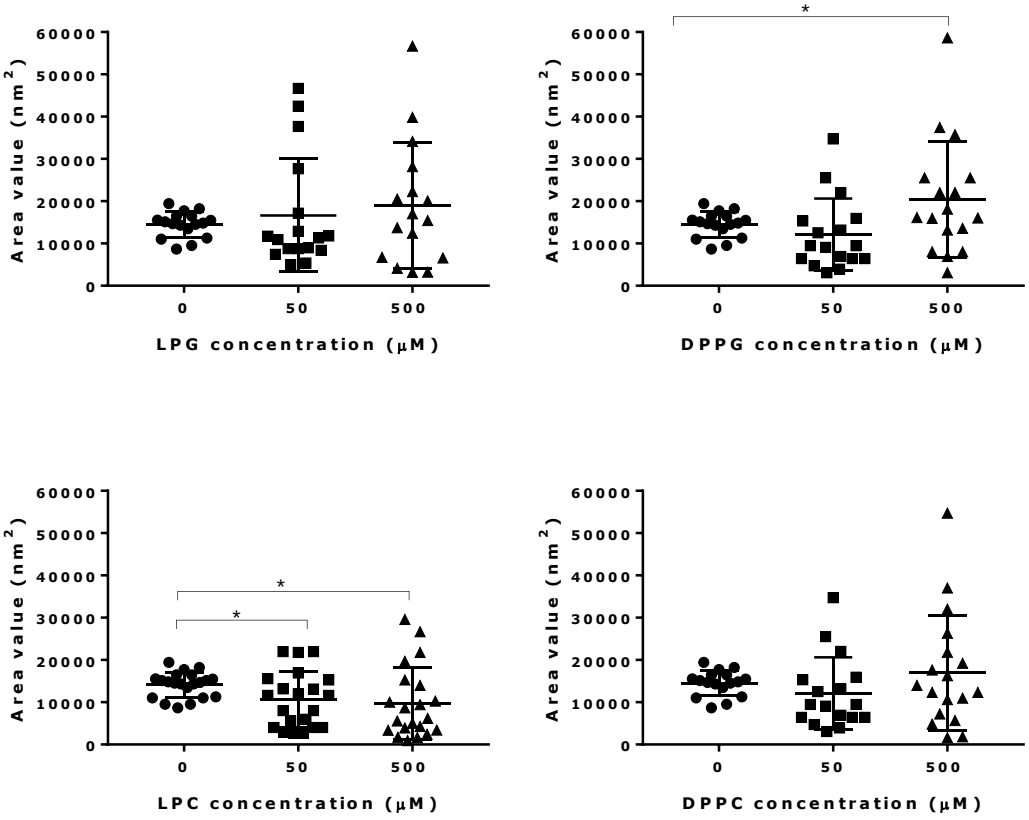

Figure 5:10 Surface area measurement of H2N3 influenza virus with or without pre-treatment with phospholipids.
LPAI H2N3 virus treated with A (LPG), B (DPPG), C (LPC), D (DPPC). The measured surface area of LPAI H2N3 pre-treated with LPG and DPPC did not change significantly ($p > 0.05$; One way ANOVA). However, incubation of 500 μM of DPPG or 50 and 500 μM of LPC showed a significant increase in the mean viral surface area ($*p < 0.05$).

5.6 Discussion

Influenza A viruses are pleomorphic enveloped viruses, and the EM images presented here show the characteristic structure of spherical (H2N3) and filamentous (H3N8) influenza viruses in untreated samples (Sarachai et al., 2014, Zhirnov and Manykin, 2015). Furthermore, both H2N3 and H3N8 influenza viruses clearly showed viral glycoprotein spikes protruding from the viral lipid layer. These glycoproteins are HA, NA and M2, which appear as characteristic spikes (Rowse et al., 2015). The RNP core of the virus differs between filamentous and spherical influenza virus. In the filamentous, it is mostly ordered in eight strands, varying in size, which explains the flexibility of NP-NP interaction that enables influenza virus to make more use of the host cell and undergo successful replication (Gallagher et al., 2017). Genetic analyses have revealed that in the H3N8 strains the viral segment 7 (M1) could play an important role in changing virus morphology (Elton et al., 2013).

Our TEM results showed that the LPAI H2N3 without treatment is mostly spherical (diameter ~100–120 nm) with visible viral glycoproteins with an aspect ratio approximately equal to one. In similar conditions (i.e. without treatment), the LPAI H3N8 is filamentous with characteristic spikes on the outer surface of the virion particles. Treating influenza H2N3 and H3N8 viruses with exogenous phospholipids changed the morphology of viruses. It was found that 500 μM of phospholipids with the exception of DPPC change

H2N3 morphology through the extensive fusion of multiple numbers of virions and liposomes, causing a noticeable increase in virus size with indistinct viral outer spikes. Similarly, some of the H3N8 virions show membrane rupture when treated with 500 μM of LPG, LPC; also with uncharacteristic visible spikes. This suggests that the exogenous lipids may have inserted into only one leaflet of the virion, which may explain the disruption of the viral envelope.

There is an apparent change in influenza virus H2N3 and H3N8 morphology when treated with 50 μM of LPG, LPC, and DPPG with aggregation of virus particles, neck-like structures, and absence of clear outer spikes that could also block the ability of viruses to infect host cells. Inhibition of influenza virus fusion through incubation of virus with the anti-fusion reagent (Z-3-(bicyclo [2.2.1] heptan-2-yl)-5-((5-(4'-chlorophenyl)-3-(3-(piperazin-1-yl) pentyl) furan-2-yl) methylene)-2-thioxothiazolidin-4-one, called 136 compound) prevents the viral fusion and the aggregation with liposomes and other virions (Rowse et al., 2015). The formation of a stable neck structure when interacting with liposomes is thought of as a partial viral fusion due to the destabilisation of HA outer spikes. These results demonstrate that virus morphology can be affected by phospholipid treatment but that it depends on the type of lipid used.

Host cell factors also have been reported to have an impact on influenza morphology. For example, extraction of cellular cholesterol

not only perturbs the function of viral M2 protein (Rossman et al., 2010) and disrupts cortical actin (Simpson-Holley et al., 2002) of filamentous H3N2 but also, the virions budding from infected cells, instead of being filamentous, become spherical. Furthermore, it was found that the surface density of HA glycoprotein or the lipids topology changes the virus morphology and that these were the assumed reasons for the reduction in influenza virus infectivity (Leser and Lamb, 2005).

The addition of exogenous phospholipids to LPAI H2N3 virus appeared to impact more on the aspect ratio of the virus than its surface area. This further suggests that exogenous lipids insert into the outer leaflet of virions to change their three-dimensional symmetry from spherical to oblate (Seifert, 1997). The fusion of multilamellar lipid liposomes made of phosphatidylcholine, cholesterol, and ganglioside GM3 with influenza virus H3N2 visualised through Cryo-EM has also demonstrated altered virus morphology (Bonnafous et al., 2014).

Chapter 6: Influence of exogenous lipids on influenza virus binding and entry into cells

6.1 Introduction

Influenza viruses derive their lipid envelope from the host cell membrane during virus budding. Influenza viruses are characterised by their pleomorphic shape ranging from spherical to filamentous up to 20 μm. Filamentous viruses show a difference in virus entry pathway as the large size of the filamentous virions precludes their entry through canonical clathrin-coated pits. It was reported that filamentous viruses use macropinocytosis as an alternate entry pathway whereas the spherical strain is capable of entering cells via clathrin-mediated endocytosis (Rossman et al., 2012). Moreover, the endocytic trafficking pathway of influenza virus after binding to the host cell surface required (i) early endosomes (10-15 mins pi) and (ii) late endosomes (35-40 min pi) for successful infection (Sieczkarski and Whittaker, 2003). The ability of H2N3 and H3N8 strains to bind with MDCK and A549 cells before and after treatment with exogenous lipids was examined in order to understand the effect of these lipids on reducing virus binding to the host cell. In this way, we sought to develop our understanding of lipid–influenza virus interaction, which could help inform future therapies against influenza virus.

6.1.1 Interaction of Influenza virus with phospholipids

The interaction of HA glycoprotein of influenza virus with receptors found on the surface membrane of the host cell is key to start the viral life cycle through mediating both attachment and internalisation

of viral particles to the host cells (Ramos and Fernandez-Sesma, 2012). The viral binding to the host cell membrane involves the specific interaction of influenza HA with host cell sialic acids. Endocytosis and fusion follow the attachment step, ultimately leading to successful replication and the release of new virions (Critchley and Dimmock, 2004).

It has been reported that influenza virus binding to liposomes depends on the liposome composition and temperature of incubation. With regards to the effect of liposome composition, virus binding to the liposomes at 37°C increased from 3% for liposomes composed of phosphatidylcholine to 39% for a liposome composed of both phosphatidylcholine and glycosphingolipid. When determining the effect of temperature, it was recorded that for a liposome composed of phosphatidylcholine and glycosphingolipid, virus binding to the liposomes increased from 14% at 0°C to 39% at 37°C (Haywood and Boyer, 1985).

In addition, endocytosis of IAV depends upon the conformational change of HA to HA1 and HA2 subunits. This leads to the fusion of the viral membrane with the host endosomal membrane and the release of the viral complex leading to specific transcription processes inside the host cell. This transcription step is followed by the aggregation of viral proteins on the plasma membrane of the cell using the host cell lipids as a future envelope in cooperation with viral glycoproteins. Then, the viral glycoprotein, neuraminidase, plays a critical role in

releasing the newly formed virions (Haywood and Boyer, 1985, Wilks et al., 2012, Victor et al., 2015).

During the viral fusion process, the mixing of the lipids from the virus and the host cell membranes has been suggested to lead to the rearrangement of host lipids, helping the virus to fuse with the host cell membrane (Victor et al., 2015). In particular, the influenza HA peptide has been shown to reorganize the host lipid domains through the insertion of backbone amines into the polar head region of lipids composed of the host cell membrane; which leads to both the disturbance of the H-bonding lipid phosphate group and a reduction in the repulsion forces between the polar head groups. Consequently, this process causes a reduction in both the lipid bilayer thickness and the ordering of the adjacent lipids (Légaré and Lagüe, 2014).

6.1.2 **Haemagglutination testing**

Haemagglutination testing with the use of chicken RBCs has been carried out to detect influenza virus infection and test the efficacy of new anti-viral medications in vitro. Although this approach is less sensitive in comparison to other techniques, such as immunofluorescence and RNA hybridisation (Rimmelzwaan et al., 1998), it is more cost effective and allows measurement of virus titre and the efficacy of antiviral medication using the endpoint dilution assay. This assay is employed as a diagnostic tool to assess live and inactivated viruses from amniotic–allantoic fluids of embryonated hens' eggs (Killian, 2014) or the titre of progeny viruses from cells

(Rimmelzwaan et al., 1998, Van Baalen et al., 2014). The HA assay is, therefore, a quantitative tool to determine the endpoint dilution which is defined as the virus dilution giving a negative result that can be seen as chicken RBCs forming a 'red dot' in a V-bottom well. A positive result is obtained when chicken RBCs agglutinate together forming a 'red blanket' in the well (Figure 6.1). It has been demonstrated that haemagglutination involves HA glycoproteins on the surface of the influenza virus since the use of specific antibodies blocking HA molecule interferes with the agglutination process (Webster et al., 2014).

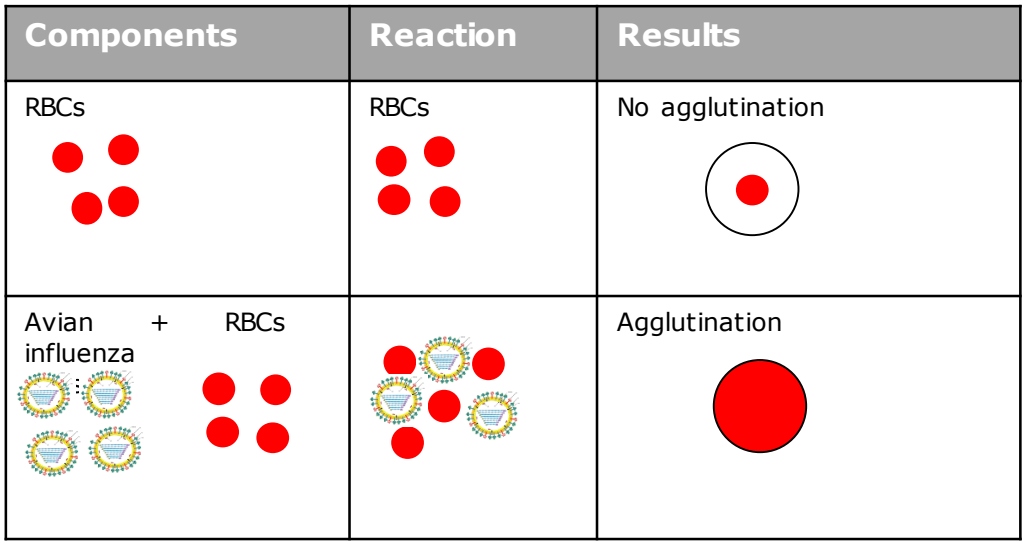

Figure 6:1 Haemagglutination assay for influenza A virus.

6.1.3 **Aims and objectives**

The aims of the work presented in this chapter was to investigate the use of several techniques to determine the impact of exogenous phospholipids on the binding and entry of influenza virus into host cells. We also sought to determine whether exogenous phospholipids

inhibit binding and uptake of filamentous equine influenza virus H3N8 greater than avian influenza virus H2N3 (a virus with spherical morphology); which we hypothesise may occur to the greater surface area of the filamentous virus.

The main objectives of this chapter are

1. To investigate the influence of different concentrations of phospholipids in reducing or blocking avian influenza virus haemagglutination in chicken RBCs.
2. To assess whether avian influenza virus pre-treated with exogenous phospholipids inhibits viral binding to MDCK cells in suspension, using flow cytometry.
3. To determine whether the exogenous phospholipids inhibit binding and uptake of H3N8 or H2N3 by adherent MDCK or A549 cells, using immunofluorescence.

6.2 Material and Methods

Haemagglutination (HA), flow cytometry, and immunofluorescence were used to analyse influenza A virus binding and uptake by cells after treatment with different doses of exogenous phospholipids.

6.2.1 Assessment of the effect of lipids on influenza virus binding using haemagglutination

An HA test was conducted using a serial dilution of phospholipids to treat IAV H2N3 with chicken RBCs following a standard protocol (Salk, 1944). Virus haemagglutination units (HAU) were determined to measure endpoint dilutions.

6.2.1.1 Preparation of 0.5% chicken RBCs

Chicken blood cells in Alsever's solution (TCS Biosciences Ltd, UK) were used to prepare a 0.5% RBC suspension. For the test, a 5 ml sample of chicken blood was pipetted into a 15 ml centrifuge tube and centrifuged at a speed of 500 xg for 5 mins. The supernatant was then discarded without disturbing the RBC pellet. Sterile PBS was added to 5 ml, and the sample was re-centrifuged at the same speed and washed twice. After the final washing, enough PBS was added to form a working solution of 0.5% RBC, determined by measuring the packed cell volume (PCV) using microhematocrit centrifuge (Selby and Eichner, 1994).

6.2.1.2 **Haemagglutination test**

Fifty microliters of PBS were added to each well of a V-bottom 96-well plate. For positive control, 50 µL of H2N3 was added, followed by the serial transfer of 50 µL from well 1 to well 12 in order to obtain a two-fold serial dilution. The final 50 µL from well 12 was discarded. Following this, 50 µL of RBCs working suspension at 0.5% was added to all the wells. The solution was mixed and the results were read after 30 mins at RT. Positive results were identified according to the presence of agglutination or partial agglutination and negative results were observed as a discrete "dot" of cells. The HAU was determined by identifying the highest viral dilution giving agglutination.

6.2.1.3 **Haemagglutination test for LPAI H2N3 pre-treated with lipids**

PBS (50 µL) was added to each well of a V-bottom 96-well plate. A serial dilution of lipid solution was started at a concentration of 500 µM and then transferred to consecutive wells via two-fold serial dilution (50 µL) as indicated above. Then 50 µL of H2N3 virus at a given titration (either 2, 4, 8, 16 or 32 HAU) was added to each well of the plate and incubated for 30 min at 37°C. Finally, 50 µL of 0.5% RBC suspension was added to each well, mixed gently, then left for 30 mins at RT. The negative control comprised of either 50 µL of PBS (wells 1 to 12) or 50 µL of lipid at a concentration of 500 µM with two-fold serial dilution.

6.2.2 **Measurement of the impact of lipids on virus binding using flow cytometry**

Flow cytometry was used to detect AI virus binding to MDCK cells following infection.

6.2.2.1 **Preparing individual MDCK cell suspensions**

Sub-confluent (90–95% confluent) MDCK cells were cultured in a T75 flask (Nunc) using DMEM; the cells were then detached by washing them twice with cold PBS (4°C) followed by incubation with Versene, as described in Section 3.3.1.4.1. Cells were harvested then washed once with infection medium and then re-suspended in infection medium at a concentration of 1 x 10^6 cells per mL.

6.2.2.2 **Determining the optimum timing for influenza virus binding to the MDCK cells**

The binding of influenza virus to the host cell was investigated using flow cytometry; optimisation of the LPAI H2N3–MDCK cells' binding period was carried out through the incubation of single suspension MDCK cells with H2N3 at MOI of 5 for different times (5, 10, 15, 20, 25 and 30 mins) at 37°C. Infected cells were washed three times with ice cold PBS, and then fixed using 1% PFA for 20 mins at RT; the cells were then re-suspended with cold PBS and kept overnight at 4°C prior to analysis.

6.2.2.3 **Staining protocol for flow cytometry samples**

Virus infected individual MDCK cell suspensions were immunostained in order to detect influenza binding to the host cells with or without pre-treatment with lipids. The fixed cells were blocked by using PBS-B (PBS + 1% bovine serum albumin [BSA], Fisher, UK) for 20 mins at RT followed by incubation with the primary antibody; purified anti-serum against influenza H2N3 (chicken anti-H2; kindly provided by Veterinary Laboratories Agency, UK) at RT for 1 hr. The cells were then washed three times using cold PBS before a final incubation with FITC-conjugated goat anti-chicken IGY (H+L) polyclonal secondary antibody (Novex, UK) for 1 hr at RT. The cells were then washed three times with cold PBS before re-suspending the cell pellets in PBS-B and examining them using an FC500 Flow Cytometer (Beckman Coulter, UK).

6.2.2.4 **Determining the optimum concentration of primary and secondary antibodies**

Fixed suspensions of MDCK cells infected with H2N3 were stained using the same protocol described in Section 6.2.2.3, while the specific anti serum against HA (chicken anti-H2) was optimised as various dilutions: 1:500, 1:750, 1:1000, and 1: 1250. The secondary antibody, FITC-conjugated goat anti-chicken IGY (H+L) was titrated at 1:1000, 1:2000, and 1:4000.

6.2.2.5 **Measurement of influenza virus binding to individual MDCK cells at 37°C by flow cytometry and the effect of phospholipid pre-treatment**

Lipids were prepared as described in Section 2.4, and LPAI H2N3 virus was incubated with lipids (LPG, LPC, LPS, DPPG, DPPC, and DPPS) at concentrations of 5, 50 and 500μM for 30 mins at 37°C. MDCK single cell suspensions were incubated with LPAI H2N3 with or without pre-treatment with phospholipids for 10 mins at 37°C. This was followed by centrifugation at 1000 x g for 6 mins followed by three washes with cold PBS. Finally, mock and infected cells were fixed in 1% PFA for 20 mins at RT, after which the cells were spun and re-suspended in cold PBS overnight, prior to flow cytometry. The data were analysed using the Weasel software program version 3.0 (Walter and Eliza Hall Institute, Australia)

6.2.2.6 **Measurement of influenza virus binding to individual MDCK cells at 4°C by flow cytometry and the effect of phospholipid pre-treatment**

Pre-incubated LPAI H2N3 at MOI 5 with each lipid (LPG, LPC, LPS, DPPG, DPPC, and DPPS) was prepared at 5, 50 and 500 μM concentrations for 30 mins at 37°C and lipids in excess were removed through centrifugation using an Amicon Ultra-15 filter (50K MWCO) (as described in Section 2.4). MDCK cells were counted using a hemocytometer, and 10^6 cells were incubated with an H2N3 virus with or without pre-treatment with phospholipid for 10 mins at 4°C, followed by three washes with cold PBS. Finally, the infected and

uninfected cells were either fixed directly in 1% PFA for 20 mins at RT (considered as the 0 min time point) or allowed further incubation time at 37°C for 10, 20 and 30 mins to determine virus uptake and allow the bound virus at 4°C to internalise MDCK cells. Fixed cells were washed three times with cold PBS and the cell pellets were re-suspended in PBS-B and kept overnight at 4°C prior to examination with flow cytometry (Figure 6.2).

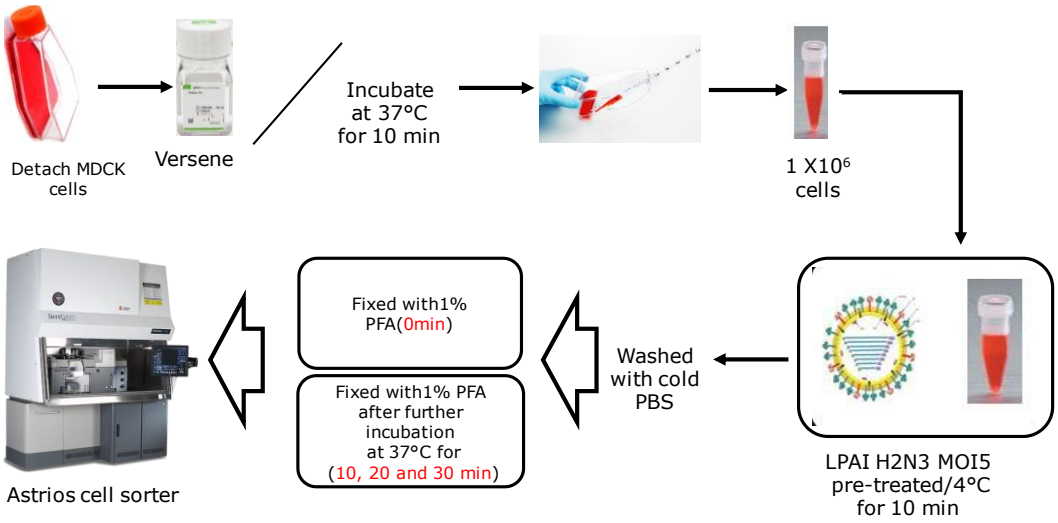

Figure 6:2 Detection of H2N3 binding and/or cell entry by flow cytometry.

Data involving LPAI H2N3 virus pre-treated with DPPG, LPG, LPC, and DPPC followed by MDCK cells infection for 0, 10, 20 and 30 mins were analysed by Weasel flow cytometry software. The number of counts vs FITC intensities were plotted for each sample, using the negative control (untreated cells) to determine the negative gate. By removing the negative gate from the results of infected cells with H2N3 with or without phospholipids treatment, the proportion of H2N3 bound to cells was determined. In particular, the number of cells that fell within

the positive gate was divided by the total cell count to obtain a percentage value (or probability) of positively labelled cells (Figure 6.3).

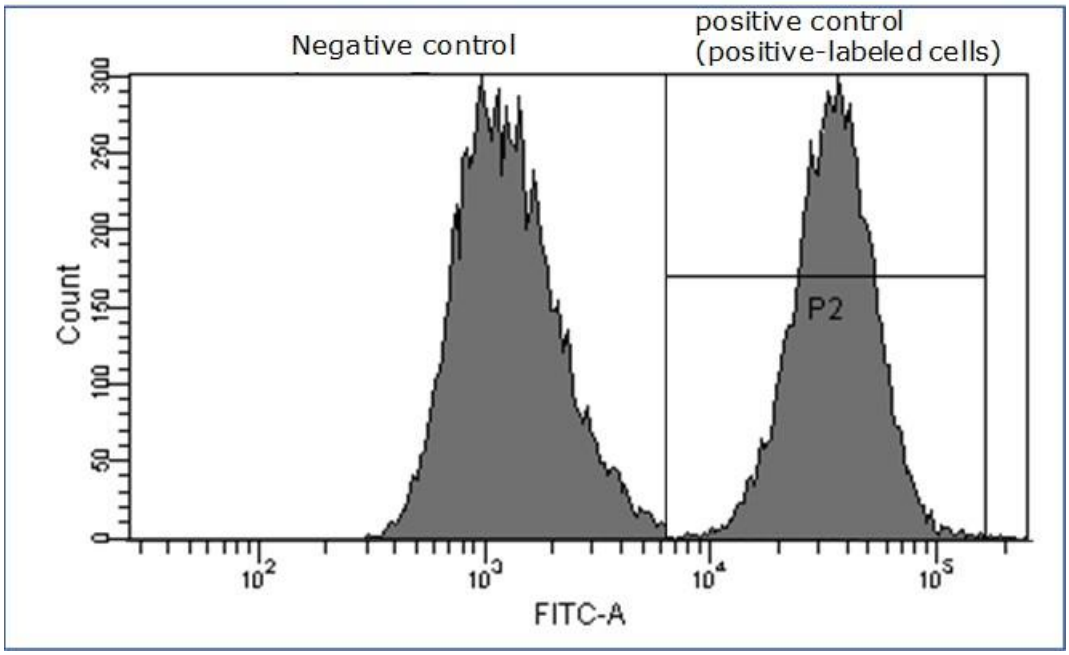

Figure 6:3 Histogram data for the surface marker expression analysed by flow cytometry.
Single parameter histogram demonstrates both negative, positive populations through measuring cell count (vertical axis) and the fluorescence intensity (horizontal axis) using the negative and positive control.

6.2.3 **Assessment of the impact of lipid treatment on virus binding using immunofluorescence**

6.2.3.1 **Influence of exogenous phospholipids on the binding of influenza A viruses analysed through immunofluorescence**

MDCK and A549 cells were grown on 13 mm glass coverslips in a 24 well plate incubated in 1mL DMEM-10 at 37°C. After 48 hrs, cells reached about 90% confluence. At this time, the MDCK or A549 cells were washed three times with PBS and infected at 4°C for 10 mins with H2N3 (spherical strain) in IM at MOI of 5. MDCK cells only were

used for infections with the filamentous strain H3N8 in IM at MOI of 5. The cells were washed three times with ice cold PBS and some of these cells were fixed with 4% PFA for 20 mins at RT. The fixed cells were washed with PBS and considered as the 0 min time. Other cells were further cultured with fresh IM for 10, 20, and 30 mins at 37°C. Subsequently, the cells were washed three times with ice cold PBS and were fixed with 4% PFA for 20 mins at RT. Finally, the fixed cells were washed with ice cold PBS and prepared for immunofluorescence staining.

6.2.3.2 **Immunofluorescence staining and imaging**

Fixed cells were blocked using 1% BSA at RT for 1 hr; then both infected and uninfected cells were incubated for 1 hr with 300µL of specific purified antiserum against viral HA (chicken anti-H2; Veterinary Laboratories Agency, UK, 1/750 dilution) with 1% BSA. The cells were then washed carefully three times, for 5 mins each, with ice cold PBS followed by incubation with 300 µl of secondary antibody Alexa Fluor® 488 (goat anti-chicken IgY (H+L), Invitrogen, 1/1000) for 1hr at RT in a dark environment. The cells were then washed three times with cold PBS. The coverslips were mounted onto microscope slides using 20 µL of Prolong® Gold Anti–Fade Reagent with 4', 6–diamidino–2–phenylindole DAPI (Life Technologies), sealed with nail varnish and kept at 4°C overnight until viewed and imaged by the Leica DM 5000B epifluorescence imaging system.

6.3 Results

6.3.1 Investigation of influenza virus H2N3 binding to RBCs through HA testing

Haemagglutination test results were presented to show the endpoint dilutions of H2N3 with or without phospholipid pre-treatment.

6.3.1.1 Haemagglutination results for H2N3

A two-fold serial dilution of H2N3 was used to measure viral HAU using chicken RBC. The positive control LPAI H2N3 HAU titre was 64U, as shown in Figure 6.4.

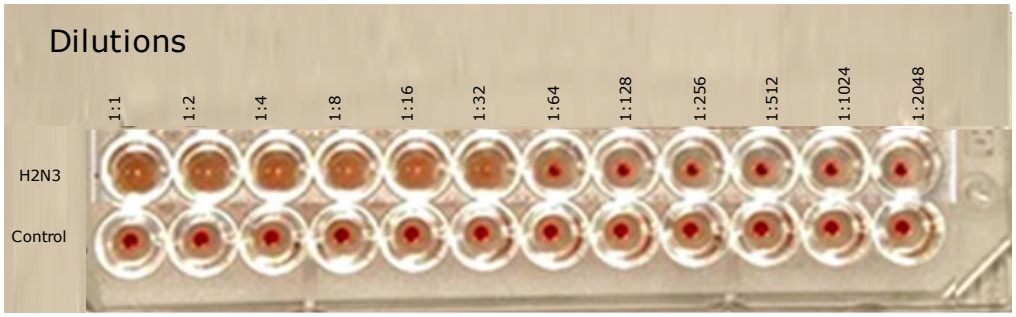

Figure 6:4 HA test for each LPAI H2N3.
The HA image shows that the endpoint dilutions (HAU) of LPAI H2N3 is 64 U/50 µL.

6.3.1.2 Impact of phospholipid lipid pre-treatment on inhibiting virus haemagglutination

We sought to examine the influence of the different kinds of phospholipids on the binding of LPAI H2N3 to chicken RBC via haemagglutination. Using positive haemagglutination results elicited by our viral H2N3 stocks (2, 4, 8, 16, and 32 HAU) together with

phospholipids pre-treatments revealed that at all the concentrations used, the phospholipids had no effect on blocking or reducing virus HA with concentrations of 2, 4, and 8 HAU (Figure 6.5). Interestingly, DPPG at concentrations ≥ 500 µM and DPPS at a concentration of 31.2 µM inhibited H2N3 haemagglutination at a concentration of 16 HAU (Figure 6.6).

Sample number	Sample name
1	DPPG
2	DPPC
3	DPPS
4	LPG
5	LPS
6	LPC
7	H2N3
8	Control

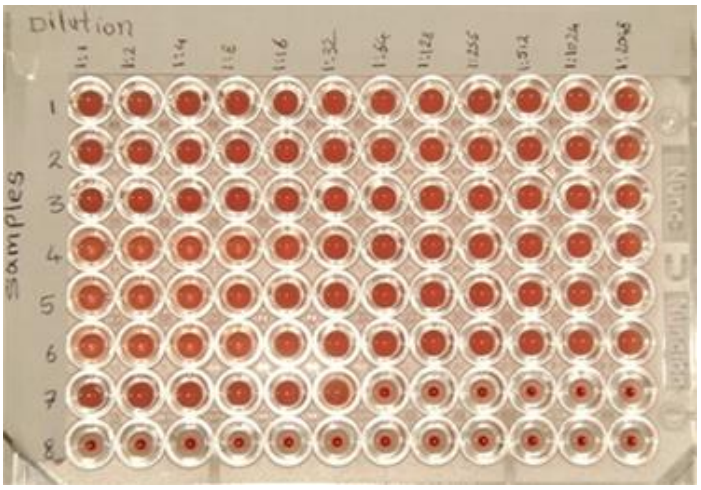

Figure 6:5 HA test for certain LPAI H2N3 HAU concentrations pre-incubated with phospholipids.

The HA image shows that the six phospholipids used with dilutions from 1:1 to 1:2058 had no effect on preventing RBC agglutination when using LPAI H2N3 virus at a concentration of 2 HAU. Sample number 7 shows the serial dilution of the virus without lipid; the endpoint dilutions (HAU) of LPAI H2N3 is 64 U/50 µL.

Sample number	Sample name	Minimum concentration of phospholipid inhibiting HA
1	DPPG	>=500μM
2	DPPC	NE
3	DPPS	31.2μM
4	LPG	NE
5	LPS	NE
6	LPC	NE

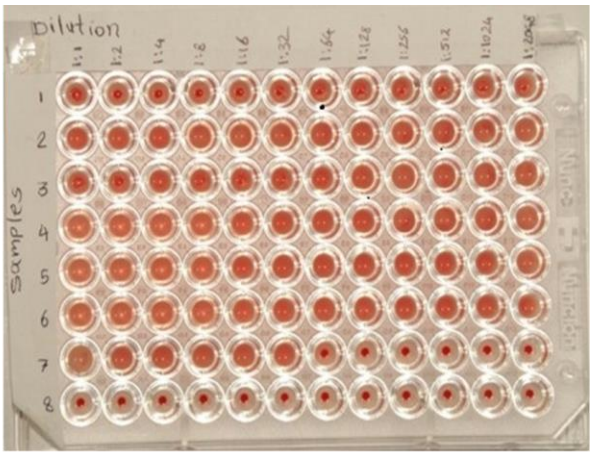

Figure 6:6 Lattice formation from incubated H2N3 16 HAU pre-treated with serial dilutions of phospholipids. NE (No endpoint).

The HA table shows the minimum concentration of phospholipids that inhibits H2N3 hemagglutinin RBCs. Both DPPG (1) and DPPS (3) at concentrations ≥ 500 μM and 31.2 μM, respectively; had an impact on blocking the binding of LPAI H2N3 at a concentration 16 HAU with chicken RBCs through the inhibition of haemagglutination of RBCs; none of the other phospholipids used in our study inhibited virus HA.

Two-fold serial dilutions of DPPG, DPPC, and DPPS incubated with 32

HAU of LPAI also inhibited viral hemagglutinin of RBCs. However,

lysolipids did not show any effect (Figure 6.7).

Sample number	Sample name	Minimum concentration of phospholipid inhibiting HA
1	DPPG	250
2	DPPC	>=500μM
3	DPPS	>=500μM
4	LPG	NE
5	LPS	NE
6	LPC	NE
7	H2N3	64HAU
8	Control	0

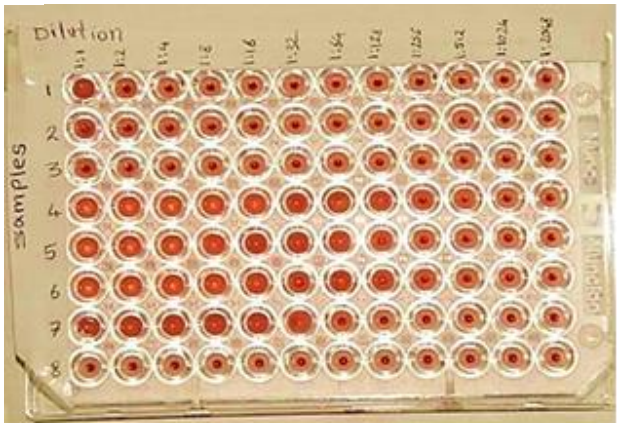

Figure 6:7 Lattice formation from H2N3 32 HAU pre-treated with serial dilutions of phospholipids.
The phospholipids DPPG, DPPC, and DPPS at concentrations of 250 μM, 500 μM, and ≥500 μM respectively; inhibited RBCs agglutination mediated by influenza virus H2N3.

6.3.2 **Analysis of influenza H2N3 virus binding to MDCK cells by flow cytometry**

6.3.2.1 **Optimisation of timing for virus binding**

Cells were gated using uninfected cells (Figure 6.8A). A higher percentage of positively-immunostained MDCK cells was observed at 10 and 15 mins post-infection with 97.9% of cells being immunostained. For 5, 20, 25, and 30 mins, the percentage of cells labelled were 95.9, 92.9, 92.4 and 89.8%, respectively (Figure 6.8 shows data collected at 5, 10 and 20 min). For the subsequent experiments, the time-point chosen was 10 mins.

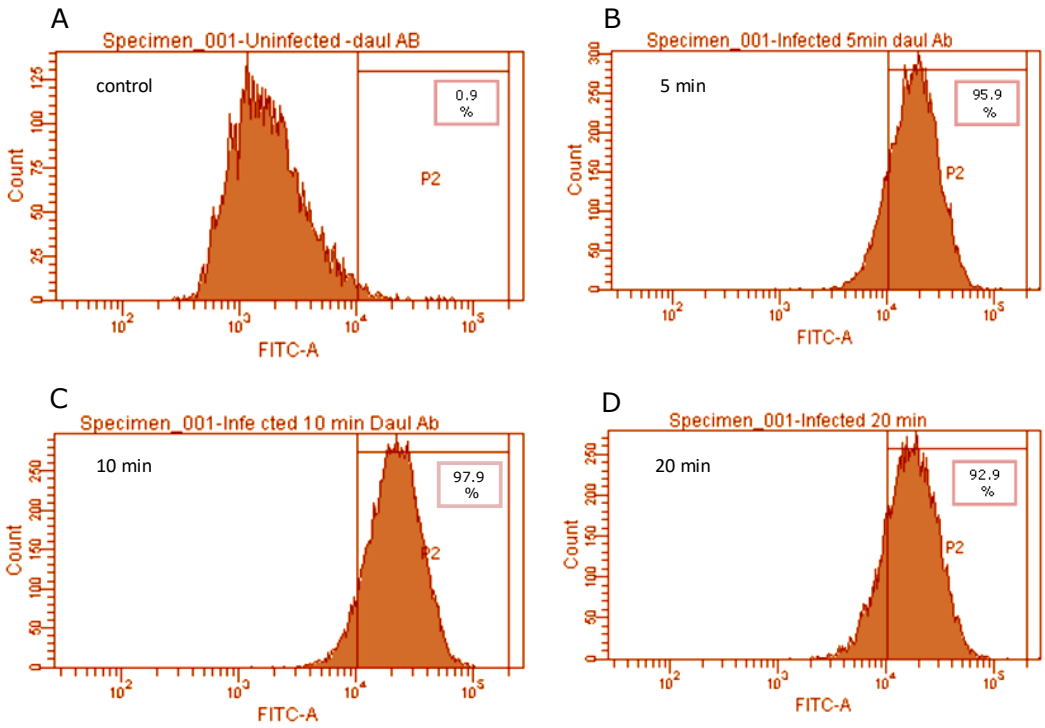

Figure 6:8 Influenza virus binding time optimisation of MDCK cells. A) Control uninfected cells, B) 5 min PI, C) 10 mins PI, D) 20mins PI, represented the Percentage of H3N2 (MOI 5) positively labelled cells (P2) at different time points post-infection.

6.3.2.2 **Optimisation of primary and secondary antibody dilutions**

The optimisation of the primary and secondary antibodies for the detection of the binding of influenza virus using flow cytometry showed that the dilutions 1:750 (Primary Ab) and 1:2000 (secondary Ab) had the highest proportion of infected cells (99.8%) when compared to other dilutions (Figure 6.9). These dilutions were therefore used for subsequent experiments.

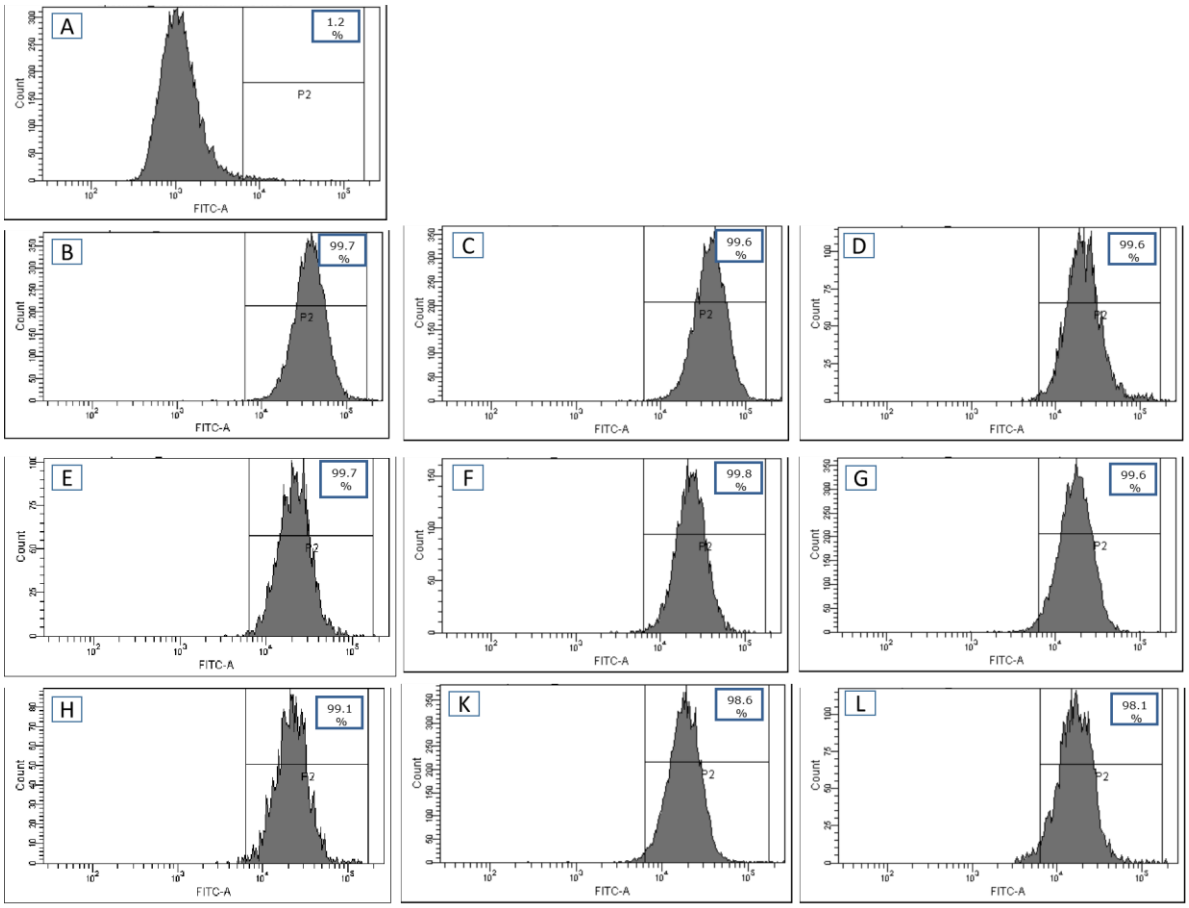

Figure 6:9 Primary and secondary Ab optimisations for flow cytometry of infected MDCK cells.
The virus H2N3 was labelled using different dilutions of primary anti-influenza A H2N3 polyclonal antibody from 1:500 to 1:1250 and FITC-conjugated secondary goat anti-chicken IgG from 1:1000 to 1:4000.
A) Control, B) 1° 1:500: 2 °1:1000, C) 1° 1:750: 2° 1:1000, D, 1° 1: 1250: °1 1:1000, E) 1° 1:500: 2° 1:2000, F) 1° 1:750: 2° 1:2000,
G)1° 1:1250: 2° 1:2000, H) 1° 1:500: 2°1:4000, K) 1° 1:750: 2°1:4000, L) 1° 1:1250: 2° 1:4000. Percentages represent positively labelled cells (P2).

6.3.2.3 **Influence of phospholipid pre-treatment on influenza H2N3 virus binding to MDCK cells at 37°C**

MDCK cell suspensions were infected with AI virus H2N3 at MOI 5 with or without pre-treatment with phospholipids for 10 mins at 37°C followed by these cells being fixed and then immunostained. The percentage of cells infected with H2N3 without treatment was around 90% while pre-treatment with LPG at 500 μM significantly reduced virus binding to MDCK cells to approximately 70% ($p < 0.01$). Pre-treatment of virus with LPG at concentrations of 5 and 50 μM produced a non-significant reduction in virus binding.

Pre-treatment of virus with DPPG at 5 or 50 μM reduced virus binding to 82% and 79%, respectively and this was further reduced to 67% with 500 μM of DPPG ($p<0.0001$) compared to untreated virus. However, phosphatidylcholine (DPPC and LPC) showed no significant reduction of H2N3 virus binding ($p > 0.05$) (Figure 6.10).

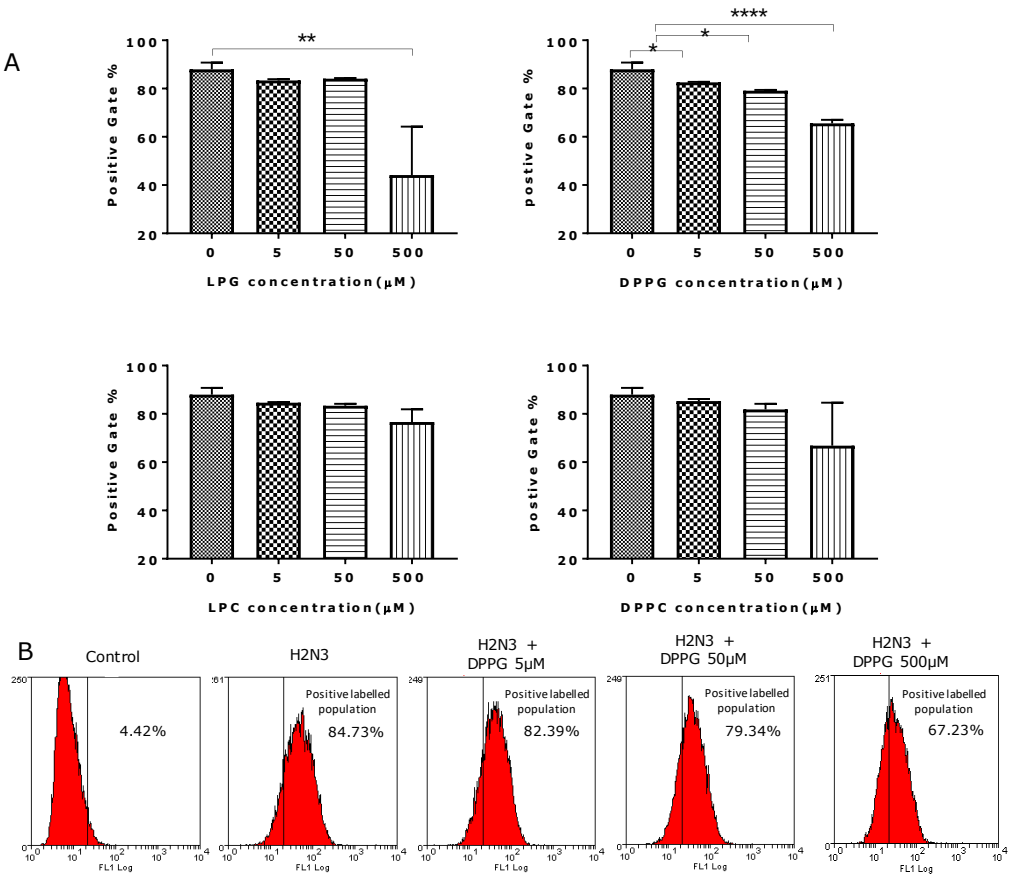

Figure 6:10 Influence of phospholipid pre-treatment on virus binding to MDCK cell

(A) A significant reduction of H2N3 binding pre-treated with DPPG (at all concentrations) or LPG (at 500 μM) (*p < 0.05, ** p < 0.01, **** p < 0.0001; one-way ANOVA) were measured. However, DPPC and LPC showed no significant effects on the reduction of H2N3 binding (p > 0.05; one-way ANOVA). (B) Control cells (uninfected and untreated) were used to set the gate for subsequent analysis. The histograms of the positive gated population show the percentage of cells binding H2N3 without treatment or with DPPG treatment at three concentrations: 5, 50 and 500μM.

6.3.2.4 **Influence of phospholipids on influenza H2N3 virus binding to the MDCK cells at 4°C**

The current study evaluated influenza H2N3 virus attachment to the MDCK cell surface as well as virus internalisation in relation to the total amount of cells, which was represented by a positive percentage. of immunostained cells. It was noticed that the amount of bound virus decreases over time and this reduction was most likely due to H2N3

virus entry into MDCK cells as the percentage of immunostained cells was reduced from around 80% at 0 min to about 70 to 62 % at 10 mins pi, followed by consistent reduction from 60-50% at 20 mins and to approximately 40% at 30 mins pi (Figure 6.11).

Pre-incubation of H2N3 virus with LPG at a concentration 5μM or 50μM showed no significant reduction in virus binding to MDCK cells at any time pi, except for 10 min pi at 50μM, which showed a significant ($p<0.05$) reduction of around 20% in the binding of the untreated virus. A significant ($p<0.05$) reduction by approximately 25% of virus binding was also seen for the pi time points 0, 10 and 20 mins with 500μM of LPG, while at 30 mins, the percentage of virus binding was reduced by 33% ($p<0.01$; Figure 6.11).

Pre-treatment of H2N3 virus with 5 μM of DPPG showed no significant reduction in virus binding over time when compared to 'time-controls' while 50 μM of DPPG produced approximately a 30% reduction in virus binding at 0, 10 and 20 mins pi ($p<0.05$). A more significant ($p<0.001$) reduction of virus binding was shown with 500 μM of DPPG to around 50% at 0 and 10 min pi, while a smaller reduction of 35% ($p<0.05$) was seen at 20 and 30 min pi.

Pre-treatment with phosphatidylcholine (LPC or DPPC) showed no significant reduction in the binding of the virus with 5 and 50 μM at any time point pi. A significant reduction was shown with 500 μM of LPC of < 20% at 0 and 10mins pi ($p<0.001$, $p<0.01$) with a further

reduction in virus binding at 20 mins and 30 mins pi respectively, as they both showed over 20% reduction of virus binding when compared to untreated virus at the same time points. Similarly, DPPC 500 μM showed significant reductions of about 30% of virus binding over the time points when compared to the untreated virus at the same time points.

Pre-treatment of H2N3 virus with DPPS showed no significant impact at 5, 50 and 500 μM, on virus binding for all post infection times. However, pre-incubation of H2N3 with 5 or 50 μM of LPS showed a reduction by about 10-50% in virus binding between 0 up to 30 min pi. A more significant reduction of virus binding was shown with H2N3 virus treated with 500 μM of LPS, as a gradual decrease was apparent in the reduction of virus binding percentage during the post infection time points 0 and 10 mins as virus binding was reduced by around 50%, whilst at 20 mins and 30 mins reductions were around 30% and 20%, respectively.

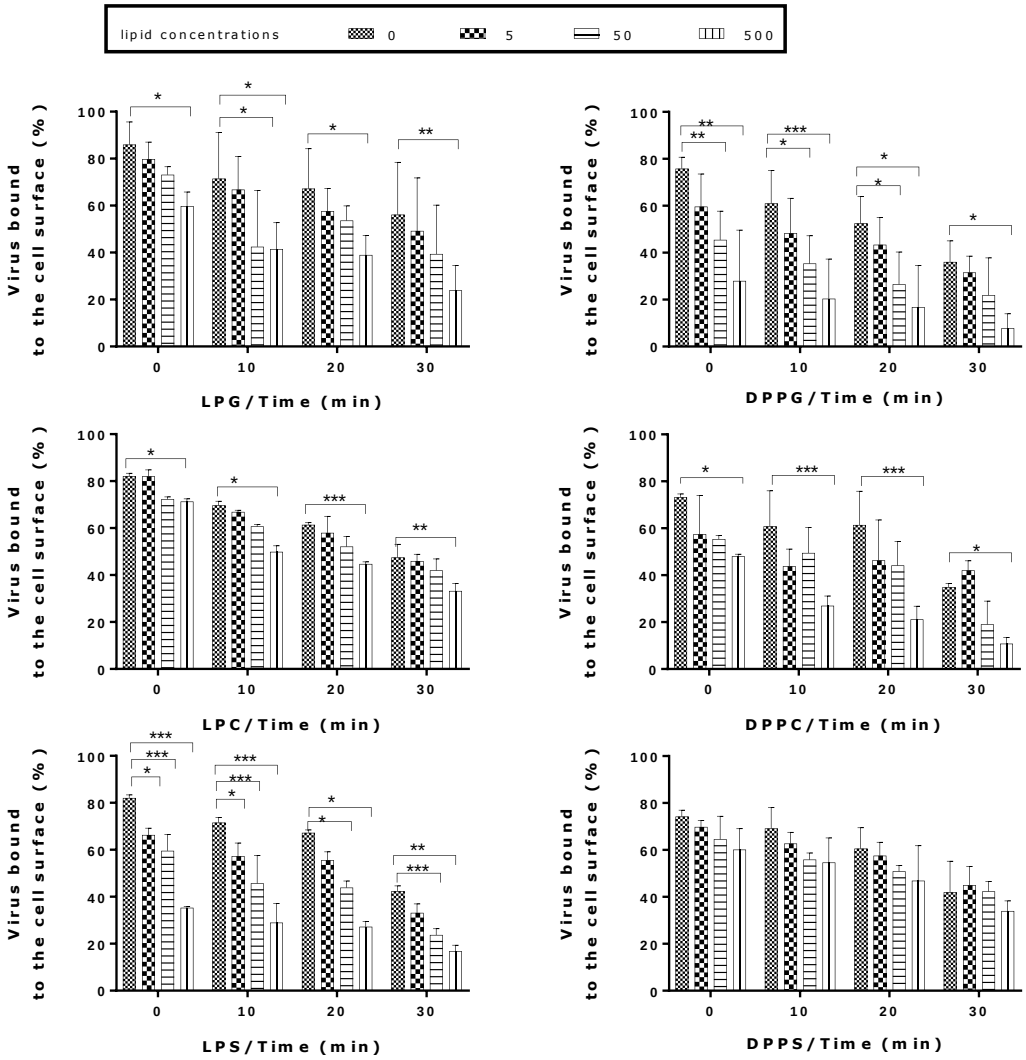

Figure 6:11 Influence of phospholipids on the probability of virus
Flow cytometry analysis of infected MDCK cells with H2N3 pre-treated with phospholipids in relation to the percentage of immunostained cells which showed that DPPG, LPG, LPC, and LPS lead to a significant reduction in virus binding (*p < 0.05, **p < 0. 01, ***p < 0.001; one-way ANOVA). DPPC at 500 μM concentration significantly reduced virus binding (*p < 0.05; one way ANOVA). However, DPPS showed no significant impact on the reduction of the virus binding to the cell surface (p > 0.05; one way ANOVA).

To determine the kinetics of virus internalisation for each pre-treatment the percentage of viruses bound to MDCK cells over time was reported to the initial fluorescence intensities measured (at time zero) for each pre-treatment. We assumed that there was minimal loss in staining intensity due to virus becoming unbound from cells Virus entry was unaffected by most treatments. However, H2N3 pre-treated with 500 μM of LPC at 10 min and DPPC at 20 min pi at

concentrations showed a significant increase in virus entry (*p < 0.05, **p < 0.01; one-way ANOVA) (Figure 6.12).

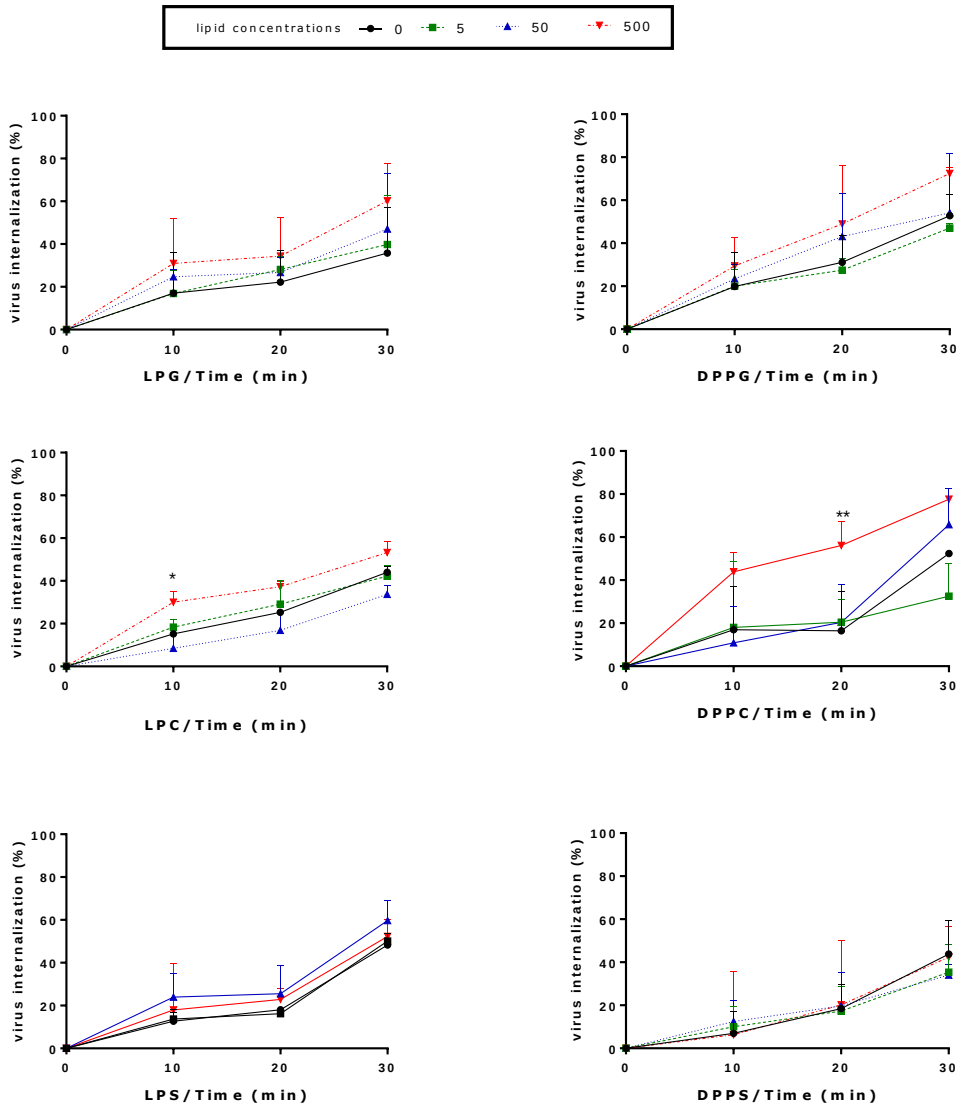

Figure 6:12 Influence of phospholipids on virus internalisation in MDCK.

Results demonstrate that with 500 µM of LPC and DPPC a significant increase in virus internalisation is measured (*p < 0.05, **p < 0.01, one-way ANOVA). There was no significant impact of other phospholipids on virus entry into MDCK cells.

6.3.3 Determining the effect of pre-treatment of influenza virus with exogenous phospholipids by immunostaining of MDCK cells for influenza HA

Staining of the influenza virus surface glycoprotein HA (H2 or H3) was merged with nuclear (DAPI) staining to visualise the impact of exogenous phospholipid pre-treatment on the binding of avian H2N3 and equine influenza H3N8 viruses to MDCK cells.

6.3.3.1 Immunological staining of LPAI H2N3 pre-treated with LPG infected MDCK and A549 cells

The uninfected MDCK cells showed no evidence of immunostaining for virus HA. LPAI H2N3 without lipid treatment at 0 mins showed clear evidence of green fluorescence at the cell surface indicating virus binding to the cells which were reduced by LPG at 50 and 500 μM, while no marked reduction was noticed at 5 μM. At 10 mins the fluorescence signal was reduced in all of the infected wells suggesting that the HA is inaccessible to antibody staining which might due to the virus having been trafficked near to the cell periphery . At 20 mins a diffused cytoplasmic staining of HA was visible in cells infected with the untreated virus, which was further reduced in virus treated with LPG. At 30 mins the majority of cells infected with the untreated virus had been trafficked in the perinuclear region of the cells and showed strong cytoplasmic staining for HA, which was reduced with 500uM of LPG. A reduction in fluorescence was noticeable with LPG pre-treatment of 5 and 50 μM when compared to the virus without treatment (Figure 6.13).

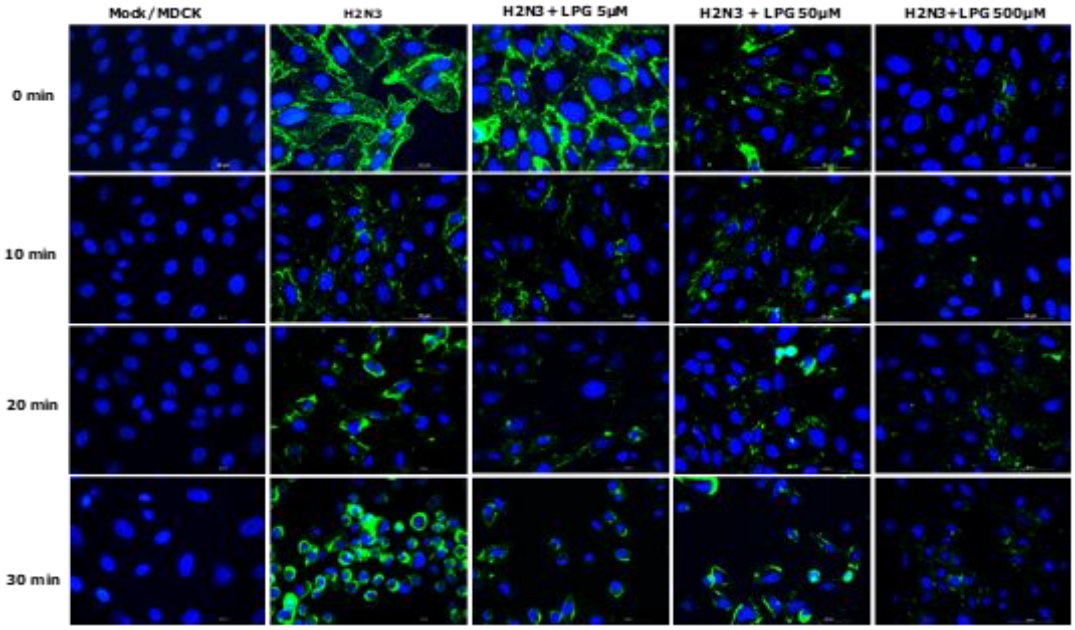

Figure 6:13 Fluorescent-labelled MDCK cells infected with H2N3 virus following pre-incubation with LPG.
Immunostaining of mock uninfected and infected MDCK cells with LPAI H2N3 at MOI 5 with or without pre-treatment with 5, 50 or 500 µM of LPG. MDCK nuclei (blue) were stained with DAPI, staining virus surface HA (green) by using green fluorescent Alexa Flour® 488. Images were captured using a Leica fluorescent microscope.

Similarly, a high impact of 50 and 500 µM LPG was observed on the reduction of the green fluorescent signals corresponding to influenza HA (H2) at 0 and 10 mins pi and a notable decrease of influenza virus binding to A549 cells was shown at 20 and 30 mins pi (Figure 6.14) This reduction in virus binding to A549 cells appeared more dramatic than that observed for MDCK cells.

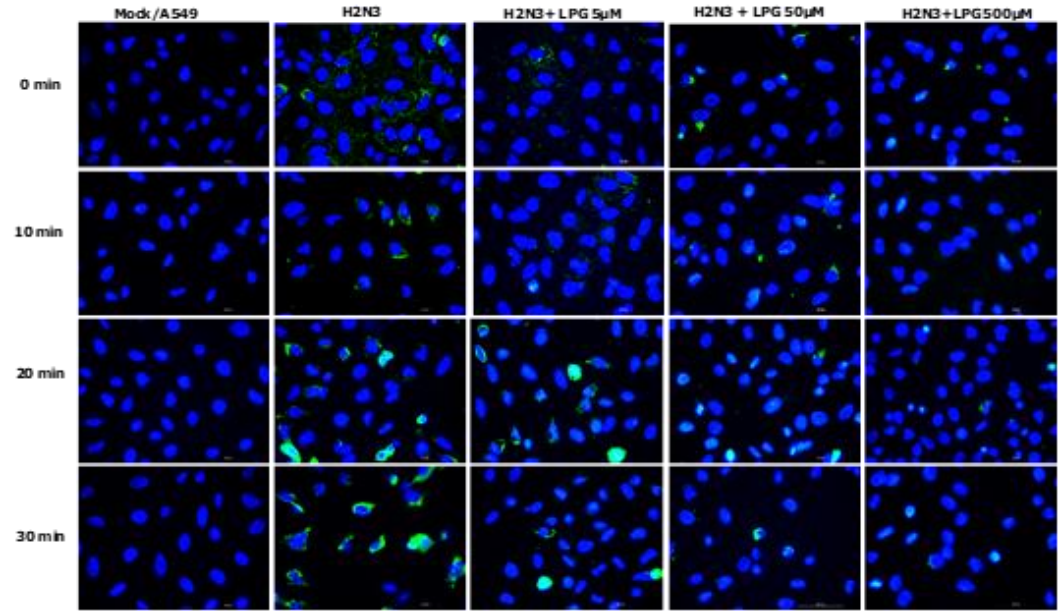

Figure 6:14 Fluorescent-labelled A549 cells infected with H2N3 virus following a pre-incubation with LPG.
Immunofluorescent images of LPAI H2N3 at MOI 5 pre-treated with LPG using A549 cells showed that treated H2N3 loses its ability to bind A549 cells. Surface virus HA (green) were stained with green fluorescent Alexa Flour® 488, A549 nuclei (blue) were stained with DAPI. Images were captured using a Leica fluorescent microscope.

6.3.3.2 **Immunological staining of LPAI H2N3 pre-treated with DPPG using MDCK and A549 cells**

The fluorescent signals were not detected at the cell surface of the uninfected control MDCK and A549 cells, whereas it was apparent at the cell surface of infected cells with untreated H2N3 at 0 mins. Pre-treating the virus with DPPG had a greater impact in reducing virus binding and fluorescent signals of influenza HA (H2) that appeared on the cell surface of MDCK, especially at concentrations 50 and 500 µM when compared to untreated virus. Infected MDCK cells with H2N3 (with or without DPPG treatment) showed a reduction in the green fluorescent signals at 10 mins pi which might be due to the inaccessibility of viral HA to the antibody staining and localization of viral particles at the cell periphery in the early endosomes At 20 mins a diffuse cytoplasmic staining of HA was noticed, which was reduced

when the virus was pre-treated with 500 μM of DPPG. At 30 mins, cells infected with untreated virus showed notable cytoplasmic staining of HA and it is probable that there was co-localization of virions in perinuclear region in the late endosomes. Virus pre-treated with 500 μM of DPPG showed reduced flourescence at 30 mins. Furthermore, a partial reduction was noticed with 50 μM of DPPG compared to untreated virus, however no notable reduction was noticed with 5 μM (Figure 6.15)

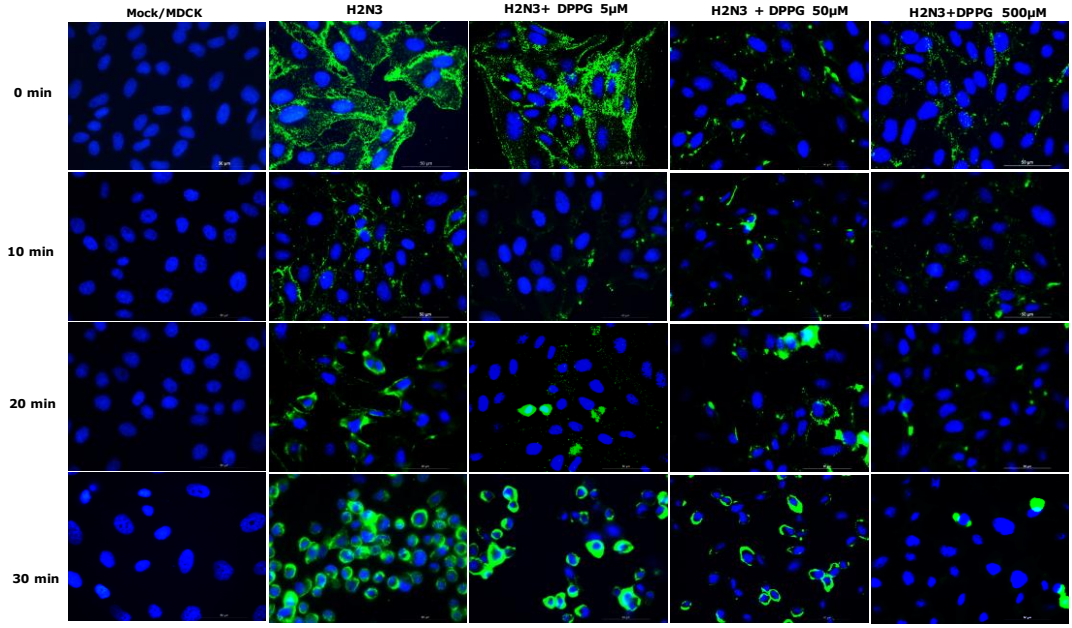

Figure 6:15 Fluorescent-labelled MDCK cells infected with H2N3 virus following a pre-incubation with DPPG.
Images of LPAI H2N3 virus binding to the MDCK cell show a reduced binding of the virus at 50 and 500 μM at all-time points. However, the virus seemed internalised at 30 min although the proportion of virus uptake by cells decreases as the concentration of DPPG increases. Surface virus HA (green) and MDCK nuclei (blue) were stained Images were captured using a Leica fluorescent microscope.

DPPG showed a higher inhibition of virus binding on A549, particularly a concentration of 500 μM (Figure 6.16) when compared with MDCK cells.

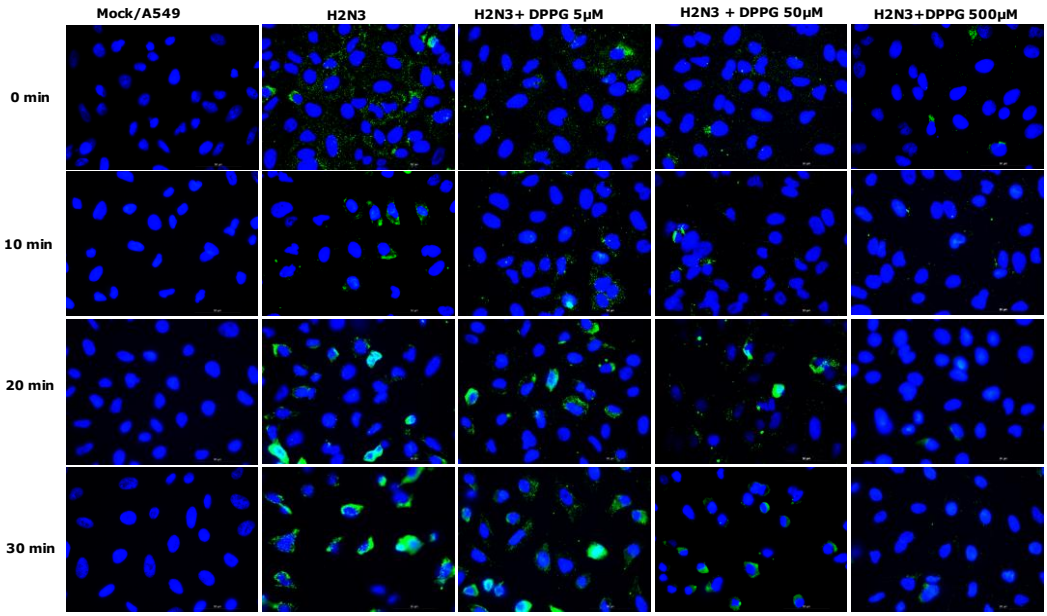

Figure 6:16 Fluorescent-labelled A549 cells infected with H2N3 virus following a pre-incubation with DPPG.
Uninfected and infected A549 cells with H2N3 pre-treated with DPPG were immunostained with surface virus HA (green) and nuclei (blue) showing that DPPG at concentration 50 and 500 μM reduced LPAI H2N3 virus from binding to A549 cell surface at 20 and 30 min. Images were captured using a Leica fluorescent microscope.

6.3.3.3 **Immunological staining of LPAI H2N3 pre-treated with phosphatidylcholine using MDCK infected cells**

The cell surface of MDCK cells (control uninfected) did not show any immunofluorescent staining for HA at all incubation time (0-30 mins), whereas these signals were obvious in the cells infected with H2N3 without treatment at 0-30 mins. Pre-treatment of AI virus with the two aliphatic chain phospholipid DPPC, at the doses of 5, 50 and 500μM, prior to incubating the virus with MDCK cells did not reduce virus binding to the cells at 0 mins when compared to the untreated virus at the same time point. At 10 mins DPPC did not reduce virus binding to the cell surface where the signals seemed to be already reduced (in untreated virus infected cells) and it was assumed that as the virus entered the cell, and antibody staining was not able to reach the HA. Cells infected with H2N3, without treatment, for 20 mins

showed diffuse cytoplasmic staining of HA which became more noticeable at 30 mins.

Pre-treatment of virus with DPPC at 5 and 50 μM concentrations did not reduce the fluorescent signals at either 20 or 30 mins. In the meantime, 500 μM displayed some reduction in the green fluorescent signal of influenza HA (H2) at 20 and 30 mins (Figure 6.17).

The one aliphatic chain LPC showed a reduction in fluorescent signals of LPAI H2N3 glycoprotein at a concentration of 50 μM, especially at incubation times 0 and 10 mins. It also specified that with 500 μM, there was a noticeable reduction in virus binding at 20 and 30 mins incubation periods (Figure 6.18).

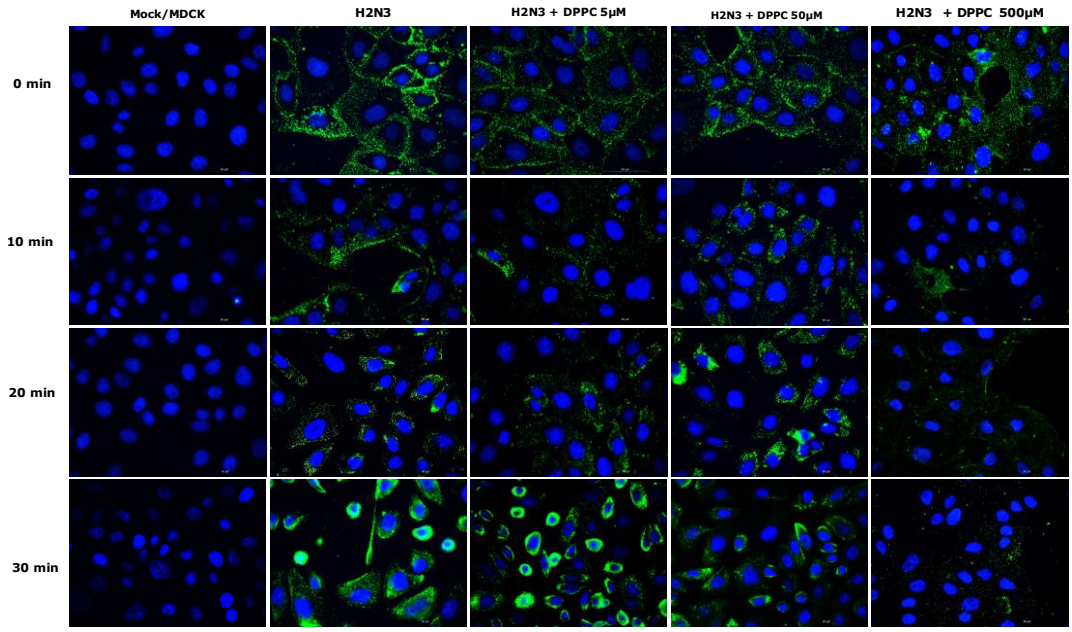

Figure 6:17 Fluorescent-labelled MDCK cells infected with H2N3 virus following a pre-incubation with DPPC.
Double labelling of MDCK with both DAPI and Alexa flour 488 revealed that the green fluorescent signals corresponding to H2N3 decreases as the concentration of the phospholipid DPPC increases. Images were captured using a Leica fluorescent microscope.

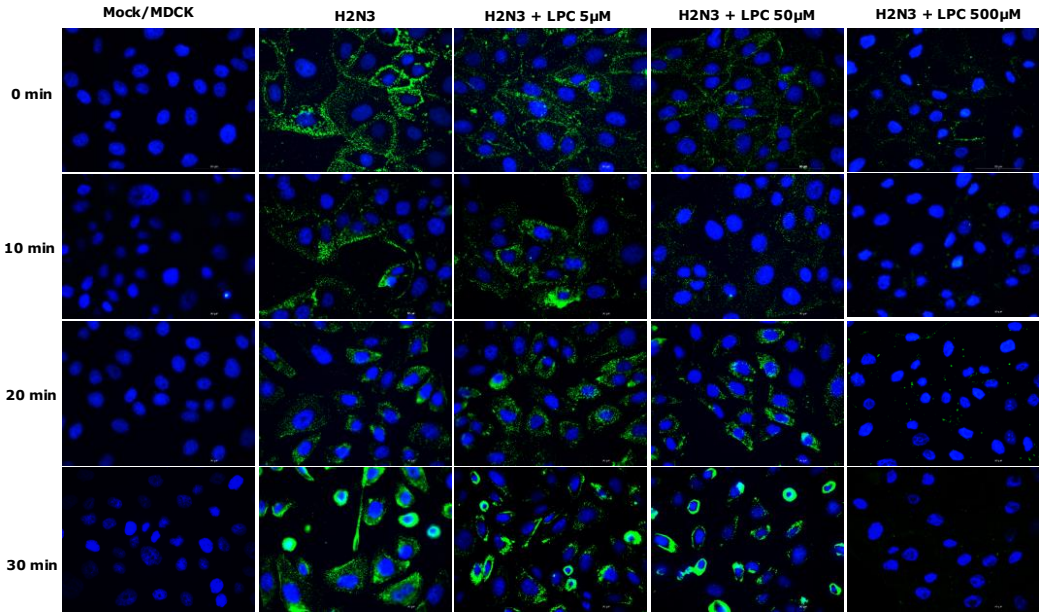

Figure 6:18 Fluorescent-labelled MDCK cells infected with H2N3 virus following a pre-incubation with LPC.
Double labelling of MDCK with both DAPI and Alexa flour 488 revealed that the green fluorescent signals corresponding to H2N3 decreases as the concentration of the phospholipid increase for all the time points used. Images were captured using a Leica fluorescent microscope.

6.3.3.4 **Immunological staining of LPAI H2N3 pre-treated with DPPS using MDCK**

Surface glycoprotein HA of influenza virus H2N3 binding to the MDCK cells was labelled using immunofluorescence. The fluorescent staining in the infected MDCK cells with H2N3 without treatment did not show change or reduction on pre-treatment of H2N3 at MOI of 5 with DPPS at the concentrations 5, 50, and 500 µM whatever time point considered (Figure 6.19) when compared to cells infected with untreated virus.

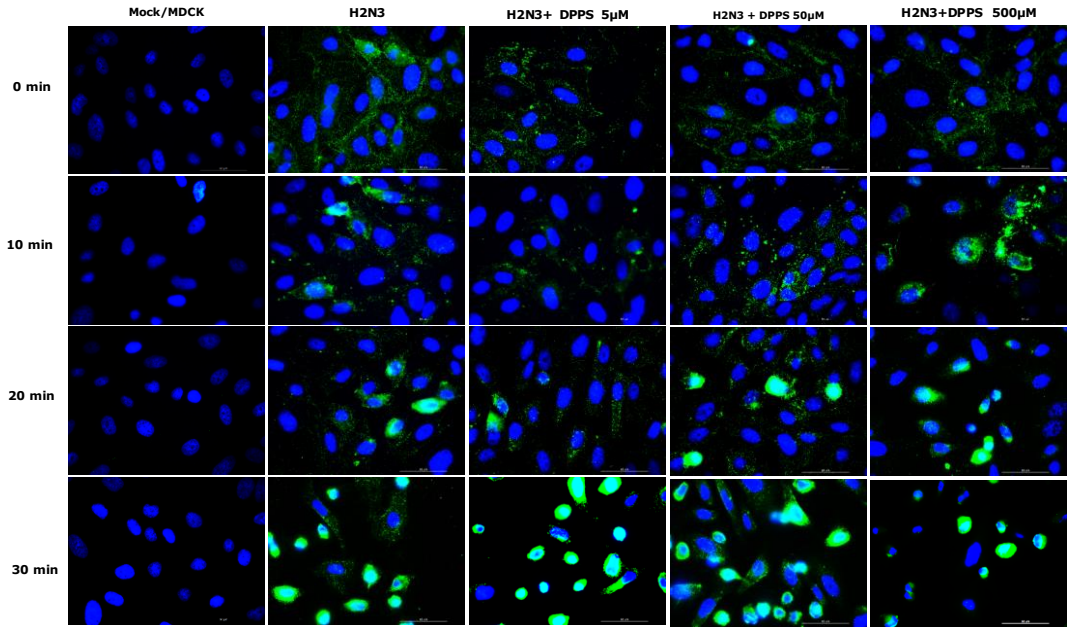

Figure 6:19 Fluorescent–labelled MDCK cells infected with H2N3 virus following a pre-incubation with DPPS.
The immunostaining of influenza virus H2N3 pre-treated with 5, 50 and 500 μM concentrations of DPPS showed no obvious differences in virus binding between control and treatments. Surface virus HA (green) and MDCK nuclei (blue) were stained Images were captured using a Leica fluorescent microscope.

6.3.3.5 **Immunological staining of H3N8 virus pre-treated with DPPG or LPG using MDCK cells**

The immunofluorescence images of uninfected MDCK cells showed no green fluorescence on their cell surface, which was clear at 0 mins on the cell surface of infected cells with H3N8 without treatment indicating virus binding to the cell surface (however, this was less than the fluorescent signals in MDCK cells infected with H2N3). Pre-treatment of H3N8 with LPG showed a reduction in virus binding with 500μM concentration but not with 5 or 50 μM. At 10 mins a reduction of the fluorescent signals was observed in all infected cells and it was assumed that the virus had been trafficked near to the cell periphery. At the same time, there was no apparent reduction in the fluorescent staining between treated and untreated virus. At 20 mins, cells

infected with H3N8 without treatment showed a diffuse cytoplasmic staining of HA, which was reduced in virus treated with 50 and 500 μM of LPG. A further reduction was noticed in the fluorescent staining of cells infected with H3N8 pre-treated with LPG at concentration 50 and 500 μM at 30 min (Figure 6.20).

Similarly, pre-treatment of H3N8 with 500μM of DPPG showed a notable reduction in virus presence at 20 and 30 min suggesting that there was localization of virions in perinuclear region (Figure 6.21).

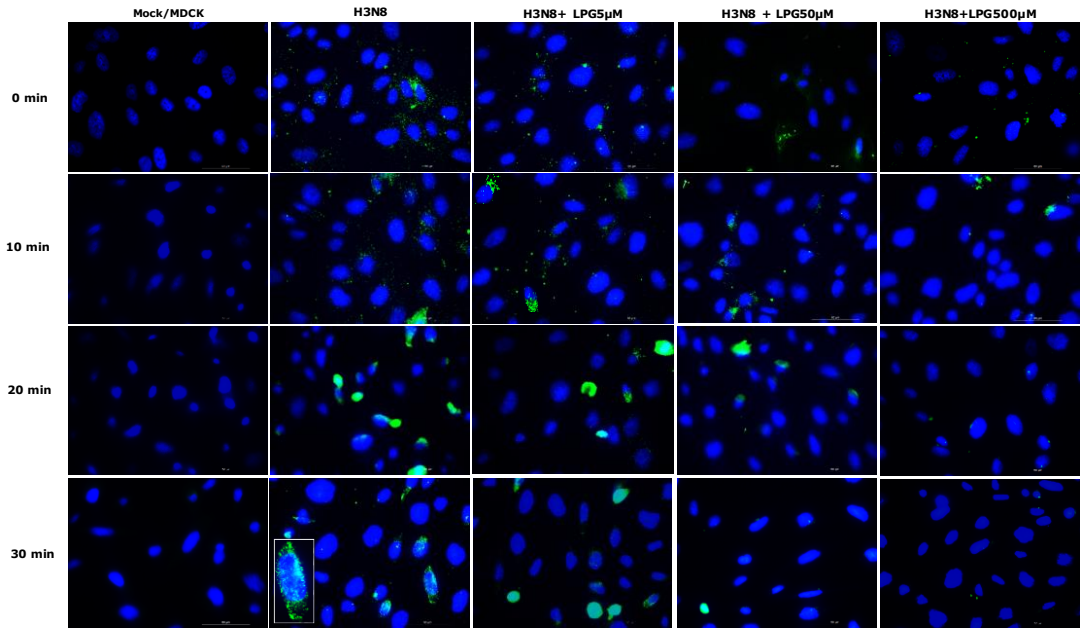

Figure 6:20 Fluorescently labelled MDCK cells infected with H3N8 virus following a pre-incubation with LPG.
The immunostaining of equine influenza virus (EIV) H3N8 pre-treated with 5, 50, and 500 μM of LPG followed by incubation with MDCK cells indicated a drop in the fluorescence signal at different time points. However, the initial control biding (time zero) was relatively low compared to H2N3. Surface virus HA (green) and MDCK nuclei (blue) were stained Images were captured using a Leica fluorescent microscope.

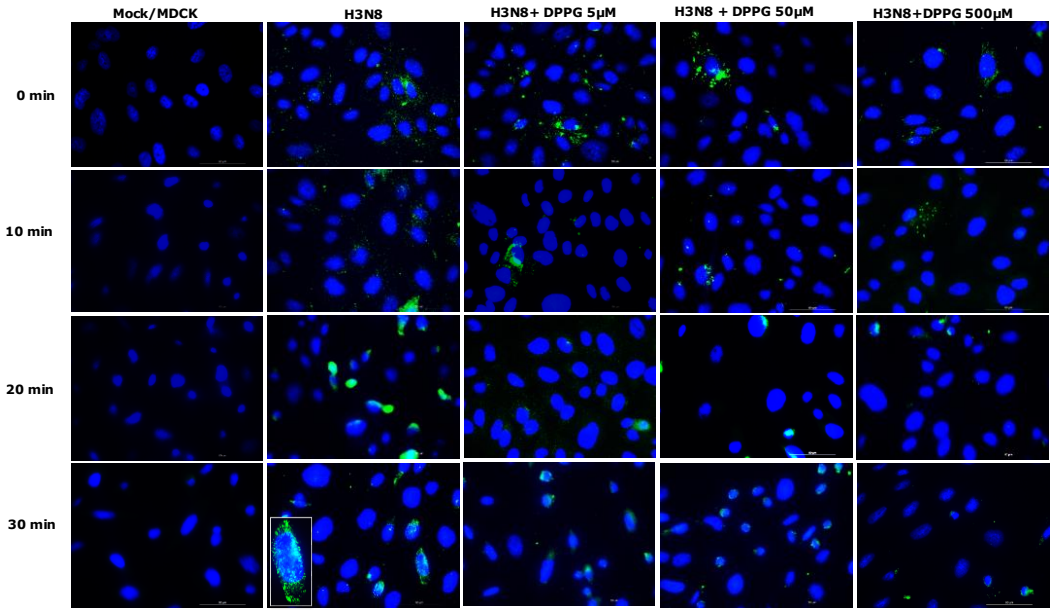

Figure 6:21 Influence of DPPG on binding EIV H3N8 to MDCK cells. The immunostaining of equine influenza virus (EIV) H3N8 pre-treated with 5, 50, and 500 µM of DPPG followed by incubation with MDCK cells indicated a drop in the fluorescence signal at different time points. However, the initial control biding (time zero) was relatively low compared to H2N3. Surface virus HA (green) and MDCK nuclei (blue) were stained. Images were captured using a Leica fluorescent microscope.

6.4 Discussion

Influenza A virus binding to the host cell receptor and the membrane fusion between the viral envelope and the endosomal membrane, are key events in the virus lifecycle with the viral surface glycoprotein HA, a target for researchers to find novel anti-viral agents against influenza (Russell et al., 2008, Mair et al., 2014, Wu et al., 2015).

Double aliphatic chain (DPPG, DPPC or DPPS) and single aliphatic chain (LPG, LPC, LPS) phospholipids did not inhibit the haemagglutination of H2N3 at concentrations of 2, 4, and 8 HAU. Interestingly, the dipalmitoyl phospholipids inhibited the haemagglutination of H2N3 at both 16 and 32 HAU. DPPG inhibited H2N3 virus at 16 and 32 HAU at concentrations ≥ 500 μM and 250 μM respectively. Similarly, DPPS blocked virus agglutination at concentrations of 31.2 μM or ≥ 500 μM for H2N3 virus at 16 or 32 HAU, respectively and DPPC ≥ 500 μM blocked agglutination by 32 HAU of H2N3. Previous researchers have shown that enveloped viruses binding to liposomes depend on the phospholipid head group rather than the acyl chain composition, as enveloped viruses bind to negatively charged lipids to a greater extent (Yamada and Ohnishi, 1986). However, owing to their unique physicochemical structure, lyso-lipids tend to penetrate the cell membrane more readily suggesting that the impact of these specific lipids on chicken RBCs may be linked to this property.

Flow cytometry was successfully used to detect viral HA bound to target cells at a very early stage of viral infection before cell entry (Schulze-Horsel et al., 2008). H2N3 binding time to cells and antibody dilutions were optimised to produce an assay that could be used to rapidly quantify the impact of phospholipids on virus binding to target cells. In this context, flow cytometry results demonstrated a high impact of negatively charged phospholipids. DPPG blocked virus binding to MDCK cell at 37°C for 10 mins, at doses as low as 5 μM. This was confirmed for both suspension and adherent MDCK cells in flow cytometry and immunofluorescent assays, respectively. Similarly, LPG treatment produced a significant reduction in virus binding at 37°C, especially at 500μM. Likewise, MDCK cells infected with LPG and DPPG at 4°C for 10 mins and then cultured at 37°C for further incubation time showed a significant reduction in virus binding at different incubation times especially at lipid concentrations of 50 and 500 μM.

The physicochemical structure of the lipid head has an impact on influenza virus adhesion and fusion to liposomes. It was observed to be higher with PS and cardiolipin (CL) than with neutral lipids including PC/PE/ganglioside. In this context, it is suggested that the fusion process relies, to some extent, on the electrostatic interaction between the virus and the lipids (Stegmann et al., 1989). Liposomes with negative charge displayed a higher binding affinity with Sendai virus (Nir et al., 1986, Stegmann et al., 1989).

Detection of virus binding to adherent MDCK using immunofluorescence similarly demonstrated that LPG and DPPG at concentrations 50 and 500 μM reduce H2N3 binding to MDCK and A549 cells after incubation times from 0 to 20 mins. At 30 min, virus pre-treated with 500μM concentrations of LPG or DPPG showed a marked reduction in the green fluorescent signals of influenza viral glycoprotein HA when compared to untreated virus. However, this assay unexpectedly detected virus internalisation despite the fact that cells were not permeabilised prior to antibody staining. Furthermore, inaccessibility of influenza viral HA in the immunofluorescence assay suggests that the virus might be inside the endosomes which could be confirmed using endosomal markers. It has been documented, using endosomal markers, that influenza virus vRNP is co-localizes first with early endosomes and then late endosomes and that both endosomal compartments are required for productive infection (Sieczkarski and Whittaker, 2003). Consistent with the above explanations and the time of infection (0-30 mins) used in the current study it is suggested that the lipid may have had an impact on the fusion stage of virus life cycle and impaired release of vRNP. It has been documented that DPPG phospholipid markedly inhibits orthopox virus attachment to pneumocytes especially at 4°C incubation (Perino et al., 2011).

H2N3 pre-treated with phosphatidylcholines LPC and DPPC, both polar phospholipids with no net charge, showed no significant reduction of virus binding to MDCK cells at 37°C even at concentrations as high as

500μM. However, performing the same experiment at 4°C incubation showed a reduction on H2N3 binding to MDCK cells at concentrations of 50 and 500 μM for LPC and 500 μM for DPPC. Furthermore, the 4°C incubation had a long lasting impact on virus infectivity at 37°C after 10, 20, and 30 mins incubation times. Similar results were observed using both flow cytometry and immunofluorescence microscopy.

On the other hand, the two aliphatic chain of phosphatidylserine DPPS which carries polar residues and a net negative charge did not show any significant reduction in virus binding to MDCK cells in suspension for any incubation times, at 4°C. These results were confirmed using immunofluorescence. These results suggest that while the negative charge is essential to block virus binding, more complex chemical interactions may hinder the potential impact of lipids used. However, LPS showed a significant reduction of LPAI H2N3 virus binding to the individual MDCK cells in suspension in a dose-dependent manner at different time points. This suggests that single aliphatic chain lipids facilitate virus blocking. It was found that binding of the vesicular stomatitis virus (VSV) with liposome was dependent on the head domain of phospholipids as VSV was bound more efficiently with phosphatidylserine than phosphatidylcholine (Yamada and Ohnishi, 1986).

H3N8 pre-treated with phosphatidylglycerol LPG and DPPG showed a notable reduction of virus fluorescent staining of MDCK cells at 4°C. Incubation with LPG and DPPG also reduced virus staining at 37°C

after 20 and 30 mins incubation times. Although the impact of phospholipids on H3N8 virus had been expected to be greater due to the filamentous structure of the virus, that was not the case as similar results as for the H2N3 virus binding was found. However, the initial amount of H3N8 virus bound to cells was remarkably low, despite using an MOI of 5.0.

Overall, pre-incubating the virus with phospholipids seems to have an impact on the ability of the virus to bind either by inhibiting virus binding to cellular receptors or causing disruption of the viral envelope. So, specific lipids could be considered as a potential new inhibiting factor for influenza infection.

Chapter 7: Measurement of the effect of phospholipids on influenza virus and host gene expression using quantitative RT-PCR

7.1 Introduction

7.1.1 Induction of cytokine responses following influenza A infection

The innate immune response to the infection of the respiratory epithelial cells by influenza is triggered by Pattern Recognition Receptors (PRRs) present on host cells including tracheobronchial and alveolar epithelial cells. These PRRs including TLRs (such as TLR3 and TLR7), RIG-I-like receptors (RLRs) and NOD-like receptors (Kanneganti, 2010) contribute to the detection of viral infections and enhance the release of cytokines and type I interferons (IFNs) (Le Goffic et al., 2007, García-Sastre, 2011). IFN-α and -β play a vital role in the immune response against influenza virus by a number of mechanisms including the upregulation of monocyte chemotactic protein (MCP) and IFN-inducible protein 10 (IP-10) expression of which mediate the migration of monocytes/macrophages and Th1-type cells to the site of infection. IFN-α and -β also enhance the adaptive immune response, for example, by increasing antigen presentation of macrophages and dendritic cells (DCs) and enhancing NK and T cell expression of IFN-γ (Julkunen et al., 2000). Other cytokines such as interleukins IL-1, IL-6 and CXCL10 are upregulated early; 3 to 6 hrs after influenza infection, followed by the expression of TNF-α and IL-8 (Lam et al., 2010, Kawai and Akira, 2011). These cytokines enhance the migration of leukocytes to the infected airway cells. IL-1α/β increases the immunoglobulin IgM antibody response and enhances monocyte and neutrophil recruitment after influenza

viral infection (Schmitz et al., 2005). Others report that RIG-I activates nuclear factor kappa B (NF-kB) signalling, which in turn upregulates secretion of IL-1β and IL-18 after influenza viral infection, promoting NLRP3 inflammasome activity (Kanneganti, 2010, Poeck et al., 2010).

Distinct patterns and kinetics of chemokines released post infection of influenza virus have also been reported, as within 2 to 4 hrs post infection, CXCL16, CXCL1, CXCL2 and CXCL3 expression is upregulated, allowing the migration of leukocyte, cytotoxic T cells and natural killer (NK) cells to the site of infection. After 8 to 12 hrs, the expression and release of CXCL8, CCL3, CCL4, CCL5, CXCL9, CXCL10 and CXCL11 cytokines results in the attraction and activation of effector memory T cells. Subsequently, 24-48 hrs post infection, DCs residing in lymphoid tissues activate the adaptive immune response through the chemotaxis of T- and B- lymphocytes (Piqueras et al., 2006). TNF-α belongs to a family of tumour necrosis factors (TNFs) and their receptors are expressed in different cell types, regulating many cell functions including proliferation, apoptosis and inflammatory response to pathogens. TNF-α is considered to be a potent stimulant for the production of many inflammatory cytokines, prostaglandins and platelet activating factor (Parameswaran and Patial, 2010). Infection of airway epithelial cells with influenza A virus enhances the early production of TNF-α as well as IFN-α, IFN-β and IL-1, which are associated with many clinical symptoms commonly related to influenza, such as fever, lethargy and lack of appetite. TNF-

α activates antiviral activity through upregulating MCP-1 and MCP-3 gene expression levels which, in turn, stimulates maturation of macrophages and DC (Julkunen et al., 2000). Furthermore, TNF-α has a profound effect on increasing the adhesion of leukocytes to the vascular endothelium. Subsequently, this is followed by an increase in concentration and activation of neutrophils and macrophages at the site of infection mediated by neutrophil-attracting cytokines-8 (IL-8) and monocyte-attracting chemokines (Van Reeth, 2000). Chemokines bind to receptors on leukocytes, allowing them to change their shape and behaviour and migrate to the site of inflammation (Julkunen et al., 2000). The biological activity of IL-8 comes from its specific amino acid sequence, namely the glutamic acid-leucine-arginine (ELR), which is essential for the binding of IL-8 to its receptor found in different cell types, especially in monocytes and macrophages (Remick, 2005).

Influenza virus spreading from the initial site of infection relies on its ability to evade the immune system. Many molecular/cellular strategies are involved including the blocking of IFNs, inhibition of RIG-I activation and the STAT transcription factor expression, mediated by the viral NS-1 protein (Wang et al., 2000, Mibayashi et al., 2007, Munir et al., 2011). However, excessive cytokine expression in response to highly pathogenic strains of influenza virus can also lead to lung-tissue damage (Oslund and Baumgarth, 2011, Kuchipudi et al., 2014).

Gene quantification and RNA copy number measurements were obtained through quantitative reverse transcription polymerase chain reaction (qRT–PCR). This is a very sensitive and specific method for measuring mRNA (Lee and Suarez, 2004). Likewise, the method has been shown to be valuable for determining cytokine transcription levels including IL-6, IL-8, IL-1a, IL-1B and TNFa in equine influenza (Allen et al., 2007). Real-time PCR assays are reliable and sensitive for the quantification of M gene transcription levels in clinical and experimental samples (Ward et al., 2004, Panning et al., 2009).

7.2 Aims and objectives

Objective

To determine if pre-treatment of virus with phospholipids reduces the transcription of pro-inflammatory cytokines and IFN-β in cells following influenza infection.

Aims

1. To measure the mRNA expression level of cytokines TNF-α and IL-8 from MDCK or A549 cells infected with H2N3, H3N8 or H1N1, with or without phospholipid pre-treatment.

2. To measure the mRNA expression level of IFN-β in MDCK cells infected with H2N3, with or without phospholipid pre-treatment.

3. To measure the expression of the viral M gene from H2N3-infected MDCK and A549 cells or H3N8-infected MDCK cells with or without lipid pre-treatment.

7.3 Materials and Methods

7.3.1 Influenza A virus pre-treated with phospholipids and infection of MDCK and A549 cells

H2N3, H3N8 or H1N1 were treated with 500 μM of LPG or DPPG (prepared as detailed in Section 2.4) for 30 min at 37°C and lipids in excess were removed through centrifugation twice using Amicon filtration. MDCK cells and A549 cells were infected with H2N3, while MDCK cells were only used for H3N8 or H1N1 strain (all MOI of 5). Both cell types (MDCK and A549) were either pre-treated with lipids, LPG or DPPG of 500 μM (pre-centrifuged using an Amicon filtration) without virus, or incubated for 2hrs at 37°C with 1 mL of IM containing influenza A virus with and without pre-treatment with lipids. Cells were rinsed three times with PBS and then incubated in IM at 37°C with 5% CO_2 for 22 hrs. At 24hrs post-infection (2 hrs + 22 hrs), the cells were washed three times with PBS, cells lysates were prepared in 350μL of RLT plus buffer (Qiagen) and kept at -80°C.

7.3.2 RNA extraction

Viral RNA was extracted from mock (non-infected) cells with or without phospholipid treatment and infected cells with influenza virus subtypes with or without phospholipid treatment using QIAamp viral RNA purification kit (Qiagen), according to the manufacturer's instructions. Fifty microlitres of RNA was extracted from each cell

lysate using the RLT buffer. The concentration and quality of RNA were measured with a NanoDrop 8000 spectrophotometer (Thermo Scientific, UK) by UV absorption according to manufacturer's instructions. RNA purity was determined via the measurement of the absorbance ratio (260nm/ 280nm), considering a ratio of 1.8-2.1 to be ideal. Samples were kept at -80°C until further use.

7.3.3 **First strand cDNA synthesis**

The reverse transcription reaction of the viral RNA to cDNA was performed using a SensiFAST™ cDNA Synthesis Kit (Bioline). For the reaction, manufacturer's instructions were followed with 1 µl of Reverse Transcriptase enzyme, 4µl of Trans Buffer and 1 µg RNA solution per sample; the samples were made up to a final volume of 20µl with diethyl-pyrocarbonate (DEPC) treated water. cDNA was synthesised using a thermal cycler (XP cycler) at 25 °C for 10 min for primer annealing, followed by the reverse transcription at 42 °C for 15 min and 48°C for 15 min. The reaction was stopped by incubation for 5 min at 85°C. Samples were diluted using a 1:5 ratio (cDNA: DNase/RNase free-Water) and were then kept at -20°C until used in subsequent quantitative PCR assays.

7.3.4 **Quantitative PCR**

7.3.4.1 **Quantitative PCR for cellular RNA**

cDNA obtained by reverse transcription was amplified by qPCR using human (for RNA extracted from A549 cells) or canine (for RNA extracted from MDCK cells) gene specific primers for IL-8, TNFα and

IFN-β. 18S rRNA was used as a reference gene , previously shown to be suitable for analysis of a range of cells infected with influenza A (Kuchipudi et al., 2012) (Table 7.1). All primers were synthesised by Sigma Aldrich.

Table 7:1 Primers used for RT–PCR amplification.

Gene name	Forward primer (5'-3')	Reverse primer (3'-5')	Species
18S	TGTGCCGCTAGAGGTGAAATT	TGGCAAATGCTTTCGCTTT	Human
18S	AGAAACGGCTACCACATCC	CACCAGACTTGCCCTCCA	Canine
IL-8	GTTTTTGAAGAGGGCTGAG	TTTGCTTGAAGTTTCACTGG	Human
IL-8	CTAAAGAAGGCTGAGAAAC	TTTGAAGTCTCATTGGCATC	Canine
TNF α	AGGCAGTCAGATCATCTTC	TTATCTCTCAGCTCCACG	Human
TNF α	TAGCTCATGTTGTAGCAAAC	AGTAGATGAGGTACAACCC	Canine
IFN-β	CCAGTTCCAGAAGGAGGACA	TGTCCCAGGTGAAGTTTTCC	Canine

Quantitative PCR was performed using a SensiFAST™ SYBR® No-ROX Kit (Bioline) with cDNA as reaction template. The PCR master mix was prepared in RNase-free conditions following the manufacturer's instructions (Table 7.2). Quantitative PCR was performed using one cycle at 95 °C for 2 min, followed by 45 cycles of 5 s at 95°C, 10 s at 60°C and 15 s at 72°C.

Table 7:2 Example of components and concentrations of a master mix for the quantitative PCR of cellular mRNA

Components	Volume/ reaction μL
2x SensiFAST SYBR® No-ROX Mix 1x	10 μL
10 μM forward primer (used at final concentration of 400 nM)	0.8 μL
10 μM reverse primer (used at final concentration of 400 nM)	0.8 μL
Template	5 μL
DNase (Deoxyribonuclease)/RNase free-Water	3.4 μL
Final volume	20 μL

The relative expression of cellular genes was determined using the 2^-ΔΔCt method (Livak and Schmittgen, 2001). The Ct values of the infected samples were normalised to 18S housekeeping gene Ct value, relative to the expression in untreated, uninfected cells. Data were analysed (one-way ANOVA; $p < 0.05$) using Graph Pad Prism software (version 7.02).

7.3.4.2 **Quantitative PCR for influenza virus (M gene) RNA**

Influenza matrix gene (M gene) was quantified using the SensiFAST™ probe No-ROX Kit (Bioline) (Table 7.3). A forward primer (5'–3') AGA TGA GTC TTC TAA CCG AGT CG and reverse primer TGC AAA AAC ATC TTC AAG TCT, with a hydrolysis probe (5'–3') [6FAM]TCAGGCCCCCTCAAAGCCGA[BHQ1] were used to amplify a 101 bp region of the M gene as previously described (Spackman et al., 2002, Slomka et al., 2009).

Table 7:3 Example of components and concentrations of master mix for real-time PCR quantification of influenza M gene

Components	Volume/reaction μL
2x SensiFAST Probe No-ROX Mix 1x	10 μL
10 μM forward primer (used at final concentration of 400 nM)	0.8 μL
10 μM reverse primer (used at final concentration of 400 nM)	0.8 μL
10 μM probe (used at final concentration of 100 nM)	0.2μL
Template	5 μL
DNase/RNase free-Water	3.2 μL
Final volume	20 μL

Fifteen microliters of master mix were added to each required well of a 96–well plate (Thermo Scientific), followed by 5 µl of RNA template for each sample. Each assay was run as follows: one cycle at 50°C for 30 min, one cycle at 95°C for 2 min and 40 cycles of 95°C for 15 s and 60°C for 1 min.

In vitro transcribed influenza M gene RNA (a kind gift from Dr Suresh Kuchipudi) was used to provide a standard with a known copy number. The total RNA concentration was determined using a NanoDrop 8000 spectrophotometer and a serial dilution of the M-gene standard was made and analysed using RT-qPCR. An 18S reference gene standard curve was used to estimate the cell number per reaction. Total RNA was extracted from MDCK cells using QIAamp viral RNA purification kit (Qiagen) and RNA concentration determined using the NanoDrop 8000 (1530 ng/µL, equivalent to approximately 19200 cells/µL). A five-fold dilution series was prepared (1:5 to 1:15625) and used as a standard curve to determine the cell number in each sample. The absolute expression of viral M gene was determined by dividing the gene copy number of M gene in treated and untreated samples by the gene copy number of 18S rRNA. All RT-qPCR reactions were analysed using Light Cycler® 480 software version 1.5 (Jiang et al., 2016). Data were analysed (one-way ANOVA; $p < 0.05$) using Graph Pad Prism software (version 7.02).

7.4 Results

7.4.1 Measurement of the matrix and 18S gene copy number by quantitative RT-PCR

A standard curve of the influenza virus mRNA M gene was prepared using RT-qPCR. Then, the CT values obtained were plotted against a log10 scale of the known M gene copy number (R^2=0.972, slope of -2.684, efficiency of 2.05). The curve was subsequently used as a standard for quantification of M-gene transcripts following viral infection (Figure 7.1).

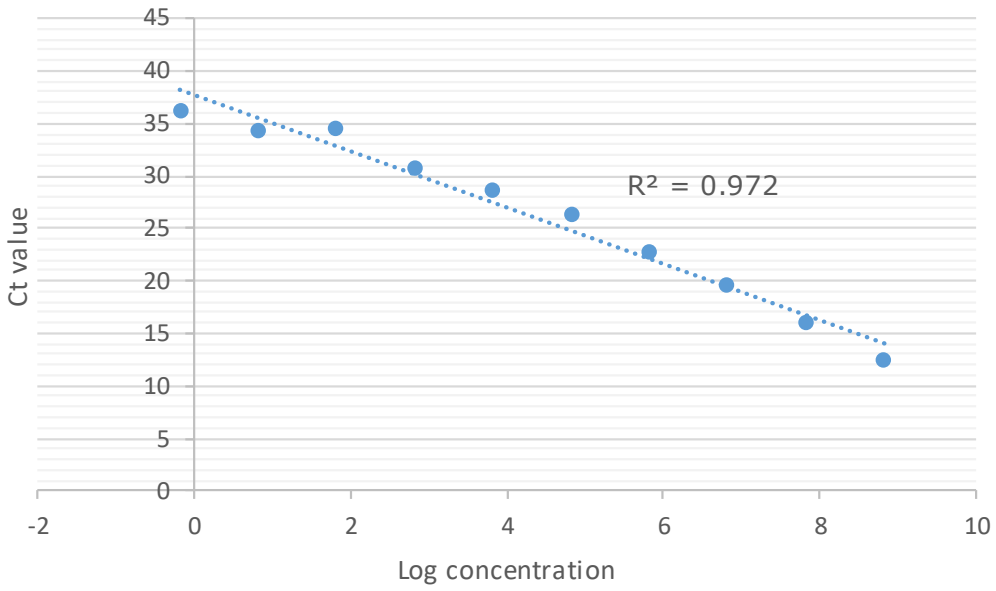

Figure 7:1 Standard curve of the M gene.
The X-axis shows the M gene copy number. Y-axis represents the average of Ct values for a given M-gene copy number.

The 18S gene standard curve was prepared using RT-qPCR, the Ct values were plotted against a log10 scale of known 18S reference

gene concentration (equivalent to cell number, efficiency of 2.01) (Figure 7.2).

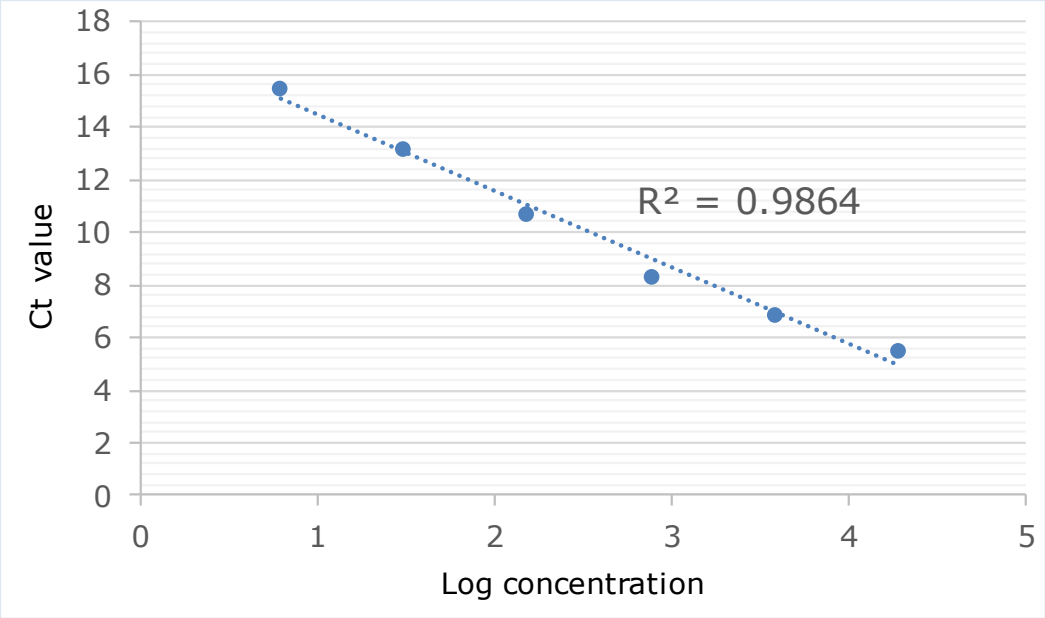

Figure 7:2 Standard curve for 18S gene copy number.
The X-axis shows the estimated cell number per reaction. Y-axis represents the average of Ct value.

7.4.2 Impact of phospholipid treatment of influenza A on IL-8 expressions from MDCK and A549 cells

MDCK cells infected with LPAI H2N3 virus induced approximately a ten-fold increase in IL-8 expression ($p<0.05$) compared to uninfected cells. However, pre-treatment of H2N3 with 500 μM of DPPG or LPG significantly reduced IL-8 cytokine expression when compared with MDCK cells infected with H2N3 virus without treatment. Cells treated with 500 μM of DPPG or LPG only, i.e. without viruses, showed no significant change in IL-8 expression compared with untreated cells (Figure 7.3A).

A similar upregulation (~5-7 fold) of IL-8 expression was seen in MDCK cells following H3N8 or H1N1 infection when compared to uninfected cells (Figure 7.3 B and C respectively). Reduced IL-8 expression was observed ($P<0.05$, $P<0.01$) following DPPG or LPG pre-treatment of H1N1 or H3N8 virus compared to MDCK cells infected with H1N1 or H3N8 virus without lipid pre-treatment. There was no significant difference in IL-8 expression from the mock-treated MDCK cells with 500 μM of DPPG or LPG when compared to mock untreated cells. There is an apparent reduction in IL-8 gene expression in MDCK cells treated with 500 μM of LPG in Figure 7.3A (although this is not statistically significant when compared to mock untreated cells). This apparent reduction in IL-8 expression on treatment with 500 μM of DPPG was not observed in further experiments using the same experimental conditions (Figure 7.3B & C).

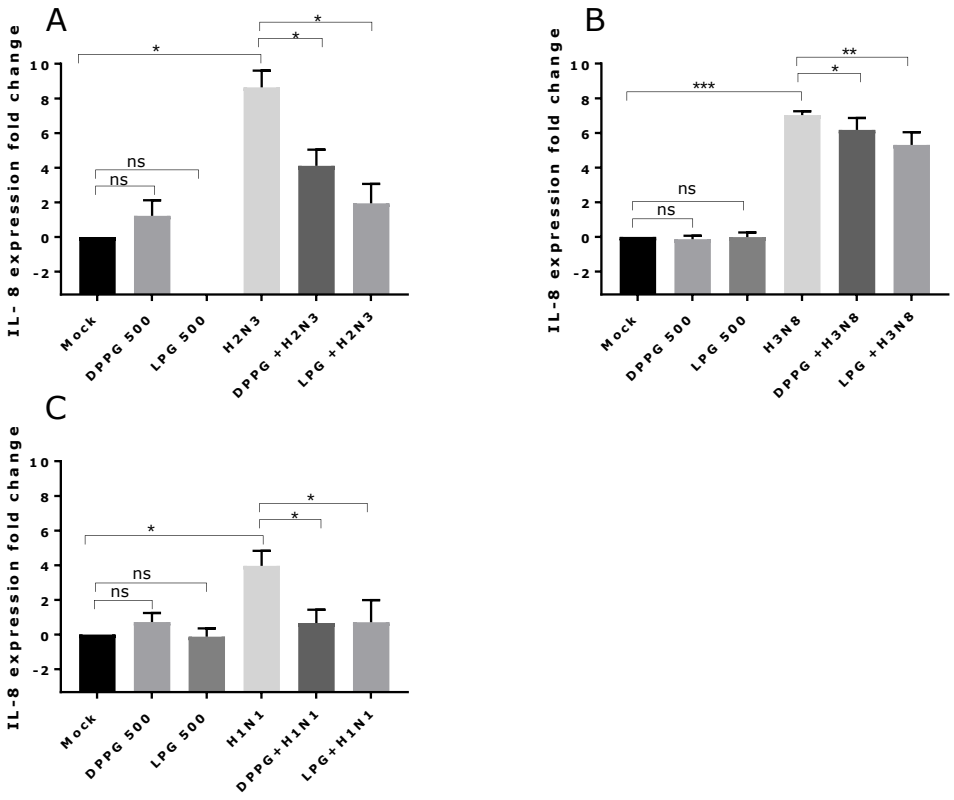

Figure 7:3 IL-8 cytokine expression levels from infected cells with influenza A viruses.
A) H2N3 infected MDCK cells, B) H3N8 infected MDCK cells, C) H1N1 infected MDCK cells. Infected cells for 24hrs with influenza viruses H2N3, H3N8 and H1N1 induced significant expression of IL-8 (*P<0.05) when compared to uninfected cells. Infected cells with influenza virus subtypes pre-treated with 500μM of DPPG or LPG reduced IL-8 expression significantly when compared to infected cells with lipid-untreated influenza virus subtypes (*P<0.05, **P<0.01). No significant differences were shown in the expressions of IL-8 from mock cells–treated with LPG or DPPG when compared to mock untreated cells. Data points are the mean of three biological replicates with SD as an error bar.

Similarly to IL-8 expression in MDCK cells infected with H2N3, IL-8 expression was also upregulated approximately nine fold in A549 cells in the presence of the virus (P<0.01). Pre-treatment of the virus with DPPG or LPG significantly reduced IL-8 expression (Figure 7.4). There were no significant differences in the expression of IL-8 in MDCK treated with 500 μM of DPPG or LPG only when compared to untreated cells. However, elevated expression levels of IL-8 were observed in

A549 cells treated with 500 μM of DPPG when compared to mock untreated A549 cells (Figure 7.4).

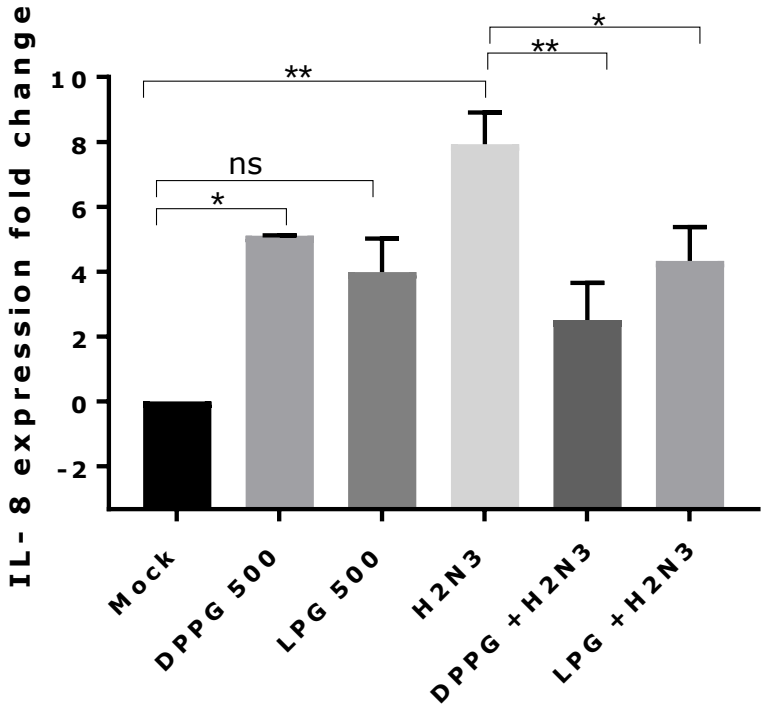

Figure 7:4 IL-8 cytokine expression levels from infected A549 cells with H2N3 virus.
H2N3 infected A549 cells. Cells infected with the H2N3 virus for 24 hrs induced significant expression of IL-8 (*P<0.05). Infected cells with H2N3 virus pre-treated with 500μM of DPPG or LPG reduced IL-8 expressions significantly (*P<0.05, **P<0.01) when compared to infected cells. No significant differences were shown in the expressions level of IL-8 from mock cells–treated with 500μM of DPPG or LPG when compared to mock untreated cells. However, a slight upregulation of IL-8 expression was shown only with mock A549 treated cells with 500 DPPG μM. Data points are the mean of three biological replicates with SD as an error bar.

7.4.3 **Impact of phospholipid treatment of influenza A on TNF-α cytokine expression from MDCK cells and A549 cells**

The expression level of TNF-α from MDCK cells infected with H2N3 for 24hr was significantly upregulated by eight-fold (P<0.01). However, the expression of TNF-α was markedly downregulated when H2N3 was pre-treated with 500 μM of DPPG or LPG (Figure 7.5A).

H3N8-infected MDCK cells showed a significantly ($P<0.01$) increased expression of TNF-α around five-fold when compared to uninfected cells. However, pre-treatment with DPPG or LPG showed no significant reduction in the expression of TNF-α in MDCK cells (Figure 7.5B). In contrast, MDCK cells infected with H1N1 pre-treated with DPPG or LPG showed a significant reduction of TNF-α expression ($P<0.001$) reaching a value close to the expression level of mock uninfected cells (Figure 7.5C). There is a reduction of IL-8 expression level of MDCK cells treated with 500 μM of DPPG in graph A but not significant when compared to untreated MDCK cells. Generally, mock MDCK cells treated with 500 μM of LPG or DPPG (Figure 7.5 A, B and C) did not show any significant differences in TNF-α expression when compared to untreated MDCK cells.

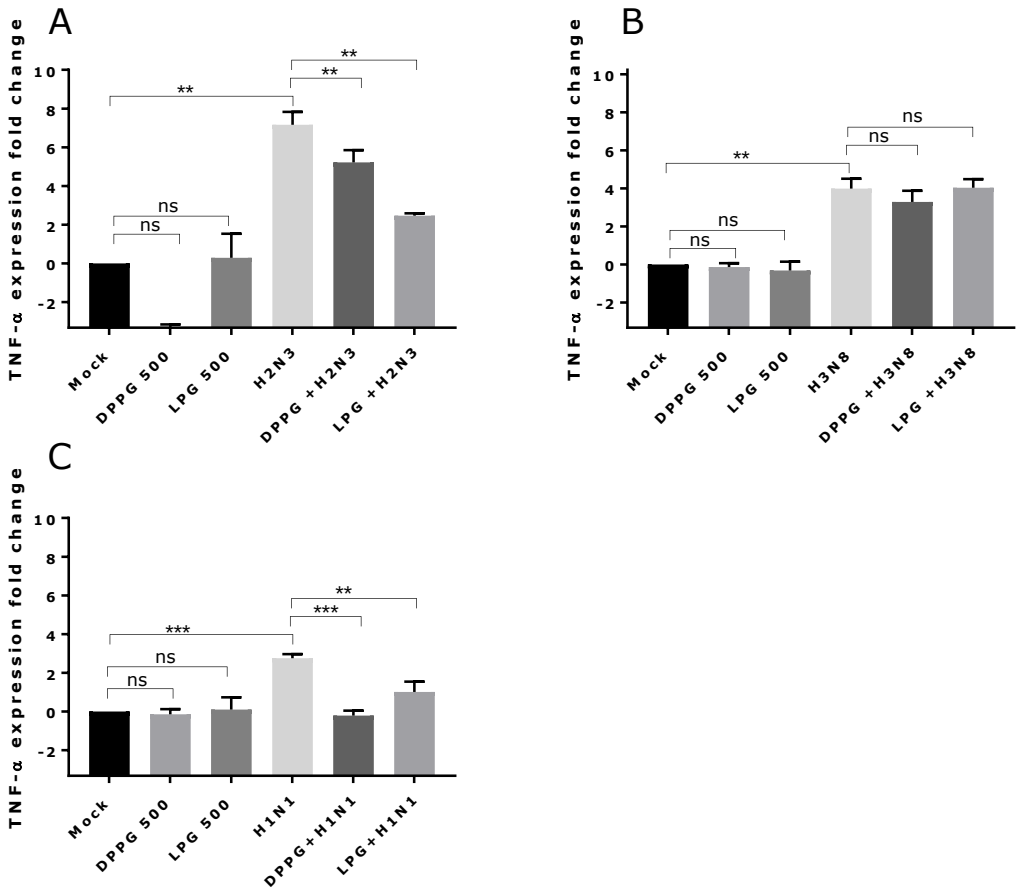

Figure 7:5 TNF- α cytokine expression from infected MDCK cells with influenza A viruses.
A) H2N3 infected MDCK cells, B) H3N8 infected MDCK cells, C) H1N1 infected MDCK cells. Mock infected cells for 24hr with influenza viruses H2N3, H3N8 and H1N1 induced significant expression of TNF-α (**P<0.01) when compared to mock uninfected cells. Pre-treating influenza A viruses H2N3, H1N1 with DPPG and LPG showed a marked reduction in TNF-α expression levels (**P <0.01, ***P <0.001). However pre-treated equine influenza virus H3N8 with DPPG and LPG did not show any significant reduction in TNF-α expression levels. Mock–treated cells with LPG or DPPG did not show any significant differences in TNF-α expressions when compared to mock-untreated MDCK cells. Data point are the mean of three biological replicates with SD as an error bar.

Similarly to TNF-α expression by MDCK cells infected with H2N3 virus, TNF-α expression by H2N3-infected A549 cells at 24hr was increased by ten-fold (P<0.01) when compared to uninfected cells. However, the expression of cytokine TNF-α was downregulated significantly (P<0.05, P<0.01) when the virus was pre-incubated with 500μM of DPPG or LPG, respectively (Figure 7.6). DPPG treated uninfected

MDCK and A549 cells did not show a significant difference in the expression of TNF-α when compared to untreated cells. However, a regulated expression of TNF-α was seen in A549 cells treated with 500μM of LPG (Figure 7.6).

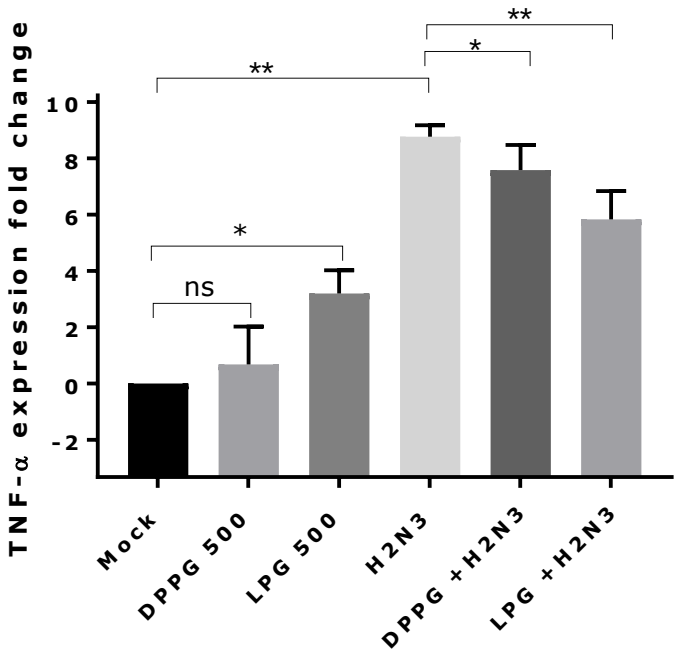

Figure 7:6 TNF-α cytokine expression from infected A549 cells with H2N3 virus.
H2N3 infected A549 cells. Mock infected cells for 24hr with H2N3 virus induced significant (**P<0.01) expression of TNF-α. Cells infected with H2N3 virus pre-treated with 500μM of DPPG or LPG downregulate TNF-α expression (*P<0.05, **P < 0.01). A difference in the expression of TNF-α was noted when A549 cells are treated with 500 μM LPG only. Data points are the mean of three biological replicates with SD as an error bar.

7.4.5 **Impact of phospholipids on IFN-β cytokine expression following H2N3 infection**

The expression level of IFN-β from MDCK cells infected with H2N3 without lipid treatment was significantly upregulated by twelve-fold at 6 hrs pi ($P<0.01$) when compared to uninfected cells, which was then reduced to eight-fold 24hrs post infection (Figure 7.7). While no significant ($P>0.05$) reduction was noted at 6 hrs pi following pre-treatment of H2N3 with DPPG, a reduction in IFN-β expression was observed at 24 hrs pi ($P<0.05$). However a significant reduction in IFN-β expression was noted at 6 hrs (four-fold, $P<0.05$) and 24 hrs (six-fold, $P<0.01$) pi following LPG treatment of virus. IFN-β expression levels were not significantly changed when compared with uninfected MDCK cells mock treated with 500 μM of DPPG or LPG at 6 and 24 hrs.

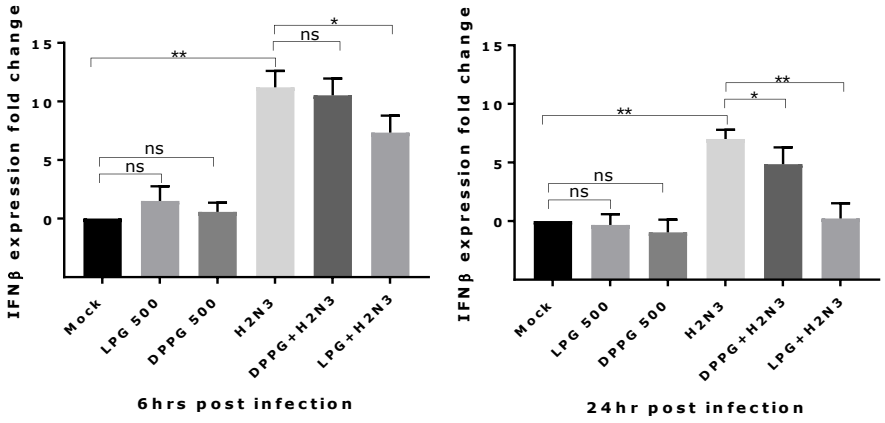

Figure 7:7 IFN-β expression from infected MDCK cells with H2N3 virus pre-treated with DPPG or LPG.
Mock infected cells for 6 and 24hrs with H2N3 virus MOI of 0.1 induced significant expression of IFN-β (**$P<0.01$) when compared to mock uninfected cells. Infected MDCK cells with H2N3 pre-treated with DPPG and LPG showed a marked reduction (*$P<0.05$, **$P<0.01$) in IFN-β expression levels at 24hrs pi compared to Infected cells with the untreated virus. Mock–treated cells with LPG or DPPG did not show any significant difference in the IFN-β expression levels compared to mock-untreated MDCK cells. Data points are the mean of four biological replicates with SD as an error bar.

7.4.6 **M gene copy number quantification by RT-qPCR**

MDCK and A549 cells infected with H2N3 virus showed an up-regulation of M gene expression levels. However, a significant reduction ($P<0.05$, $P<0.01$) of viral M gene expression to 42% and 37% was observed at 24hrs pi in MDCK cells incubated with H2N3 pre-treated with DPPG or LPG, respectively, when compared to infected MDCK cells with H2N3 without lipid pre-treatment (100%)(Figure 7.8A).

Reduction in M gene expression levels was also noticeable when A549 cells were infected with H2N3 pretreated with phospholipids, as the percentage of M gene was significantly ($P<0.05$) reduced to 13 % with DPPG and 58 % with LPG. (Figure 7.8B).

The expression levels of M gene were upregulated in infected MDCK cells with H3N8 pre-treated with DPPG or LPG (99%). No significant differences ($P>0.05$) of viral M gene expression were seen in MDCK cells infected with H2N3 pre-treated with DPPG(80%) or LPG(99%) when compared to infected cell with H2N3 without lipid pre-treatment (100%) (Figure 7.8C).

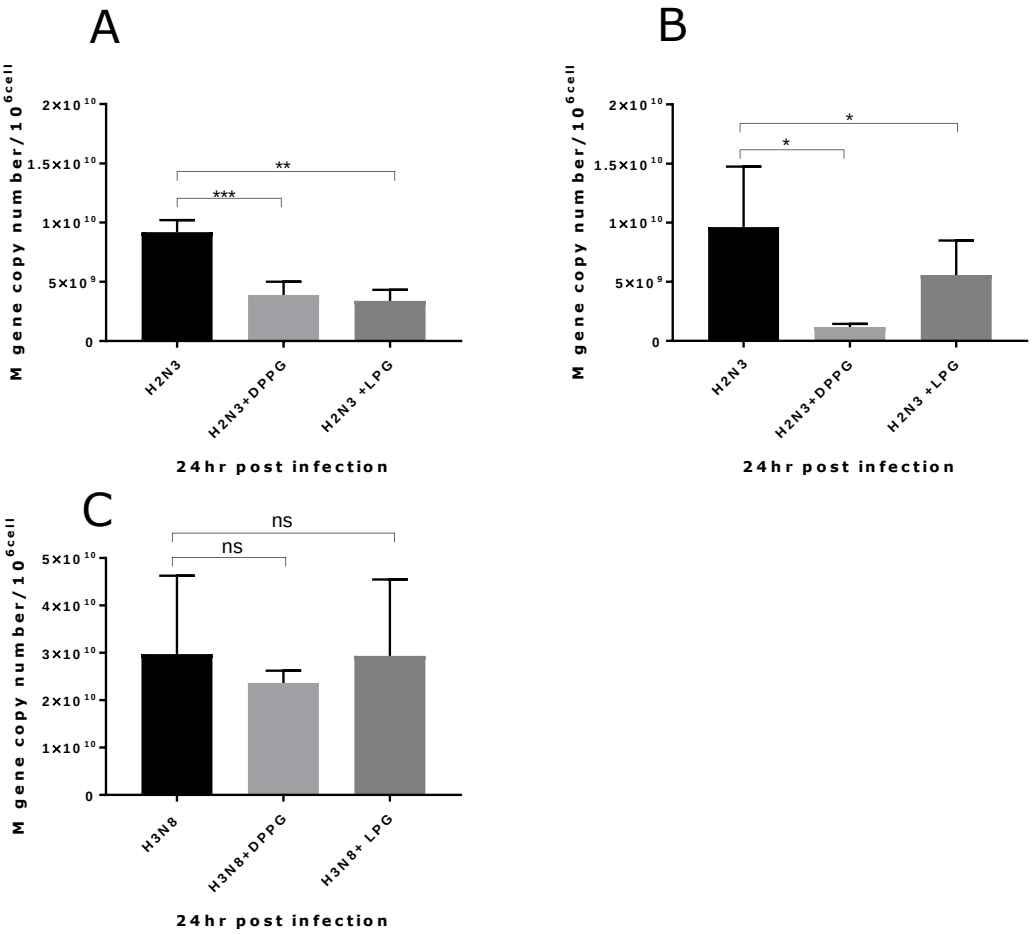

Figure 7:8 M gene copy number for Influenza A viruses pre-treated with DPPG and LPG 24 hr post infection.
(A) H2N3 infected MDCK cells, (B) H2N3 infected A549 cells, (C) H3N8 infected MDCK cells. DPPG or LPG demonstrate a significant impact on the number of copies of the M gene normalised to 18S rRNA only with the LPAI H2N3 virus. Data points show the mean and standard error of triplicate well (* $p < 0.05$, ** $p < 0.01$, *** $p < 0.001$; one-way ANOVA).

7.5 Discussion

Influenza A viral infection enhances cytokine and chemokine production, recruiting mononuclear blood cells to the site of infection and activating the antiviral immune response (Julkunen et al., 2000). It has also been documented that IL-8, IL-6 and TNF alpha (LITAF) are upregulated following avian influenza (H5N1) infection of chicken cells (Kuchipudi et al., 2014) and the severity of influenza virus H1N1 in humans has been correlated to the expression level of IL-6, IL-5, IL-8 and TNF-α cytokines (Hagau et al., 2010). Results from the present study confirmed that host cells infected with influenza A virus H2N3, H3N8 or H1N1 were associated with a significantly higher expression of TNF-α, IL-8 and IFN-β when compared to mock uninfected cells. Consequently, we hypothesised that pre-treatment of virus with phospholipids might reduce the expression of TNF-α, IL-8 and IFN-β.

In this context the expression levels of IL-8 were significantly reduced when measured 24 hrs pi using H2N3, H3N8 or H1N1 following pre-treatment with DPPG or LPG, in either MDCK or A549 cells. These results are comparable to the findings that POPG reduced the infectivity of respiratory syncytial virus and inhibited the upregulation of IL-6 and IL-8 in bronchial epithelial cells (Numata et al., 2010). There is a major difference, however, in the fact that in this present study it is the viruses that are pretreated with the lipids and not the cells as described in Numata et al. (2010).

TNF-α has been demonstrated to be a major cytokine upregulated in response to influenza infection, leading to the enhancement of the NF-κB transcription factor activity within an hour of virus infection. NF-kB activation leads to the expression of other cytokines (Simmons and Farrar, 2008, Park et al., 2015) including IFN-β (Piqueras et al., 2006).

TNF-α expression was significantly reduced in MDCK or A549 cells infected with LPAI H2N3 pre-treated with 500μM of DPPG or LPG. A similar significant reduction of TNF-α expression from MDCK cells infected with H1N1 virus following pre-treatment with DPPG or LPG was also noted. Neither DPPG nor LPG demonstrated an impact on TNF-α expression by MDCK cells infected with equine influenza virus H3N8. The present results agree in principle with the observation that POPG (which has the same lipid head domain as is used in this study; PG) inhibits TNF-α expression in pulmonary alveolar cells pre-treated with phospholipids prior to incubation with lipopolysaccharide, which is purified from *Escherichia coli* (Kuronuma et al., 2009).

IFNα/β is a crucial cytokine produced by epithelial cells or macrophages infected with influenza virus. A significant upregulation in IFN-β expression levels in MDCK cells infected with H2N3 for 6 and 24hrs were measured. This result is in agreement with the finding that IFN-β expression is upregulated in MDCK cells infected with canine influenza virus (Park et al., 2015) and with human influenza virus H5N1 (Chan et al., 2005). We observed that pre-treatment of

virus with DPPG or LPG reduced IFN-β expression 24 hrs post-infection with levels approaching those of uninfected cells. These findings are in agreement with others showing that PG reduced cytokine expression (Hashimoto et al., 2003) and that POPG inhibited eicosanoids production from macrophages while palmitoyl-oleoyl-phosphatidylcholine (POPC) did not (Kandasamy et al., 2011).

However, at the present time, it is unclear as to why, with our filtration method that should remove any excess of lipids, DPPG and LPG upregulate, respectively, IL-8 and TNF-a, in A549 cells and not in MDCK cells. Although this needs further clarification, we may hypothesise that this may be related to the cell type used and possibly to the low residual concentration of lipids in the supernatant that may exist following Amicon filtration.

Nonetheless a marked reduction of IFN-β was observed in MDCK cells infected for 24hrs with influenza A virus pre-treated with 500μM of DPPG and LPG. As IFN-β expression is the result of virus infecting cells then this result agrees with data obtained in Chapter 4 when the same MOI of 0.1 was used. Indeed, it was observed lower kinetics of infectivity were observed at this MOI, which may suggest that the virus may have been altered upon lipid pre-treatment explaining the low IFN-β expression levels. However, the infectivity is a time-dependent process meaning that even with a low initial binding due to lipid pre-treatments, viruses can still bud out from cells following their replication and infect more surrounding cells which could explain

why treated viruses are still able to stimulate cell cytokine responses over time at 24 hrs. Likewise, the decrease in expression of IL-8 and TNF-a may also be related to a lower initial amount of viruses bound to cells due to lipid treatments. However, over time the infection may proceed when low MOI are used.

The M gene copy number of both MDCK and A549 cells infected for 24 hrs with H2N3 was significantly reduced after the virus pre-treatment with DPPG or LPG. However, the M gene copy number of equine influenza virus H3N8 was not significantly reduced under the same conditions when compared to H3N8 without treatment which showed a high expression of viral M gene. Our results agree, at least in principle, with data of Numata et al. (2012) which showed that 1 mg/ml of Palmitoyl-oleoyl-phosphatidylglycerol inhibited M gene expression by 75% in H3N2 infected MDCK cells. POPG has the same small and negatively charged lipid head domain as DPPG and LPG lipids used in this study. DPPG, however has a saturated phospholipid tail while POPG has an unsaturated phospholipid tail. In contrast, M gene expression was not reduced by lipid treatment with Palmitoyl-oleoyl-phosphatidylcholine (POPC) (Numata et al., 2012). POPC has the same large and neutral lipid head domain as DPPC used in this study, however, DPPC has a saturated phospholipid tail while POPC has an unsaturated phospholipid tail.

Chapter 8: General discussion

8.1 General discussion

The influenza virus has a serious effect on human and animal health causing thousands of deaths per year, or even more during deadly pandemic episodes involving the emergence of new virion subtypes (Campbell and Ellis, 2013). Influenza virus is an enveloped virus that belongs to the Orthomyxoviridae family and uses the host cell's machinery to replicate and produce new virions. Viruses derive their lipid envelope from the host cell's plasma membrane (Nayak et al., 2009). Inactivated vaccines against influenza A and B have been used to prevent and control influenza virus infection, in addition to prophylactic treatment attempts by using antiviral drugs including amantadine or sialic acid analogs like zanamivir. Still, significant research efforts are needed to control influenza viral infection.

Monitoring the shape of chicken RBCs treated with phospholipids and prepared with two different approaches demonstrated that phospholipids with two aliphatic chains are less potent than lyso-lipids (one aliphatic chain) in changing the shape and surface area of RBCs. However, the potencies of lipids vary according to their polar heads, and whether or not they are subjected to micro-centrifugation and multiple washes prior to incubation with RBCs. The role of membrane lipid composition in RBCs has already been reported. It was reported that the abnormal shape of the human RBC (spherocytosis state) results from a change in the interaction between the lipid bilayer and the underlying cortical cytoskeleton (Mohandas and Evans, 1994). Furthermore, it has been demonstrated that oxidative degradation of

the lipids and alteration in the packing of their acyl chains deforms human RBCs (Sugihara et al., 1991). Besides, the biochemical analysis demonstrated that anomalies in the lipid metabolism and membrane composition lead to increased RBC membrane fragility deforming RBC shape including a 7% increase in the mean corpuscular volume (MCV) (Suda et al., 2002). To further address the impact of phospholipids on the cells used, the size and granularity of individual MDCK cell in suspensions pre-treated with phospholipids was determined by light scattering using flow cytometry. Flow cytometry results showed that phospholipids affect cell size and complexity and are potentially toxic to cells in the absence of removal by ultra-filtration (using Amicon filters). In this context, lipid toxicity can be controlled through appropriate protocols with cells. However, the clinical use of these lipids would need to be assessed as far as their toxicity is involved prior to any use in animals or humans.

Influenza virus relies on specific viral membrane proteins for fusion, i.e. HA, NA and M2, whose stereochemistry and collective structure are central for successful infectivity (Crisci et al., 2013, Pflug et al., 2014). These proteins, or at least their organisation or collective structure, could be altered by exogenous lipids. This is not unexpected as in mammalian cells the mechanical perturbation of the bilayer membrane, through the exogenous inclusion of amphipathic materials, e.g. phospholipids, has been shown to affect the function of ion channels (Sukharev and Sachs, 2012), drug transporters (Omran et al., 2017), endocytosis (Rauch and Farge, 2000) and

exocytosis (Baba et al., 2001). A similar membrane perturbation pattern could occur for influenza virions, although at a much smaller scale. If true, it would be worth considering what structure of lipid(s) would be reliable at disrupting the organisation of the membrane of viruses and consequently reducing their infectivity.

To develop a better understanding of the role of the membrane of influenza virus in infectivity, exogenous cholesterol was added to H2N3; cholesterol would be expected to "stiffen" the cell membrane, but there was no impact on infectivity. However, the addition of MβCD, a cholesterol depleting agent, decreased influenza infectivity suggesting that specific states of the viral membrane namely the lipid-to-protein ratio are key to alter infection. A similar result was obtained using HIV-1 where 0.5mM MβCD reduced virus infectivity by 50% (Hawkes et al., 2015). Results from the present study showed that the degree to which phospholipids reduce virus infectivity is dependent mostly on the lipid used, as the pre-incubation of H2N3 virus with a negatively charged small lipid heads, such as DPPG, reduced virus infectivity more significantly than when DPPS (negative net charge and large head) or DPPC (no net charge and large head) were used. However, the mono-acyl lipids, such as LPC, LPG, and LPS, significantly reduced H2N3 virus infectivity and almost completely blocked the viral infectivity at 500μM concentration, suggesting that a single aliphatic chain may be more potent in reducing infectivity. These results show the analogous impact on infectivity, i.e. drop in

infectivity, which was measured when pre-incubating DPPG, LPG or LPC with influenza A virus subtypes H3N8 and H1N1.

The impact of LPG and DPPG in reducing H2N3 infectivity was not related to cell type as the reduction in virus infectivity was similar in MDCK and A549 cells. The alteration in kinetics of infectivity (6-72 hrs pi times) for H2N3 pre-treated with 50 or 500μM of LPG and 500μM of DPPG was significant. The influence of phospholipid on virus infectivity in the current study are in agreement with previous observations, showing that the pulmonary surfactant phosphatidylglycerol (PG), which functions as the main innate immunity regulator in the lungs, blocks pulmonary viral infections (Quintero and Wright, 2000) such as respiratory syncytial virus (RSV). This, could provide an explanation for the higher concentration of phosphatidylglycerol in the lung compared to other body organs (Numata et al., 2013).

EM has revealed the multiple morphologies of IAV, ranging from spherical to filamentous, and underlined that viral NP residues could have an impact on virus morphology (Bialas et al., 2014). In our study, as in others (Bialas et al., 2014), LPAI H2N3 has a spherical shape while LPAI H3N8 is filamentous. Outer glycoprotein spikes were evenly distributed around the outer surface of the viral strains in avian and equine influenza viruses. The negative staining of H2N3 and H3N8 virions treated with 500 μM of endogenous lysophospholipids showed the extensive interaction between virus particles and liposomes as

well as the incorporation of exogenous lipids into the virus membrane, as some virions became giant particles and / or had localised membrane "ruptures". Furthermore, treatment of virus with 500 μM of DPPG revealed a large swollen uncharacteristic viral morphology in comparison to the untreated virus. The morphology changes in addition to the fusion of many virions with the liposomes as discussed in chapter 5 could suggest a reason behind the impact of lipids on the first stages of influenza virus life cycle (attachment and the fusion with the endosomes to release vRNP to start virus replication), which could also explain the significant reduction in virus infectivity when pre-treated with the lipids in chapter 4. Interestingly, other studies have shown that the disturbance of the lipid raft microdomains of influenza virus occurs by depleting the cholesterol from the viral envelope, which lead to the reduction of virus infectivity and affects virus morphology; with virions showing nicks or holes in parts of the viral envelope (Barman and Nayak, 2007). Electron spin resonance and electron micrography demonstrated that the influenza virus binds efficiently with mixed liposomes composed of different phospholipids including PtdCho/PtdEtn/PtdSer/cholesterol which occurred within the first 15 minutes (Maeda et al., 1981), a time course similar to the one used in this thesis.

DPPG and DPPS (both with a net negative charge) seemed to be most efficient at blocking haemagglutination at a high viral concentration (16 HAU) in our study. This agrees with previous research showing that liposomes containing a mixture of the phospholipids DOPC, DOPE

and DOPG inhibit haemagglutination and reduce the infectivity of influenza virus (Hendricks et al., 2013). In contrast, lysophospholipids did not affect virus haemagglutination but had a disruptive impact on RBC morphology. One way through which di-acyl phospholipids could act is through a "rupture" of the viral membrane as treating influenza virus with 0.1% Triton X-100 has also been shown to reduce the HA titre (Sun and Whittaker, 2003).

Treatment of influenza virus with phospholipid revealed a significant reduction in the percentage of H2N3 binding to MDCK cells. The immunofluorescent staining of MDCK cells infected with H2N3 pre-treated with LPG, LPC or DPPG confirmed the results obtained with flow cytometry. With regard to equine influenza virus H3N8 pre-treated with phospholipids, it was also found that LPG or DPPG reduced virus binding to MDCK cells. Interestingly, influenza virus pre-treated with lipids, especially at 50 and 500μM concentration reduced the viral immunofluorescence signals at 0-30 min (chapter 6) in addition to changing virus morphology. Uneven distribution of virus glycoprotein and viral fusion with liposomes (chapter 5) following phospholipid treatment likely impacts the process of virus entry and fusion and potentially virus trafficking within endosomes at 10-30min post infection. Further studies using endosome markers to localize virus within infected cells would help understand this further. An *in vitro* study has documented the interaction of vaccinia virus with 0.4mM DPPG leading to a significant reduction in virus infectivity (Perino et al., 2011). VSV binding to liposomes was dependent on the head group of phospholipids and this binding had higher affinity with

liposomes composed of PS when compared to liposomes made of PC (Yamada and Ohnishi, 1986) correlating with a reduced VSV infectivity (Schlegel et al., 1983). On some occasions, nanoparticles composed of lipids and antiviral drugs have been shown to be more potent. For example, DMPC vesicles bound to the broad-spectrum antiviral Arbidol, which is known as an anti-influenza drug, showed more significant inhibition of hepatitis C virus (HCV) infectivity when compared to Arbidol alone (Teissier et al., 2011). These results may suggest that lipids may be used to enhance the activity of existing antiviral drugs.

The airway epithelium is a primary barrier between the environment and the host, enhancing inflammatory and chemokine production targeting influenza viral infections and improving innate antiviral immunity (Sanders et al., 2011). Results of the current study showed the impact of DPPG and LPG in suppressing IL-8 and TNF-α cytokine expression in both MDCK and A549 cells infected with H2N3. In addition, these phospholipids led to a reduction in the copy number of the H2N3 viral M gene 24 hr post infection. Similarly, DPPG and LPG pre-treatment of pandemic H1N1 virus showed a marked reduction in IL-8 and TNF-α expression from infected MDCK cells 24 hr pi. Even though these phospholipids showed an impact on reducing IL-8 expression levels in infected MDCK cells using H3N8, no significant reduction was noticed in TNF-α.

Taking into account the low binding affinity of H3N8 filamentous virus infecting MDCK cells when treated with lipid (Chapter 6), the high impact of lipid pre-treatments in altering H3N8 virus morphology (see EM pictures, Chapter 5) and its reduced infectivity 6 hrs pi although the use of DPPG on the filamentous virus showed less reduction in virus infectivity than that of H2N3 and H1N1(Chapter 4), it is unclear why neither M-gene nor TNF-α cytokine production seem to be affected by the lipid pre-treatments of H3N8 at 24 hrs. Our hypothesis is that H3N8 virus has a greater ability to replicate inside MDCK cells in comparison to H2N3 or H1N1. The different response of the influenza viruses used in this study to the lipid treatment, may be due to differences in the surface structure of different virus strains or may be due to differences in morphology. This could be clarified by comparing influenza strains that are genetically engineered to be either filamentous or spherical in a similar manner to that described for equine influenza virus (Elton et al., 2013). It would also be of interest to investigate the influence of cell type on the efficacy of lipid treatment using cells derived from avian or equine hosts and to use more sophisticated in vitro techniques such as tracheal explants.

The potential use of phospholipids as a novel antiviral treatment has previously been shown using pulmonary surfactant phospholipid POPG at a concentration of 1mg/ml, which reduced respiratory syncytial viral infection and pro-inflammatory processes within the lung, reducing IL-8 by 80% and virus titres by 2 to 6 viral plaque log units at 24 hrs post infection (Numata et al., 2013). Similarly, POPG liposomes suppress the cytopathic effect induced by influenza A virus

(Wu et al., 2015) and inhibit viral replication by blocking viral attachment.

8.2 Summary and future work

In summary, findings from the current study revealed that the treatment of influenza A virus with phospholipids could have a marked effect on reducing virus infectivity. This study has improved our understanding of the role that these phospholipids may have *in vivo* and underlines their potential as novel protective agents against influenza virus.

To provide a better picture regarding lipid-virus interaction different biophysical techniques could be used such as magnetic resonance. Indeed by incubating cells with radioactive lipids (or lipid components), the virus budding from infected cells would also bear radioactive lipids. Then the measure of the spin of lipids and therefore their level of confinement, or degree of freedom of their in-plane/membrane rotation in the viral membrane could then be assessed. This could permit a better measurement of the surface tension of the viral membrane generated exogenously by lipid addition. Other less accurate methods could involve the use of fluorescent lipids to measure the amount of lipid incorporation into the viral membrane. However, one limitation of these fluorescent lipids is that physico-chemical changes associated with the addition

of fluorophore groups may perturb their ability to interact with the viral membrane.

Further studies are necessary to optimise the pharmacological dose of lipids to be used *in-vivo* to reduce their toxicity and the lung histopathological lesions that these lipids may generate. Furthermore, measuring virus budding from infected cells could give more information as to whether pre-treatment with exogenous/endogenous lipids impact this aspect of the virus life cycle.

To explore the possibility of using phospholipids in vivo as antiviral therapy, the following issues must be considered: delivery to the target cell or tissue with as few side effects as possible, whether it is possible to reduce dosage frequency, drug toxicity, and increase drug stability whilst being a cost-effective treatment. In addition to that, determination of drug interactions, including synergism, additive effect, and antagonism at all doses or effect levels will effectively evaluate how to beneficially use one or multiple phospholipids or modalities in combination therapies.

The high biocompatibility of phospholipids has been used to increase the bioavailability of therapeutic agents for example with the use of poly-ethylene glycerol (PEG)-phospholipid. The use of liposomes (such as DOPC and DPPG) as carriers of antitumour, antifungal, analgesic and vaccines has been widely accepted; their use in antiviral

therapy remains to be established (Knop et al., 2010, Vishvakrama and Sharma, 2014).

Researchers have reviewed how to deliver drugs into every part of the body. The pulmonary route is one of the possible routes which might be used to deliver phospholipids, which showed a notable reduction in influenza virus infectivity in our study, like PG (DPPG or LPG or combination) or with other phospholipids and cholesterol through pushing liquid phospholipid formulations through very tiny nozzles or delivery of fine dry-powder aerosols to the lungs. This might need input from other fields; chemistry, biomaterials, engineering and pharmaceutical sciences.

References

ADAMS, S. & SANDROCK, C. 2010. Avian influenza: update. *Medical Principles and Practice,* 19**,** 421-432.

ADAN, A., ALIZADA, G., KIRAZ, Y., BARAN, Y. & NALBANT, A. 2017. Flow cytometry: basic principles and applications. *Critical Reviews in Biotechnology,* 37**,** 163-176.

AKILA, K., BALAMURUGAN, P. & RAJASEKARAN, E. 2012. The nature of proteins in influenza. *Health,* 4**,** 991.

ALEXANDER, D. J. 2000. A review of avian influenza in different bird species. *Veterinary Microbiology,* 74**,** 3-13.

ALLEN, C. A., PAYNE, S. L., HARVILLE, M., COHEN, N. & RUSSELL, K. E. 2007. Validation of quantitative polymerase chain reaction assays for measuring cytokine expression in equine macrophages. *Journal of Immunological Methods,* 328**,** 59-69.

ÁLVAREZ-BARRIENTOS, A., ARROYO, J., CANTÓN, R., NOMBELA, C. & SÁNCHEZ-PÉREZ, M. 2000. Applications of flow cytometry to clinical microbiology. *Clinical Microbiology Reviews,* 13**,** 167-195.

ARRANZ, R., COLOMA, R., CHICHON, F. J., CONESA, J. J., CARRASCOSA, J. L., VALPUESTA, J. M., ORTIN, J. & MARTIN-BENITO, J. 2012. The structure of native influenza virion ribonucleoproteins. *Science,* 338**,** 1634-7.

BABA, T., RAUCH, C., XUE, M., TERADA, N., FUJII, Y., UEDA, H., TAKAYAMA, I., OHNO, S., FARGE, E. & SATO, S. B. 2001. Clathrin-dependent and clathrin-independent endocytosis are differentially sensitive to insertion of poly (ethylene glycol)-derivatized cholesterol in the plasma membrane. *Traffic,* 2**,** 501-512.

BAGATOLLI, L. A., IPSEN, J. H., SIMONSEN, A. C. & MOURITSEN, O. G. 2010. An outlook on organization of lipids in membranes: searching for a realistic connection with the organization of biological membranes. *Progress in Lipid Research,* 49**,** 378-389.

BAKER, S. F., NOGALES, A., FINCH, C., TUFFY, K. M., DOMM, W., PEREZ, D. R., TOPHAM, D. J. & MARTINEZ-SOBRIDO, L. 2014. Influenza A and B Virus Intertypic Reassortment through Compatible Viral Packaging Signals. *Journal of Virology,* 88**,** 10778-10791.

BALS, R. & HIEMSTRA, P. 2004. Innate immunity in the lung: how epithelial cells fight against respiratory pathogens. *European Respiratory Journal,* 23**,** 327-333.

BARMAN, S. & NAYAK, D. P. 2007. Lipid raft disruption by cholesterol depletion enhances influenza A virus budding from MDCK cells. *Journal of Virology,* 81**,** 12169-12178.

BELSHE, R. B. 2005. The origins of pandemic influenza—lessons from the 1918 virus. *New England Journal of Medicine,* 353**,** 2209-2211.

BIALAS, K. M., BUSSEY, K. A., STONE, R. L. & TAKIMOTO, T. 2014. Specific nucleoprotein residues affect influenza virus morphology. *Journal of Virology,* 88**,** 2227-2234.

BONNAFOUS, P., NICOLAÏ, M.-C., TAVEAU, J.-C., CHEVALIER, M., BARRIÈRE, F., MEDINA, J., LE BIHAN, O., ADAM, O., RONZON, F. & LAMBERT, O. 2014. Treatment of influenza virus with beta-propiolactone alters viral membrane fusion. *Biochimica et Biophysica Acta (BBA)-Biomembranes,* 1838**,** 355-363.

CAMPBELL, T. W. & ELLIS, C. K. 2013. *Avian and exotic animal hematology and cytology*, John Wiley & Sons.

CARNEIRO, F. A., VANDENBUSSCHE, G., JULIANO, M. A., JULIANO, L., RUYSSCHAERT, J.-M. & DA POIAN, A. T. 2006. Charged residues are involved in membrane fusion mediated by a hydrophilic peptide located in vesicular stomatitis virus G protein. *Molecular Membrane Biology,* 23**,** 396-406.

CARRAT, F. & FLAHAULT, A. 2007. Influenza vaccine: the challenge of antigenic drift. *Vaccine,* 25**,** 6852-6862.

CHAN, M., CHEUNG, C., CHUI, W., TSAO, S., NICHOLLS, J., CHAN, Y., CHAN, R., LONG, H., POON, L. & GUAN, Y. 2005. Proinflammatory cytokine responses induced by influenza A (H5N1) viruses in primary human alveolar and bronchial epithelial cells. *Respiratory Research,* 6**,** 135.

CHAN, R. B., TANNER, L. & WENK, M. R. 2010. Implications for lipids during replication of enveloped viruses. *Chemistry and Physics of Lipids,* 163**,** 449-459.

CHERNOMORDIK, L. V., FROLOV, V. A., LEIKINA, E., BRONK, P. & ZIMMERBERG, J. 1998. The pathway of membrane fusion catalyzed by influenza hemagglutinin: restriction of lipids, hemifusion, and lipidic fusion pore formation. *The Journal of Cell Biology,* 140**,** 1369-1382.

CHUKKAPALLI, V., HEATON, N. S. & RANDALL, G. 2012. Lipids at the interface of virus–host interactions. *Current Opinion in Microbiology,* 15**,** 512-518.

CIECHONSKA, M. & DUNCAN, R. 2014. Lysophosphatidylcholine reversibly arrests pore expansion during syncytium formation mediated by diverse viral fusogens. *Journal of Virology,* 88**,** 6528-6531.

CLAAS, E. C., OSTERHAUS, A. D., VAN BEEK, R., DE JONG, J. C., RIMMELZWAAN, G. F., SENNE, D. A., KRAUSS, S., SHORTRIDGE, K. F. & WEBSTER, R. G. 1998. Human influenza A H5N1 virus related to a highly pathogenic avian influenza virus. *The Lancet,* 351**,** 472-477.

COIL, D. A. & MILLER, A. D. 2005. Enhancement of enveloped virus entry by phosphatidylserine. *Journal of Virology,* 79**,** 11496-11500.

CRISCI, E., MUSSÁ, T., FRAILE, L. & MONTOYA, M. 2013. Influenza virus in pigs. *Molecular Immunology,* 55**,** 200-211.

CRITCHLEY, P. & DIMMOCK, N. J. 2004. Binding of an influenza A virus to a neomembrane measured by surface plasmon resonance. *Bioorganic & Medicinal Chemistry,* 12**,** 2773-2780.

CURY-BOAVENTURA, M. F., POMPÉIA, C. & CURI, R. 2004. Comparative toxicity of oleic acid and linoleic acid on Jurkat cells. *Clinical Nutrition,* 23**,** 721-732.

DAIDOJI, T., KOMA, T., DU, A., YANG, C.-S., UEDA, M., IKUTA, K. & NAKAYA, T. 2008. H5N1 avian influenza virus induces apoptotic cell death in mammalian airway epithelial cells. *Journal of Virology,* 82**,** 11294-11307.

DALY, J. M., MACRAE, S., NEWTON, J. R., WATTRANG, E. & ELTON, D. M. 2011. Equine influenza: a review of an unpredictable virus. *The Veterinary Journal,* 189**,** 7-14.

DANIELLI, J. F. & DAVSON, H. 1935. A contribution to the theory of permeability of thin films. *Journal of Cellular Physiology,* 5**,** 495-508.

DAVIS, A. S., TAUBENBERGER, J. K. & BRAY, M. 2015. The use of nonhuman primates in research on seasonal, pandemic and avian influenza, 1893–2014. *Antiviral Research,* 117**,** 75-98.

DIERKES, R., WARNKING, K., LIEDMANN, S., SEYER, R., LUDWIG, S. & EHRHARDT, C. 2014. The Rac1 inhibitor NSC23766 exerts anti-influenza virus properties by affecting the viral polymerase complex activity. *PloS One,* 9**,** e88520.

DISCHER, D. E. & CARL, P. 2001. New insights into red cell network structure, elasticity, and spectrin unfolding-a current review. *Cellular and Molecular Biology Letters,* 6**,** 593-606.

DUDEK, S. E., WIXLER, L., NORDHOFF, C., NORDMANN, A., ANHLAN, D., WIXLER, V. & LUDWIG, S. 2011. The influenza virus PB1-F2 protein has interferon antagonistic activity. *Biological Chemistry,* 392**,** 1135-1144.

DUNHAM, S. P. 2002. The application of nucleic acid vaccines in veterinary medicine. *Research in Veterinary Science,* 73**,** 9-16.

DUNNING, R. A., DOMANSKA, M. K., DRYDEN, K., YEAGER, M. & KASSON, P. M. 2015. Effect of Cholesterol Depletion on HA Distribution in the Viral Membrane of Influenza. *Biophysical Journal,* 108**,** 406a-407a.

EDIDIN, M. 2003. The state of lipid rafts: from model membranes to cells. *Annual Review of Biophysics and Biomolecular Structure,* 32**,** 257-283.

EISFELD, A. J., NEUMANN, G. & KAWAOKA, Y. 2014. Influenza A virus isolation, culture and identification. *Nature Protocols,* 9**,** 2663-2681.

EKIERT, D. C., BHABHA, G., ELSLIGER, M.-A., FRIESEN, R. H., JONGENEELEN, M., THROSBY, M., GOUDSMIT, J. & WILSON, I. A. 2009. Antibody recognition of a highly conserved influenza virus epitope. *Science,* 324**,** 246-251.

ELTON, D., BRUCE, E. A., BRYANT, N., WISE, H. M., MACRAE, S., RASH, A., SMITH, N., TURNBULL, M. L., MEDCALF, L. & DALY, J. M. 2013. The genetics of virus particle shape in equine influenza A virus. *Influenza and Other Respiratory Viruses,* 7**,** 81-89.

ELTON, D., DIGARD, P., TILEY, L. & ORTIN, J. 2006. Structure and function of the influenza virus RNP. *Influenza Virology: Current Topics. Caister Academic Press, Wymondham, United Kingdom***,** 1-36.

FERA, A., FARRINGTON, J. E., ZIMMERBERG, J. & REESE, T. S. 2012. A negative stain for electron microscopic tomography. *Microscopy and Microanalysis,* 18**,** 331-335.

FERGUSON, L., ECKARD, L., EPPERSON, W. B., LONG, L.-P., SMITH, D., HUSTON, C., GENOVA, S., WEBBY, R. & WAN, X.-F. 2015. Influenza D virus infection in Mississippi beef cattle. *Virology,* 486**,** 28-34.

FERNANDEZ-SESMA, A., MARUKIAN, S., EBERSOLE, B. J., KAMINSKI, D., PARK, M.-S., YUEN, T., SEALFON, S. C., GARCÍA-SASTRE, A. & MORAN, T. M. 2006. Influenza virus evades innate and adaptive immunity via the NS1 protein. *Journal of Virology,* 80**,** 6295-6304.

FONTANA, J. & STEVEN, A. C. 2015. Influenza virus-mediated membrane fusion: structural insights from electron microscopy. *Archives of Biochemistry and Biophysics,* 581**,** 86-97.

FRENSING, T., KUPKE, S. Y., BACHMANN, M., FRITZSCHE, S., GALLO-RAMIREZ, L. E. & REICHL, U. 2016. Influenza virus intracellular replication dynamics, release kinetics, and particle morphology during propagation in MDCK cells. *Applied Microbiology and Biotechnology,* 100**,** 7181-7192.

FUJII, Y., GOTO, H., WATANABE, T., YOSHIDA, T. & KAWAOKA, Y. 2003. Selective incorporation of influenza virus RNA segments into virions. *Proceedings of the National Academy of Sciences,* 100**,** 2002-2007.

GALLAGHER, J. R., TORIAN, U., MCCRAW, D. M. & HARRIS, A. K. 2017. Structural studies of influenza virus RNPs by electron microscopy indicate molecular contortions within

NP supra-structures. *Journal of Structural Biology,* 197**,** 294-307.

GARCÍA-SASTRE, A. 2011. Induction and evasion of type I interferon responses by influenza viruses. *Virus Research,* 162**,** 12-18.

GARTEN, W. & KLENK, H.-D. 1999. Understanding influenza virus pathogenicity. *Journal of Virology,* 68**,** 3120-3128.

GASPARINI, R., AMICIZIA, D., LAI, P. L., BRAGAZZI, N. L. & PANATTO, D. 2015. Compounds with anti-influenza activity: present and future of strategies for the optimal treatment and management of influenza. Part I: influenza life-cycle and currently available drugs. *Journal of Preventive Medicine and Hygiene,* 55**,** 109–129.

GERL, M. J., SAMPAIO, J. L., URBAN, S., KALVODOVA, L., VERBAVATZ, J.-M., BINNINGTON, B., LINDEMANN, D., LINGWOOD, C. A., SHEVCHENKO, A. & SCHROEDER, C. 2012. Quantitative analysis of the lipidomes of the influenza virus envelope and MDCK cell apical membrane. *The Journal of Cell Biology,* 196**,** 213-221.

GHARAGOZLOO, M., RAFIEE, A., CHEN, D. W. & FOLDVARI, M. 2015. A flow cytometric approach to study the mechanism of gene delivery to cells by gemini-lipid nanoparticles: an implication for cell membrane nanoporation. *Journal of Nanobiotechnology,* 13**,** 62.

GHOSH, S., MISHRA, R., SARKAR, D., MISHRA, R. & MUKHERJEE, D. C. 2014. morphological alteration of Red Blood Cell. *Journal of the Indian Chemical Society,* 91**,** 1601-1610.

GIVAN, A. L. 2013. *Flow cytometry: first principles*, John Wiley & Sons.

GLASSER, J. R. & MALLAMPALLI, R. K. 2012. Surfactant and its role in the pathobiology of pulmonary infection. *Microbes and Infection,* 14**,** 17-25.

GOLDSMITH, C. S. & MILLER, S. E. 2009. Modern uses of electron microscopy for detection of viruses. *Clinical Microbiology Reviews,* 22**,** 552-563.

GORTER, E. & GRENDEL, F. 1925. On bimolecular layers of lipoids on the chromocytes of the blood. *Journal of Experimental Medicine,* 41**,** 439-443.

GUBAREVA, L. V., KAISER, L. & HAYDEN, F. G. 2000. Influenza virus neuraminidase inhibitors. *The Lancet,* 355**,** 827-835.

GÜNTHER-AUSBORN, S., PRAETOR, A. & STEGMANN, T. 1995. Inhibition of influenza-induced membrane fusion by lysophosphatidylcholine. *Journal of Biological Chemistry,* 270**,** 29279-29285.

HAGAU, N., SLAVCOVICI, A., GONGANAU, D. N., OLTEAN, S., DIRZU, D. S., BREZOSZKI, E. S., MAXIM, M., CIUCE, C., MLESNITE, M. & GAVRUS, R. L. 2010. Clinical aspects and

cytokine response in severe H1N1 influenza A virus infection. *Critical Care,* 14**,** R203.

HALE, B. G., KNEBEL, A., BOTTING, C. H., GALLOWAY, C. S., PRECIOUS, B. L., JACKSON, D., ELLIOTT, R. M. & RANDALL, R. E. 2009. CDK/ERK-mediated phosphorylation of the human influenza A virus NS1 protein at threonine-215. *Virology,* 383**,** 6-11.

HAN, S. & MALLAMPALLI, R. K. 2015. The role of surfactant in lung disease and host defense against pulmonary infections. *Annals of the American Thoracic Society,* 12**,** 765-774.

HARRIS, A., CARDONE, G., WINKLER, D. C., HEYMANN, J. B., BRECHER, M., WHITE, J. M. & STEVEN, A. C. 2006. Influenza virus pleiomorphy characterized by cryoelectron tomography. *Proceedings of the National Academy of Sciences,* 103**,** 19123-19127.

HARRIS, J. R. 2015. Transmission electron microscopy in molecular structural biology: a historical survey. *Archives of Biochemistry and Biophysics,* 581**,** 3-18.

HAWKES, D., JONES, K. L., SMYTH, R. P., PEREIRA, C. F., BITTMAN, R., JAWOROWSKI, A. & MAK, J. 2015. Properties of HIV-1 associated cholesterol in addition to raft formation are important for virus infection. *Virus Research,* 210**,** 18–21.

HAYWOOD, A. M. & BOYER, B. P. 1985. Fusion of influenza virus membranes with liposomes at pH 7.5. *Proceedings of the National Academy of Sciences,* 82**,** 4611-4615.

HEATON, N. S. & RANDALL, G. 2011. Multifaceted roles for lipids in viral infection. *Trends in Microbiology,* 19**,** 368-375.

HENDRICKS, G. L., WEIRICH, K. L., VISWANATHAN, K., LI, J., SHRIVER, Z. H., ASHOUR, J., PLOEGH, H. L., KURT-JONES, E. A., FYGENSON, D. K. & FINBERG, R. W. 2013. Sialylneolacto-N-tetraose c (LSTc)-bearing liposomal decoys capture influenza A virus. *Journal of Biological Chemistry,* 288**,** 8061-73.

HEROLD, S., LUDWIG, S., PLESCHKA, S. & WOLFF, T. 2012. Apoptosis signaling in influenza virus propagation, innate host defense, and lung injury. *Journal of Leukocyte Biology,* 92**,** 75-82.

HRUBY, D. E. & FRANKE, C. A. 1993. Viral acylproteins: greasing the wheels of assembly. *Trends in Microbiology,* 1**,** 20-25.

HUANG, R. T. 1976. Sphingolipids of influenza viruses. *Biochimica et Biophysica Acta (BBA)-lipids and Lipid Metabolism,* 424**,** 90-97.

HUANG, R. T., LICHTENBERG, B. & RICK, O. 1996. Involvement of annexin V in the entry of influenza viruses and role of phospholipids in infection. *FEBS Letters,* 392**,** 59-62.

INGÓLFSSON, H. I., MELO, M. N., VAN EERDEN, F. J., ARNAREZ, C. M., LOPEZ, C. A., WASSENAAR, T. A., PERIOLE, X., DE VRIES, A. H., TIELEMAN, D. P. & MARRINK, S. J. 2014. Lipid organization of the plasma membrane. *Journal of the American Chemical Society,* 136**,** 14554-14559.

ISRAELACHVILI, J. N. 2011. *Intermolecular and surface forces*, Academic press.

IVANOVA, P. T., MYERS, D. S., MILNE, S. B., MCCLAREN, J. L., THOMAS, P. G. & BROWN, H. A. 2015. Lipid composition of viral envelope of three strains of influenza virus–not all viruses are created equal. *ACS Infectious Diseases,* 1**,** 435-442.

IWASAKI, A. & PILLAI, P. S. 2014. Innate immunity to influenza virus infection. *Nature Reviews Immunology,* 14**,** 315-328.

JIANG, L., TIXEIRA, R., CARUSO, S., ATKIN-SMITH, G. K., BAXTER, A. A., PAONE, S., HULETT, M. D. & POON, I. K. 2016. Monitoring the progression of cell death and the disassembly of dying cells by flow cytometry. *Nature Protocols,* 11**,** 655-663.

JULKUNEN, I., MELÉN, K., NYQVIST, M., PIRHONEN, J., SARENEVA, T. & MATIKAINEN, S. 2000. Inflammatory responses in influenza A virus infection. *Vaccine,* 19**,** S32-S37.

KANDASAMY, P., ZARINI, S., CHAN, E. D., LESLIE, C. C., MURPHY, R. C. & VOELKER, D. R. 2011. Pulmonary surfactant phosphatidylglycerol inhibits Mycoplasma pneumoniae-stimulated eicosanoid production from human and mouse macrophages. *Journal of Biological Chemistry,* 286**,** 7841-7853.

KANNEGANTI, T.-D. 2010. Central roles of NLRs and inflammasomes in viral infection. *Nature Reviews Immunology,* 10**,** 688.

KAPOOR, S. & DHAMA, K. 2014. Introduction. *Insight into Influenza Viruses of Animals and Humans.* Springer.

KASSON, P. M. & PANDE, V. S. 2008. Structural basis for influence of viral glycans on ligand binding by influenza hemagglutinin. *Biophysical Journal,* 95**,** L48-L50.

KAWAI, T. & AKIRA, S. 2011. Toll-like receptors and their crosstalk with other innate receptors in infection and immunity. *Immunity,* 34**,** 637-650.

KAWAOKA, Y. & NEUMANN, G. 2012. *Influenza virus: methods and protocols*, Humana Press.

KHURANA, S., KREMENTSOV, D. N., DE PARSEVAL, A., ELDER, J. H., FOTI, M. & THALI, M. 2007. Human immunodeficiency virus type 1 and influenza virus exit via different membrane microdomains. *Journal of Virology,* 81**,** 12630-12640.

KILLIAN, M. L. 2014. Hemagglutination assay for influenza virus. *Animal Influenza Virus*

1611**,** 3-9.

KNIPE, D. M. & HOWLEY, P. M. 2013. *Fields Virology*, Wolters Kluwer Health.

KNOP, K., HOOGENBOOM, R., FISCHER, D. & SCHUBERT, U. S. 2010. Poly (ethylene glycol) in drug delivery: pros and cons as well as potential alternatives. *Angewandte Chemie International Edition,* 49**,** 6288-6308.

KOÇER, Z. A., JONES, J. C. & WEBSTER, R. G. 2013. Emergence of influenza viruses and crossing the species barrier. *Microbiol Spectrum*1**,** 1-15.

KOHN, A., GITELMAN, J. & INBAR, M. 1980. Unsaturated free fatty acids inactivate animal enveloped viruses. *Archives of Virology,* 66**,** 301-307.

KOOPMANS, M., WILBRINK, B., CONYN, M., NATROP, G., VAN DER NAT, H., VENNEMA, H., MEIJER, A., VAN STEENBERGEN, J., FOUCHIER, R. & OSTERHAUS, A. 2004. Transmission of H7N7 avian influenza A virus to human beings during a large outbreak in commercial poultry farms in the Netherlands. *The Lancet,* 363**,** 587-593.

KREIJTZ, J., FOUCHIER, R. & RIMMELZWAAN, G. 2011. Immune responses to influenza virus infection. *Virus Research,* 162**,** 19-30.

KUCHIPUDI, S. V., TELLABATI, M., NELLI, R. K., WHITE, G. A., PEREZ, B. B., SEBASTIAN, S., SLOMKA, M. J., BROOKES, S. M., BROWN, I. H. & DUNHAM, S. P. 2012. 18S rRNA is a reliable normalisation gene for real time PCR based on influenza virus infected cells. *Virology Journal,* 9**,** 230.

KUCHIPUDI, S. V., TELLABATI, M., SEBASTIAN, S., LONDT, B. Z., JANSEN, C., VERVELDE, L., BROOKES, S. M., BROWN, I. H., DUNHAM, S. P. & CHANG, K.-C. 2014. Highly pathogenic avian influenza virus infection in chickens but not ducks is associated with elevated host immune and pro-inflammatory responses. *Veterinary Research,* 45**,** 118.

KURONUMA, K., MITSUZAWA, H., TAKEDA, K., NISHITANI, C., CHAN, E. D., KUROKI, Y., NAKAMURA, M. & VOELKER, D. R. 2009. Anionic pulmonary surfactant phospholipids inhibit inflammatory responses from alveolar macrophages and U937 cells by binding the lipopolysaccharide interacting proteins CD14 and MD2. *Journal of Biological Chemistry,* 284**,** 25488-500.

LAM, W., YEUNG, A. C., CHU, I. M. & CHAN, P. K. 2010. Profiles of cytokine and chemokine gene expression in human

pulmonary epithelial cells induced by human and avian influenza viruses. *Virology Journal,* 7**,** 344.

LANGE, Y. & SLAYTON, J. M. 1982. Interaction of cholesterol and lysophosphatidylcholine in determining red cell shape. *Journal of Lipid Research,* 23**,** 1121-1127.

LE GOFFIC, R., POTHLICHET, J., VITOUR, D., FUJITA, T., MEURS, E., CHIGNARD, M. & SI-TAHAR, M. 2007. Cutting Edge: Influenza A virus activates TLR3-dependent inflammatory and RIG-I-dependent antiviral responses in human lung epithelial cells. *The Journal of Immunology,* 178**,** 3368-3372.

LEE, C.-W. & SUAREZ, D. L. 2004. Application of real-time RT-PCR for the quantitation and competitive replication study of H5 and H7 subtype avian influenza virus. *Journal of Virological Methods,* 119**,** 151-158.

LEE, S. M., CHEUNG, C.-Y., NICHOLLS, J. M., HUI, K. P., LEUNG, C. Y., UIPRASERTKUL, M., TIPOE, G. L., LAU, Y.-L., POON, L. L. & IP, N. Y. 2008. Hyperinduction of cyclooxygenase-2-mediated proinflammatory cascade: a mechanism for the pathogenesis of avian influenza H5N1 infection. *The Journal of Infectious Diseases,* 198**,** 525-535.

LÉGARÉ, S. & LAGÜE, P. 2014. The influenza fusion peptide promotes lipid polar head intrusion through hydrogen bonding with phosphates and N-terminal membrane insertion depth. *Proteins: Structure, Function, and Bioinformatics,* 82**,** 2118-2127.

LEI, H., PENG, X., OUYANG, J., ZHAO, D., JIAO, H., SHU, H. & GE, X. 2015. Protective immunity against influenza H5N1 virus challenge in chickens by oral administration of recombinant Lactococcus lactis expressing neuraminidase. *BMC Veterinary Research,* 11**,** 85.

LEKKALA, M., LEVINE, A. M., LINKE, M. J., CROUCH, E. C., LINDERS, B., BRUMMER, E. & STEVENS, D. A. 2006. Effect of lung surfactant collectins on bronchoalveolar macrophage interaction with Blastomyces dermatitidis: inhibition of tumor necrosis factor alpha production by surfactant protein D. *Infection and Immunity,* 74**,** 4549-4556.

LESER, G. P. & LAMB, R. A. 2005. Influenza virus assembly and budding in raft-derived microdomains: a quantitative analysis of the surface distribution of HA, NA and M2 proteins. *Virology,* 342**,** 215-227.

LESKAWA, K. C., HOGAN, E. L., DASGUPTA, S., CHIEN, J.-L., ERWIN, R. E. & BROSTOFF, S. W. 1986. Lipid content of swine influenza and other vaccines. *Lipids,* 21**,** 342-346.

LESSE, A. J. 2016. Emerging Infections: Influenza, Avian Influenza, and Pandemic Influenza. *Respiratory Infections,* 232**,** 271.

LEUNG, K., KIM, J.-O., GANESH, L., KABAT, J., SCHWARTZ, O. & NABEL, G. J. 2008. HIV-1 assembly: viral glycoproteins segregate quantally to lipid rafts that associate individually with HIV-1 capsids and virions. *Cell Host & Microbe,* 3**,** 285-292.

LEVENTAL, K. R., LORENT, J. H., LIN, X., SKINKLE, A. D., SURMA, M. A., STOCKENBOJER, E. A., GORFE, A. A. & LEVENTAL, I. 2016. Polyunsaturated lipids regulate membrane domain stability by tuning membrane order. *Biophysical Journal,* 110**,** 1800-1810.

LEVINE, A. M., KURAK, K. E., BRUNO, M. D., STARK, J. M., WHITSETT, J. A. & KORFHAGEN, T. R. 1998. Surfactant protein-A-deficient mice are susceptible to Pseudomonas aeruginosa infection. *American Journal of Respiratory Cell and Molecular Biology,* 19**,** 700-708.

LEVINE, J. S., KOH, J. S., TRIACA, V. & LIEBERTHAL, W. 1997. Lysophosphatidic acid: a novel growth and survival factor for renal proximal tubular cells. *American Journal of Physiology-renal Physiology,* 273**,** F575-F585.

LI, X. D., ZOU, S. M., ZHANG, Y., BAI, T., GAO, R. B., ZHANG, X., WU, J. & SHU, Y. L. 2014. A Novel Reassortant H2N3 Influenza Virus Isolated from China. *Biomedical and Environmental Sciences,* 27**,** 240-249.

LIEBER, M., TODARO, G., SMITH, B., SZAKAL, A. & NELSON-REES, W. 1976. A continuous tumor-cell line from a human lung carcinoma with properties of type II alveolar epithelial cells. *International Journal of Cancer,* 17**,** 62-70.

LIGON, B. L. Avian influenza virus H5N1: a review of its history and information regarding its potential to cause the next pandemic. Seminars in pediatric iInfectious diseases, 2005. Elsevier, 326-335.

LIVAK, K. J. & SCHMITTGEN, T. D. 2001. Analysis of relative gene expression data using real-time quantitative PCR and the 2− ΔΔCT method. *Methods,* 25**,** 402-408.

LÓPEZ, C. A., DE VRIES, A. H. & MARRINK, S. J. 2011. Molecular mechanism of cyclodextrin mediated cholesterol extraction. *PLOS Computational Biology,* 7**,** e1002020.

LOREGIAN, A., MERCORELLI, B., NANNETTI, G., COMPAGNIN, C. & PALÙ, G. 2014. Antiviral strategies against influenza virus: towards new therapeutic approaches. *Cellular and molecular life sciences,* 71**,** 3659-3683.

LUCAS, A. M. & JAMROZ, C. 1961. *Atlas of Avian Hematology*, Washington, D.C.: United States Department of Agriculture.

LUCKEY, M. 2014. *Membrane structural biology: with biochemical and biophysical foundations*, Cambridge University Press.

MAEDA, T., KAWASAKI, K. & OHNISHI, S.-L. 1981. Interaction of influenza virus hemagglutinin with target membrane lipids is a key step in virus-induced hemolysis and fusion at pH 5.2. *Proceedings of the National Academy of Sciences,* 78**,** 4133-4137.

MAIR, C. M., LUDWIG, K., HERRMANN, A. & SIEBEN, C. 2014. Receptor binding and pH stability - how influenza A virus hemagglutinin affects host-specific virus infection. *Biochimica et Biophysica Acta* 1838**,** 1153-68.

MARTÍN-ACEBES, M. A., VÁZQUEZ-CALVO, Á., CARIDI, F., SOBRINO, F. & SAIZ, J.-C. 2013. *Lipid involvement in viral infections: present and future perspectives for the design of antiviral strategies*, INTECH Open Access Publisher.

MAURER-STROH, S. & EISENHABER, F. 2004. Myristoylation of viral and bacterial proteins. *Trends in Microbiology,* 12**,** 178-185.

MAZZON, M. & MERCER, J. 2014. Lipid interactions during virus entry and infection. *Cellular Microbiology,* 16**,** 1493-502.

MEDINA, R. A. & GARCÍA-SASTRE, A. 2011. Influenza A viruses: new research developments. *Nature Reviews Microbiology,* 9**,** 590-603.

MERRILL JR, A. H. 2011. Sphingolipid and glycosphingolipid metabolic pathways in the era of sphingolipidomics. *Chemical Reviews,* 111**,** 6387-6422.

MIBAYASHI, M., MARTÍNEZ-SOBRIDO, L., LOO, Y.-M., CÁRDENAS, W. B., GALE, M. & GARCÍA-SASTRE, A. 2007. Inhibition of retinoic acid-inducible gene I-mediated induction of beta interferon by the NS1 protein of influenza A virus. *Journal of Virology,* 81**,** 514-524.

MOHANDAS, N. & EVANS, E. 1994. Mechanical properties of the red cell membrane in relation to molecular structure and genetic defects. *Annual Review of Biophysics and Biomolecular Structure,* 23**,** 787-818.

MOHANDAS, N. & GALLAGHER, P. G. 2008. Red cell membrane: past, present, and future. *Blood,* 112**,** 3939-3948.

MOHANDAS, N., GREENQUIST, A. C. & SHOHET, S. B. 1978. Bilayer balance and regulation of red cell shape changes. *Journal of Supramolecular Structure,* 9**,** 453-458.

MUNGER, J., BENNETT, B. D., PARIKH, A., FENG, X.-J., MCARDLE, J., RABITZ, H. A., SHENK, T. & RABINOWITZ, J. D. 2008. Systems-level metabolic flux profiling

identifies fatty acid synthesis as a target for antiviral therapy. *Nature Biotechnology,* 26**,** 1179-1186.

MUNIR, M., ZOHARI, S. & BERG, M. 2011. Non-structural protein 1 of avian influenza A viruses differentially inhibit NF-κB promoter activation. *Virology Journal,* 8**,** 383.

MUNIR, M., ZOHARI, S., IQBAL, M., ABBAS, M., PEREZ, D. R. & BERG, M. 2013. The non-structural (NS) gene segment of H9N2 influenza virus isolated from backyard poultry in Pakistan reveals strong genetic and functional similarities to the NS gene of highly pathogenic H5N1. *Virulence,* 4**,** 612-623.

MURCH, O., COLLIN, M., SEPODES, B., FOSTER, S. J., MOTA-FILIPE, H. & THIEMERMANN, C. 2006. Lysophosphatidylcholine reduces the organ injury and dysfunction in rodent models of Gram-negative and Gram-positive shock. *British Journal of Pharmacology,* 148**,** 769-777.

NAYAK, D. P., BALOGUN, R. A., YAMADA, H., ZHOU, Z. H. & BARMAN, S. 2009. Influenza virus morphogenesis and budding. *Virus Research,* 143**,** 147-161.

NEERGAARD, K. V. 1929. Neue auffassungen über einen grundbegriff der atemmechanik. *Zeitschrift Für Die Gesamte Experimentelle Medizin,* 66**,** 373-394.

NELLI, R. K., KUCHIPUDI, S. V., WHITE, G. A., PEREZ, B. B., DUNHAM, S. P. & CHANG, K.-C. 2010. Comparative distribution of human and avian type sialic acid influenza receptors in the pig. *BMC Veterinary Research,* 6**,** 4.

NELSON, M. I. & VINCENT, A. L. 2015. Reverse zoonosis of influenza to swine: new perspectives on the human–animal interface. *Trends in Microbiology,* 23**,** 142-153.

NEUMANN, G. & KAWAOKA, Y. 2015. Transmission of influenza A viruses. *Virology,* 89**,** 8453-8461.

NEUMANN, G., NODA, T. & KAWAOKA, Y. 2009. Emergence and pandemic potential of swine-origin H1N1 influenza virus. *Nature,* 459**,** 931-939.

NICOLSON, G. L. & ASH, M. E. 2014. Lipid replacement therapy: a natural medicine approach to replacing damaged lipids in cellular membranes and organelles and restoring function. *Biochimica et Biophysica Acta (BBA)-Biomembranes,* 1838**,** 1657-1679.

NIR, S., KLAPPE, K. & HOEKSTRA, D. 1986. Mass action analysis of kinetics and extent of fusion between Sendai virus and phospholipid vesicles. *Biochemistry,* 25**,** 8261-8266.

NODA, T. 2012. Native morphology of influenza virions. *Frontiers in Microbiology,* 2**,** 269.

NODA, T. & KAWAOKA, Y. 2010. Structure of influenza virus ribonucleoprotein complexes and their packaging into virions. *Reviews in Medical Virology,* 20**,** 380-391.

NOMURA, F., INABA, T., ISHIKAWA, S., NAGATA, M., TAKAHASHI, S., HOTANI, H. & TAKIGUCHI, K. 2004. Microscopic observations reveal that fusogenic peptides induce liposome shrinkage prior to membrane fusion. *Proceedings of the National Academy of Sciences,* 101**,** 3420-3425.

NUMATA, M., CHU, H. W., DAKHAMA, A. & VOELKER, D. R. 2010. Pulmonary surfactant phosphatidylglycerol inhibits respiratory syncytial virus–induced inflammation and infection. *Proceedings of the national academy of sciences,* 107**,** 320-325.

NUMATA, M., KANDASAMY, P., NAGASHIMA, Y., POSEY, J., HARTSHORN, K., WOODLAND, D. & VOELKER, D. R. 2012. Phosphatidylglycerol suppresses influenza A virus infection. *American Journal of Respiratory Cell and Molecular Biology,* 46**,** 479-487.

NUMATA, M., NAGASHIMA, Y., MOORE, M. L., BERRY, K. Z., CHAN, M., KANDASAMY, P., PEEBLES, R. S., MURPHY, R. C. & VOELKER, D. R. 2013. Phosphatidylglycerol provides short-term prophylaxis against respiratory syncytial virus infection. *Journal of Lipid Research,* 54**,** 2133-2143.

OFFLU. 2018. *Influenza A Cleavage Sites* [Online]. Available: http://www.offlu.net/fileadmin/home/en/resource-centre/pdf/Influenza_A_Cleavage_Sites.pdf [Accessed 12/12/2018].

OMRAN, Z., SCAIFE, P., STEWART, S. & RAUCH, C. Physical and biological characteristics of multi drug resistance (MDR): an integral approach considering pH and drug resistance in cancer. Seminars in Cancer Biology, 2017. Elsevier, 42-48.

OPASAWATCHAI, A. & MATANGKASOMBUT, P. 2015. iNKT cells and their potential lipid ligands during viral infection. *Frontiers in Immunology,* 6**,** 378.

OSLUND, K. L. & BAUMGARTH, N. 2011. Influenza-induced innate immunity: regulators of viral replication, respiratory tract pathology & adaptive immunity. *Future Virology,* 6**,** 951-962.

OVSYANNIKOVA, I. G., WHITE, S. J., ALBRECHT, R. A., GARCÍA-SASTRE, A. & POLAND, G. A. 2014. Turkey versus guinea pig red blood cells: hemagglutination differences alter hemagglutination inhibition responses against influenza A/H1N1. *Viral Immunology,* 27**,** 174-178.

OXFORD, J. & LAMBKIN, R. 2006. Influenza is now a preventable disease. *International Journal of Antimicrobial Agents,* 27**,** 271-273.

OZAWA, M., FUJII, K., MURAMOTO, Y., YAMADA, S., YAMAYOSHI, S., TAKADA, A., GOTO, H., HORIMOTO, T. & KAWAOKA, Y. 2007. Contributions of two nuclear localization signals of influenza A virus nucleoprotein to viral replication. *Journal of Virology,* 81**,** 30-41.

PAGET, W., MEERHOFF, T. & MEIJER, A. 2005. Epidemiological and virological assessment of influenza activity in Europe during the 2003-2004 season. *Euro Surveillance: Bulletin Europeen Sur Les Maladies Transmissibles= European Communicable Disease Bulletin,* 10**,** 107-111.

PANDIT, H., GOPAL, S., SONAWANI, A., YADAV, A. K., QASEEM, A. S., WARKE, H., PATIL, A., GAJBHIYE, R., KULKARNI, V. & AL-MOZAINI, M. A. 2014. Surfactant protein D inhibits HIV-1 infection of target cells via interference with gp120-CD4 interaction and modulates pro-inflammatory cytokine production. *PloS One,* 9**,** e102395.

PANNING, M., EICKMANN, M., LANDT, O., MONAZAHIAN, M., OLSCHLÄGER, S., BAUMGARTE, S., REISCHL, U., WENZEL, J., NILLER, H. & GÜNTHER, S. 2009. Detection of influenza A (H1N1) v virus by real-time RT-PCR. *Euro Surveillance: Bulletin Européen Sur Les Maladies Transmissibles= European Communicable Disease Bulletin,* 14.

PARAMESWARAN, N. & PATIAL, S. 2010. Tumor necrosis factor-α signaling in macrophages. *Critical Reviews™ in Eukaryotic Gene Expression,* 20**,** 87-103.

PARK, W.-J., PARK, B.-J., SONG, Y.-J., LEE, D.-H., YUK, S.-S., LEE, J.-B., PARK, S.-Y., SONG, C.-S., LEE, S.-W. & CHOI, I.-S. 2015. Analysis of cytokine production in a newly developed canine tracheal epithelial cell line infected with H3N2 canine influenza virus. *Archives of Virology,* 160**,** 1397-1405.

PEREZ-GIL, J. & WEAVER, T. E. 2010. Pulmonary surfactant pathophysiology: current models and open questions. *Physiology,* 25**,** 132-141.

PERINO, J., CROUZIER, D., SPEHNER, D., DEBOUZY, J.-C., GARIN, D., CRANCE, J.-M. & FAVIER, A.-L. 2011. Lung surfactant DPPG phospholipid inhibits vaccinia virus infection. *Antiviral Research,* 89**,** 89-97.

PFLUG, A., GUILLIGAY, D., REICH, S. & CUSACK, S. 2014. Structure of influenza A polymerase bound to the viral RNA promoter. *Nature,* 516**,** 355-360.

PIQUERAS, B., CONNOLLY, J., FREITAS, H., PALUCKA, A. K. & BANCHEREAU, J. 2006. Upon viral exposure, myeloid and plasmacytoid dendritic cells produce 3 waves of distinct chemokines to recruit immune effectors. *Blood,* 107**,** 2613-2618.

POECK, H., BSCHEIDER, M., GROSS, O., FINGER, K., ROTH, S., REBSAMEN, M., HANNESSCHLÄGER, N., SCHLEE, M., ROTHENFUSSER, S. & BARCHET, W. 2010. Recognition of RNA virus by RIG-I results in activation of CARD9 and inflammasome signaling for interleukin 1β production. *Nature Immunology,* 11**,** 63.

QUINTERO, O. A. & WRIGHT, J. R. 2000. Metabolism of phosphatidylglycerol by alveolar macrophages in vitro. *American Journal of Physiology-lung Cellular and Molecular Physiology,* 279**,** L399-L407.

RAGHAVENDRAN, K., WILLSON, D. & NOTTER, R. 2011. Surfactant therapy for acute lung injury and acute respiratory distress syndrome. *Critical Care Clinics,* 27**,** 525-559.

RAMOS, I. & FERNANDEZ-SESMA, A. 2012. Cell receptors for influenza a viruses and the innate immune response. *Frontiers in Microbiology,* 3**,** 117.

RAUCH, C. 2009a. On the relationship between drug's size, cell membrane mechanical properties and high levels of multi drug resistance: a comparison to published data. *European Biophysics Journal,* 38**,** 537-546.

RAUCH, C. 2009b. Toward a mechanical control of drug delivery. On the relationship between Lipinski's 2nd rule and cytosolic pH changes in doxorubicin resistance levels in cancer cells: a comparison to published data. *European Biophysics Journal,* 38**,** 829-846.

RAUCH, C. & FARGE, E. 2000. Endocytosis switch controlled by transmembrane osmotic pressure and phospholipid number asymmetry. *Biophysical Journal,* 78**,** 3036-3047.

RAUT DEEPIKA, B., SAKHARE RAM, S., DADGE KETAN, K. & HALLE, P. 2013. Resealed Erythrocyte Drug Delivery: A Review. *Hemoglobin,* 33**,** 6-7.

REMICK, D. G. 2005. Interleukin-8. *Critical Care Medicine,* 33**,** S466-S467.

RIMMELZWAAN, G., BAARS, M., CLAAS, E. & OSTERHAUS, A. 1998. Comparison of RNA hybridization, hemagglutination assay, titration of infectious virus and immunofluorescence as methods for monitoring influenza virus replication in vitro. *Journal of Virological Methods,* 74**,** 57-66.

RISS, T. L., MORAVEC, R. A., NILES, A. L., DUELLMAN, S., BENINK, H. A., WORZELLA, T. J. & MINOR, L. 2004. Cell Viability Assays. *In:* SITTAMPALAM, G. S., COUSSENS, N. P., BRIMACOMBE, K., GROSSMAN, A., ARKIN, M., AULD, D., AUSTIN, C., BAELL, J., BEJCEK, B., CAAVEIRO, J. M. M., CHUNG, T. D. Y., DAHLIN, J. L., DEVANARYAN, V., FOLEY, T. L., GLICKSMAN, M., HALL, M. D., HAAS, J. V., INGLESE, J., IVERSEN, P. W., KAHL, S. D., KALES, S. C.,

LAL-NAG, M., LI, Z., MCGEE, J., MCMANUS, O., RISS, T., TRASK, O. J., JR., WEIDNER, J. R., WILDEY, M. J., XIA, M. & XU, X. (eds.) *Assay Guidance Manual.* Bethesda (MD): Eli Lilly & Company and the National Center for Advancing Translational Sciences.

ROBERTS, K. L., LESER, G. P., MA, C. & LAMB, R. A. 2013. The amphipathic helix of influenza A virus M2 protein is required for filamentous bud formation and scission of filamentous and spherical particles. *Journal of Virology,* 87**,** 9973-82.

ROSSMAN, J. S., JING, X., LESER, G. P., BALANNIK, V., PINTO, L. H. & LAMB, R. A. 2010. Influenza virus m2 ion channel protein is necessary for filamentous virion formation. *Journal of Virology,* 84**,** 5078-5088.

ROSSMAN, J. S., LESER, G. P. & LAMB, R. A. 2012. Filamentous influenza virus enters cells via macropinocytosis. *Journal of Virology,* 86**,** 10950-11.

ROWSE, M., QIU, S., TSAO, J., YAMAUCHI, Y., WANG, G. & LUO, M. 2015. Reduction of Influenza Virus Envelope's Fusogenicity by Viral Fusion Inhibitors. *ACS Infectious Diseases,* 2**,** 47-53.

RUIGROK, R. W., BARGE, A., DURRER, P., BRUNNER, J., MA, K. & WHITTAKER, G. R. 2000. Membrane interaction of influenza virus M1 protein. *Virology,* 267**,** 289-298.

RUIGROK, R. W., CREPIN, T., HART, D. J. & CUSACK, S. 2010. Towards an atomic resolution understanding of the influenza virus replication machinery. *Current Opinion in Structural Biology,* 20**,** 104-13.

RUSSELL, R. J., KERRY, P. S., STEVENS, D. J., STEINHAUER, D. A., MARTIN, S. R., GAMBLIN, S. J. & SKEHEL, J. J. 2008. Structure of influenza hemagglutinin in complex with an inhibitor of membrane fusion. *Proceedings of the National Academy of Sciences,* 105**,** 17736-17741.

RYBORG, A., DELEURAN, B., THESTRUP-PEDERSEN, K. & KRAGBALLE, K. 1994. Lysophosphatidylcholine: a chemoattractant to human T lymphocytes. *Archives of Dermatological Research,* 286**,** 462-465.

SALK, J. E. 1944. A simplified procedure for titrating hemagglutinating capacity of influenza-virus and the corresponding antibody. *Journal of Immunology,* 49**,** 87-98.

SAMJI, T. 2009. Influenza A: understanding the viral life cycle. *The Yale Journal of Biology and Medicine,* 82**,** 153.

SANDERS, C. J., DOHERTY, P. C. & THOMAS, P. G. 2011. Respiratory epithelial cells in innate immunity to influenza virus infection. *Cell and Tissue Research,* 343**,** 13-21.

SARACHAI, C., SASIPREEYAJAN, J. & CHANSIRIPORNCHAI, N. 2014. Characterization of avian influenza H5N1 virosome. *Pakistan Veterinary Journal,* 34**,** 201-204.

SCHLEGEL, R., TRALKA, T. S., WILLINGHAM, M. C. & PASTAN, I. 1983. Inhibition of VSV binding and infectivity by phosphatidylserine: is phosphatidylserine a VSV-binding site? *Cell,* 32**,** 639-646.

SCHMIDT, N. W., MISHRA, A., WANG, J., DEGRADO, W. F. & WONG, G. C. 2013. Influenza virus A M2 protein generates negative Gaussian membrane curvature necessary for budding and scission. *The Journal of the American Chemical Society,* 135**,** 13710-9.

SCHMITZ, N., KURRER, M., BACHMANN, M. F. & KOPF, M. 2005. Interleukin-1 is responsible for acute lung immunopathology but increases survival of respiratory influenza virus infection. *Journal of Virology,* 79**,** 6441-6448.

SCHRAMLOVÁ, J., ARIENTOVA, S. & HULINSKA, D. 2010. The role of electron microscopy in the rapid diagnosis of viral infections. *Folia Microbiologica,* 55**,** 88-101.

SCHULZE-HORSEL, J., GENZEL, Y. & REICHL, U. 2008. Flow cytometric monitoring of influenza A virus infection in MDCK cells during vaccine production. *BMC Biotechnology,* 8**,** 45.

SCHÜRCH, S., BACHOFEN, H. & POSSMAYER, F. 2001. Surface activity in situ, in vivo, and in the captive bubble surfactometer. *Comparative Biochemistry and Physiology Part A: Molecular & Integrative Physiology,* 129**,** 195-207.

SEIFERT, U. 1997. Configurations of fluid membranes and vesicles. *Advances in Physics,* 46**,** 13-137.

SELBY, G. B. & EICHNER, E. R. Hematocrit and performance: the effect of endurance training on blood volume. Seminars in Hematology, 1994. 122.

SEO, Y.-J., BLAKE, C., ALEXANDER, S. & HAHM, B. 2010. Sphingosine 1-phosphate-metabolizing enzymes control influenza virus propagation and viral cytopathogenicity. *Journal of Virology,* 84**,** 8124-8131.

SHI, Y., WU, Y., ZHANG, W., QI, J. & GAO, G. F. 2014. Enabling the'host jump': structural determinants of receptor-binding specificity in influenza A viruses. *Nature Reviews Microbiology,* 12**,** 822-831.

SHOHET, S. B. & NATHAN, D. G. 1970. Incorporation of phosphatide precursors from serum into erythrocytes. *Biochimica et Biophysica Acta (BBA)-lipids and Lipid Metabolism,* 202**,** 202-205.

SIDORENKO, Y. & REICHL, U. 2004. Structured model of influenza virus replication in MDCK cells. *Biotechnology and Bioengineering,* 88**,** 1-14.

SIMMONS, C. & FARRAR, J. 2008. Insights into inflammation and influenza. *The New England Journal of Medicine,* 359**,** 1621–1623.

SIMPSON-HOLLEY, M., ELLIS, D., FISHER, D., ELTON, D., MCCAULEY, J. & DIGARD, P. 2002. A functional link between the actin cytoskeleton and lipid rafts during budding of filamentous influenza virions. *Virology,* 301**,** 212-225.

SLOMKA, M. J., PAVLIDIS, T., COWARD, V. J., VOERMANS, J., KOCH, G., HANNA, A., BANKS, J. & BROWN, I. H. 2009. Validated RealTime reverse transcriptase PCR methods for the diagnosis and pathotyping of Eurasian H7 avian influenza viruses. *Influenza and Other Respiratory Viruses,* 3**,** 151-164.

SMRT, S. T., DRANEY, A. W. & LORIEAU, J. L. 2014. The Influenza Hemagglutinin Fusion Domain is an Amphipathic Helical-Hairpin that Functions by Inducing Membrane Curvature. *Journal of Biological Chemistry,* 290**,** 228-238.

SONG, J. M., CHOI, C. W., KWON, S. O., COMPANS, R. W., KANG, S. M. & KIM, S. I. 2011. Proteomic characterization of influenza H5N1 virus-like particles and their protective immunogenicity. *Journal of Proteome Research,* 10**,** 3450-9.

SPACKMAN, E., SENNE, D. A., MYERS, T., BULAGA, L. L., GARBER, L. P., PERDUE, M. L., LOHMAN, K., DAUM, L. T. & SUAREZ, D. L. 2002. Development of a real-time reverse transcriptase PCR assay for type A influenza virus and the avian H5 and H7 hemagglutinin subtypes. *Journal of Clinical Microbiology,* 40**,** 3256-3260.

STEGMANN, T., NIR, S. & WILSCHUT, J. 1989. Membrane fusion activity of influenza virus. Effects of gangliosides and negatively charged phospholipids in target liposomes. *Biochemistry,* 28**,** 1698-1704.

STOCKERT, J. C., BLÁZQUEZ-CASTRO, A., CAÑETE, M., HOROBIN, R. W. & VILLANUEVA, Á. 2012. MTT assay for cell viability: Intracellular localization of the formazan product is in lipid droplets. *Acta Histochemica,* 114**,** 785-796.

SUDA, T., AKAMATSU, A., NAKAYA, Y., MASUDA, Y. & DESAKI, J. 2002. Alterations in erythrocyte membrane lipid and its fragility in a patient with familial lecithin: cholesterol acyltrasferase (LCAT) deficiency. *Journal of Medical Investigation,* 49**,** 147-155.

SUGIHARA, T., RAWICZ, W., EVANS, E. A. & HEBBEL, R. P. 1991. Lipid hydroperoxides permit deformation-dependent leak of monovalent cation from erythrocytes. *Blood,* 77**,** 2757-2763.

SUGITA, Y., NODA, T., SAGARA, H. & KAWAOKA, Y. 2011. Ultracentrifugation deforms unfixed influenza A virions. *Journal of General Virology,* 92**,** 2485-2493.

SUKHAREV, S. & SACHS, F. 2012. Molecular force transduction by ion channels–diversity and unifying principles. *Journal of Cell Science,* 125**,** 3075-3083.

SUN, X. & WHITTAKER, G. R. 2003. Role for influenza virus envelope cholesterol in virus entry and infection. *Journal of Virology,* 77**,** 12543-12551.

TAKEDA, M., LESER, G. P., RUSSELL, C. J. & LAMB, R. A. 2003. Influenza virus hemagglutinin concentrates in lipid raft microdomains for efficient viral fusion. *Proceedings of the National Academy of Sciences,* 100**,** 14610-14617.

TAN, T. S., HASSAN, S. S. & YAP, W. B. 2016. Significant Replication Time-points of Avian Influenza A Virus Strain H5N1 in Madin-Darby Canine Kidney Cells. *Malaysian Journal of Health Sciences,* 14**,** 17-21.

TAUBENBERGER, J. K. & MORENS, D. M. 2006. 1918 Influenza: the mother of all pandemics. *Annual Review of Biomedical Engineering,* 17**,** 69-79.

TEISSIER, E., ZANDOMENEGHI, G., LOQUET, A., LAVILLETTE, D., LAVERGNE, J.-P., MONTSERRET, R., COSSET, F.-L., BÖCKMANN, A., MEIER, B. H. & PENIN, F. 2011. Mechanism of inhibition of enveloped virus membrane fusion by the antiviral drug arbidol. *PloS One,* 6**,** e15874.

THAA, B., HERRMANN, A. & VEIT, M. 2009. The polybasic region is not essential for membrane binding of the matrix protein M1 of influenza virus. *Virology,* 383**,** 150-155.

TREANOR, J. J. 2014. Influenza viruses. *Viral Infections of Humans.* Springer.

TSCHERNE, D. M. & GARCÍA-SASTRE, A. 2011. Virulence determinants of pandemic influenza viruses. *The Journal of Clinical Investigation,* 121**,** 6-13.

VALE, F., CORREIA, A., MATOS, B., MOURA NUNES, J. & ALVES DE MATOS, A. 2010. Applications of transmission electron microscopy to virus detection and identification. *Microscopy: Science, Technology, Applications and Education***,** 128-136.

VAN BAALEN, C., ELS, C., SPRONG, L., VAN BEEK, R., VAN DER VRIES, E., OSTERHAUS, A. & RIMMELZWAAN, G. 2014. Detection of nonhemagglutinating influenza a (h3) viruses by enzyme-linked immunosorbent assay in quantitative influenza virus culture. *Journal of Clinical Microbiology,* 52**,** 1672-1677.

VAN MEER, G., VOELKER, D. R. & FEIGENSON, G. W. 2008. Membrane lipids: where they are and how they behave. *Nature Reviews Molecular Cell Biology,* 9**,** 112.

VAN REETH, K. 2000. Cytokines in the pathogenesis of influenza. *Veterinary Microbiology,* 74**,** 109-116.

VANCE, J. E. 2008. Thematic Review Series: Glycerolipids. Phosphatidylserine and phosphatidylethanolamine in mammalian cells: two metabolically related aminophospholipids. *Journal of Lipid Research,* 49**,** 1377-1387.

VIALLAT, A. & ABKARIAN, M. 2014. Red blood cell: from its mechanics to its motion in shear flow. *International Journal of Laboratory Hematology,* 36**,** 237-243.

VICTOR, B. L., LOUSA, D., ANTUNES, J. M. & SOARES, C. U. M. 2015. Self-assembly molecular dynamics simulations shed light into the interaction of the influenza fusion peptide with a membrane bilayer. *Journal of Chemical Information and Modeling,* 55**,** 795-805.

VISHVAKRAMA, P. & SHARMA, S. 2014. Liposomes: an overview. *Journal of Drug Delivery and Therapeutics***,** 47-55.

WANG, X., LI, M., ZHENG, H., MUSTER, T., PALESE, P., BEG, A. A. & GARĆıA-SASTRE, A. 2000. Influenza A virus NS1 protein prevents activation of NF-κB and induction of alpha/beta interferon. *Journal of Virology,* 74**,** 11566-11573.

WARD, C., DEMPSEY, M., RING, C., KEMPSON, R., ZHANG, L., GOR, D., SNOWDEN, B. & TISDALE, M. 2004. Design and performance testing of quantitative real time PCR assays for influenza A and B viral load measurement. *Journal of Clinical Virology,* 29**,** 179-188.

WEBSTER, R., COX, N. & STOHR, K. 2014. WHO Manual on Animal Influenza Diagnosis and Surveillance (World Health Organization, Geneva, Switzerland).

WILKS, S., DE GRAAF, M., SMITH, D. J. & BURKE, D. F. 2012. A review of influenza haemagglutinin receptor binding as it relates to pandemic properties. *Vaccine,* 30**,** 4369-4376.

WILLSON, D. F., CHESS, P. R., WANG, Z. & NOTTER, R. H. 2009. Pulmonary surfactant: biology and therapy. *The Respiratory Tract in Pediatric Critical Illness and Injury.* Springer.

WORLD HEALTH ORGANIZATION 2002. WHO manual on animal influenza diagnosis and surveillance.

WU, W., LI, R., LI, X., HE, J., JIANG, S., LIU, S. & YANG, J. 2015. Quercetin as an antiviral agent inhibits influenza A virus (IAV) entry. *Viruses,* 8**,** 6.

YAMADA, S. & OHNISHI, S. 1986. Vesicular stomatitis virus binds and fuses with phospholipid domain in target cell membranes. *Biochemistry,* 25**,** 3703-3708.

YAMASHITA, M., TOMOZAWA, T., KAKUTA, M., TOKUMITSU, A., NASU, H. & KUBO, S. 2009. CS-8958, a prodrug of the new neuraminidase inhibitor R-125489, shows long-acting anti-influenza virus activity. *Antimicrobial agents and chemotherapy,* 53**,** 186-192.

YAN, J.-J., JUNG, J.-S., LEE, J.-E., LEE, J., HUH, S.-O., KIM, H.-S., JUNG, K. C., CHO, J.-Y., NAM, J.-S. & SUH, H.-W. 2004. Therapeutic effects of lysophosphatidylcholine in experimental sepsis. *Nature Medicine,* 10**,** 161.

YEWDELL, J. W., BENNINK, J. R., SMITH, G. L. & MOSS, B. 1985. Influenza A virus nucleoprotein is a major target antigen for cross-reactive anti-influenza A virus cytotoxic T lymphocytes. *Proceedings of the National Academy of Sciences,* 82**,** 1785-1789.

YORK, A. & FODOR, E. 2013. Biogenesis, assembly, and export of viral messenger ribonucleoproteins in the influenza A virus infected cell. *RNA Biology,* 10**,** 1274-1282.

ZAMBON, M. C. 1999. Epidemiology and pathogenesis of influenza. *Journal of Antimicrobial Chemotherapy,* 44**,** 3-9.

ZHIRNOV, O. & MANYKIN, A. 2015. Abnormal morphological vesicles in influenza A virus exposed to acid pH. *Bulletin of Experimental Biology and Medicine,* 158**,** 776-780.